

Electronic Thesis and Dissertation Repository

---

6-28-2019 2:00 PM

## Neoadjuvant Stereotactic Ablative Radiotherapy To Treat Early Stage Breast Cancer Patients: The Role Of DCE-MRI

Matthew Mouawad  
*The University of Western Ontario*

Supervisor  
Gaede, Stewart  
*The University of Western Ontario* Co-Supervisor  
Gelman, Neil  
*The University of Western Ontario*

Graduate Program in Medical Biophysics  
A thesis submitted in partial fulfillment of the requirements for the degree in Doctor of Philosophy  
© Matthew Mouawad 2019

Follow this and additional works at: <https://ir.lib.uwo.ca/etd>



Part of the [Oncology Commons](#)

---

### Recommended Citation

Mouawad, Matthew, "Neoadjuvant Stereotactic Ablative Radiotherapy To Treat Early Stage Breast Cancer Patients: The Role Of DCE-MRI" (2019). *Electronic Thesis and Dissertation Repository*. 6264.  
<https://ir.lib.uwo.ca/etd/6264>

This Dissertation/Thesis is brought to you for free and open access by Scholarship@Western. It has been accepted for inclusion in Electronic Thesis and Dissertation Repository by an authorized administrator of Scholarship@Western. For more information, please contact [wlsadmin@uwo.ca](mailto:wlsadmin@uwo.ca).

# Abstract

The current standard of breast conserving therapy is lumpectomy followed by whole breast radiotherapy which is prohibitively long for many patients (4-6 weeks). In addition, the need for treating the whole breast has been questioned. The London Regional Cancer Program is enrolling early stage breast cancer patients in a prospective Phase I/II clinical trial (SIGNAL) to assess the safety/efficacy of neoadjuvant stereotactic ablative radiotherapy (SABR) to the tumour alone to reduce treatment times. This provides a unique opportunity to assess tumour response to SABR using non-invasive imaging. Patients received a pre-SABR dynamic contrast-enhanced (DCE)-MRI to guide target volume delineation. A subset also received post-SABR DCE-MRI to facilitate response assessment.

Recent safety concerns of long-term retention of gadolinium-based contrast agents (GBCA) in brain and bone led us to reduce the dose of GBCA to half the clinical dose part way through SIGNAL. Chapter 2 presents an investigation of the impact of this reduction on the inter- and intra-observer variability for target volume delineation and we found no significant decreases. These results are important for any context that requires repeated administrations of GBCAs to patients.

Chapter 3 presents an investigation of the impact of intra-session image registration on the voxel-by-voxel application of the Tofts model. Image registration led to significant reductions in the uncertainty in model parameter estimates and unphysical parameter estimates. Also, we showed that computation time could be reduced by a factor of two without affecting these results.

Chapter 4 presents an investigation of DCE-MRI based assessment of treatment response to SABR in early stage breast cancer. The analysis included two time delays post-SABR (6-7 or 16-19 days) and two SABR fractionation schemes (21Gy/1fraction or 30Gy/3fractions). DCE-MRI response assessment one-week post-SABR was confounded by acute inflammatory effects whereas 2.5 weeks appeared sufficiently long to minimize these effects. Kinetic parameters

measured 2.5 weeks post-SABR in both fractionation groups were indicative of response, but only the single fraction led to enhancement in tissue surrounding the tumour. Such metrics will be valuable in adapting treatment to patients and in future studies that will investigate higher ablative doses with the potential to eliminate surgery.

**Keywords:** Accelerated Partial Breast Irradiation (APBI), Early Stage Breast Cancer, Stereotactic Ablative Radiotherapy (SABR), Gadolinium Contrast Agent Safety, Deformable Registration, Tofts Model, 3D Slicer, Dynamic contrast enhanced (DCE) MRI, Response Imaging

## Summary for Lay Audience

The current standard of treatment for low-risk early stage breast cancer patients is a lumpectomy followed by 4-7 weeks of whole breast radiotherapy. This treatment time length has been shown to be prohibitively long for many patients, particularly elderly or rural patients. The London Regional Cancer Program is conducting a clinical trial with the aim of assessing the safety and efficacy of treating low-risk early stage breast cancer with 1-3 treatments of radiation therapy 1-3 weeks prior to surgery. This new treatment approach may significantly improve the quality of life for many patients but also provides a unique opportunity to assess treatment response to the high dose radiation using non-invasive imaging, which may allow for the development of prognostic biomarkers of tumour response. The main objective of this thesis was to explore the role of an imaging technique called dynamic contrast enhanced (DCE) MRI in non-invasively assessing tumour response in patients receiving high dose radiotherapy.

Recent findings have shown long-term retention of contrast agents used in DCE-MRI in brain and bone which led us to reduce the dose of these contrast agents part-way through the clinical trial. Chapter 2 presents an investigation of the impact that this reduction has on patient care, specifically the effect on the radiotherapy delivery process. We found that we could lower the contrast dose used without compromising patient care.

Chapter 3 investigates the role that motion correction strategies play in the analysis of DCE-MRI and was an important step in the analysis of DCE-MRI. Building off these results, Chapter 4 presents the results that address the original objective of investigating DCE-MRI in assessing tumour response to high dose radiation therapy. This work presents novel insights into the vascular response to high dose radiotherapy and shows that DCE-MRI may be a good candidate to assess tumour response – so long as the imaging time post-radiotherapy is sufficiently long to avoid confounding acute inflammatory effects due to the radiation. The work presented in this thesis sets the stage for future studies that will investigate even higher doses of radiotherapy with the potential to eliminate surgery altogether.

## Co-Authorship Statement

Chapter 2 of this thesis is an original research article that was submitted and published in *Radiotherapy and Oncology* entitled, "Reducing the dose of gadolinium-based contrast agents for DCE-MRI guided SBRT: The effects on inter and intra observer variability for preoperative target volume delineation in early stage breast cancer patients" by Matthew Mouawad, Heather Biernaski, Muriel Brackstone, Michael Lock, Brian Yaremko, Tracy Sexton, Edward Yu, Robert E. Dinniwell, Kalan Lynn, George Hajdok, Frank S. Prato, R. Terry Thompson, Neil Gelman, and Stewart Gaede (DOI: <https://doi.org/10.1016/j.radonc.2018.11.020>). Heather Biernaski, Muriel Brackstone, and Michael Lock were integral to the collection of data. George Hajdok suggested the project and contributed to the design of the study. Kalan Lynn collated patient data. Brian Yaremko, Tracy Sexton, Edward Yu, and Robert E. Dinniwell provided target volume delineations. All authors provided feedback and contributed to the writing of the manuscript. I designed the study, choose and implemented the methods of analysis, interpreted the results, and wrote the manuscript under the co-supervision of Dr. Neil Gelman and Dr. Stewart Gaede.

Chapter 3 of this thesis is currently under peer-review as a submission to the *Journal of Digital Imaging* entitled, "The effect of registration on voxel-wise Tofts model parameters and uncertainties from DCE-MRI of early stage breast cancer patients using 3DSlicer" by Matthew Mouawad, Heather Biernaski, Muriel Brackstone, Michael Lock, Anat Kornecki, Olga Shmuilovich, Ilanit Ben Nachum, Frank S. Prato, R. Terry Thompson, Stewart Gaede, and Neil Gelman. Heather Biernaski, Muriel Brackstone, Michael Lock, Anat Kornecki, Olga Shmuilovich, and Ilanit Ben Nachum, Stewart Gaede, and Neil Gelman are investigators on the SIGNAL trial and were integral to the design of the study and collection of data. Frank Prato and Terry Thompson provided funding and guidance on the image acquisition and project design. I performed the entirety of the analysis, interpreted the results and wrote the manuscript

under the co-supervision of Dr. Stewart Gaede and Dr. Neil Gelman.

Chapter 4 will be submitted as an original research article to the journal *Radiotherapy & Oncology* entitled: "The influence of single fraction versus three fraction SABR and imaging delay time post-radiotherapy on DCE-MRI response assessment in early stage breast cancer patients" by Matthew Mouawad, Heather Biernaski, Muriel Brackstone, Michael Lock, Brian Yaremko, Olga Shmuilovich, Anat Kornecki, Ilanit Ben Nachum, Giulio Muscedere, Frank S. Prato, R. Terry Thompson, Stewart Gaede, Neil Gelman. Heather Biernaski, Muriel Brackstone, Michael Lock, Brian Yaremko, Olga Shmuilovich, Anat Kornecki, Ilanit Ben Nachum, Giulio Muscedere, Stewart Gaede, and Neil Gelman were investigators on the SIGNAL trial from which the data was acquired and all provided feedback on the manuscript. Frank Prato and Terry Thompson provided funding and input in the study design. I analyzed the data, interpreted the results, and wrote the manuscript under the co-supervision of Dr. Stewart Gaede and Dr. Neil Gelman.

Appendix F is an original research article included for completeness. It has been accepted to the journal called *Current Oncology* and is entitled: "Stereotactic Image-Guided Neoadjuvant Ablative Single Dose Radiation Then Lumpectomy (Signal) For Early Breast Cancer: A Prospective Single Arm Trial Of Single Dose Radiation Therapy" by Keegan Guidolin, Brian Yaremko, Kalan Lynn, Stewart Gaede, Anat Kornecki, Giulio Muscedere, Ilanit Ben Nachum, Olga Shmuilovich, Matthew Mouawad, Edward Yu, Tracy Sexton, Neil Gelman, Vitali Moiseenko, Muriel Brackstone, Michael Lock. As part of this work, I collated data to provide the dose to the various organs. The citation is located at the end of Appendix F.

## Acknowledgments

No PhD is met without barriers and obstacles. I have been fortunate over the years to have developed a strong network of support - the people who have contributed enormously to my development and completion of this thesis. In what follows, I thank some of the most prominent figures in my life, with the understanding that I simply do not have the space to thank everyone who has helped me over the years.

To begin, I would like to both acknowledge and thank my supervisors, Dr. Neil Gelman and Dr. Stewart Gaede, for giving me the opportunity to be a part of this project. They have given me an immense amount of their time, effort, and consideration over the past five years. Both have consistently pushed me to become a better student and scientist, but also have instilled a philosophy of patience, leadership, and caring. I hope that in the future I will be able to emulate their approach to mentorship.

I would like to thank my committee members, Dr. Frank Prato, Dr. George Hajdok, and Dr. Michael Kovacs. While we only met as a group once a year, each meeting propelled the project further and helped immensely in terms of setting goals. They were always engaged and helpful in providing both feedback and constructive criticism. I would like to thank Frank for making time to discuss some of the finer details of the projects, as well as providing support in terms of funding, advice, and manuscript editing. I would also like to thank George for putting forth the idea for the project presented in chapter 2 - his initial idea led to a novel and innovative paper as well as allowing for continuation of the post-radiotherapy imaging that comprises the third project presented in this thesis.

I would like to thank all co-investigators on the SIGNAL trial. Without their help, the projects here could not have been completed. Particularly, I would like to thank Dr. Muriel Brackstone and Dr. Michael Lock for providing additional guidance on all aspects of SIGNAL and for taking into consideration my needs along with theirs. I would like to give additional thanks to Heather Biernaski and John Butler for providing their time, experience, and guidance

in designing the PET and MRI acquisitions that we used for SIGNAL.

Thank you to the staff of the London Regional Cancer Program, particularly Barb Barons, who helped me through all my administrative needs, and Scott Karnas, who helped with generation of figures. I would also like to thank Jeff Kempe who made sure to keep me humble, but who also provided input into some technical aspects of the various projects I worked on over the years. I would like to thank my lab mates, both current and past, for being willing to provide input and discuss various topics (like my love for the DICOM file format).

On a personal note, I would like to thank my parents, Caroline and Tony, my aunt and uncle, Penny and Dave, and my Grandpa, Michael Turnnidge, for their support, love, and motivation over the years. They have always shown interest in the direction I have chosen and supported the decisions I have made, providing whatever wisdom they could along the way. I know that, regardless of where the future takes me, their primary concern is my happiness and knowing this has been fundamental to my success.

I would also like to thank my soon-to-be in-laws. Tom, Karen, Cory, and Marlee have welcomed me whole-heartedly into their family and provided much-needed breaks from schooling life.

Finally, I would like to thank my fiancée and soon-to-be wife, Brittany Kosir. She is quite literally my other half and I could not imagine where I would be without her. She has been there to support me through all of university and been a continuous source of happiness and personal inspiration. I cannot wait to begin the next chapter of my life with her by my side.



# Table of Contents

<b>Abstract</b>	
<b>Summary for Lay Audience</b>	<b>ii</b>
<b>Co-Authorship Statement</b>	<b>iii</b>
<b>Acknowledgements</b>	<b>v</b>
<b>List of Figures</b>	<b>xiii</b>
<b>List of Tables</b>	<b>xvi</b>
<b>List of Abbreviations</b>	<b>xvii</b>
<b>List of Appendices</b>	<b>xix</b>
<b>Chapter 1: Introduction</b>	<b>1</b>
1.1 Cancer . . . . .	1
1.1.1 Overview . . . . .	1
1.1.2 Tissue Response to Radiotherapy and the Linear Quadratic Model . . . . .	1
1.1.3 The Evolution of External Beam Radiation Therapy . . . . .	5
1.1.4 Stereotactic Radiotherapy and the Linear Quadratic Model . . . . .	7
1.1.5 Summary . . . . .	8
1.2 Breast Cancer . . . . .	8
1.2.1 Overview . . . . .	8

1.2.2	Current Standard for Early Stage Breast Cancer Treatment . . . . .	9
1.3	Accelerated Partial Breast Irradiation . . . . .	10
1.3.1	Overview . . . . .	10
1.3.2	Treatment Evaluation . . . . .	11
1.3.3	Brachytherapy Accelerated Partial Breast Irradiation . . . . .	13
1.3.4	Intra-Operative Accelerated Partial Breast Irradiation . . . . .	15
1.3.5	External Beam Accelerated Partial Breast Irradiation . . . . .	17
1.4	Neoadjuvant Stereotactic Body Radiotherapy . . . . .	21
1.4.1	Prone Positioning . . . . .	21
1.4.2	Stereotactic Radiotherapy . . . . .	22
1.4.3	Treating neoadjuvant to surgery . . . . .	23
1.5	The SIGNAL trial . . . . .	24
1.6	Image Assessment of Treatment Response . . . . .	26
1.6.1	Overview . . . . .	26
1.6.2	Vascular Response to Radiotherapy . . . . .	27
1.7	Dynamic Contrast Enhanced MRI . . . . .	29
1.7.1	Overview . . . . .	29
1.7.2	DCE-MRI Contrast Agents . . . . .	30
1.7.3	Contrast Agent Dose in SIGNAL . . . . .	32
1.7.4	Image Acquisition . . . . .	32
	Dynamic Contrast Enhanced MRI acquisition . . . . .	33
	Native $T_1$ ( $T_{10}$ ) and $B_1$ Mapping for Signal to Concentration Conversion	36
1.7.5	Intra-Session Image Registration . . . . .	37
	Similarity Metric . . . . .	37
	Transformation Model . . . . .	40
1.7.6	Analysis . . . . .	43
	Non-parametric analysis of DCE-MRI . . . . .	43

Parametric analysis of DCE-MRI . . . . .	44
MRI Signal to Concentration . . . . .	44
The Tofts Model . . . . .	45
1.7.7 DCE-MRI Response Assessment to SABR . . . . .	49
1.8 Research Hypothesis . . . . .	52
1.9 Research Objectives . . . . .	52
1.10 Thesis Outline . . . . .	53
1.10.1 Reducing the dose of gadolinium-based contrast agents for DCE-MRI guided SBRT: The effects on inter and intra observer variability for pre- operative target volume delineation in early stage breast cancer patients (Chapter 2) . . . . .	53
1.10.2 The effect of registration on voxel-wise Tofts model parameters and uncertainties from DCE-MRI of early stage breast cancer patients using 3DSlicer (Chapter 3) . . . . .	53
1.10.3 DCE-MRI assessment of response to neoadjuvant SABR in early stage breast cancer: Comparisons of single versus three fraction schemes and two different imaging time delays post-SABR (Chapter 4) . . . . .	54
1.10.4 Conclusions and Future Work (Chapter 5) . . . . .	55
1.11 Bibliography . . . . .	56
<b>Chapter 2: Reducing the dose of gadolinium-based contrast agents for DCE- MRI guided SBRT: The effects on inter and intra observer variability for preoperative target volume delineation in early stage breast cancer patients</b>	<b>83</b>
2.1 Introduction . . . . .	83
2.2 Materials and Methods . . . . .	85
Patients . . . . .	85
Image Acquisition . . . . .	85

	Target Volume Delineation . . . . .	87
	Data Analysis . . . . .	88
	Statistics . . . . .	90
2.3	Results . . . . .	91
2.4	Discussion . . . . .	94
2.5	Bibliography . . . . .	98
<b>Chapter 3:</b>	<b>The effect of registration on voxel-wise Tofts model parameters and uncertainties from DCE-MRI of early stage breast cancer patients using 3DSlicer</b>	<b>104</b>
3.1	Introduction . . . . .	104
3.2	Materials and Methods . . . . .	107
3.3	Results . . . . .	111
3.4	Discussion . . . . .	115
3.5	Conclusion . . . . .	119
3.6	Bibliography . . . . .	120
<b>Chapter 4:</b>	<b>DCE-MRI assessment of response to neoadjuvant SABR in early stage breast cancer: Comparisons of single versus three fraction schemes and two different imaging time delays post-SABR</b>	<b>125</b>
4.1	Introduction . . . . .	125
4.2	Methods . . . . .	127
4.2.1	Patients . . . . .	127
4.2.2	Image Acquisition . . . . .	129
4.2.3	Image Registration . . . . .	130
4.2.4	Analysis . . . . .	131
	Signal Enhancement Volume . . . . .	131
	Tumour Segmentation . . . . .	131

Kinetic analysis . . . . .	133
Statistical Analysis . . . . .	134
4.3 Results . . . . .	134
4.4 Discussion . . . . .	137
4.5 Conclusion . . . . .	140
4.6 Bibliography . . . . .	141
<b>Chapter 5: Conclusions and Future Works</b>	<b>149</b>
5.1 Summary and Conclusions . . . . .	149
5.2 Limitations . . . . .	152
5.3 Future Work . . . . .	154
5.4 Bibliography . . . . .	158
<b>Appendix A: SIGNAL inclusion/exclusion criteria</b>	<b>162</b>
<b>Appendix B: The Effect of Partial Volume on <math>T_{10}</math> Estimation Using the Variable Flip Angle Method</b>	<b>165</b>
<b>Appendix C: Response assessment - detailed methodology for image registration and post-SABR contour generation</b>	<b>169</b>
<b>Appendix D: Response assessment - <math>B_1</math> and <math>T_{10}</math> variation within the tumour for Chapter 4</b>	<b>172</b>
<b>Appendix E: Appendix A-C Bibliography</b>	<b>174</b>
E.1 Bibliography . . . . .	174
<b>Appendix F: Stereotactic Image-Guided Neoadjuvant Ablative Single Dose Radiation Then Lumpectomy (Signal) For Early Breast Cancer: A Prospective Single Arm Trial Of Single Dose Radiation Therapy</b>	<b>175</b>
F.1 Introduction . . . . .	175

F.2	Methods . . . . .	178
F.3	Results . . . . .	181
F.4	Discussion . . . . .	185
F.5	Bibliography . . . . .	191
<b>Appendix G: Chapter 2 copyright form</b>		<b>197</b>
<b>Appendix H: Curriculum Vitae</b>		<b>198</b>

## List of Figures

Figure 1.1 Cell survival in fractionated vs unfractionated treatments with high and low $\alpha / \beta$ values . . . . .	4
Figure 1.2 Example case of two radiotherapy plans using whole-breast versus 3D-CRT for a patient enrolled in the RAPID trial . . . . .	18
Figure 1.3 Schematic diagram of imaging and treatment schedule for patients enrolled in the SIGNAL trial . . . . .	25
Figure 1.4 Schematic of the acquisition and analysis of DCE-MRI . . . . .	30
Figure 1.5 Pulse diagram of the SPGRE sequence (SIEMENS VIBE) method with fat suppression . . . . .	34
Figure 1.6 Visual demonstration of the differences between a rigid, affine, and deformable registration. . . . .	40
Figure 1.7 Simplified diagram of the free-form deformation algorithm with BSplines interpolation . . . . .	41
Figure 1.8 Diagram of the two-compartment Tofts model . . . . .	46
Figure 2.1 Demonstration of observer contours in two patients from the full and half dose contrast groups . . . . .	92
Figure 2.2 Column scatter plots for the volume and coefficient of variation metrics for the GTV and CTV . . . . .	93
Figure 3.1 Image acquisition timing diagram for SIGNAL . . . . .	106
Figure 3.2 An example mask defined over a patients' breast for the DCE-MRI intra-session image registration . . . . .	108

Figure 3.3	Computation time for deformable registration as a function of percent sampling . . . . .	109
Figure 3.4	Parametric maps for $K^{\text{trans}}$ and $v_e$ across percent sampling cases for a representative patient . . . . .	112
Figure 3.5	Median and 90th percentile values for parameter estimate and standard error of $K^{\text{trans}}$ across percent sampling cases . . . . .	113
Figure 3.6	Median $v_e$ percentage of voxels with $v_e > 1$ , median $\sigma v_e$ and percentage of voxels where $\sigma v_e$ exceeded 0.2 for unregistered and registered images (all percent sampling cases) . . . . .	114
Figure 3.7	Changes in the percentage of voxels where the standard error of $v_e$ exceeded certain thresholds for all percent sampling cases . . . . .	116
Figure 3.8	The change in RMSE as a function of percent sampling . . . . .	117
Figure 4.1	Flowchart of the analysis of the DCE-MRI data for response assessment . . . . .	128
Figure 4.2	Detailed schematic of the contour generation process for DCE-MRI response assessment . . . . .	132
Figure 4.3	Subtraction images and threshold versus signal enhancement volume curves from representative patients for the three response assessment groups demonstrating the change in signal enhancement post-SABR . . . . .	135
Figure 4.4	Changes in the spatial mean and standard deviation of $K^{\text{trans}}$ and $v_e$ following SABR for the three fractionation and imaging groups . . . . .	137
Figure B.1	Representation of a partial volumed voxel with different percentages ("P") of fat and fibroglandular tissue . . . . .	167
Figure B.2	Estimated $T_{10}$ values as a function of the percentage of fat in the partial volumed voxel. The purple dashed line represents the "true" value of fibroglandular tissue and the red dashed lines is the "true" value of fat . . . . .	168



Figure C.1 Schematic showing the intra-session image registration procedure for the variable flip angle and  $B_1$  images to the DCE-MRI images . . . . . 170

Figure C.2 Schematic of how the post-SABR contour was generated from the pre-SABR tumour contour. Corr = correction, Gd = gadolinium contrast . . . 171

Figure D.1 Additional Results for Chapter 4 showing variation of  $B_1$  and  $T_{10}$  across patients . . . . . 173

Figure F.1 Study schema showing the entire course of the experimental protocol undergone by patients in this study . . . . . 177

Figure F.2 Sample size of the different cohorts of patients included in SIGNAL . . . 179

## List of Tables

Table 1.1	General overview of CTCAE system for grading adverse events . . . . .	11
Table 1.2	Review of studies that investigated brachytherapy APBI . . . . .	14
Table 1.3	Review of studies that investigated EBRT APBI . . . . .	19
Table 1.4	Review of studies that investigated DCE-MRI or DCE-CT response assessment to stereotactic radiotherapy . . . . .	50
Table 2.1	Patient characteristics for the full versus half clinical dose groups . . . . .	86
Table 2.2	Summary of spatial metrics used to assess inter-observer variation between the full and half dose groups . . . . .	94
Table 2.3	Inter- and intra-observer reliability coefficients for the full and half dose groups . . . . .	95
Table 3.1	Results of statistical comparisons between parameters obtained with unregistered images versus registered images (at any PS level) . . . . .	111
Table 4.1	Study and patient information for DCE-MRI response assessment . . . . .	129
Table 4.2	Acquisition Parameters for MRI sequences used in this study. . . . .	130
Table 4.3	Pre-SABR contour volume and the change in the signal enhancement volume following SABR for the three response assessment groups . . . . .	136
Table F.1	Normal Tissue Dosimetric Limits – Original and Revised . . . . .	182
Table F.2	As-Treated Target Dosimetry . . . . .	183
Table F.3	Patient Demographics: Baseline and Tumour Characteristics . . . . .	184
Table F.4	Toxicity, Cosmesis, and Quality of Life Outcomes Pre- and Post-Treatment	185

## List of Abbreviations

$T_1$	Longitudinal Relaxation Time
$T_{10}$	Native $T_1$
3D	Three-Dimensional
3D-CRT	3D Conformal Radiotherapy
AFI	Actual Flip Angle
AIF	Arterial Input Function
ANOVA	Analysis Of Variance
APBI	Accelerated Partial Breast Irradiation
ASTRO	American Society For Radiation Oncology
BCS	Breast Conserving Surgery
BCT	Breast Conserving Therapy
BED	Biologically Effective Dose
BI-RADS	Breast Imaging-Reporting And Data System
C	$B_1$ Correction Factor
CE	Contrast Enhanced
CI	Conformity Index
$CI_{gen}$	Generalized Conformity Index
CT	Computed Tomography
CTCAE	Common Terminology Criteria For Adverse Events
CTV	Clinical Target Volume
CV	Coefficient Of Variation
DCE	Dynamic Contrast Enhanced
DCOM	Distance Between Centers Of Mass
EB-APBI	External Beam Accelerated Partial Breast Irradiation
EBRT	External Beam Radiotherapy
EES	Extracellular Extravascular Space
ELIOT	Electron Intra-operative Radiotherapy
FAZA	Fluoroazomycin Arabinoside
FDG	$^{18}\text{F}$ -Fluorodeoxyglucose
FFD	Free-form Deformation
FLT	Fluorothymidine
GBCA	Gadolinium Based Contrast Agent
GTV	Gross Target Volume
Gy	Gray
HASTE	Half-Fourier Acquisition Single-shot Turbo Spin Echo
$IAUC_t$	Initial Area Under The Curve To Time Point $T$
IBTR	Ipsilateral Breast Tumour Recurrence
IMRT	Intensity Modulated Radiotherapy

IORT	Intra-operative Radiotherapy
J	Joules
Kg	Kilogram
KV	Kilo-voltage
LD <sub>50</sub>	Lethal Dose That Kills 50% Of A Test Population
LQ model	Linear-quadratic Model
MCIB	Multi-catheter Interstitial Brachytherapy
MLC	Multileaf Collimator
MRI	Magnetic Resonance Imaging
NSF	Nephrogenic Systemic Fibrosis
PET	Positron Emission Tomography
PS	Percent Sampling
PSA	Permeability-surface Area Product
PTV	Planning Target Volume
QA	Quality Assurance
QOL	Quality Of Life
RAPID	Randomized Trial Of Accelerated Partial Breast Irradiation
RECIST	Response Evaluation Criteria In Solid Tumors
RF	Radiofrequency
RMSE	Root-mean-square-error
RO	Radiation Oncologist
ROI	Region-of-interest
RT	Radiotherapy
SABR	Stereotactic Ablative Radiotherapy
SBRT	Stereotactic Body Radiotherapy
SC	Shape Circularity
SFRT	Single-fraction Radiotherapy
SIGNAL	Stereotactic Image Guided Neoadjvant Ablation Then Lumpectomy
SNR	Signal-to-noise Ratio
SPGRE	Spoiled-Gradient Recalled Echo
SRS	Stereotactic Radiosurgery
SS-PRE	Slice-selective Pre-conditioning RF Pulse
TARGET-A	Targeted Intraoperative Radiotherapy Alone
TR	Repetition Time
USC	Universal Survival Curve
VMAT	Volumetric Modulated Arc Therapy
WBRT	Whole Breast Radiotherapy
WHO	World Health Organization

## List of Appendices

Appendix A SIGNAL inclusion/exclusion criteria . . . . .	162
Appendix B The Effect of Partial Volume on $T_{10}$ Estimation Using the Variable Flip Angle Method . . . . .	165
Appendix C Response assessment - detailed methodology for image registration and post-SABR contour generation . . . . .	169
Appendix D Response assessment - $B_1$ and $T_{10}$ variation within the tumour for Chap- ter 4 . . . . .	172
Appendix E Appendix A-C Bibliography . . . . .	174
Appendix F Stereotactic Image-Guided Neoadjuvant Ablative Single Dose Radiation Then Lumpectomy (Signal) For Early Breast Cancer: A Prospective Single Arm Trial Of Single Dose Radiation Therapy . . . . .	175
Appendix G Chapter 2 copyright form . . . . .	197
Appendix H Curriculum Vitae . . . . .	198

# Chapter 1

## 1 Introduction

### 1.1 Cancer

#### 1.1.1 Overview

Over their lifetime, 1 out of every 2 Canadians will be diagnosed with cancer [1,2]. In addition, cancer is one of the leading causes of death worldwide [1,3]. Cancer is a highly diverse disease requiring several different modalities of treatment including radiotherapy, systemic chemical therapies, and surgical procedures. However, radiotherapy is unique in that it is ubiquitous across most to all cancers. It is estimated that at least two-thirds of all cancer patients are treated with radiation therapy throughout their treatment course [4]. As such, it is important to understand the mechanisms of radiation therapy as well as the way it has developed over the past years. In the following section, we review radiotherapy in the context of cancer.

#### 1.1.2 Tissue Response to Radiotherapy and the Linear Quadratic Model

Radiation therapy involves the delivery of ionizing radiation to a target site. Ionizing radiation consists of high energy x-rays, gamma rays, or charged particles that are capable of ionizing atoms. This ionization causes deposition of energy which can lead to harmful and potentially lethal effects to living organisms. One measure of energy deposition that is important in cancer radiotherapy is the "absorbed dose," which is the amount of energy deposited (in joules (J)) per unit mass (kilogram (kg)). The SI unit of absorbed dose is called the "gray (Gy)". In the context

of cancer, the goal of using ionizing radiation for treatment is to deliver enough radiation to destroy cancer cells in the target site while minimizing the amount delivered to surrounding normal tissues.

In terms of the mechanistic cause of cell killing due to ionizing radiation, there is a large body of experimental evidence that demonstrates that the most important target for inducing cell death is through DNA damage [5]. On a cellular scale, as the radiation deposits its energy, there is a chance for the radiation to induce either single or double strand DNA breaks. This occurs either through direct or indirect action. In the case of an x-ray photon, one mode of interaction is with an electron on an atom that has the potential to liberate it (i.e., ionize the atom). This electron can then interact with the DNA causing damage (direct action), or create free radicals that then interact with DNA causing damage (indirect action) [6]. If the DNA damage is not repaired, the resulting effects are either DNA mutation or cellular death (the desired effect in cancer).

Early experiments into the effect of radiation on cellular systems established that the biological effect of radiation was influenced by factors such as the total dose, the dose rate, the dose per fraction, the overall treatment time, the type of tissue, *etc.* The interplay between dose delivery schema and inherent properties of the tissue are encapsulated by the "5 R's of radiobiology" which provide a framework for understanding how altering our radiation delivery scheme will affect tumour cell killing [6, 7]. The 5 R's are:

1. **Repair** of sublethal DNA damage
2. **Repopulation** of cells after a radiotherapy fraction
3. **Redistribution** of cells within the cell cycle
4. **Reoxygenation** of the surviving cells
5. Intrinsic cell **Radiosensitivity**

The interplay between these factors depends on the way that the radiation is delivered and the

type of tissue under study. For example, if we divide the total dose into a number of treatment sessions (fractionate), redistribution and reoxygenation lead to increased cell killing whereas repopulation and repair allow for potentially increased tumour cell survival [7]. Attempting to predict how these factors interact with living systems is important for determining optimal treatment techniques in terms of sparing normal tissue while maximally damaging tumour tissue [8].

A ubiquitous model predicated on these ideas and that has been in use for many years is the linear-quadratic model (LQ model). This model allows for comparison and conversion between different dose schemes, as well as a prediction of the biological effect that a certain dose scheme will have based on the properties of the tissue i.e., it can calculate isoeffective doses. In this model, it is assumed that single strand breaks rarely lead to cellular death, and so, the primary focus of cell killing is the ability of the dose scheme to induce double strand breaks. A double strand break can be caused by a single track of radiation or the cooperative effort of two radiation tracks that break a single strand of DNA "close" in time and space such that repair mechanisms fail. Then, the log of the number of cells surviving is related to dose through the following:

$$SF = e^{-(\alpha D + \beta D^2)} \quad (1.1)$$

where  $SF$  is the cell survival fraction,  $D$  is the dose,  $\alpha$  specifies the slope of the survival curve as  $D \rightarrow 0$ , and  $\beta$  specifies the relative contribution of the "quadratic component," which is related to the effectiveness of the DNA repair mechanisms. In other words,  $\alpha D$  is the yield of double strand breaks due to a single track of radiation and  $\beta D^2$  is the yield of double strand breaks due to cooperating tracks of radiation.

A parameter that is used to describe the relative sensitivity of a cell line to repeated smaller doses of radiation (i.e., fractionation) is the  $\alpha/\beta$ . Large values of  $\alpha/\beta$  indicate that the survival of the cell line does not largely depend on fractionation scheme (i.e., the cell of interest has



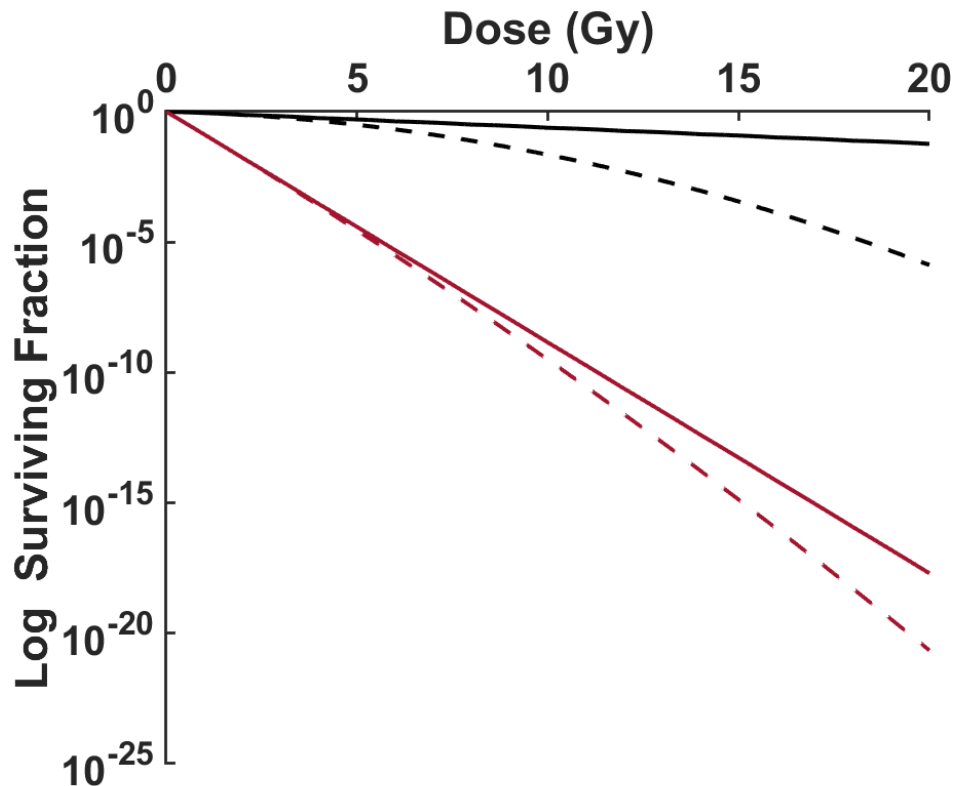


**Figure 1.1:** An example of the effect of fractionation on cell survival as predicted by the linear quadratic model. The black lines are tissues with a low  $\alpha/\beta$  and the red is a tissue with a high  $\alpha/\beta$ . The solid lines represent a fractionated scheme and the dotted lines represents a single fraction dose at different dose levels.

poor repair mechanisms). This is often the case for tumours with a typically assumed  $\alpha/\beta$  value of 10 [6]. Small  $\alpha/\beta$  are indicative of strong DNA repair mechanisms and that the cell is sensitive to fractionation. This is the case with "normal" tissue which is often assumed to have a value of 3 and is why fractionated radiation therapy has been the standard method of treatment for decades. Fractionating allows for a minimization of damage to normal tissue while not significantly affecting damage to the tumour [6]. Figure 1.1 shows this when comparing early (high  $\alpha/\beta$ ) versus late (low  $\alpha/\beta$ ) responding tissues. Fractionation leads to approximately equivalent cell killing in tissue with a high  $\alpha/\beta$  (i.e., tumours) but to tissue sparing effects in tissues with a low  $\alpha/\beta$  (i.e., normal tissue).

From this model, a parameter called the biologically effective dose (BED) can be derived

that allows for comparisons between different dose fractionation schemes:

$$BED = \frac{-\log(SF)}{\alpha} \quad (1.2)$$

$$BED = nd \left( 1 + \frac{d}{\alpha/\beta} \right) \quad (1.3)$$

where  $n$  is the number of fractions,  $d$  is the dose per fraction, and  $\alpha/\beta$  is as described above. This essentially specifies any dose scheme as if it had been given in an infinite number of small doses. This metric allows for comparisons of dose schedules based on the relative effect they would have on tissue cell killing [6].

### 1.1.3 The Evolution of External Beam Radiation Therapy

While different techniques exist to delivery radiotherapy, a commonly used method is through external beam radiotherapy. In this technique, radiation therapy is delivered external to the target site, typically with linear accelerators.

Before the advent of contemporary imaging (i.e., computed tomography (CT)), it was typical to treat a very large portion or the entirety of the affected organ up to the prescription dose using multiple static fixed x-ray fields. With the advent of CT imaging and the ability to visualize the target and surrounding tissues/organs, it became possible to treat more conformally, facilitating increased normal tissue sparing. One of the first examples of this was in the use of 3D conformal radiotherapy (3D-CRT), a technique where beam angles were chosen based on what structures could be seen through the "beams-eye-view" in an attempt to minimize the dose to the surrounding tissues and organs [9]. In addition, physical blocks or metallic multileaf collimators (MLCs) were used to statically shape the beam to further spare surrounding organs. This type of treatment design is called "forward planning" where the beam intensities are chosen and the resulting dose distribution is calculated [9].

It became evident that this method of planning had inherent flaws - we *know* the type of dose distribution that we want (or at least specific characteristics such as maximal dose to nor-

mal tissues). What if, instead, we could start from our dose distribution characteristics and find the optimal beam positions? This type of treatment technique is called intensity modulated radiotherapy (IMRT) and implements the paradigm of “inverse planning” where the beam shape and intensity is optimized to provide the desired dose distribution [9, 10]. The use of IMRT has grown immensely and has shown success in many cancer sites [10]. Even still, radiation was most commonly delivered in 1.8-2 Gy fractions per day to minimize normal tissue toxicities.

A technical advancement of IMRT is to deliver the therapy from an entire  $360^\circ$  arc while simultaneously modulating the intensity and shape of the beam instead of delivering the therapy from fixed angles. This method of delivery is called volumetric modulated arc therapy (VMAT). Due to the fact that it is typically used for highly targeted radiation, it requires extensive image-guidance. This has introduced a new era to treatment delivery design for cancer by delivering highly focused dose distributions to a target with steep dose fall-off [11]. Furthermore, the delivery was more efficient than typical IMRT techniques that use fixed beams, both in terms of the amount of radiation used over the treatment as well as reductions in the overall treatment time [11]. Finally, it has also enabled for the escalation of the dose per fraction into stereotactic regimes resulting in shorter treatment courses for patients (typically 1-10 fractions) [11, 12]. In terms of nomenclature, stereotactic radiotherapy is typically referred to as stereotactic radiosurgery (SRS) for single fraction treatments (typically in brain and head and neck cancer cases) and stereotactic ablative radiotherapy (SABR) (or stereotactic body radiotherapy (SBRT)) for extra-cranial stereotactic radiotherapy. Stereotactic techniques have been used successfully in several sites including head and neck, prostate, and lung cancers [11]. Its use for breast cancer has been limited primarily due to the fact that breast cancer radiotherapy is post-lumpectomy which results in large treatment volumes. This will be discussed in more depth in the following sections, particularly in section 1.4.2.

### 1.1.4 Stereotactic Radiotherapy and the Linear Quadratic Model

The LQ model has proved successful in traditional radiotherapy schemes [7]. However, deficiencies have been identified in high dose per fraction regimes, particularly since it assumes complete repair of sub-lethal DNA damage between fractions which may not be valid in stereotactic treatments [13] as evident by potential repair saturation effects [14]. Researchers have generally identified that the linear-quadratic model fails to predict cell survival accurately at doses  $> 10$  Gy per single fraction and overestimates the cell killing effect in tumours while underestimating cell killing in normal tissues [14, 15], though this is controversial [7]. In any case, development and implementation of alternative models that better predict cell killing effects and account for potentially differential cell killing effects at stereotactic doses are necessary [16].

Several models have been proposed to try and better describe tumour cell killing in higher single fraction doses than has previously been used [17]. One such model is the universal survival curve (USC) which merges the linear quadratic model, which explains cell killing effectively at lower doses, and another empirical model called the multi-target model, which fits empirical data well at higher doses [14]. The equation describing the log cell survival is [14]:

$$\ln S(d) = \begin{cases} -\alpha d - \beta d^2 & \text{if } d \leq D_T \\ -\frac{1}{D_0}d + \frac{D_q}{D_0} & \text{if } d \geq D_T \end{cases}$$

where  $S$  is the survival fraction,  $d$  is the dose,  $D_T$  is the threshold dose where the model transitions from the LQ model to the multi-target model,  $D_0$  is the characteristic dose required to deliver one inactivating event, on average, per cell,  $D_q$  is the quasi-threshold dose i.e., where the linear portion of the curve intersects with the x-axis (see Figure 2 in reference [14]). The parameters  $\alpha$  and  $\beta$  have been explained previously in section 1.1.2.

The USC model has been used to some success but requires an additional 2 parameters

which increases the complexity of data fitting [7, 14] - a difficulty for all proposed models [17]. Furthermore, unlike the linear quadratic model, the USC model does not provide any mechanistic explanation for the predictions at higher doses (a deficiency of the multi-target model). It is clear however that, in the stereotactic regime, we need to carefully consider the dose used, as a naive application of the LQ model to determine equivalent stereotactic dose schemes compared to standard fractionation schemes could potentially result in insufficient dose being delivered to the tumour or an under-estimation of the expected normal tissue toxicities [15].

### **1.1.5 Summary**

The previous sections have been given a broad overview of the radiotherapy field in terms of the mechanism behind radiotherapy cell killing and methods of radiation delivery. The remainder of this thesis will be focused on breast cancer.

## **1.2 Breast Cancer**

### **1.2.1 Overview**

Breast cancer is the most commonly diagnosed cancer and the second leading cause of cancer death in woman in Canada [2]. Fortunately, 80% of woman are diagnosed with early stage breast cancer i.e., as either Stage I or II, primarily due to organized screening programs [2]. Furthermore, early stage breast cancer is highly treatable [18] with 5-year survival rates of 100% and 93% for stage I and II, respectively [2]. As such, research into breast cancer therapies has generally shifted towards investigating methods to reduce the physical and emotional burden on patients.

## 1.2.2 Current Standard for Early Stage Breast Cancer Treatment

The current treatment options for early stage breast cancer are either radical mastectomy or breast conserving therapy (BCT). Radical mastectomy, introduced by Halstead and Meyer in 1894 (later modified to spare the pectoralis major muscle), was the standard of care well into the 1980s [18,19]. Investigation into new techniques has continued to focus on further conservation of breast tissue while maintaining tumour control. Most recently, several prospective clinical studies have investigated using a BCT technique where a lumpectomy is performed followed by external beam whole breast radiotherapy (WBRT) (Figure 1.2a, 1.2c). The radiotherapy is delivered in 2 Gy fractions per day over 25 fractions for a total dose of 50 Gy. This is typically followed by a 16 Gy boost to the surgical bed delivered in 2 Gy fractions [20,21]. The radiation following surgery has shown to be essential for minimizing tumour recurrence [22–25] and increasing overall survival [23,25]. These studies have demonstrated an equivalent cure rate to total mastectomy [18,22,26,27].

Despite the apparent benefits of BCT, its utilization has been limited [28,29]. This 5-8 week treatment schedule has been shown to be prohibitively long for many patients, particularly elderly and rural patients or patients who live in under-served areas [29,30]. Depending on the region being studied, 10-80% of patients who are eligible for BCT opt to undergo mastectomy instead [20]. Furthermore, 15-30% of patients who undergo BCT do not return for the adjuvant WBRT after the lumpectomy [20].

There has been an increased investigation into reducing the treatment time for patients to try and encourage them to return for the adjuvant radiotherapy as it is important in minimizing recurrence. Several studies have investigated an alternative to the 50 Gy in 25 fractions WBRT in which the dose is increased per fraction (i.e., hypo-fractionated). In the so-called “Canadian” scheme, radiation is delivered in 2.66 Gy fractions over 16 fractions for a total of 42.5 Gy and has shown to provide equivalent tumour control and equivalent cosmetic outcome [21]. This scheme has thus become the standard for adjuvant WBRT radiotherapy [31]. Even still,

this requires 3-5 weeks of treatment, again depending on the use of a boost of radiation to the tumour bed. Ideally, the dose per fraction would be increased further to reduce the treatment time but this is not possible without increasing the risk of normal tissue and organ complications, particularly for the heart and lungs [32]. If smaller volumes could be treated then it may be possible to increase the dose per fraction.

Fortunately, large randomized prospective trials have established that recurrence tends to occur local to the surgical bed [22, 26, 27], and that recurrence at other sites distal from the original target was comparable to rates in the contra-lateral breast [26]. This has prompted researchers to question whether it is necessary to deliver radiation to the entire breast. If it is indeed true that we could treat a smaller volume, this would motivate reductions in the treatment volume and would allow for further escalations of the dose per fraction. This method of treatment has been termed accelerated partial breast irradiation (APBI) and has been investigated by several researchers and institutions [20].

## **1.3 Accelerated Partial Breast Irradiation**

### **1.3.1 Overview**

Similar to WBRT, APBI typically begins with a lumpectomy where the tumour plus a margin is removed, followed by targeted radiotherapy. The radiation is prescribed to the lumpectomy plus a margin that accounts for microscopic disease as well as uncertainties in the delivery of the radiation (due to motion, setup reproducibility *etc.*). This allows for escalation of the dose per fraction resulting in typical treatment times of a week or less [20]. APBI can be performed using three different techniques: brachytherapy, intra-operative radiotherapy (IORT), or external beam radiotherapy (EBRT). The largest prospective, randomized trial comparing the three methods of APBI to WBRT is the NSABP B-39/RTOG 0413 clinical trial [33], the results of which are highly anticipated (the interim results reported for 3D-CRT are discussed in section 1.3.5). In the meantime, many single-institution or smaller multi-institution studies have

**Table 1.1:** A general description of the five grades in the criteria for adverse events (CTCAE) system.

Grade of Adverse Event	General Description
Grade 1 (Mild)	Asymptomatic or mild symptoms Clinical or diagnostic observations only Intervention not indicated.
Grade 2 (Moderate)	Minimal, local or noninvasive intervention indicated Limits age appropriate activities of daily living
Grade 3 (Severe)	Medically significant but not immediately life threatening hospitalization or prolongation of hospitalization indicated Disabling Limiting of self care activities of daily living
Grade 4 (Life Threatening)	Urgent intervention indicated
Grade 5 (Death)	Death Related to adverse event

arisen to investigate APBI, though typically limited to just one of the aforementioned delivery methods.

In the following sections, we begin by describing the general concepts of ipsilateral breast tumour recurrence (IBTR), cosmesis assessment, and toxicity evaluation. This is important as it, along with the concept of BED introduced in section 1.1.2, form a framework for comparing new methodologies to the current standards of treatment as well as for comparing between studies. Following this, a brief description of each APBI technique is given as well as associated studies that have quantified cosmetic outcomes and IBTR - with a focus on more recent studies (within last 10 years).

### 1.3.2 Treatment Evaluation

Most studies investigating APBI base their assessment and outcomes on the primary and secondary endpoints of the NSABP B-39/RTOG 0413 trial.

While there are many different treatment evaluation metrics, the ones of focus are cosmesis, normal tissue and organ toxicities, and IBTR. IBTR is defined as a tumour recurrence that



occurs within the affected breast after treatment. Contralateral breast and other regional recurrences are also generally reported but rates are low in early stage breast cancer [34] and so will not generally be discussed here. Cosmesis evaluation and toxicity are related but distinct evaluations. Toxicities are pathological side effects in the surrounding tissue as a result of our treatment. Cosmesis outcomes are macroscopic deterioration in the overall look, feel, or shape of the treated breast. Cosmesis outcomes are linked to toxicological effects but a toxicity does not necessarily present as a short- or long-term cosmetic deterioration.

In terms of toxicity reporting, the most commonly used system for side effect reporting is the common terminology criteria for adverse events (CTCAE), which provides a standardized framework for reporting system for toxicological side effects [35]. Generally, the adverse events reported are specific to the organ under study and graded on a scale from 1-5 (or highest grade that fits within the context of the current adverse events importance) which describes the severity of the adverse event (table 1.1). For breast treatment, particularly due to radiation, we are primarily concerned with adverse events related to breast under "Reproductive system and breast disorders" as well as "Skin and subcutaneous tissue disorders." The most prevalent assessments reported are skin toxicities (erythema, telangiectasia), fat necrosis, breast pain, and fibrosis.

Cosmesis is typically evaluated by both patients and physicians or caregivers [36]. The first formal system was developed in 1979 by Harris *et al.* who introduced a subjective assessment scheme utilizing a four-point scale where the affected breast is compared to the untreated breast [37]. The cosmetic outcome is typically grouped into four categories: excellent, good, fair, or poor with most studies reporting the total proportion of patients that experienced excellent or good cosmesis as rated by patients or physicians as a combined metric. Other authors have attempted to provide more objective measures over the years but the Harris system (also referred to as the Harvard scale) continues to be ubiquitous in the context of assessing breast cosmesis outcomes.

### 1.3.3 Brachytherapy Accelerated Partial Breast Irradiation

Brachytherapy is a technique that uses encapsulated radioactive sources ("seeds") to deliver radiation over short distances. Due to the nature of radiation fall-off with distance (inverse square law), this technique results in sharp dose gradients [38]. This makes it a prime candidate for delivering focal radiotherapy to the target location for APBI. In the context of APBI, three methods exist for its application: 1) interstitially using multi-catheter interstitial brachytherapy (MCIB), 2) intracavitary using balloon-based techniques, or 3) using hybrid approaches.

MCIB uses multiple catheters that are inserted into the breast tissue in multiple planes which allow the radioactive seeds to deliver their dose to the tissue [20]. The interstitial applicators can be placed at the time of surgery or in a follow-up if pathology and margin status need to be evaluated before treatment [20, 34, 39].

Most studies that report long-term patient follow-up and evaluation were performed with MCIB (Table 1.2) [20]. Generally, IBTR rates are equivalent to WBRT (Table 1.2). One of the first series of successful studies involving brachytherapy APBI used interstitial implants to deliver the radiotherapy following a lumpectomy [34]. These promising results lead to the development of the RTOG-9517 trial where patients were treated over the course of 5 days using MCIB - a significant reduction in treatment time [40]. Follow-up with patients continues to show long term breast cancer control rates after more than 10 years [40]. Another large multi-institution study conducted in European countries comparing WBRT versus MCIB APBI found a IBTR of 1.44% vs 0.92%, respectively. This supports the idea that breast recurrence tends to occur local to the surgical bed and further motivates continued investigation into APBI.

In terms of cosmesis and toxicity, results tend be favorable (Table 1.2 [20, 39]). RTOG-9517 showed a patient rated cosmesis of 66% at 5 years which was comparable to to WBRT at the time [41, 42]. Johansson *et al.* reported a very low cosmetic outcome of 51% but explain that this may be due to the fact that patients were planned before the era of CT based planning which necessitated large margins for radiotherapy i.e., a large amount of the surrounding breast

**Table 1.2:** A list of studies reporting cosmetic outcome as well as IBTR with a focus on studies from the last 10 years. Cosmetic outcome was determined using the Harvard Harris Criteria as indicated previously. The cosmesis and IBTR are specified for the median follow-up time

Reference	# Cases	Method	Median Follow up (months)	Good/Excellent Cosmesis	IBTR
Mann [45]	111	Mammosite	66	97%	2.700%
Shah / Nelson [46] [47]	1449	Mammosite	63.1	91%	2.800%
Vargo [48]	157	Mammosite	66.33	93%	2.500%
Johansson [43]	51	MCIB	86	51%	6.000%
Antonucci [49]	199	MCIB	105.6	98%	5.000%
Strnad [50]	274	MCIB	63	90%	2.900%
Polgar [51]	128	MCIB	122.4	85%	5.500%
White / Rabinovitch [40] [42]	100	MCIB	145.2	66%	6.200%
Polgar / Strnd [52] [53]	633	MCIB	78	92%	1.400%
Gabani [54]	175	MCIB	120	95%	5.700%
Khan [55]	200	MCIB / Balloon	19	97%	0.005%

received a high dose of radiation in a shorter amount of time. They also identified that close to 50% of negative cosmesis rating were due to surgery [43]. Even with these promising results, this techniques success relies heavily on accurate placement of the catheters, requiring a very high degree of expertise and experience. As such, its implementation into regular clinical use has been limited [20, 34, 44].

Intracavitary or balloon based brachytherapy APBI involves placement of a saline filled balloon into the surgical cavity during or after the lumpectomy. The first to be developed was the Mammosite® brachytherapy system (Hologic, Marlborough, MA) which provided a more reproducible and easily applied methodology, requiring much less expertise. However, this system only contained one central channel for an Iridium-192 high dose rate source to traverse and deliver the dose resulting. This resulted in an inflexibility to shape the dose distribution resulting in inhomogeneous dose distributions. In addition, the materials used lacked contrast on x-ray or CT requiring injection of a contrast agent for visualization. Despite these shortcomings, it has shown relatively good cosmesis and toxicity (Table 1.2), though longer follow

up is needed [20]. Other technologies such as the Axxent Electronic brachytherapy system (Xoft, Fremont, CA), the Contura device (SenoRx, Inc, Aliso Viejo, Ca), *etc.* improve on these aspects by introducing multiple channels for better dose distribution shaping, or use of kilo-voltage x-ray sources to allow less stringent shielding requirements and greater system mobility [20, 34], though clinical outcome data is currently lacking.

Finally, hybrid techniques have been developed to take advantage of the dose distribution shaping versatility of MCIB with the ease-of-use and convenience of balloon based brachytherapy systems. These systems are surgically implanted in patients and typically have several channels for entry of radioactive sources.

These studies taken together show that brachytherapy APBI is generally well tolerated by patients and can reduce treatment time to approximately five days. However this technique is highly invasive, sometimes requiring a second surgery for implantation of the devices into the surgical cavity. It also has an increased risk of infection. Normal tissue toxicity is generally acceptable but depends on factors such as tumour location, surgical excision irregularity, breast size, and the expertise of the physician performing the operation which likely present as a barrier for widespread adoption.

### **1.3.4 Intra-Operative Accelerated Partial Breast Irradiation**

In IORT, a single high dose of radiation is delivered to the tumour bed during surgery. In this way, large doses can be delivered in a single fraction while minimizing toxicities to the normal tissue since the radiation does not have to traverse the normal tissues to reach the target. Radiation was originally delivered using a standard linear accelerator by transporting the patient from the operating room to the radiotherapy bunker, but recent development of portable linear accelerators allow for patients to be treated without the additional logistical complications of transporting them [56]. Linear accelerator miniaturization technologies has improved greatly over recent years and is making this technique more appealing. In addition, IORT eliminates the risk of patients not returning for their treatment and eliminates the risk of miss due to respi-

ratory motion since the radiotherapy can be delivered under direct visualization of the tumour bed.

There are only a few studies that have long term follow up for patients that received IORT due to the previous logistical difficulties [57]. The two largest prospective trials with longer term follow-up are the targeted intraoperative radiotherapy alone (TARGIT-A) trial and the electron intra-operative radiotherapy (ELIOT) trial.

TARGIT-A compared external beam WBRT to single dose IORT [58]. IORT was delivered using a 1.5-5 cm spherical applicator and an intrabeam device that used 50 kilo-voltage (kV) energy x-rays to deliver the radiation. The surface of the tumour bed received 20 Gy which attenuated to 5-7 Gy at 1 cm depth. Using a non-inferiority statistical design, the authors showed that IORT did not perform worse than WBRT at the prescribed non-inferiority margin, though there was indeed a significant increase in IBTR for the IORT arm (3.3% versus 1.3%). Concerning toxicity, a study on a subsample of patients from the TARGIT-A trial showed that patients enrolled in the IORT arm were twice as likely to have excellent or good cosmetic scores as compared to WBRT using an objective camera based system, demonstrating that IORT was well tolerated by patients [59].

The ELIOT trial was similar in design to the TARGIT-A trial but used a mobile electron linear accelerator to deliver the therapy. While they found that there was a significant increase in the IBTR rate for the IORT arm compared to WBRT, it was within the pre-specified equivalence margin. They further commented that this increase was likely due to inclusion of patients who would be selected as "unsuitable" according to American Society for Radiation Oncology (ASTRO) consensus criteria for patient selection and showed no significant difference in recurrence rate between IORT and WBRT when selecting favorable candidates [60]. In several subsequent analyses on subsets of patients, toxicity profiles tended to favor IORT [61].

While IORT is generally well tolerated with acceptable IBTR in correctly selected patients, its use has generally been low due to the logistical difficulties of having to transfer patients from the surgical room to the radiotherapy treatment machines [62]. While mobile linear ac-

celerators are renewing interest in this technique they still require a large cost investment as well as additional quality assurance (QA) procedures and expertise. One of the largest criticisms is that treatment occurs before final pathology has been determined and re-excision may be required once pathology is established. Devices are being constructed that allow for detection of positive or negative margins at the time of surgery and may help to increase the use of IORT [56].

### **1.3.5 External Beam Accelerated Partial Breast Irradiation**

External beam accelerated partial breast irradiation (EB-APBI) utilizes linear accelerators to treat patients non-invasively using the superposition of radiation beams. Most investigations into APBI providing long-term follow-up have delivered the treatment in accordance to the specifications of NSABP B-39/RTOG 0413 [20, 63] i.e., using 3D-CRT. Patients are setup in the supine position and radiation is delivered using 3-5 non-coplanar static photon fields, with the goal of minimizing dose to the uninvolved ipsilateral breast, the contra-lateral breast, the heart, and the lungs.

However, other techniques have been developed since the initiation of NSABP B-39/RTOG 0413 that allow for better dose shaping. IMRT is a technique that modulates the beam intensities at each treatment angle using using the multi-leaf collimators that provides further target conformity [64]. For this reason, other studies have performed investigations for its use in APBI [65].

For both 3D-CRT and IMRT, the gross target volume (GTV) is defined as the lumpectomy cavity, visualized with CT, plus a margin for radiation treatment delivery uncertainties. Typical expansions of the GTV are 1.5cm for microscopic disease (clinical target volume (CTV)) and 1cm to account for the uncertainties in target position due to respiratory motion and the generally mobile nature of the breast in the supine position as well as setup errors day-to-day (planning target volume (PTV)). The most common dose scheme is 38.5 Gy total dose in 10 fractions twice per day with a minimal delay interval of 6 hours to allow for repair mechanisms

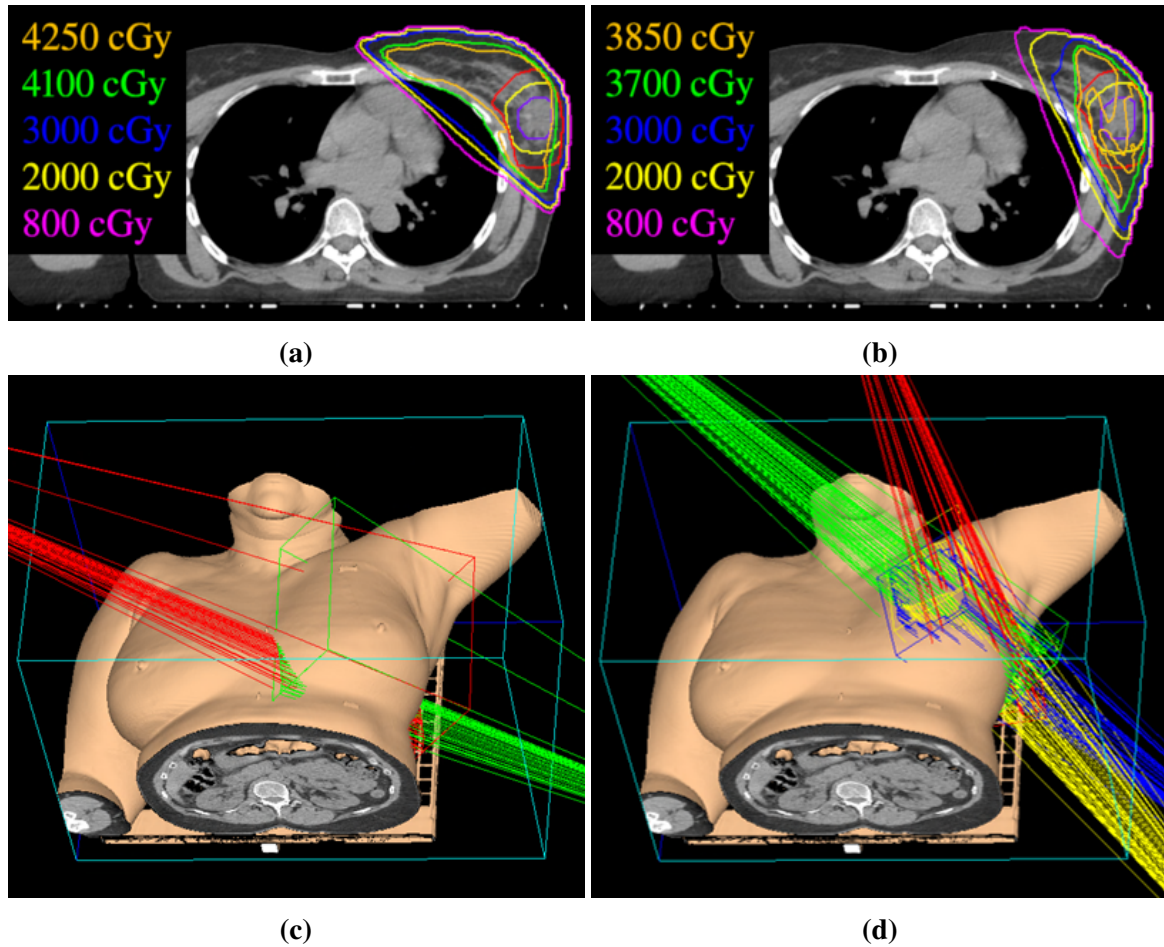


**Figure 1.2:** A patient from the RAPID trial showing the differences between whole breast radiotherapy and 3D-conformal radiotherapy. (A) and (B) show the dose distributions for the whole breast and 3D-CRT plan, respectively. The GTV (lumpectomy), CTV, and PTV are shown as purple, yellow, and red contours. The orange isodose line represents 100% of the prescription dose and the green represents the 95% (prescription) isodose line. (C) and (D) show a visual representation of the spatial geometry of the beams for whole breast and the 3D-CRT plans, respectively. Thanks to Dr. Scott Karnas from the London Regional Cancer Program for providing the dosimetry plans for this representative patient.

in normal tissue.

The main advantages of APBI delivered using EBRT compared to brachytherapy and intra-operative techniques are: 1) it is non-invasive, 2) the technology is widespread, requiring a standard linear accelerator, 3) requires less expertise for planning which results in more uniform treatment across centers and easier comparisons, 4) more likely to have uniform dose distributions compared to brachytherapy techniques, and 5) does not require subjecting the

**Table 1.3:** A list of studies reporting cosmetic outcome (using Harvard Harris Criteria) as well as IBTR with a focus on studies from the last 10 years. The cosmesis and IBTR are specified for the median follow-up time. 3D-CRT = 3 dimensional conformal radiotherapy, IMRT = intensity modulated radiotherapy

Reference	Pub Year	# Cases	Method	Median Follow up (months)	Good/Excellent Cosmesis	IBTR
Hepel [66]	2009	60	3D-CRT	15	82%	0.00%
Chen [67]	2010	94	3D-CRT	50.4	89%	1.10%
Berrang [68]	2011	104	3D-CRT	37	82%	1.00%
Formenti [69]	2012	98	3D-CRT <sup>a</sup>	64	89%	1.00%
Lewin [70]	2012	36	IMRT	44.8	97%	3.00%
Rodriguez [71]	2013	51	3D-CRT	60	75%	0.00%
Lei [72]	2013	136	IMRT	53.1	88%	0.70%
Bergom [73]	2013	20	IMRT <sup>a</sup>	18.9	95%	0.00%
Liss [74]	2014	30	IMRT	60	73%	3.00%
Galland-Girodet [75]	2014	98	Proton 3D-CRT	82.5	62%	11.00%
Galland-Girodet [75]	2014	98	3D-CRT	82.5	94%	4.00%
Livi [76]	2015	260	IMRT	60	100%	1.40%
Peterson [77]	2015	569	3D-CRT	36	71%	NS
Horst [78]	2016	141	3D-CRT	60	95%	0.70%
Rabinovitch [79]	2016	52	3D-CRT	96	64%	7.70%
Coles [80]	2017	669	IMRT	72.2	NS	0.50%

<sup>a</sup>Patients were setup prone  
NS = not specified

patient to additional surgeries as well as verification of the tumour pathology before treatment [20, 34, 39].

EB-APBI has seen a large increase in use, again owing to its high availability. Table 1.3 summarizes relevant contemporary studies. Most studies report IBTR rates similar to those of other APBI techniques and WBRT, again supporting the notion that local recurrence tends to occur local to the surgical bed. However, mixed results have been seen in terms of the long term cosmesis outcomes.

In a single institution study, Rodriguez *et al.* randomized patients to either WBRT or



APBI using 3D-CRT [71]. In terms of IBTR, there was no significance differences between the two arms. However, they found significant reductions in the Good/Excellent cosmesis outcomes at a median follow up of 60 months (90% compared to 75%). The randomized trial of accelerated partial breast irradiation (RAPID) trial, a large multi-institution Canadian trial, performed an interim analysis comparing WBRT and 3D-CRT in 164 and 171 patients, respectively. They found that there was a significant reduction in cosmesis for patients enrolled in the 3D-CRT arm of 71% Good/Excellent compared to 83% in the WBRT. As a result, the trial was terminated early [77,81]. Liss *et al.* also showed a significant reduction in cosmesis in a single institution study with 30 patients using IMRT. With a median follow up of 60 months, they found a cosmesis of Good/Excellent in only 73% of patients [74].

While there is mixed results in terms of toxicity and cosmesis, researchers claim that the poor outcomes in these trials is largely due to patient selection criteria and, in particular, the large volumes of normal breast tissue that receives radiation - especially for large tumours or patients with large breasts [15]. A primary factor of these large treatment volumes is the large margins that are used that account for patient respiratory motion and treatment setup inaccuracies. For example, in NSABP B39/RTOG 0413 [33] and RAPID [81] PTV margins of 1 cm were used in addition to a 1.5 cm margin for the CTV. Furthermore, because this is delivered post-lumpectomy, the GTV will contain both the original tumour volume as well as the surgical margins, which are typically 1cm or more. These factors compound resulting in large amount of normal tissue being exposed to radiation. As was demonstrated in section 1.1.2, normal tissue is sensitive to fractionation scheme, and so, the hypofractionation leads to additional normal tissue complications compared to WBRT (which allows for appropriate repair). Figure 1.2 shows a patient from the RAPID trial (from the London Regional Cancer Program) that was planned with both WBRT and APBI. It is evident that even though we are treating more focally, a large amount of normal breast tissue still receives a high dose of radiation (see 2000 cGy isodose) but over a shorter treatment period. This is most likely causing sub-lethal damage to become lethal in the surrounding tissue as there is not sufficient

time for DNA repair.

Despite these negative findings, there is a large motivation for addressing these shortcomings due to the potential widespread availability of this technique and its non-invasive nature. To address the poor cosmesis seen in several studies, investigation into techniques that reduce the amount of radiation normal tissue receives is at the forefront of EB-APBI research. Reductions in the margins added to the GTV to account for the poor setup reproducibility and patient motion is a primary area of investigation. In addition, more conformal techniques as well as other potential treatment schemes need to be investigated.

## **1.4 Neoadjuvant Stereotactic Body Radiotherapy**

Each of the techniques outlined above have their advantages and disadvantages. The largest focus of research in the past several years is EB-APBI as it holds the greatest promise for wide adoption and low patient burden. Most, if not all, cancer centres have a linear accelerator and so, if we could address some of the short-comings of EBRT, we would be able to significantly improve patient care while potentially decreasing the cost per patient [82]. Particularly, developing better treatment techniques to reduce dose to the surrounding normal tissue are of high interest as the poor cosmesis in some studies most likely relates to large treatment volumes due to the PTV expansion. Three ways of reducing the treatment volumes as well as minimizing dose to the surrounding normal tissue are of primary interest: 1) treating patients prone, 2) using VMAT, and 3) treating neoadjuvant (before) surgery.

### **1.4.1 Prone Positioning**

One method that may potentially be able to reduce treatment volumes, improve dose homogeneity (particularly for large breast patients) as well as reduce dose to lung, chest wall, and heart, is by treating patients prone [69, 83–87]. Formenti *et al.* [69] were one of the first to demonstrate the efficacy of the prone setup in reducing setup error as well as reductions in the

PTV volume needed by 1 cm compared to NSABP B-39/RTOG 0413. They note that this had a pronounced effect in patient inclusion as in the NSABP B-39/RTOG 0413 study, 1/3 of patients had to be excluded due to the final treatment volume exceeding the prescribed limits. Other researchers have also shown its benefit; Bergon *et al.* [73] used image guided prone IMRT with a CTV to PTV expansion of 0.5 cm - a large reduction compared to typical NSABP B-39/RTOG 0413. They did indicate this techniques required per-session image guidance beyond the standard weekly orthogonal pair of MV and KV images to maintain the 0.5 cm expansion which led to longer treatment times and more demand on personnel.

There is the potential that larger GTV volumes are contoured when treating patients prone. In one study Lakosi *et al.* [88] compared target volume size in patients planned in both the supine and prone position using CT. They found a significant increase in the CTV and PTV volumes when delineated on the prone images compared to the supine. They hypothesized that this difference in delineation volume may be due to the expansion of the seroma cavity in the prone position which lead to better visualization of the tumour bed and larger contour volumes. In any case, the increased setup reproducibility and reductions in the expansions needed would likely outweigh potential increases in contour volume size, as seen in the studies mentioned above, so long as appropriate set-up imaging is performed [87].

Even with the strong evidence that prone setup could improve setup reproducibility and minimize respiratory motion, it requires additional immobilization devices and a large bore CT scanner [83]. This has most likely inhibited its wide adoption. In the context of APBI however, its value increases as it may provide a way to decrease the margins needed to account for setup error and patient motion, as well as minimizing lung and heart dose [83].

## 1.4.2 Stereotactic Radiotherapy

Technological advances in dose distribution shaping will be imperative for further tissue sparing and target conformality.

As discussed in section 1.1.3, a notable technological advancement that allowed for SABR

is a technique called VMAT. Instead of using static, fixed angles to delivery the radiation, this method delivers radiation continuously over an arc while the radiation beam intensity and shape is modulated through dose rate and multi-leaf collimators. This results in exceptionally high doses at the target location and very low doses to the surrounding normal tissue with a shorter treatment time [11]. It should be noted that an important aspect of this type of therapy is image guidance; it is imperative that the radiation is delivered accurately when high doses are delivered to a focal spot.

Only a few studies have investigated VMAT in the context of treating breast cancer - and most are relegated to feasibility or treatment planning studies comparing different EBRT delivery techniques [11]. At the time of writing, there is only one study that has reported follow up using VMAT for APBI. In a feasibility study in France [89], nine patients with early stage breast cancer were treated with VMAT in the supine position. Patients were treated in 4 Gy fractions, twice per day over 5 consecutive days. At a median follow-up of 26 months, no grade 2 or greater toxicities were observed and there was no evidence of IBTR. While this study used a typical APBI delivery scheme, the ability to create highly contoured dose distributions with steep dose gradients cannot be understated in terms of its importance for delivery of ablative doses of radiation per fraction to the target while minimizing dose to the normal tissue.

### **1.4.3 Treating neoadjuvant to surgery**

One of the simplest proposals for reducing the treatment volume is by treating before surgery. Doing so would localize the dose to a small intact breast tumour and adjacent tissue, rather than treating a large seroma volume post-surgery. In effect, this reduces the volume of normal tissue exposed to radiation. Furthermore, a reduced inter-observer variability has been found when contouring the tumour in the pre-operative setting compared to contouring the seroma [90], though a contrast agent is required in the pre-operative setting [91, 92].

Very few studies have reported long-term follow-up for patients treated with EBRT neoadjuvant to surgery. In one study [90], patients were treated with 40 Gy in 10 fractions over two

weeks before lumpectomy. At median follow-ups of 6 months and 3 years, the Good/Excellent cosmesis rating was 77% and 100%, respectively - showing a remarkable increase in cosmesis over time. This increase over time is in contrary to typical APBI studies such as in RAPID [77, 81] and provides a strong motivation for implementing APBI before surgery.

In addition to the potential margin reductions by treating before surgery, it also enables the investigation of response biomarkers. In this regime, since the tumour and surrounding tissue are intact after the radiation, it is possible to investigate ways to assess treatment response non-invasively in both the tumour and surrounding tissue [15]. Doing so could provide ways to verify delivery of the radiation, as well as allow adaptation of our treatment to the patient, providing highly patient-centric care. It also allows for investigating the general radio-biological effects of high dose radiotherapy, a topic not well studied in humans. Particularly in breast, this has been seldom explored due to the removal of the tumour and surrounding tissue (which forms the surgical bed) before radiotherapy.

## 1.5 The SIGNAL trial

The London Regional Cancer Program is conducting a phase I/II clinical trial called stereotactic image guided neoadjuvant ablation then lumpectomy (SIGNAL) to assess the safety and efficacy of using neoadjuvant stereotactic body radiotherapy for treating low-risk early stage breast cancer patients [93]. The trial has undergone two iterations which will be referred to as SIGNAL 1.0 and SIGNAL 2.0. Inclusion and exclusion criteria and presented in appendix A. Figure 1.3 shows the workflow for patients that are enrolled in SIGNAL. At the time of tumour core biopsy, a metallic surgical clip (HydroMARK<sup>®</sup>, Biopsy Science, Clearwater, FL) is placed adjacent to, or within the tumour. Patients then undergo imaging on a hybrid positron emission tomography (PET)/magnetic resonance imaging (MRI) which includes a dynamic contrast enhanced (DCE)-MRI that will be used in conjunction with the radiation treatment planning CT simulation to help target volume delineation. For SIGNAL 1.0, all patients were treated with

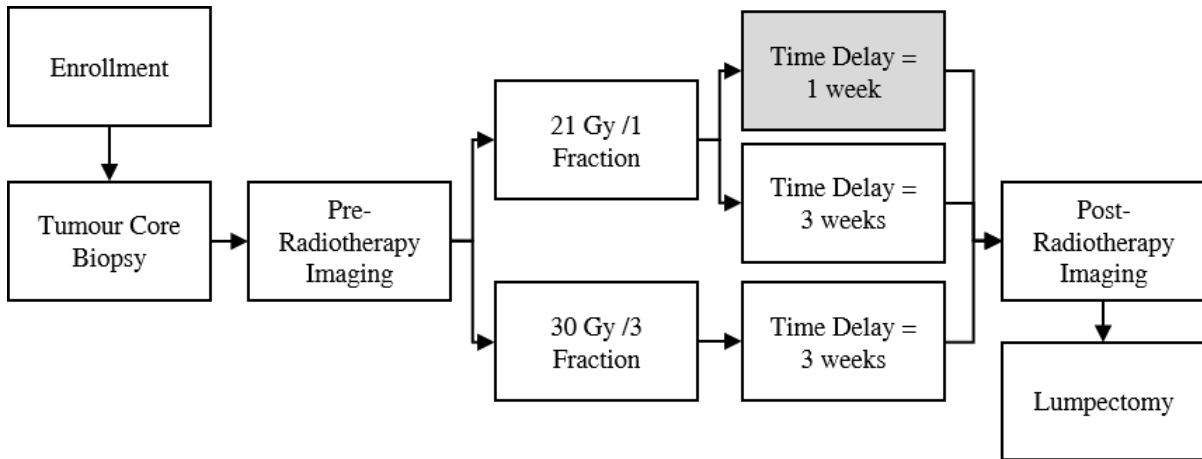


**Figure 1.3:** Schematic diagram showing the general process for a patient enrolled in the SIGNAL trial. At the time of the tumour core biopsy, a metallic surgical clip was placed adjacent to or within the tumour (HydroMARK<sup>®</sup>, Biopsy Science, Clearwater, FL). For SIGNAL 1.0, all patients were treated with 21 Gy/1 fraction and imaged at 1 week post-SABR (gray box). However for SIGNAL 2.0, patients were randomized to either 21 Gy / 1 fraction or 30 Gy / 3 fractions every other day following the pre-radiotherapy imaging. The post-radiotherapy imaging session was performed as close to the surgery as logistically possible which, again, was initially one week post-radiotherapy for SIGNAL 1.0 but was moved to three weeks for SIGNAL 2.0. Finally, all patients received a lumpectomy.

21 Gy in 1 treatment fraction (21 Gy / 1) with the purpose of determining the feasibility of SABR for early stage breast cancer patients. However, following the success of this cohort of patients ([93] and appendix F), SIGNAL was modified such that patients were randomized to receive either 21 Gy / 1 or 30 Gy / 3. This was related to recent findings that fractionated SABR may lead to immune priming effects that increase tumour cell killing [94, 95].

The doses used in this study are approximately equivalent to the standard whole breast prescription dose. The 30 Gy / 3 dose scheme has the same BED as 50 Gy / 25 assuming an  $\alpha/\beta$  of 10. However, the 21 / 1 fraction dose has a slightly higher BED compared to the traditional scheme as it has been adjusted for the fact that the linear quadratic model potentially overestimates cell killing at high single fraction doses [15] (see section 1.1.2). This dose was selected based on previous studies that showed little to no recurrence and generally low toxicity and cosmesis [60, 96, 97].

The primary endpoints of SIGNAL are normal tissue toxicities and cosmesis outcomes.

However, as previously mentioned, treating neoadjuvantly enables monitoring of treatment response using non-invasive imaging. As such, following treatment, patients are imaged as close to the lumpectomy as logistically possible - again using a 3T hybrid PET/MRI which included another DCE-MRI acquisition. The pre- and post-SABR DCE-MRI acquisitions will allow for interrogation of radio-biological effects to the SABR alone based on changes in the vasculature and fibrosis.

## **1.6 Image Assessment of Treatment Response**

### **1.6.1 Overview**

Imaging has become a ubiquitous tool for researchers to assess in-vivo anatomical and physiological measures. The earliest standardized methodologies to assess treatment response was the World Health Organization (WHO) and response evaluation criteria in solid tumors (RECIST) which were originally developed to assess tumour response to cytotoxic chemotherapeutic drugs. These measures are solely based on the anatomical size changes of the tumour or tumours. While these provide a common framework for evaluating response, weaknesses have been identified. Particularly, it has been shown that tumour size does not always change immediately in response to a therapy and that other physiological effects can lead to false assessment of progression [98,99]. For example, fibrosis development post-SABR can lead to an effect called pseudo-progression, where size estimates indicate progression when in fact, the effect observed is due to benign injury due to the radiation. In the case of lung cancer, SABR treatment can lead to the development of pneumonitis and fibrosis which presents as increased CT density and the appearance of a growing tumour [100, 101]. It became evident that methods of assessing the underlying functional and metabolic changes could prove more valuable for assessing response, particularly if assessment is desired at early timepoints in the patient's course of treatment.

Several methodologies have been developed that allow for the non-invasive assessment

of treatment response using metabolic and functional information such as glucose metabolism (using tracers that mimic glucose and PET), markers of cellular proliferation (using tracers such as fluorothymidine (FLT) and PET), and physiological properties such as blood flow, vessel permeability, and vessel density [98]. Concerning the latter three, in the context of cancer, image-based measures that provide information related to the vasculature are important as angiogenesis plays a significant role in both the growth and control of the tumour [98].

## 1.6.2 Vascular Response to Radiotherapy

It has been generally thought that the primary mode of tumour control from radiotherapy is through damage to the DNA that leads to induction of apoptosis. However, there is a growing body of evidence that the microvasculature plays a key role in tumour response to high doses of radiation [102–108]. In particular, there is evidence that high doses of radiotherapy cause significant dysfunction and destruction of endothelial cells due to induction of irreversible senescence and apoptosis of these cells which leads to increased tumour cell death, potentially due to hypoxia [16, 102, 106, 108].

The time course of the vascular response to SABR presents as a dynamic process. Previous studies have established that vascular physiological changes depend on time post-therapy and are due to the influence of acute inflammatory effects [104, 106, 109]. Previous work investigating vascular changes to high doses of radiotherapy has primarily been conducted in the context of pre-clinical studies or in cancer sites other than breast.

Park *et al.* performed an in depth literature review looking into the role of radiation induced vascular damage in tumours. They investigated vascular changes in human tumours, human tumour xenografts in rodents, and mice or rat tumours [102]. The human studies were from patients that received traditional doses per fraction on the order of 2 Gy / fraction with 10-25 fractions. Patients were imaged at various time points, primarily during treatment (both early and mid treatment) with a few studies providing longer term follow up (~a few weeks to a few months post-treatment). Response assessment was performed using a variety of techniques



including DCE-MRI, DCE-CT, colour doppler ultrasound, and immunostaining. The general conclusion drawn from the analysis by Park *et al.* was that, in response to standard fractionation schemes (i.e., 2Gy/fraction), blood flow remained unchanged or slightly increased at early times during treatment but decreased towards the end of treatment. In one study that provided follow-up 4-6 weeks following treatment, there continued to be a decrease in perfusion values as measured using DCE-MRI [110]. Park *et al.* summarized these findings, stating that the cancer cell death due to radiotherapy lead to decreased demand for perfusion, rendering the microvasculature beds nonfunctional.

In regards to higher doses of radiation, Park *et al.* summarized available pre-clinical studies (mice and rat) performed over several decades. They conclude that, generally, the following responses are seen: After a single exposure of 5-10 Gy, tumour blood flow tends to initially increase and then return to pre-irradiation levels within 2-3 days. In studies that used doses of 10-15 Gy in 1 or 2 fractions, blood flow decreases shortly after the therapy and remains decreased for varying lengths of time, occasionally returning to baseline. Finally, most tumours that are exposed to 15-20 Gy in a single exposure, there are rapid decreases in blood flow (2 hours - 2 days) followed by a deterioration of the vasculature, resulting in both a decrease in the functional vasculature but also increases in vessel permeability. However, there was some variation in the response measured between studies. Park *et al.* highlight the important fact that there were varying volumes of adjacent "normal" tissues that received radiation. It is likely that the varying amount of radiation delivered to the normal tissue vasculature would influence tumour response measurements.

Several studies have categorized the response to radiation into "early" (during treatment or within a few weeks after completion) vs "late" effects (a few months to years following treatment) [102, 104–106, 109]. There is evidence to suggest that at early time points, response assessment reflects acute inflammatory effects due to the radiotherapy [104, 105]. As such, measures related to blood flow and permeability, as well as microvasculature function will have different values depending on the timepoint following the therapy. For acute effects of

radiation, Corre *et al.* [109] identify several early endothelial processes following high dose radiation ( $> 15$  Gy) that are not seen with traditional fractionation schemes. In particular, endothelial apoptosis, recruitment of inflammatory cells, and increased permeability changes are observed. Late effects include microvessel collapse, and irreversible senescence [106]. It has been stipulated by several reports of studies in the pre-clinical setting that there exists a "threshold dose" of radiation that causes endothelial cell death but this remains to be seen in clinical data [104, 106, 109, 111].

With the importance that the vasculature plays in tumour response to radiotherapy, techniques that allow for characterization of vascular physiology and changes following therapy would allow for interrogation of the radiobiology of SABR as well as provide assessment of response.

## 1.7 Dynamic Contrast Enhanced MRI

### 1.7.1 Overview

Dynamic contrast enhanced (DCE) imaging techniques allow for the non-invasive assessment of tissue vascular function related to angiogenesis and perfusion [112]. This technique provides insight into normal and tumour tissue treatment response through measurement of the changes in parameters related to blood flow, vessel permeability, and volume of the extracellular extravascular space (EES) space. DCE imaging refers to the dynamic acquisition of images over time before and after injection of a low molecular weight contrast agent. Two common imaging modalities used in conjunction with DCE techniques are CT and MRI. The focus of this thesis is on DCE-MRI as it is the most widely used in breast cancer assessment due to its superior soft tissue contrast over CT.

In the case of DCE-MRI, the contrast agent contains a paramagnetic ion that causes longitudinal relaxation time ( $T_1$ ) (and  $T_2$ ) shortening resulting in hyper-intense signal for  $T_1$ -weighted images in areas of contrast agent accumulation. The changes in the  $T_1$  relaxation rate ( $1/T_1$ )

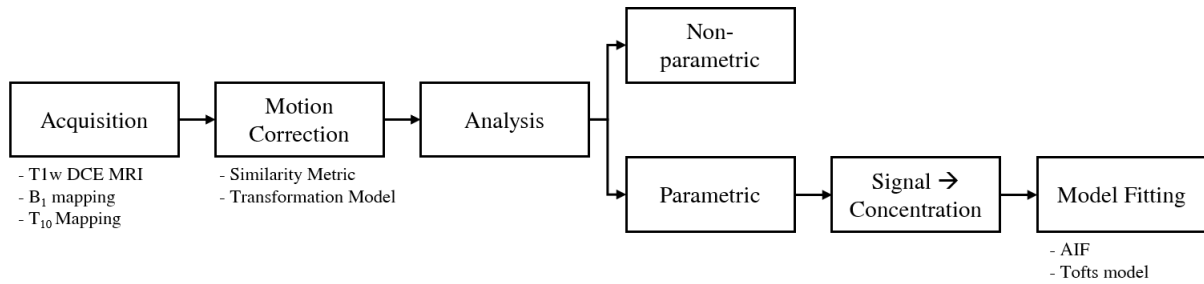


**Figure 1.4:** General schematic overview of the acquisition and analysis of DCE-MRI.  $T_{1w} = T_1$  weighted, AIF = arterial input function.

are proportional to the contrast agent concentration in the tissue [113]. From the time-resolved images, non-parametric (model free) or parametric (model-based) analyses can be used to derive parameters related to vascular function of the tissue of interest. This is particularly useful in the context of oncology since cancerous tissue has poorly developed vasculature with high vessel density and high permeability [114].

In the sections below I will first discuss potential health effects of MRI contrast agents. This will be followed by individual sections describing the components involved in the acquisition and analysis of DCE MRI. Figure 1.4 shows an overview of these DCE-MRI acquisition and analysis components. Finally, I will summarize currently available literature which reports the application of DCE-MRI for response assessment to SABR techniques at an early time-point post-therapy.

## 1.7.2 DCE-MRI Contrast Agents

The most common contrast agents for DCE-MRI are chelates of gadolinium with a low molecular weight ligand (~500 Daltons) [115]. The gadolinium ion is paramagnetic, and hence, uptake of contrast agent leads to reduced  $T_1$  relaxation times and increased signal intensity on  $T_1$  weighted imaging in tissue regions where this uptake occurs due to dipole-dipole interactions between the bound Gadolinium and water molecules. Free gadolinium is toxic as it interferes with calcium channels and directly competes with biological processes that require calcium ions due to its similar size [116, 117]. In addition, free gadolinium accumulates in the liver,

spleen, kidney, and bones. In mice the lethal dose that kills 50% of a test population ( $LD_{50}$ ) for free gadolinium is 0.2 mmol/kg [117]. The chelated form of the contrast agent experiences minimal interactions with the organism and leads to vastly reduced toxic side effects compared to free gadolinium [116, 117]. The ligand can be categorized as either linear or macrocyclic. In the case of macrocyclic contrast agents, the ligand forms a rigid cage around the gadolinium ion, whereas, the linear form is more flexible and does not fully enclose the gadolinium ion. Generally, the macrocyclic agents are more thermodynamically stable.

The first contrast enhanced MRI was acquired in 1983 [113] and since then, more than 300 million doses have been used worldwide with 30 million doses used each year [118]. These agents were initially considered exceptionally safe with the belief that essentially all of the contrast agent was excreted by the kidneys [113]. However, in 2006 (23 years later), two independent reports demonstrated a causative link between a degenerative disease called nephrogenic systemic fibrosis (NSF) and contrast exposure in patients with poor renal function [119, 120]. Since then, renal function screening is generally performed prior to contrast injection to prevent patients with poor kidney function from undergoing contrast enhanced MRI. This has led to the incidence of NSF being effectively eliminated [113, 121]. In patients with sufficient renal function, contrast agents were still considered to be fully excreted.

In 2014 and 2016, two studies (one in-vivo and the other post-mortem) reported long-term gadolinium retention in brain and bone for patients who had healthy renal function and were exposed to at least one contrast-enhanced MRI over their lifetime [121, 122]. In addition, there was a clear dose response relationship observed between the level of gadolinium in tissue and the total contrast agent exposure over their lifetime (dose from all MRI scans). Studies continue to investigate in what form (free ion or intact chelated) the gadolinium is retained with some studies indicating that de-chelation may be occurring, at least for the linear agents [123]. In addition, it is unclear if this retention has any associated pathologies. While no studies thus far have reported causative links between pathological side effects and gadolinium deposition, patient advocacy groups have taken an active role in providing public communications regarding

what they believe to be potential acute and long term side-effects of gadolinium retention from contrast agent exposure [124]. Some researchers have proposed including gadolinium retention from contrast agent exposure to a broad class of gadolinium associated disorders [124].

### **1.7.3 Contrast Agent Dose in SIGNAL**

Based on the findings of gadolinium retention following DCE-MRI, post-SABR imaging within the SIGNAL trial was temporarily halted. However, after some delay, we proposed using half the clinical dose of contrast agent for patients that were to receive both a pre- and post-SABR imaging session. In reviewing the literature, it seemed that the dose of contrast agent now considered as the clinical standard dose (0.1 mmol/kg) may have been initially justified from a study of high risk multiple metastatic brain cancer patients imaged at a field strength of 0.25-0.5 T. In this study it was observed that contrast agent doses below 0.1 mmol/kg led to clinically unacceptable tumour visualization [125]. Given that our study is performed at a much higher field strength and in early stage breast cancer (rather than metastatic brain cancer), we felt that a dose as high as 0.1 mmol/kg might not be required. Furthermore, we noticed that in the patient data that we had already acquired (pre-SABR only) that tumour visualization appeared to be sufficient for images that were not fully enhanced (i.e., earlier or later than the occurrence of the maximal enhancement). After implementation of this lower dose level (0.05 mmol/kg), the radiation oncologists involved in the SIGNAL study were satisfied that tumours were still well visualized on the pre-SABR images. This provided a unique opportunity to quantitatively assess the effect of reducing the dose on target volume delineation by comparing tumour delineation from patients that received this half dose with those that had received the full standard dose. This is the subject of chapter 2.

### **1.7.4 Image Acquisition**

This section will outline the acquisition techniques and considerations for  $T_1$ -weighted DCE-MRI.

### **Dynamic Contrast Enhanced MRI acquisition**

Spatial and time resolution are important imaging parameters that affect the quality of analysis as well as the specificity of information related to the extent of angiogenesis and tissue perfusion characteristics that can be extracted from the dynamic signal intensity curves. On the one hand, the time resolution of an image acquisition dictates the fastest hemodynamic process that can be measured. For example, for plasma flow to be measured, it is recommended that the time resolution be on the order of a few seconds or less [126]. On the other hand, spatial resolution is important for minimizing partial volume effects in assessing contrast agent enhancement of the tumour. A clear example of how spatial and time resolution play conflicting roles is in measurement of the arterial input function (AIF) - a patient specific (or often population averaged) characterization of the contrast agent concentration versus time in the plasma (ideally within an artery feeding the tumour). This curve is necessary for parametric-type analyses (see section 1.7.6). For accurate measurement of the AIF, high temporal resolution on the order of 3 seconds is necessary [127]. In opposition to this, high spatial resolution is required to minimize partial volume effects which could potentially corrupt the measurement of this AIF curve. The highest time and spatial resolution possible for an acquisition also depends on required tissue volume of tissue coverage. For breast imaging large coverage is often required unless the precise location of the lesions is known prior to imaging, which is often not the case. Thus, the typical time resolution in most breast DCE-MRI studies to date have been on the order of 60 seconds per image with a spatial resolution on the order of 1mm and complete breast coverage [112]. Even with a spatial resolution on the order of 2mm it is difficult to achieve temporal resolution below 20s with full breast coverage, making it impractical to measure the AIF with clinically used sequences and breast coils.

The most common sequences used in DCE-MRI are those based on the Three-Dimensional (3D)-Spoiled-Gradient Recalled Echo (SPGRE). This is a steady state  $T_1$ -weighted sequence that provides relatively fast acquisition of 3D volumes. Essentially, the longitudinal magnetization is subjected to repeated radiofrequency (RF) pulses at uniform time intervals (repetition

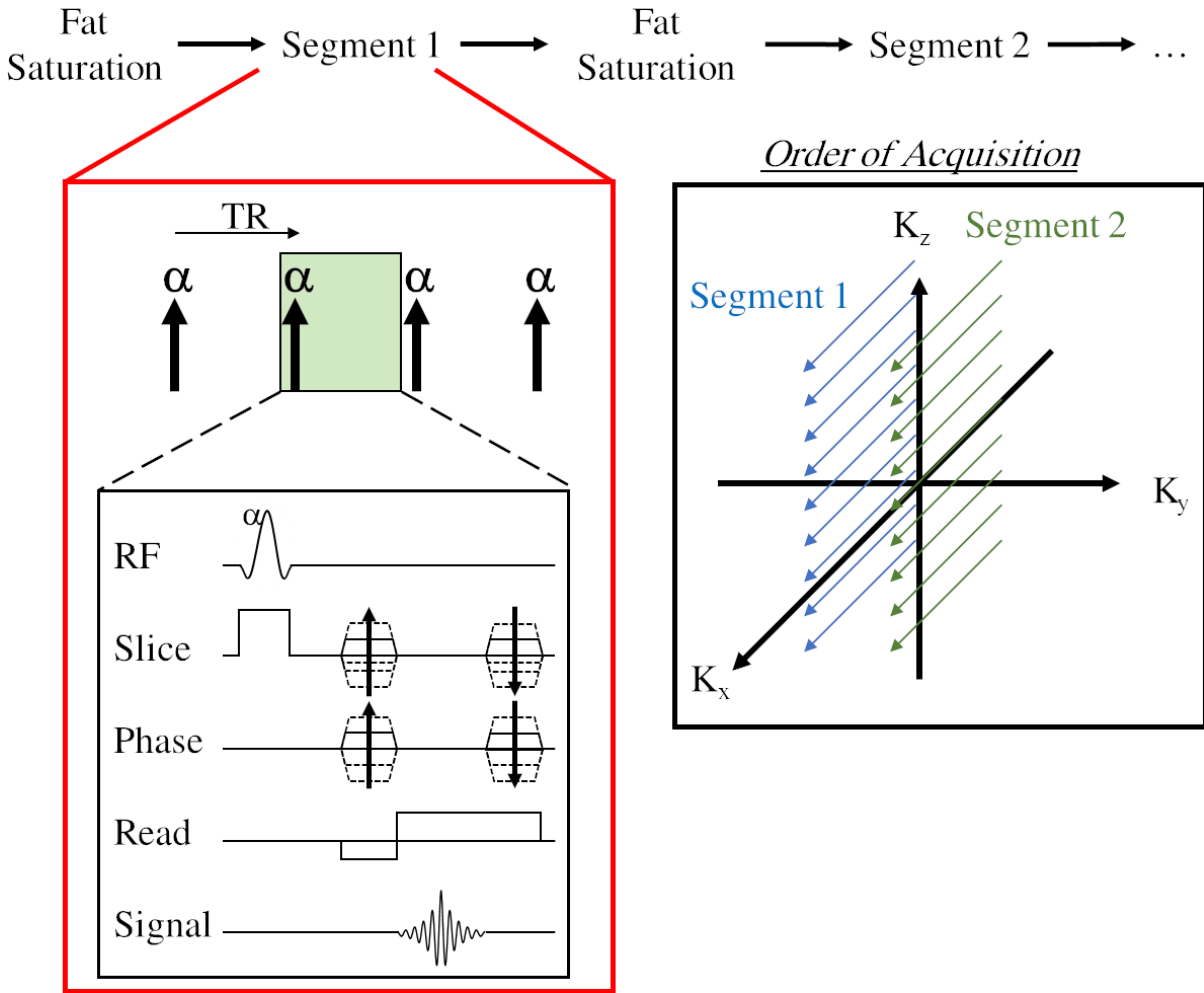


**Figure 1.5:** Schematic representation of the SPGRE sequence combined with fat suppression. Frequency selective fat saturation RF pulses are applied which selectively suppresses magnetization of the lipid signal. This is followed by the acquisition of a  $k_x$  by  $k_z$  plane. The inset outlined in red shows the gradients and signal following each RF pulse. A slab selective RF pulse is applied followed by activation of slice and phase gradients. The echo signal is recorded and is followed by an extended read gradient as well rewinding gradients which are required as part of the RF spoiling technique. Following acquisition of each segment, fat saturation is then re-applied before the next segment is acquired. The "order of acquisition" inset shows the order that segments of k-space are acquired.

time (TR)). Signals are measured via gradient echoes at echo time  $T_E$ . The repeated application of RF pulses results in a steady state longitudinal magnetization ( $M_z$ ) which is a balance between suppression of  $M_z$  from the RF pulses and regrowth due to  $T_1$  relaxation.  $T_1$  weighting is achieved by destruction or "spoiling" of the transverse magnetization before the next RF pulse. The equation that describes the steady state signal intensity is:

$$S = kM_0 \sin \alpha \frac{1 - \exp(-T_R/T_1)}{1 - \cos \alpha \exp(-T_R/T_1)} \exp(-T_E/T_2^*) \quad (1.4)$$

where  $S$  is the signal intensity,  $k$  is a proportionality coefficient related to scanner hardware/adjustments and patient loading,  $M_0$  is the equilibrium magnetization of the sample and related to proton density,  $\alpha$  is the flip angle,  $T_R$  is the repetition time,  $T_1$  is the tissue longitudinal relaxation time with the presence contrast agent,  $T_E$  is the echo time, and  $T_2^*$  is the rate of signal decay as a function of  $T_E$  for gradient recalled echo sequences. If  $T_E$  is chosen such that  $T_E \ll T_2^*$ , then the factor  $\exp(-T_E/T_2^*)$  approaches unity, allowing for this term to be effectively ignored [128].

Spatial encoding for 3D SPGR involves frequency encoding in one direction and phase encoding in the other two directions. At our institution this is performed with the Siemens VIBE sequence [129] that utilizes slab selective rf pulses for excitation. For the projects in this thesis, the frequency encoding direction is along the anterior-posterior direction to avoid respiratory and cardiac related ghosting artifacts from interfering with image signal in the breast region. The slab selective RF pulses are applied with the slab plane perpendicular to the inferior-superior direction to prevent aliasing (along this phase-encode direction).

Spoiling of the transverse magnetization for our acquisitions is accomplished using so-called RF spoiling. This includes (1) a scheme of phase increments between each RF pulse (2) an extended read gradient and (3) phase encode rewinding. Details of this method can be found elsewhere [130].

The SPGRE sequence is often accompanied by a fat suppression to increase the conspicuity of structures of interest (such as enhancing tumour tissue). One fat suppression technique is fat spectrally selective saturation which exploits the resonance frequency difference between fat and water ( $\sim 420$  Hz at 3T [131]). Essentially, a spectrally selective RF pulse tuned to the peak fat resonance frequency is applied to rotate the fat magnetization into (or close to) the transverse plane. This fat excitation is followed by spoiling of the fat transverse magnetization leading to a nulled fat magnetization immediately after the spoiling. Although the fat longitudinal



magnetization then increases with time following this fat nulling, it remains relatively small for the period over which a series of SPGRE signals are acquired, and hence, contributes minimally to those signals. Fat suppression will slightly increase image acquisition time.

Figure 1.5 shows how the fat suppression is applied with the SPGRE acquisition. In this case, a fat saturation sequence is applied before acquisition of each slice plane. Following this, a segment is acquired using the SPGRE sequence as described above. A slab selective RF pulse is applied followed by slice and phase encoding. The signal is then read followed by transverse spoiling through the use of an extended read gradient [130]. Finally, slice and phase rewinding gradients are applied. This is repeated until a full  $k_x$  by  $k_z$  plane is acquired (a full segment). This series of steps is repeated until the full slab has been sampled.

### **Native $T_1$ ( $T_{10}$ ) and $B_1$ Mapping for Signal to Concentration Conversion**

In order to convert the DCE signal to an estimate of contrast agent concentration (section 1.7.6), image based native  $T_1$  ( $T_{10}$ ) maps are required. These are needed strictly for parametric analysis. For characterizing the tissue  $T_{10}$ , the SPGRE sequence can again be used (pre-contrast injection), but in this case, with varying flip angles. From this, non-linear fitting can be applied to the flip angle versus signal intensity data which allows for estimation of  $M_0$  and  $T_{10}$  in equation 1.4.

Finally, both the conversion from signal to concentration and  $T_{10}$  mapping require knowledge of the actual flip angle. However, at higher field strengths (such as 3T), the flip angle  $\alpha$  can vary substantially with spatial position due to the spatial variation of the  $B_1$  magnetic field [112]. To provide accurate local values of the flip angle,  $B_1$  mapping can be performed. Two sequences that have been shown to be useful (and are used in this thesis) are the "actual flip angle (AFI)" and the "slice-selective pre-conditioning RF pulse (SS-PRE)" sequences. The details of these sequences can be found elsewhere [132, 133]. Images obtained with these  $B_1$

mapping sequences allow for calculation of a "B<sub>1</sub> correction factor (C)" defined as:

$$C = \frac{\alpha_{true}}{\alpha_{nominal}} \quad (1.5)$$

where  $\alpha_{true}$  is the measured flip angle and  $\alpha_{nominal}$  is the prescribed flip angle. The SPGRE steady state equation can be modified to incorporate this correction:

$$S = CkM_0 \frac{1 - \exp(-T_R/T_1)}{1 - \cos(C \alpha_{nominal}) \exp(-T_R/T_1)} \sin(C \alpha_{nominal}) \quad (1.6)$$

where the factor  $\exp(-TE/T_2^*)$  in equation 1.6 has been omitted by assuming  $T_E \ll T_2^*$ .

### 1.7.5 Intra-Session Image Registration

An important step in the analysis of DCE-MRI is correcting for intra-session patient movement. It has been shown that patient movement between images in the DCE-MRI data can severely corrupt the signal enhancement curves.

Pairwise image registration is a commonly used method to correct for movement between a "fixed" (or reference) and moving image [134]. The moving image is iteratively transformed until it "matches" the reference image. Between each transform iteration, the degree of "sameness" is assessed through the evaluation of a similarity metric, which is a function that characterizes the degree of similarity between two images. This iterative process is continued until there is there is a sufficient similarity between the two images. There are two important aspects of interest for this thesis: 1) the specific similarity metric used and 2) the type of transformation used.

#### Similarity Metric

The similarity metric quantifies the relationship between the fixed and moving images. It is optimized over the course of iterative transformations in order to obtain the closest spatial correspondence of the two images. Typical metrics are based on the extent to which the image

intensity profiles of the two images match. As an example, a simple intensity-based similarity metric that has been employed previously is the sum of squared differences between corresponding voxel intensities.

The application of signal intensity based metrics for registration involves the assumption that any differences between the two images is due to movement alone [134]. In the context of DCE-MRI, this assumption is violated as uptake of contrast agents causes local changes in intensity. Some researchers have investigated alternative ways that account for these local intensity changes, either introducing new similarity metrics [135], adding a tolerance to local variations in intensity in currently used registration algorithms [136], or through "de-enhancement" of the post-contrast images to remove the contrast enhancement before image registration [137]. However, implementation of these different strategies can be difficult and time-consuming, requiring a high degree of expertise. Several studies have shown that a metric known as mutual information is relatively robust to these local differences [136, 138, 139]. Mutual information is a measure of the statistical dependency of the of two sets of images. While its use was originally designed for multi-modal registration, it is also commonly used in the context of DCE-MRI [136, 138, 140–142]. To understand this metric, we begin with a brief introduction to information entropy.

Information entropy was developed by Shanon [143] in 1940s which is based on the definition of information created by Hartley [144]. Essentially, Hartley proposed that the information  $I$  associated with an event that has a probability  $p$  of occurring is:

$$I \equiv \log_2 \left( \frac{1}{p} \right) = -\log_2(p) \quad (1.7)$$

which has units of "bits." Intuitively this can be understood as follows: As the probability of an event occurs becomes closer to 0, more information is "gained" knowing that the event occurred. A simple example of this involves analyzing an unfair versus fair coin. In the case of the unfair coin that always turns heads, the probability of that event occurring is equal to

1 and, thus, the amount of information gained from knowing the next coin flip is equal to 0. So in conveying the next coin flip result, it would require 0 bits according to equation 1.7 - we already know the result. However, imagine we have a fair coin, knowing the result of the next coin flip would reveal information. In essence, this would require 1 bit of information to convey according to Hartley's definition of information.

Shanon information entropy is an extension of Hartley's definition of information as described in the preceding paragraph. Essentially, it is a quantification of the bits needed to convey the *expected* information from a set of possible events with probabilities of  $p$ . More formally, if an event  $i$  occurs with a probability  $p_i$  from a set of  $N$  events, the average or expected information is given by:

$$H(p_i) = - \sum_{i=1}^N p_i \log_2(p_i) \quad (1.8)$$

Whereas Equation 1.7 represents the *minimum* number of bits needed to transmit the result of some event, equation 1.8 is the average bits needed to convey the results from a set of events that can occur with different number of bits needed for each event. Another interpretation is that the entropy is the expected uncertainty associated with a set of events.

Mutual information is a further extension of entropy. In essence, it quantifies how much the uncertainty of a variable is decreased knowing information about some other variable. In other words, it is a statistical measure of the shared information between two variables. For two variables  $X$  and  $Y$ , it is defined as follows:

$$MI(X; Y) = \sum_{xy} -p_{X|Y}(x, y)(\log p_X(x) + \log p_Y(y) - \log p_{X|Y}(x, y)) \quad (1.9)$$

$$MI(X; Y) = \sum_{xy} p_{X|Y}(x, y) \log \frac{p_{X|Y}(x, y)}{p_X(x)p_Y(y)} \quad (1.10)$$

where  $p_{XY}$  is the joint probability of events  $X$  and  $Y$  occurring. As stated previously, this metric has been used extensively in DCE-MRI. In essence, by maximization of the mutual informa-

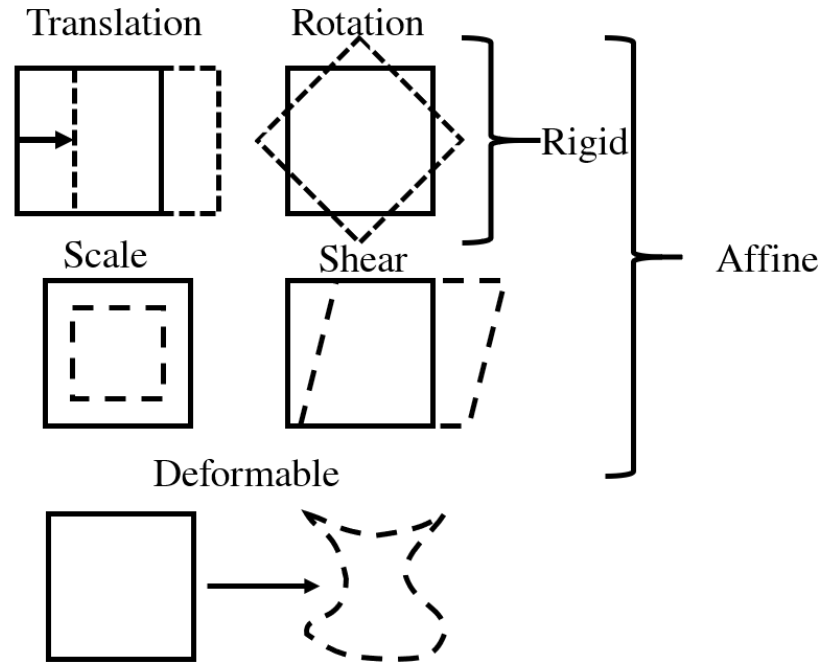


**Figure 1.6:** Visual demonstration of the differences between a rigid, affine, and deformable registration.

tion, we find the greatest similarity between the intensities for a given spatial transformation of the moving image. Since it does not rely on the spatial intensity differences between two images, it is robust in the presence of different intensity profiles.

### Transformation Model

Another important consideration for image registration involves the type of transformation used to deform the moving image onto the fixed image. Figure 1.6 shows the different transformations with increasing degrees of complexity. Rigid transformations are those that simply translate and/or rotate the moving image onto the fixed image (3-6 degrees of freedom). Affine transformations allow for translations and rotations but also scaling and "shearing" (12 degrees of freedom). Rigid and affine transformations are considered "global" registrations i.e., they act on the image as a whole. Finally, a more complex transformation that allows for complex movement characterization is deformable transformations. This type of transformation is considered a "local" transformation, capable of deforming different sections of the image

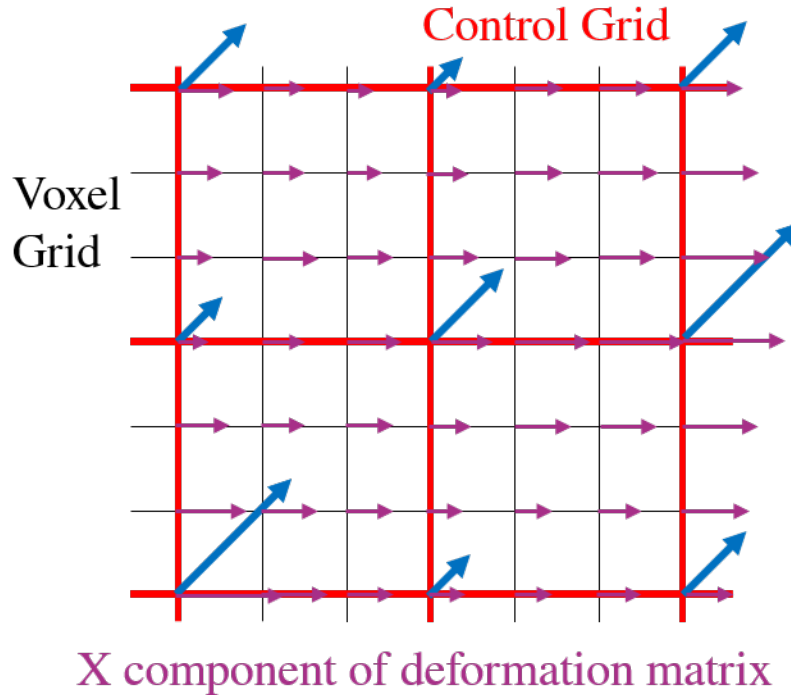


**Figure 1.7:** Simplified example of the free-form deformation transformation. Arrows represent displacement vectors with the length of the arrow representing larger displacements. The control grid (red) is superimposed on the voxel grid (black). Control points are at the intersections of the control grid. A control point is displaced as part of the registration (blue arrows). The vector for the voxels that are enclosed in a section of the control grid are generated using a BSpline interpolation scheme (purple arrows show the x-component of the interpolated deformation field from the control point displacements; y-component not shown). Finally, the deformation field is applied to the moving image to transform it.

independently. In the context of the breast image registration, deformable registration has been shown to be the most appropriate due to the deformable nature of the breast tissue [145].

The goal of deformable registration is the creation of a positional mapping function that relates the spatial position of the image voxels in the moving image to those in the fixed image. This mapping is referred to as the deformation field. The deformation field contains a vector describing the positional displacement of voxels. A particular characteristic of the deformation field is that the direction and magnitude of the deformation should be "smooth" across the image space without significant compressions or expansions [134].

One of the most commonly used algorithms for generating a deformation field is based

on the work of Rueckert *et al.* [146]. Their group devised a "free-form" deformation model whereby a set of control points are superimposed on the voxel grid at regular intervals. Figure 1.7 illustrates the deformation field for a simple hypothetical example of a free-form deformation (FFD). The control points are located at the intersection of the control grid in Figure 1.7. The displacement of these control points is interpolated onto the voxel grid which defines the deformation matrix that maps the moving image space into the fixed image space. The interpolation is performed using a cubic BSpline interpolation of the control point displacement vectors. Cubic BSplines have two particular strengths: 1) they are continuous at their junctions and generally create smoothly varying fields, 2) they are locally controlled i.e., changing one control point only affects the transformation in the local neighbourhood of that point [147, 148]. Finally, by using control points instead of the voxel grid, the dimensionality is greatly reduced which allows for faster optimization [147, 148].

In essence, the FFD process can be summarized as follows: each of the control points is moved independently leading to the generation of a voxel-by-voxel deformation field (through interpolation). The deformation field is applied to the moving image resulting in a transformed image which is then compared to the reference image using the similarity metric. This process of moving control points, generation of the deformation field, transformation of the moving image, and comparison is repeated until a convergence threshold of the similarity metric is reached.

Several authors have investigated the effect of registration on DCE-MRI by generating a "ground truth" data set through application of known deformation fields or finite element deformations (based on biomechanical models) to an image to create a simulated fixed and moving image pair. Deformable image registration is then applied to this pair. The resulting deformation field can then directly be compared to the ground truth deformation on a voxel by voxel basis to determine absolute positional deviation [135, 136, 140, 145].

Very few authors have investigated the impact of registration in the context of kinetic model application to DCE-MRI [135, 149]. To our knowledge, only one study [149] has investigated

the impact of contemporary image registration techniques on Tofts model analysis of breast DCE-MRI (see section 1.7.6). They investigated the impact of transformation model (rigid or 2D deformable registration based on FFD), similarity metric (sum of squares, Pearson correlation, or mutual information), and choice of fixed volume (i.e., pre-contrast or a post-contrast image) on the registration of breast DCE-MRI using the model goodness of fit root-mean-square-error (RMSE). They found that a deformable registration based on cubic BSpline interpolation using mutual information as the similarity metric resulted in the best performance. However, there were several limitations to their study. They performed their kinetic analysis on the average signals from regions-of-interest rather than voxel-by-voxel, which neglects the effect of registration on the assessment of tumour spatial heterogeneity. They performed a 2D registration localized to the tumour, neglecting displacements along a third dimension. Finally, they did not report the effect that registration may have on model fit parameter estimations and uncertainties (precision). Chapter 3 investigates the impact of 3D deformable registration on the Tofts model parameter estimation, uncertainty in those parameters, and validity of parameter estimates.

## 1.7.6 Analysis

### Non-parametric analysis of DCE-MRI

Non-parametric or model-free analysis of DCE-MRI involves creating quantitative measures that describe the time-signal intensity curve. In early reports, this took the form of simple classification of the "shape" of the time-intensity curves by an expert observer [150]. Other more quantitative parameters were also explored to try and remove the subjective component of this analysis [112]. A fairly exhaustive list of non-parametric parameters can be found in the review paper written by Khalifa *et al.* [151].

The strength of these non-parametric quantities is that they are straightforward to apply. Certain non-parametric parameters, such as the initial area under the curve to time point  $t$



(IAUC<sub>t</sub>) have also shown to correlate to more physiologically relevant model based parameters [112]. Several parameters have shown to be clinically valuable for breast cancer disease classification and diagnosis and these have been incorporated into Breast Imaging-Reporting and Data System (BI-RADS) [152]. However, these non-parametric quantities do not provide direct quantification of information related to underlying physiology [151, 152].

### Parametric analysis of DCE-MRI

Parametric analysis involves application of a model to the DCE-MRI data. Several models of different complexity exist that allow for quantification of parameters related to the underlying vasculature [153]. In the context of breast DCE-MRI, the most commonly used model is the Tofts model due to the typically poor temporal resolution that precludes the use of complex models [112, 153]. In the following sections, the process of applying the Tofts model is described from acquisition to application of the model.

### MRI Signal to Concentration

For DCE-MRI in breast,  $T_1$ -weighted sequences are typically used to acquire the dynamic series. As the contrast agent enters the tissue of interest, the  $T_1$  value of that tissue decreases in proportion to the concentration of contrast:

$$\frac{1}{T_1} = rC(t) + \frac{1}{T_{10}} \quad (1.11)$$

$$C(t) = \frac{\frac{1}{T_1} - \frac{1}{T_{10}}}{r} \quad (1.12)$$

where  $T_1$  is the tissue longitudinal relaxation time after contrast injection,  $T_{10}$  is the tissue longitudinal relaxation rate before contrast injection, and  $r$  is the longitudinal relaxivity at the particular field strength (Litres mmol<sup>-1</sup> s<sup>-1</sup>). The relaxivity is dependent on both the magnetic field strength and the contrast agent used. Studies exist which have measured these values [154].

In essence, there is an assumed linearity between the concentration of contrast agent and the reduction in  $T_1$  observed. From equation 1.12, we need the following to convert our signal to concentration: 1) the equation that describes how signal is related to  $T_1$ , 2) the "native" or pre-contrast  $T_1$  ( $T_{10}$ ), and 3) the relaxivity which depends on the contrast agent used and the MRI field strength. Acquisition of  $B_1$  and  $T_{10}$  values has been discussed in section 1.7.4. To determine an equation for converting the signal observed in the dynamic series to  $T_1$ , we start with an expression for the signal enhancement, which is the ratio of the enhanced to unenhanced signal and is given by:

$$\frac{S(t)}{S_0} = S_E = \frac{1 - \exp(-T_R/T_1)}{1 - \cos(C\alpha) \exp(-T_R/T_1)} \left( \frac{1 - \cos(C\alpha) \exp(-T_R/T_{10})}{1 - \exp(-T_R/T_{10})} \right) \quad (1.13)$$

If we set the second fractional term in brackets to " $K$ " and perform some additional algebra, equation 1.13 becomes:

$$\frac{1}{T_1} = -\frac{1}{T_R} \ln\left(\frac{S_E - K}{S_E \cos(C\alpha) - K}\right) \quad (1.14)$$

### The Tofts Model

With the motion corrected concentration versus time data for each voxel, it is now possible to apply a kinetic model to extract the parameters related to perfusion and angiogenesis. Kinetic analysis of DCE-MRI is based on well established tracer kinetic theory. There are many models derived from this analysis [151] but the most commonly used in breast is the Tofts model [112, 155]. The tissue of interest is represented by "compartments," which are defined as well-mixed, homogeneous components that form distinct volumes in which the contrast agent can distribute in to. Well-mixed specifically means that the concentration of contrast agent is the same everywhere within that compartment. Other assumptions of most models (including the Tofts model) are that the system is linear and time-invariant [151, 156]. More specific assumptions of the Tofts model are discussed below.

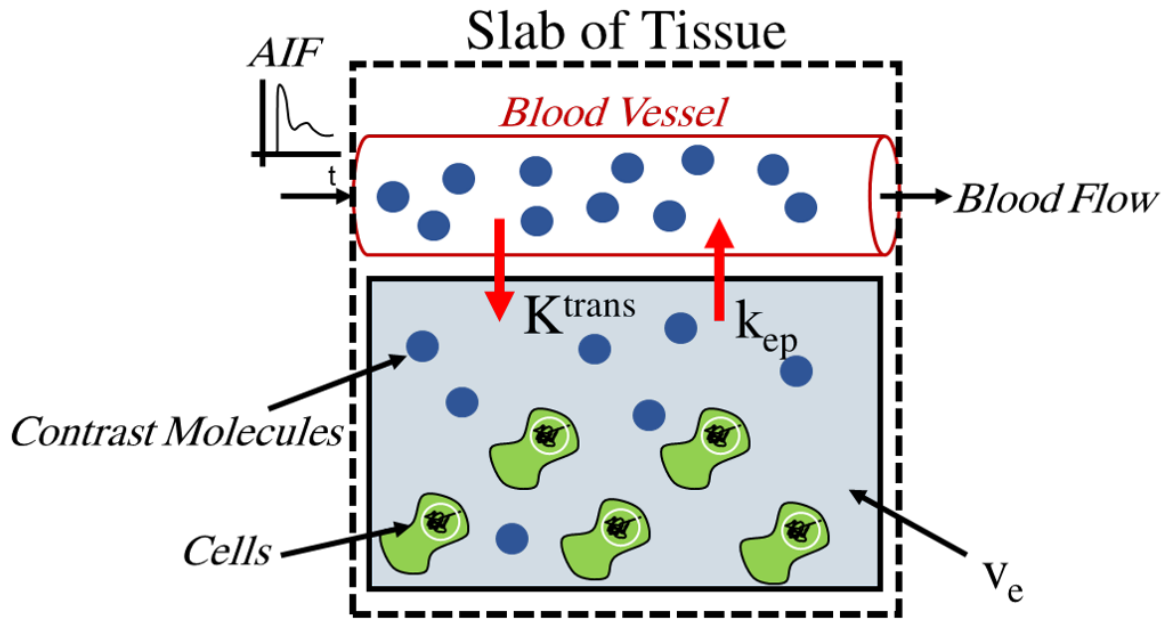


**Figure 1.8:** A schematic of the Tofts compartment model. The two compartments that comprise this model are the plasma space (represented by the blood vessel) and the extracellular-extravascular compartment (highlighted in light blue). Cells are represented by the green shapes.  $K^{trans}$ ,  $k_{ep}$ , and  $v_e$  are parameters of the Tofts model. AIF stands for arterial input function.

As depicted in Figure 1.8, the Toft model assumes two distinct compartments of the underlying tissue: the plasma space (represented by the blood vessel), and the EES (represented by the light blue rectangle but does *not* include the cells). Since the contrast agent molecules are small, leakage across the endothelium from plasma to the EES is generally assumed to be through passive diffusion. We can therefore assume that the concentration in either compartment is proportional to the difference in concentration between the two compartments [157]:

$$v_e \frac{dc_e(t)}{dt} = K^{trans} (c_p(t) - c_e(t)) \quad (1.15)$$

where  $c_e(t)$  is the concentration of contrast agent in the EES,  $v_e$  is the fractional volume of contrast agent in the EES,  $K^{trans}$  is the constant of proportionality, and  $c_p$  is the concentration in the plasma. Using the fact that the tissue concentration is  $c_t(t) = v_p c_p(t) + v_e c_e(t)$  (i.e., a combination of the plasma concentration and the EES concentration) and solving equation

1.15 for  $c_e(t)$ , the tissue concentration  $c_t$  is then given by [158]:

$$c_t(t) = v_p c_p(t) + K^{trans} \int_0^t c_p(\tau) e^{-\frac{K^{trans}(t-\tau)}{v_e}} d\tau \quad (1.16)$$

where  $v_p$  is the plasma volume and note that  $K^{trans}/v_e$  is defined as  $k_{ep}$ . Toft *et al.* [159] argued that the plasma contribution is, in some cases, sufficiently small that it can be neglected to reduce complexity of the model. In this case eqn 1.16 further reduces to:

$$c_t(t) = K^{trans} \int_0^t c_p(\tau) e^{-\frac{K^{trans}(t-\tau)}{v_e}} d\tau \quad (1.17)$$

which can also be written as the convolution (\*):

$$c_t(t) = K^{trans} c_p(t) * e^{-\frac{K^{trans}}{v_e} t} \quad (1.18)$$

where the parameters have been defined previously. Equation 1.17 is referred to as the Tofts Model and equation 1.16 is the extended Tofts model, which may provide better fits in tissues that are highly vascularized [112].

In equation 1.17, we have  $c_t(t)$  from the converted signal intensities (section 1.7.6). However, to retrieve estimates of  $K^{trans}$  and  $v_e$ , the plasma concentration versus time information,  $c_p(t)$ , is needed. This is also referred to as the AIF and describes the delivery of contrast to the tissue of interest (see Figure 1.8). For accurate quantification of  $K^{trans}$  and  $v_e$  it is generally advisable to measure this on a patient specific basis using an artery as close as possible to the tissue of interest. However, for breast imaging this is generally challenging given the required spatial resolution and field-of-view coverage required for a breast exam which precludes sufficient temporal resolution for measurement of an AIF with current clinical hardware and protocols (see section 1.7.4). In addition, if the internal mammary artery was to be used, an even greater spatial resolution would be required due to the small size of this artery, further inhibiting increases to temporal resolution. Instead, many breast DCE-MRI studies have in-

stead used a population based AIF as an approximation to individually measured AIFs. One of the most commonly used AIFs in recent years is the one generated by Parker *et al.* [160]. To determine a population averaged AIF these authors analyzed DCE-MRI data from 23 cancer patients scanned a total of 113 times. Scans were performed with high time resolution (4.97s) but limited coverage over the pelvic region. Signal from the descending aorta or iliac arteries was analyzed and fit to an empirical model to describe an average AIF. With the measured  $c_t(t)$  data and the population based AIF, non-linear fitting can be applied for extraction of parameters  $K^{\text{trans}}$  and  $v_e$  (as well as  $k_{\text{ep}}$  through the relation mentioned above). Interpretation of  $v_e$  is straightforward - it represents the fractional volume taken up by the EES within the tissue of interest. However, the interpretation of  $K^{\text{trans}}$  is less clear [161]. Strictly speaking,  $K^{\text{trans}}$  represents the forward rate of gadolinium transfer between the plasma compartment and the EES (figure 1.8). However, this rate of transfer depends on both the local blood flow, vessel permeability, and the surface area of the vessels, and so,  $K^{\text{trans}}$  is a reflection of all these parameters:

$$K^{\text{trans}} = EF_p \quad (1.19)$$

where  $E$  is the extraction fraction and  $F_p$  is the plasma flow. The extraction fraction is the proportion of tracer that leaves the plasma compartment and enters the EES in the first pass of blood through the capillary system [161]. It is related to the permeability and surface area of the capillary system (called the permeability-surface area product (PSA)) as well as the plasma flow [161]:

$$E = \frac{PSA}{PSA + F_p} \quad (1.20)$$

The interpretation of  $K^{\text{trans}}$  is characterized by three regimes of tracer exchange [159, 161]: 1) when  $PSA \ll F_p$ ,  $K^{\text{trans}}$  is directly proportional to PSA, 2) when  $PSA \gg F_p$  then  $K^{\text{trans}}$  is directly proportional to blood flow and, 3) when neither dominates then  $K^{\text{trans}}$  reflects a mixed combination of blood flow and PSA [115, 159, 161].

The Tofts model can be applied either to the average signal from a region-of-interest (ROI)

or on a voxel-by-voxel basis. ROI analysis minimizes noise as the average signal intensity is taken over a set of voxels, which can potentially improve model fitting. However, ROI fitting disallows assessment of tumour heterogeneity. It may also bias the result in that the measured value may not reflect the spatial mean across the tumour [157].

### 1.7.7 DCE-MRI Response Assessment to SABR

Response assessment using DCE-MRI has been previously investigated in the context of neoadjuvant chemotherapy and traditional schemes of radiation treatment in breast cancer [112]. There have been very few studies that investigate DCE-MRI for assessment of response to SABR at early time points post-treatment.

To our knowledge, there is only one study that has investigated response of breast cancer to SABR [165]. Wang *et al.* conducted a prospective study treating early stage breast cancer patients with either 15, 18, or 21 Gy in a single fraction and imaged patients prior to and one week following treatment. DCE-MRI images were acquired with a time resolution of one minute over 6 minutes post-contrast injection. They analyzed their data by averaging enhancement signals over regions of interest corresponding to three clinical volumes, the GTV, CTV, and PTV. They reported the initial area under the curve up to 6 minutes (non-parametric measure),  $K^{\text{trans}}$ , and  $v_e$ , though,  $K^{\text{trans}}$  and  $v_e$  were not reported for the GTV. They found no significant pre- to post-SABR changes in  $K^{\text{trans}}$  for either the CTV or PTV. However, they observed significant increases in the initial area under the curve in the CTV and PTV. Finally, they found significant increases in  $v_e$  for the CTV and PTV. They also performed a correlation analysis to determine if the change in parameters from pre- to post-SABR were related to the dose received in a single fraction. No significant correlations were found for DCE parameters except for the PTV value of  $K^{\text{trans}}$ , though from observing their plot, the data had considerable variability. There were several limitations to their study that are discussed in chapter 4. The method of averaging over the regions of interest neglects spatial heterogeneity information and may have contributed to their finding of no significant changes as the volumes used included

**Table 1.4:** Studies that report early changes in DCE parameters including both MRI and CT modalities. The table is sorted by Image delay post radiotherapy. Note that "Day X" specifies that assessment occurred *during* treatment.

Refs	Site	Method	Sample Size	Dose (Gy)/fractions	Image Delay (days)	$\Delta$ BF and Perm	$\Delta v_e$
Janssen [162]	Rectal	DCE-CT	23	25 / 5	Day 5 <sup>a</sup>	Increase	NSC
					Day 3 <sup>a</sup>	Increase	Increase
Coolens [163]	Liver	DCE-CT	6	30-54 / 6	30	Decrease	NSC
					60	Decrease	NSC
Winter [164]	Brain Met	DCE-MRI	29	15-21 / 1	3	NSC	NSC
					20	NSC	Decrease
Wang [165]	Breast	DCE-MRI	15	15-21 / 1	7	NSC	Increase
Detsky [166]	Colorectal Liver Met	DCE-CT	10	54 total <sup>b</sup>	7	Decrease <sup>c,d</sup>	N/A
					14	Increase <sup>d</sup>	NSC
Sawyer [167]	Pulmonary Met	DCE-CT	11	26 / 1	70	Decrease <sup>d</sup>	Decrease
Huang [168]	NSCLC	DCE-MRI	19	40-50 / 4-5	42	Decreased	NSC
Spratt [169]	Sarcoma Spine Met	DCE-MRI	12	9 / 3 or 10 / 3 or 24 / 1	57	Decreased	N/A
Taunk [170]	Brain met	DCE-MRI	53	21 / 1	77	Trend to decrease (p = 0.054)	NSC
Santos [171]	Chordoma	DCE-MRI	6 / 11	24 / 1	154	Decreased <sup>d</sup>	N/A

<sup>a</sup>of the treatment regime, <sup>b</sup>fractionation was not specified, <sup>c</sup>indicates blood flow in the case that it is explicitly specified, <sup>d</sup>indicates permeability in the case that it is explicitly specified

$\Delta$  = change in, BF = blood flow, Perm = permeability, NSC = no significant change, N/A = not applicable, fx = fraction, met = metastases

a large amount of tissue. In addition, they did not report kinetic model parameter ( $K^{\text{trans}}$  or  $v_e$ ) values for the GTV. The reason provided for not presenting these values was “poor model fitting”, possibly due to low signal-to-noise ratio (SNR). Another limitation was the fact that

they used ROI averaging analysis of the CTV and PTV which includes surrounding tissue that may not respond the same way as normal tissue and confound their results. Finally, although this study applied the Tofts model, the AIF used is one that, to our knowledge, has not been not widely used in recent DCE studies. This AIF, reported in 1984 [172], does not capture the fast contrast agent concentration changes believed to occur at early times post injection.

Looking beyond breast cancer, there is only sparse data with regard to the application of DCE-MRI for response assessment at an early time point post radiotherapy. Table 1.4 summarizes studies that have investigated DCE-MRI response assessment to stereotactic radiotherapy. Concerning parameters related to blood flow and vessel permeability (represented in the Tofts model by changes in  $K^{\text{trans}}$ ), most studies show transient increases in blood flow and vessel permeability at time delays less than 3-14 days, before an eventual decrease at later time points following SABR [163, 167]. Other studies have also shown decreases in these parameters when patients were evaluated from 30-154 days (table 1.4) [163, 167, 168, 170, 171]. These decreases also correlated to pathologically complete response at later follow-up [168–170]. This literature provides an indication of the "expected" course of the parameter  $K^{\text{trans}}$  changes with time.

Reports of  $v_e$  are much more variable. Since  $v_e$  represents the fraction of a voxel that is extracellular extravascular space, vascular and cellular death would likely cause it to increase. Some studies report an increase [163, 165] while others report a decrease [164, 167] or no significant changes. A requirement for estimation of  $v_e$  is sufficient measurement of the wash-out phase. The inconsistent results may be due to variable acquisition times over which the post injection DCE signals were followed. In some cases these acquisition times may be insufficient for accurate  $v_e$  characterization, which is typically stipulated to be approximately 10 minutes [157], but may be longer if there is very slow wash-out.



## 1.8 Research Hypothesis

The primary hypothesis of this thesis is that response to SABR treatment for early stage breast cancer can be detected with 3T DCE-MRI using deformable registration procedures followed by parametric analysis. Furthermore, I propose that half the standard dose of contrast agent will be sufficient for this detection. The secondary hypothesis is that using a half-dose of gadolinium-based contrast agent will not affect the inter- and intra- observer variability for target volume delineation in the radiotherapy planning process.

## 1.9 Research Objectives

The work presented in this thesis is focused on three main objectives:

1. To quantitatively assess the potential of reducing the dose of gadolinium contrast agent for DCE-MRI-based radiotherapy target volume delineation. More specifically the aim was to compare using a full versus half clinical dose of contrast agent on the inter- and intra-observer variability (Chapter 2).
2. To quantitatively evaluate the impact of 3D deformable registration on voxel-by-voxel parameter values, associated uncertainties, and goodness of fit extracted from application of the Tofts model to DCE-MRI data from breast cancer patients.
3. To determine tumour and the surrounding tissue response to SABR in early stage breast cancer patients using two different SABR fractionations and two different time delays post-SABR.

## **1.10 Thesis Outline**

### **1.10.1 Reducing the dose of gadolinium-based contrast agents for DCE-MRI guided SBRT: The effects on inter and intra observer variability for preoperative target volume delineation in early stage breast cancer patients (Chapter 2)**

In chapter 2, the effect of reducing the dose of gadolinium-based contrast agent for MRI-guided target volume delineation in the radiotherapy planning process is presented. Patients included in this analysis had received either a full clinical dose of contrast or half a clinical dose. Initially, pre-SABR imaging in SIGNAL was performed with the standard contrast agent dose, but later in the study the dose was reduced for reasons explained in Section 1.7.3 above. Five radiation oncologists from the London Regional Cancer Program contoured the gross target volume for each patient twice, with a month in-between contouring sessions. Using several metrics of agreement, we found no significant decreases in the inter- or intra-observer variability when using a half-dose of contrast agent. With the increased concern regarding gadolinium safety and long-term retention, this study is likely the first in many that will look to decrease patient exposure to gadolinium contrast agents. Such studies are particularly important for clinical applications that require repeated contrast agent administrations, such as DCE-MRI acquisition for response assessment.

### **1.10.2 The effect of registration on voxel-wise Tofts model parameters and uncertainties from DCE-MRI of early stage breast cancer patients using 3DSlicer (Chapter 3)**

As mentioned in section 1.7.5, the effect of intra-session image registration on the value and precision of Tofts model fit parameters has not been quantitatively explored. Chapter 3 ad-

dresses this gap in the literature. We quantitatively investigated the influence of image registration on Tofts model-based kinetic analysis of dynamic contrast enhanced MRI of early stage breast cancer patients. Signal enhancement curves were analyzed voxel-by-voxel using the Tofts kinetic model. The major findings of this study were that 3D deformable registration led to a significant reduction in the uncertainty of model fit parameters as well as a significant reduction in the number of voxels that had an unphysical value for one of the two Tofts model parameters. We also showed that registration computation time could be reduced by a factor of two without altering model fit quality using a lower percent sampling of voxels for estimation of the cost function. The results of this study demonstrate that deformable image registration likely contributes to the efficacy of kinetic voxel-by-voxel DCE-MRI analysis for detecting pre- to post-SABR response.

### **1.10.3 DCE-MRI assessment of response to neoadjuvant SABR in early stage breast cancer: Comparisons of single versus three fraction schemes and two different imaging time delays post-SABR (Chapter 4)**

The final project of this thesis involved quantitatively determining the effect of SABR dose fractionation and time delay post-neoadjuvant SABR on DCE-MRI parameters in early stage breast cancer patients. The results of this study suggest that performing breast DCE-MRI one-week post-SABR may be too early for response assessment, whereas 2.5 weeks appears sufficiently long to minimize confounding acute inflammatory effects. In addition, kinetic parameters measured 2.5 weeks post-SABR in both single fraction and 3 fraction groups were indicative of response, but only the single fraction protocol led to enhancement in tissue surrounding the tumor. We suspect that this increased contrast uptake in the surrounding tissue is likely due to a hypothesized endothelial cell death threshold that is seen at doses  $>8-12$  Gy. This work sets the stage for further study of treatment schemes for early stage breast cancer

that may be able to eliminate surgery all-together. This will be a subject of discussion in the final chapter (section 5.3).

#### **1.10.4 Conclusions and Future Work (Chapter 5)**

The final chapter of this thesis summarizes the main findings of the three projects that comprise this thesis. Important limitations are highlighted followed by a discussion of how the work presented here sets the stage for future directions in breast cancer radiotherapy treatment and imaging research.

## 1.11 Bibliography

- [1] F. Bray, J. Ferlay, I. Soerjomataram, R. L. Siegel, L. A. Torre, and A. Jemal, “Global cancer statistics 2018: GLOBOCAN estimates of incidence and mortality worldwide for 36 cancers in 185 countries.,” *CA: a cancer journal for clinicians*, vol. 68, pp. 394–424, nov 2018.
- [2] Canadian Cancer Statistics Advisory Committee, “Canadian Cancer Statistics 2018,” *Canadian Cancer Society*, 2018.
- [3] World Health Organization (WHO), “WHO | Cancer,” 2019.
- [4] H. H. Chen and M. T. Kuo, “Improving radiotherapy in cancer treatment: Promises and challenges,” *Oncotarget*, vol. 8, no. 37, pp. 62742–62758, 2017.
- [5] R. Baskar, J. Dai, N. Wenlong, R. Yeo, and K.-W. Yeoh, “Biological response of cancer cells to radiation treatment,” *Frontiers in Molecular Biosciences*, vol. 1, p. 24, 2014.
- [6] E. J. Hall and A. J. Giaccia, *Radiobiology for the Radiologist: 7th edition*. Lippincott Williams and Wilkins Publishing, 2012.
- [7] J. M. Brown, D. J. Carlson, and D. J. Brenner, “The tumor radiobiology of SRS and SBRT: Are more than the 5 Rs involved?,” feb 2014.
- [8] C. M. van Leeuwen, A. L. Oei, J. Crezee, A. Bel, N. A. P. Franken, L. J. A. Stalpers, and H. P. Kok, “The alfa and beta of tumours: a review of parameters of the linear-quadratic model, derived from clinical radiotherapy studies.,” *Radiation oncology (London, England)*, vol. 13, p. 96, may 2018.
- [9] B. Cho, “Intensity-modulated radiation therapy: a review with a physics perspective,” *Radiation Oncology Journal*, vol. 36, p. 1, mar 2018.

- [10] T. Bortfeld, "IMRT: A review and preview," *Physics in Medicine and Biology*, vol. 51, pp. R363–R379, jul 2006.
- [11] M. Teoh, C. H. Clark, K. Wood, S. Whitaker, and A. Nisbet, "Volumetric modulated arc therapy: a review of current literature and clinical use in practice," *The British Journal of Radiology*, vol. 84, pp. 967–996, 2011.
- [12] M. Guckenberger, N. Andratschke, H. Alheit, R. Holy, C. Moustakis, U. Nestle, and O. Sauer, "Definition of stereotactic body radiotherapy: Principles and practice for the treatment of stage I non-small cell lung cancer," *Strahlentherapie und Onkologie*, vol. 190, no. 1, pp. 26–33, 2014.
- [13] S. M. Bentzen and J. R. Yarnold, "Reports of Unexpected Late Side Effects of Accelerated Partial Breast Irradiation—Radiobiological Considerations," *International Journal of Radiation Oncology\*Biological\*Physics*, vol. 77, pp. 969–973, jul 2010.
- [14] C. Park, L. Papiez, S. Zhang, M. Story, and R. D. Timmerman, "Universal Survival Curve and Single Fraction Equivalent Dose: Useful Tools in Understanding Potency of Ablative Radiotherapy," *International Journal of Radiation Oncology Biology Physics*, vol. 70, pp. 847–852, mar 2008.
- [15] A. Rahimi and R. Timmerman, "New Techniques for Irradiating Early Stage Breast Cancer: Stereotactic Partial Breast Irradiation," 2017.
- [16] C. W. Song, E. Glatstein, L. B. Marks, B. Emami, J. Grimm, P. W. Sperduto, M.-S. Kim, S. Hui, K. E. Dusenbery, and L. Cho, "Biological Principles of Stereotactic Body Radiation Therapy (SBRT) and Stereotactic Radiation Surgery (SRS): Indirect Cell Death," *International Journal of Radiation Oncology\*Biological\*Physics*, pp. 1–14, 2019.
- [17] Y. Shibamoto, A. Miyakawa, S. Otsuka, and H. Iwata, "Radiobiology of hypofractionated stereotactic radiotherapy: what are the optimal fractionation schedules?," *Journal of radiation research*, vol. 57 Suppl 1, pp. i76–i82, aug 2016.

- [18] S. Becker, "A historic and scientific review of breast cancer: The next global healthcare challenge," *International Journal of Gynecology and Obstetrics*, vol. 131, pp. S36–S39, oct 2015.
- [19] S. Libson and M. Lippman, "A review of clinical aspects of breast cancer," feb 2014.
- [20] C. F. Njeh, M. W. Saunders, and C. M. Langton, "Accelerated Partial Breast Irradiation (APBI): a review of available techniques," *Radiation Oncology*, vol. 5, no. 90, pp. 1–28, 2010.
- [21] A. G. Waks and E. P. Winer, "Breast Cancer Treatment: A Review," *JAMA - Journal of the American Medical Association*, vol. 321, pp. 288–300, jan 2019.
- [22] U. Veronesi, E. Marubini, L. Mariani, V. Galimberti, A. Luini, P. Veronesi, B. Salvadori, and R. Zucali, "Radiotherapy after breast-conserving surgery in small breast carcinoma: Long-term results of a randomized trial," *Annals of Oncology*, vol. 12, pp. 997–1003, 2001.
- [23] V. Vinh-Hung and C. Verschraegen, "Breast-conserving surgery with or without radiotherapy: Pooled-analysis for risks of ipsilateral breast tumor recurrence and mortality," *Journal of the National Cancer Institute*, vol. 96, pp. 115–121, jan 2004.
- [24] B. Fisher, J. Dignam, N. Wolmark, E. Mamounas, J. Costantino, W. Poller, E. R. Fisher, D. L. Wickerham, M. Deutsch, R. Margolese, N. Dimitrov, and M. Kavanah, "Lumpectomy and radiation therapy for the treatment of intraductal breast cancer: Findings from National Surgical Adjuvant Breast and Bowel Project B- 17," *Journal of Clinical Oncology*, vol. 16, pp. 441–452, feb 1998.
- [25] M. Clarke, R. Collins, S. Darby, C. Davies, P. Elphinstone, V. Evans, J. Godwin, R. Gray, C. Hicks, S. James, E. MacKinnon, P. McGale, T. McHugh, R. Peto, C. Taylor, Y. Wang, and Early Breast Cancer Trialists' Collaborative Group (EBCTCG), "Effects of radio-

- therapy and of differences in the extent of surgery for early breast cancer on local recurrence and 15-year survival: an overview of the randomised trials.," *Lancet (London, England)*, vol. 366, pp. 2087–106, dec 2005.
- [26] B. Fisher, S. Anderson, J. Bryant, R. G. Margolese, M. Deutsch, E. R. Fisher, J.-H. Jeong, and N. Wolmark, "Twenty-Year Follow-up of a Randomized Trial Comparing Total Mastectomy, Lumpectomy, and Lumpectomy plus Irradiation for the Treatment of Invasive Breast Cancer," *New England Journal of Medicine*, vol. 347, pp. 1233–1241, oct 2002.
- [27] K. Holli, R. Saaristo, J. Isola, H. Joensuu, and M. Hakama, "Lumpectomy with or without postoperative radiotherapy for breast cancer with favourable prognostic features: results of a randomized study.," *British journal of cancer*, vol. 84, pp. 164–9, jan 2001.
- [28] D. C. Farrow, W. C. Hunt, and J. M. Samet, "Geographic variation in the treatment of localized breast cancer.," *The New England journal of medicine*, vol. 326, pp. 1097–1101, 1992.
- [29] J. Gu, G. Groot, C. Boden, A. Busch, L. Holtlander, and H. Lim, "Review of Factors Influencing Women's Choice of Mastectomy Versus Breast Conserving Therapy in Early Stage Breast Cancer: A Systematic Review," aug 2018.
- [30] M. Morrow, J. White, J. Moughan, J. Owen, T. Pajack, J. Sylvester, J. F. Wilson, and D. Winchester, "Factors predicting the use of breast-conserving therapy in stage I and II breast carcinoma.," *Journal of clinical oncology : official journal of the American Society of Clinical Oncology*, vol. 19, pp. 2254–62, apr 2001.
- [31] National Comprehensive Cancer Network, "Breast Cancer (Version 3.2018)," 2019.
- [32] K. S. Kim, K. H. Shin, N. Choi, and S.-W. Lee, "Hypofractionated whole breast irradiation: new standard in early breast cancer after breast-conserving surgery.," *Radiation oncology journal*, vol. 34, pp. 81–7, jun 2016.



- [33] F. Vicini, J. White, D. Arthur, R. Kuske, and R. Rabinovitch, “NSABP protocol B-39/RTOG protocol 0413: a randomized phase III study of conventional whole breast irradiation (WBI) versus partial breast irradiation for women with stage 0,I, or II breast cancer,” 2004.
- [34] D. E. Wazer, D. W. Arthur, and F. A. Vicini, eds., *Accelerated partial breast irradiation : techniques and clinical implementation*. Berlin, Heidelberg: Springer Berlin Heidelberg, 2009.
- [35] NIH, “Common Terminology Criteria for Adverse Events (CTCAE) | Protocol Development | CTEP,” 2017.
- [36] T. Corica, A. K. Nowak, C. M. Saunders, M. K. Bulsara, M. Taylor, N. R. Williams, M. Keshtgar, D. J. Joseph, and J. S. Vaidya, “Cosmetic outcome as rated by patients, doctors, nurses and BCCT.core software assessed over 5 years in a subset of patients in the TARGIT-A Trial,” *Radiation Oncology*, vol. 13, p. 68, dec 2018.
- [37] J. R. Harris, M. B. Levene, G. Svensson, and S. Hellman, “Analysis of cosmetic results following primary radiation therapy for stages I and II carcinoma of the breast,” *International Journal of Radiation Oncology, Biology, Physics*, vol. 5, pp. 257–261, feb 1979.
- [38] E. D. Podgorsak and International Atomic Energy Agency., *Radiation oncology physics : a handbook for teachers and students*. International Atomic Energy Agency, 2005.
- [39] N. R. Bennion, M. Baine, A. Granatowicz, and A. O. Wahl, “Accelerated partial breast radiotherapy: a review of the literature and future directions,” *Gland Surgery*, vol. 7, pp. 596–610, dec 2018.
- [40] J. White, K. Winter, R. R. Kuske, J. S. Bolton, D. W. Arthur, T. Scroggins, R. A. Rabinovitch, T. Kelly, L. M. Toonkel, F. A. Vicini, and B. McCormick, “Long-Term Can-

- cer Outcomes From Study NRG Oncology/RTOG 9517: A Phase 2 Study of Accelerated Partial Breast Irradiation With Multicatheter Brachytherapy After Lumpectomy for Early-Stage Breast Cancer.,” *International journal of radiation oncology, biology, physics*, vol. 95, no. 5, pp. 1460–1465, 2016.
- [41] T. J. Whelan, J.-P. Pignol, M. N. Levine, J. A. Julian, R. MacKenzie, S. Parpia, W. Shelley, L. Grimard, J. Bowen, H. Lukka, F. Perera, A. Fyles, K. Schneider, S. Gulavita, and C. Freeman, “Long-Term Results of Hypofractionated Radiation Therapy for Breast Cancer,” *New England Journal of Medicine*, vol. 362, pp. 513–520, feb 2010.
- [42] R. Rabinovitch, K. Winter, R. Kuske, J. Bolton, D. Arthur, T. Scroggins, F. Vicini, B. McCormick, and J. White, “RTOG 95-17, a Phase II trial to evaluate brachytherapy as the sole method of radiation therapy for Stage I and II breast carcinoma-year-5 toxicity and cosmesis,” *Brachytherapy*, vol. 13, pp. 17–22, jan 2014.
- [43] B. Johansson, L. Karlsson, G. Liljegren, L. Hardell, and J. Persliden, “Pulsed dose rate brachytherapy as the sole adjuvant radiotherapy after breast-conserving surgery of T1-T2 breast cancer: First long time results from a clinical study,” *Radiotherapy and Oncology*, vol. 90, pp. 30–35, 2009.
- [44] A. J. Stewart, A. J. Khan, and P. M. Devlin, “Partial breast irradiation: a review of techniques and indications.,” *The British journal of radiology*, vol. 83, pp. 369–78, may 2010.
- [45] J. M. Mann, A. D. Osian, A. Brandmaier, W. Yan, K.-J. Sung, B. Siegel, S. Fink, B. Kaplan, M. Fulman, G. Wu, P. Christos, D. Nori, and A. Ravi, “Excellent Long-term Breast Preservation Rate After Accelerated Partial Breast Irradiation Using a Balloon Device,” *Clinical Breast Cancer*, vol. 16, no. 3, pp. 217–222, 2016.
- [46] C. Shah, S. Badiyan, J. B. Wilkinson, F. Vicini, P. Beitsch, M. Keisch, D. Arthur, M. Lyden, C. Shah, and A. Surg, “Treatment Efficacy with Accelerated Partial Breast Irradia-

- tion (APBI): Final Analysis of the American Society of Breast Surgeons MammoSite<sup>®</sup> Breast Brachytherapy Registry Trial,” *Oncol*, vol. 20, pp. 3279–3285, 2013.
- [47] J. C. Nelson, P. D. Beitsch, F. A. Vicini, C. A. Quiet, D. Garcia, H. C. Snider, M. A. Gittleman, V. J. Zannis, P. W. Whitworth, R. E. Fine, A. J. Keleher, and H. M. Kuerer, “Four-year clinical update from the American Society of Breast Surgeons MammoSite brachytherapy trial,” *American Journal of Surgery*, vol. 198, no. 1, pp. 83–91, 2009.
- [48] J. A. Vargo, V. Verma, H. Kim, R. Kalash, D. E. Heron, R. Johnson, and S. Beriwal, “Extended (5-year) Outcomes of Accelerated Partial Breast Irradiation Using MammoSite Balloon Brachytherapy: Patterns of Failure, Patient Selection, and Dosimetric Correlates for Late Toxicity Radiation Oncology,” *Radiation Oncology Biology*, vol. 88, no. 2, pp. 285–291, 2014.
- [49] J. V. Antonucci, M. Wallace, N. S. Goldstein, L. Kestin, P. Chen, P. Benitez, N. Dekhne, A. Martinez, and F. Vicini, “Differences in Patterns of Failure in Patients Treated With Accelerated Partial Breast Irradiation Versus Whole-Breast Irradiation: A Matched-Pair Analysis With 10-Year Follow-Up,” *International Journal of Radiation Oncology Biology Physics*, vol. 74, no. 2, pp. 447–452, 2009.
- [50] V. Strnad, G. Hildebrandt, R. Potter, P. Potter, J. Hammer, M. Hindemith, A. Resch, K. Spiegl, M. Lotter, W. Uter, M. Bani, R.-D. Kortmann, M. W. Beckmann, R. Fietkau, and O. J. Ott, “Accelerated Partial Breast Irradiation: 5-Year Results of the German-Austrian Multicenter Phase II Trial Using Interstitial Multicatheter Brachytherapy Alone After Breast-Conserving Surgery,” *Radiation Oncology Biology*, vol. 80, pp. 17–24, 2011.
- [51] C. Polgár, J. Fodor, T. Major, Z. Sulyok, and M. Kásler, “Breast-conserving therapy with partial or whole breast irradiation: Ten-year results of the Budapest randomized trial,” *Radiotherapy and Oncology*, vol. 108, pp. 197–202, aug 2013.

- [52] C. Polgár, O. J. Ott, G. Hildebrandt, D. Kauer-Dorner, H. Knauerhase, T. Major, J. Lyczek, J. L. Guinot, J. Dunst, C. G. Miguelez, P. Slampa, M. Allgäuer, K. Lössl, B. Polat, G. Kovács, A.-R. Fishedick, R. Fietkau, A. Resch, A. Kulik, L. Arribas, P. Niehoff, F. Guedea, A. Schlamann, R. Pötter, C. Gall, W. Uter, and V. Strnad, “Late side-effects and cosmetic results of accelerated partial breast irradiation with interstitial brachytherapy versus whole-breast irradiation after breast-conserving surgery for low-risk invasive and in-situ carcinoma of the female breast: 5-year result,” *The Lancet Oncology*, vol. 18, pp. 259–268, feb 2017.
- [53] V. Strnad, O. J. Ott, G. Hildebrandt, D. Kauer-Dorner, H. Knauerhase, T. Major, J. Lyczek, J. L. Guinot, J. Dunst, C. G. Miguelez, P. Slampa, M. Allgäuer, K. Lössl, B. Polat, G. Kovács, A. R. Fishedick, T. G. Wendt, R. Fietkau, M. Hindemith, A. Resch, A. Kulik, L. Arribas, P. Niehoff, F. Guedea, A. Schlamann, R. Pötter, C. Gall, M. Malzer, W. Uter, and C. Polgár, “5-year results of accelerated partial breast irradiation using sole interstitial multicatheter brachytherapy versus whole-breast irradiation with boost after breast-conserving surgery for low-risk invasive and in-situ carcinoma of the female breast: A ran,” *The Lancet*, vol. 387, no. 10015, pp. 229–238, 2016.
- [54] P. Gabani, A. E. Cyr, J. E. Zoberi, L. L. Ochoa, M. A. Matesa, M. A. Thomas, J. Garcia, J. A. Margenthaler, M. J. Naughton, C. Ma, S. Sanati, and I. Zoberi, “Breast/Soft Tissue Long-term outcomes of APBI via multicatheter interstitial HDR brachytherapy: Results of a prospective single-institutional registry,” *Brachytherapy*, vol. 17, no. 1, pp. 171–180, 2018.
- [55] A. J. Khan, P. Y. Chen, C. Yashar, M. M. Poppe, L. Li, A. Y. Zeinab, F. A. Vicini, D. Moore, R. Dale, D. Arthur, C. Shah, B. G. Haffty, R. Kuske, and S. Kettering, “Three-Fraction Accelerated Partial Breast Irradiation (APBI) Delivered With Brachytherapy Applicators Is Feasible and Safe: First Results From the TRIUMPH-T Trial Radiation Oncology,” *Radiation Oncology Biology*, pp. 1–8, 2018.

- [56] S. L. Showalter, G. Petroni, D. M. Trifiletti, B. Libby, A. T. Schroen, D. R. Brenin, P. Dalal, M. Smolkin, K. A. Reardon, and T. N. Showalter, “A Novel Form of Breast Intraoperative Radiation Therapy With CT-Guided High-Dose-Rate Brachytherapy: Results of a Prospective Phase 1 Clinical Trial,” *International Journal of Radiation Oncology Biology Physics*, vol. 96, pp. 46–54, sep 2016.
- [57] S. A. Valente, R. D. Tendulkar, S. Cherian, C. O’rourke, J. M. Greif, L. Bailey, V. Uhl, K. P. Bethke, E. D. Donnelly, R. Rudolph, A. Pederson, T. Summer, S. C. Lottich, D. L. Ross, C. Laronga, L. Loftus, A. M. Abbott, P. Kelemen, U. Hermanto, N. B. Friedman, G. C. Bedi, J. E. Joh, W. A. Thompson Iii, R. A. Hoefler, J. P. Wilson, S. K. Kang, B. Rosen, J. Ruffer, L. Bravo, A. Police, J. M. Escallon, A. W. Fyles, D. R. Mccready, G. M. Graves, N. Rohatgi, J. A. Eaker, J. Graves, S. C. Willey, E. A. Tousimis, B. T. Collins, C. M. Shaw, L. Riley, N. Deb, T. Kelly, D. L. Andolino, M. E. Boisvert, J. Lyons, W. Small, S. R. Grobmyer, S. A. Valente, S. R. Grobmyer, and A. Surg, “TARGIT-R (Retrospective): North American Experience with Intraoperative Radiation Using Low-Kilovoltage X-Rays for Breast Cancer,” *Oncol*, vol. 23, pp. 2809–2815, 2016.
- [58] J. S. Vaidya, F. Wenz, M. Bulsara, J. Rey, S. Tobias, D. J. Joseph, M. Keshtgar, H. L. Flyger, S. Massarut, M. Alvarado, C. Saunders, W. Eiermann, M. Metaxas, E. Sperk, M. Sütterlin, D. Brown, L. Esserman, M. Roncadin, A. Thompson, J. A. Dewar, H. M. R. Holtveg, S. Pigorsch, M. Falzon, E. Harris, and A. Matthews, “Risk-adapted targeted intraoperative radiotherapy versus whole-breast radiotherapy for breast cancer: 5-year results for local control and overall survival from the TARGIT-A randomised trial,” *The Lancet Oncology*, vol. 383, p. 603, 2014.
- [59] M. R. S. Keshtgar, N. R. Williams, M. Bulsara, C. Saunders, H. Flyger, J. S. Cardoso, T. Corica, N. Bentzon, . Nikolaos, V. Michalopoulos, D. J. Joseph, N. R. Williams, M. Bulsara, C. Saunders, H. Flyger, Á. N. Bentzon, J. S. Cardoso, and D. J. Joseph, “Objective assessment of cosmetic outcome after targeted intraoperative radiotherapy

- in breast cancer: results from a randomised controlled trial,” *Breast Cancer Res Treat*, vol. 140, pp. 519–525, 2013.
- [60] U. Veronesi, R. Orecchia, P. Maisonneuve, G. Viale, N. Rotmensz, C. Sangalli, A. Luini, P. Veronesi, V. Galimberti, S. Zurrada, M. C. Leonardi, R. Lazzari, F. Cattani, O. Gentilini, M. Intra, P. Caldarella, and B. Ballardini, “Intraoperative radiotherapy versus external radiotherapy for early breast cancer (ELIOT): A randomised controlled equivalence trial,” *The Lancet Oncology*, vol. 14, pp. 1269–1277, 2013.
- [61] E. E. R. Harris, W. Small, and Jr., “Intraoperative Radiotherapy for Breast Cancer.” *Frontiers in oncology*, vol. 7, p. 317, 2017.
- [62] U. Veronesi, R. Orecchia, A. Luini, V. Galimberti, S. Zurrada, M. Intra, P. Veronesi, P. Arnone, M. C. Leonardi, M. Ciocca, R. Lazzari, P. Caldarella, N. Rotmensz, C. Sangalli, D. Sances, and P. Maisonneuve, “Intraoperative radiotherapy during breast conserving surgery: a study on 1,822 cases treated with electrons,” *Breast Cancer Research and Treatment*, 2010.
- [63] N. Surgical and A. Breast, “NSABP PROTOCOL B-39 RTOG PROTOCOL 0413 A Randomized Phase III Study of Conventional Whole Breast Irradiation ( WBI ) Versus Partial Breast Irradiation ( PBI ) for Women with Stage 0 , I , or II Breast Cancer,” 2011.
- [64] B. Cho, “Intensity-modulated radiation therapy: a review with a physics perspective.” *Radiation oncology journal*, vol. 36, pp. 1–10, mar 2018.
- [65] T. S. Hong, M. A. Ritter, W. A. Tomé, and P. M. Harari, “Intensity-modulated radiation therapy: emerging cancer treatment technology.” *British journal of cancer*, vol. 92, pp. 1819–24, may 2005.
- [66] J. T. Hepel, M. Tokita, S. G. MacAusland, S. B. Evans, J. R. Hiatt, L. L. Price, T. DiPetrillo, and D. E. Wazer, “Toxicity of Three-Dimensional Conformal Radiother-

- apy for Accelerated Partial Breast Irradiation,” *International Journal of Radiation Oncology Biology Physics*, vol. 75, no. 5, pp. 1290–1296, 2009.
- [67] P. Y. Chen, M. Wallace, C. Mitchell, I. Grills, L. Kestin, A. Fowler, A. Martinez, and F. Vicini, “Four-Year Efficacy, Cosmesis, and Toxicity Using Three-Dimensional Conformal External Beam Radiation Therapy to Deliver Accelerated Partial Breast Irradiation,” *International Journal of Radiation Oncology Biology Physics*, vol. 76, no. 4, pp. 991–997, 2010.
- [68] T. S. Berrang, I. Olivotto, D. H. Kim, A. Nichol, B. C. Cho, I. G. Mohamed, T. Parhar, J. R. Wright, P. Truong, S. Tyldesley, J. Sussman, E. Wai, and T. Whelan, “Three-year outcomes of a Canadian multicenter study of accelerated partial breast irradiation using conformal radiation therapy,” *International Journal of Radiation Oncology Biology Physics*, vol. 81, no. 5, pp. 1220–1227, 2011.
- [69] S. C. Formenti, H. Hsu, M. Fenton-Kerimian, D. Roses, A. Guth, G. Jozsef, J. D. Goldberg, and J. K. Dewyngaert, “Prone accelerated partial breast irradiation after breast-conserving surgery: Five-year results of 100 patients,” *International Journal of Radiation Oncology Biology Physics*, vol. 84, pp. 606–611, nov 2012.
- [70] A. A. Lewin, R. Derhagopian, K. Saigal, J. E. Panoff, A. Abitbol, D. J. Wiczorek, V. Mishra, I. Reis, A. Ferrell, L. Moreno, and C. Takita, “Accelerated partial breast irradiation is safe and effective using intensity-modulated radiation therapy in selected early-stage breast cancer,” *International Journal of Radiation Oncology Biology Physics*, vol. 82, no. 5, pp. 2104–2110, 2012.
- [71] N. Ria Rodríguez, X. Sanz, J. Dengra, P. Foro, I. Membrive, A. Reig, J. Quera, E. Fernández-Velilla, O. . Scar Pera, J. Lio, J. Lozano, and M. Algara, “Clinical Investigation: Breast Cancer Five-Year Outcomes, Cosmesis, and Toxicity With 3-Dimensional Conformal External Beam Radiation Therapy to Deliver Accelerated Partial Breast Irra-

- diation Radiation Oncology,” *Int J Radiation Oncol Biol Phys*, vol. 87, no. 5, pp. 1051–1057, 2013.
- [72] R. Y. Lei, C. E. Leonard, K. T. Howell, P. L. Henkenberns, T. K. Johnson, T. L. Hobart, S. P. Fryman, J. M. Kercher, J. L. Widner, T. Kaske, and D. L. Carter, “Four-year clinical update from a prospective trial of accelerated partial breast intensity-modulated radiotherapy (APBIMRT),” *Breast ca*, vol. 140, pp. 119–133, 2013.
- [73] C. Bergom, P. Prior, K. Kainz, N. V. Morrow, E. E. Ahunbay, A. Walker, X. Allen Li, and J. White, “A phase I/II study piloting accelerated partial breast irradiation using CT-guided intensity modulated radiation therapy in the prone position,” *Radiotherapy and Oncology*, vol. 108, no. 2, pp. 215–219, 2013.
- [74] A. L. Liss, M. A. Ben-David, R. Jagsi, J. A. Hayman, K. A. Griffith, J. M. Moran, R. B. Marsh, and L. J. Pierce, “Decline of cosmetic outcomes following accelerated partial breast irradiation using intensity modulated radiation therapy: Results of a single-institution prospective clinical trial,” *International Journal of Radiation Oncology Biology Physics*, vol. 89, no. 1, pp. 96–102, 2014.
- [75] S. Galland-Girodet, I. Pashtan, S. M. Macdonald, M. Ancukiewicz, A. E. Hirsch, L. A. Kachnic, M. Specht, M. Gadd, B. L. Smith, S. N. Powell, A. Recht, and A. G. Taghian, “Long-term cosmetic outcomes and toxicities of proton beam therapy compared with photon-based 3-dimensional conformal accelerated partial-breast irradiation: A phase 1 trial,” *International Journal of Radiation Oncology Biology Physics*, vol. 90, no. 3, pp. 493–500, 2014.
- [76] L. Livi, I. Meattini, L. Marrazzo, G. Simontacchi, S. Pallotta, C. Saieva, F. Paiar, V. Scotti, C. De Luca Cardillo, P. Bastiani, L. Orzalesi, D. Casella, L. Sanchez, J. Nori, M. Fambrini, and S. Bianchi, “Accelerated partial breast irradiation using intensity-modulated radiotherapy versus whole breast irradiation: 5-year survival analysis of



- a phase 3 randomised controlled trial,” *European Journal of Cancer*, vol. 51, no. 4, pp. 451–463, 2015.
- [77] D. Peterson, P. T. Truong, S. Parpia, I. A. Olivotto, T. Berrang, D. H. Kim, I. Kong, I. Germain, A. Nichol, M. Akra, I. Roy, M. Reed, A. Fyles, T. Trotter, F. Perera, S. Balkwill, S. Lavertu, E. Elliott, J. A. Julian, M. N. Levine, and T. J. Whelan, “Predictors of adverse cosmetic outcome in the rapid trial: An exploratory analysis,” *International Journal of Radiation Oncology Biology Physics*, vol. 91, no. 5, pp. 968–976, 2015.
- [78] K. C. Horst, C. Fasola, D. Ikeda, B. Daniel, G. Ognibene, D. R. Goffinet, and F. M. Dirbas, “Five-year results of a prospective clinical trial investigating accelerated partial breast irradiation using 3D conformal radiotherapy after lumpectomy for early stage breast cancer,” *Breast*, vol. 28, pp. 178–183, 2016.
- [79] R. Rabinovitch, J. Moughan, F. Vicini, H. Pass, J. Wong, S. Chafe, I. Petersen, D. W. Arthur, and J. White, “Long-Term Update of NRG Oncology RTOG 0319: A Phase 1 and 2 Trial to Evaluate 3-Dimensional Conformal Radiation Therapy Confined to the Region of the Lumpectomy Cavity for Stage I and II Breast Carcinoma,” *International Journal of Radiation Oncology Biology Physics*, vol. 96, no. 5, pp. 1054–1059, 2016.
- [80] C. E. Coles, C. L. Griffin, A. M. Kirby, J. Titley, R. K. Agrawal, A. Alhasso, I. S. Bhattacharya, A. M. Brunt, L. Ciurlionis, C. Chan, E. M. Donovan, M. A. Emson, A. N. Harnett, J. S. Haviland, P. Hopwood, M. L. Jefford, R. Kaggwa, E. J. Sawyer, I. Syndikus, Y. M. Tsang, D. A. Wheatley, M. Wilcox, J. R. Yarnold, J. M. Bliss, W. Al Sarakbi, S. Barber, G. Barnett, P. Bliss, J. Dewar, D. Eaton, S. Ebbs, I. Ellis, P. Evans, E. Harris, H. James, C. Kirwan, J. Kirk, H. Mayles, A. McIntyre, J. Mills, A. Poynter, E. Provenzano, C. Rawlings, M. Sculpher, G. Sumo, M. Sydenham, A. Tutt, N. Twyman, K. Venables, A. Winship, J. Winstanley, G. Wishart, and A. Thompson, “Partial-breast radiotherapy after breast conservation surgery for patients with early breast cancer (UK

IMPORT LOW trial): 5-year results from a multicentre, randomised, controlled, phase 3, non-inferiority trial,” *The Lancet*, vol. 390, no. 10099, pp. 1048–1060, 2017.

- [81] I. A. Olivotto, T. J. Whelan, S. Parpia, D. H. Kim, T. Berrang, P. T. Truong, I. Kong, B. Cochrane, A. Nichol, I. Roy, I. Germain, M. Akra, M. Reed, A. Fyles, T. Trotter, F. Perera, W. Beckham, M. N. Levine, and J. A. Julian, “Interim cosmetic and toxicity results from RAPID: A randomized trial of accelerated partial breast irradiation using three-dimensional conformal external beam radiation therapy,” *Journal of Clinical Oncology*, 2013.
- [82] R. A. Greenup, M. S. Camp, A. G. Taghian, J. Buckley, S. B. Coopey, M. Gadd, K. Hughes, M. Specht, and B. L. Smith, “Cost Comparison of Radiation Treatment Options After Lumpectomy for Breast Cancer,” *Annals of Surgical Oncology*, vol. 19, pp. 3275–3281, oct 2012.
- [83] N. Huppert, G. Jozsef, K. DeWyngaert, and S. C. Formenti, “The Role of a Prone Setup in Breast Radiation Therapy,” *Frontiers in Oncology*, vol. 1, 2011.
- [84] K. L. Griem, P. Fetherston, M. Kuznetsova, G. S. Foster, S. Shott, and J. Chu, “Three-dimensional photon dosimetry: A comparison of treatment of the intact breast in the supine and prone position,” *International Journal of Radiation Oncology Biology Physics*, vol. 57, no. 3, pp. 891–899, 2003.
- [85] A. M. Kirby, P. M. Evans, E. M. Donovan, H. M. Convery, J. S. Haviland, and J. R. Yarnold, “Prone versus supine positioning for whole and partial-breast radiotherapy: A comparison of non-target tissue dosimetry,” *Radiotherapy and Oncology*, vol. 96, pp. 178–184, 2010.
- [86] J. Buijsen, J. J. Jager, J. Bovendeerd, R. Voncken, J. H. Borger, L. J. Boersma, L. H. Murrer, and P. Lambin, “Prone breast irradiation for pendulous breasts,” *Radiotherapy and Oncology*, vol. 82, no. 3, pp. 337–340, 2007.

- [87] E. E. Ahunbay, J. Robbins, R. Christian, A. Godley, J. White, and X. A. Li, “Interfractional target variations for partial breast irradiation,” *International Journal of Radiation Oncology Biology Physics*, vol. 82, pp. 1594–1604, apr 2012.
- [88] F. Lakosi, A. Gulyban, S. B. M. Simoni, P. V. Nguyen, S. Cucchiaro, L. Seidel, L. January, S. Nicolas, P. Vavassis, and P. Coucke, “The Influence of Treatment Position (Prone vs. Supine) on Clip Displacement, Seroma, Tumor Bed and Partial Breast Target Volumes: Comparative Study,” *Pathology and Oncology Research*, vol. 22, no. 3, pp. 493–500, 2016.
- [89] O. Riou, P. Fenoglietto, C. Bourcier, O. Lauche, F. Boulbair, M. Charissoux, A. Duceil, N. Aillères, C. Lemanski, and D. Azria, “Feasibility of accelerated partial breast irradiation with volumetric-modulated arc therapy in elderly and frail patients,” *Radiation Oncology*, vol. 10, p. 209, dec 2015.
- [90] F. Van Der Leij, P. H. M. Elkhuisen, T. M. Janssen, P. Poortmans, M. Van Der Sangen, A. N. Scholten, C. Van Vliet-Vroegindeweyj, and L. J. Boersma, “Partial breast irradiation Target volume delineation in external beam partial breast irradiation: Less inter-observer variation with preoperative-compared to postoperative delineation q,” *Radiotherapy and Oncology*, vol. 110, pp. 467–470, 2014.
- [91] L. J. Boersma, T. Janssen, P. H. M. Elkhuisen, P. Poortmans, M. Van Der Sangen, A. N. Scholten, B. Hanbeukers, J. C. Duppen, C. Hurkmans, and C. Van Vliet, “Reducing interobserver variation of boost-CTV delineation in breast conserving radiation therapy using a pre-operative CT and delineation guidelines,” *Radiotherapy and Oncology*, vol. 103, no. 2, pp. 178–182, 2012.
- [92] M. D. den Hartogh, M. E. P. Philippens, I. E. van Dam, C. E. Kleynen, R. J. H. A. Tersteeg, R. M. Pijnappel, A. N. T. J. Kotte, H. M. Verkooijen, M. A. A. J. van den Bosch, M. van Vulpen, B. van Asselen, and H. D. van den Bongard, “MRI and CT imaging for

- preoperative target volume delineation in breast-conserving therapy,” *Radiation oncology (London, England)*, vol. 9, p. 63, feb 2014.
- [93] K. Guidolin, M. Lock, B. Yaremko, N. Gelman, S. Gaede, A. Kornecki, V. Moiseenko, J. Cao, L. Scott, and M. Brackstone, “A phase II trial to evaluate single-dose stereotactic body radiation therapy (SBRT) prior to surgery for early-stage breast carcinoma: SIGNAL (stereotactic image-guided neoadjuvant ablative radiation then lumpectomy) trial,” *Journal of Radiation Oncology*, vol. 4, no. 4, pp. 423–430, 2015.
- [94] M. Z. Dewan, A. E. Galloway, N. Kawashima, J. K. Dewyngaert, J. S. Babb, S. C. Formenti, and S. Demaria, “Fractionated but Not Single-Dose Radiotherapy Induces an Immune-Mediated Abscopal Effect when Combined with Anti-CTLA-4 Antibody,” *Clinical Cancer Research*, vol. 15, pp. 5379–5388, sep 2009.
- [95] M. Lock, A. Muinuddin, W. I. Kocha, R. Dinniwell, G. Rodrigues, and D. D’souza, “Abscopal Effects: Case Report and Emerging Opportunities,” *Cureus*, vol. 7, p. e344, oct 2015.
- [96] P. Pinnarò, S. Arcangeli, C. Giordano, G. Arcangeli, F. A. Impiombato, V. Pinzi, G. Iaccarino, A. Soriani, V. Landoni, and L. Strigari, “Toxicity and cosmesis outcomes after single fraction partial breast irradiation in early stage breast cancer,” *Radiation oncology (London, England)*, vol. 6, p. 155, jan 2011.
- [97] J. K. Horton, R. C. Blitzblau, S. Yoo, J. Geradts, Z. Chang, J. A. Baker, G. S. Georgiade, W. Chen, S. Siamakpour-Reihani, C. Wang, G. Broadwater, J. Groth, M. Palta, M. Dewhirst, W. T. Barry, E. A. Duffy, J.-T. A. T. A. Chi, and E. S. Hwang, “Preoperative Single-Fraction Partial Breast Radiation Therapy: A Novel Phase 1, Dose-Escalation Protocol With Radiation Response Biomarkers,” *International Journal of Radiation Oncology Biology Physics*, vol. 92, pp. 846–855, jul 2015.

- [98] R. G. Figueiras, A. R. Padhani, V. J. Goh, J. C. Vilanova, S. B. Gonzalez, C. V. Martin, a. G. Caamano, A. B. Naveira, and P. L. Choyke, “Novel Oncologic Drugs: What They Do and How They Affect Images,” *Radiographics*, vol. 31, no. 7, pp. 2059–2091, 2011.
- [99] L. C. Villaruz and M. A. Socinski, “The clinical viewpoint: Definitions, limitations of RECIST, practical considerations of measurement,” may 2013.
- [100] S. A. Mattonen, K. Huang, A. D. Ward, S. Senan, and D. A. Palma, “New techniques for assessing response after hypofractionated radiotherapy for lung cancer.,” *Journal of thoracic disease*, vol. 6, pp. 375–86, apr 2014.
- [101] J. Ruzevick, L. Kleinberg, and D. Rigamonti, “Imaging changes following stereotactic radiosurgery for metastatic intracranial tumors: differentiating pseudoprogression from tumor progression and its effect on clinical practice.,” *Neurosurgical review*, vol. 37, pp. 193–201; discussion 201, apr 2014.
- [102] H. J. Park, R. J. Griffin, S. Hui, S. H. Levitt, C. W. Song, H. Levitt, and C. W. Song, “Radiation-Induced Vascular Damage in Tumors: Implications of Vascular Damage in Ablative Hypofractionated Radiotherapy (SBRT and SRS),” *Radiation Research*, vol. 177, no. 3, pp. 311–327, 2012.
- [103] F. Wenz, F. Sedlmayer, C. Herskind, G. Welzel, E. Sperk, C. Neumaier, B. Gauter-Fleckenstein, J. S. Vaidya, and M. Sütterlin, “Accelerated partial breast irradiation in clinical practice,” *Breast Care*, vol. 10, pp. 247–252, aug 2015.
- [104] R. García-Figueiras, V. J. Goh, A. R. Padhani, S. Baleato-González, M. Garrido, L. León, and A. Gómez-Caamaño, “CT perfusion in oncologic imaging: A useful tool?,” *American Journal of Roentgenology*, vol. 200, pp. 8–19, jan 2013.
- [105] H. B. Stone, C. N. Coleman, M. S. Anscher, and W. H. McBride, “Effects of radiation on normal tissue: Consequences and mechanisms,” 2003.

- [106] T. Hellevik and I. Martinez-Zubiaurre, "Radiotherapy and the Tumor Stroma: The Importance of Dose and Fractionation," *Frontiers in Oncology*, vol. 4, p. 1, jan 2014.
- [107] Y. Shibamoto, A. Miyakawa, H. Iwata, and S. Otsuka, "Radiobiology of SBRT," in *Stereotactic Body Radiation Therapy: Principles and Practices*, pp. 11–25, 2015.
- [108] C. W. Song, L. C. Cho, J. Yuan, K. E. Dusenbery, R. J. Griffin, and S. H. Levitt, "Radiobiology of Stereotactic Body Radiation Therapy/Stereotactic Radio-surgery and the Linear-Quadratic Model," *International Journal of Radiation Oncology\*Biological\*Physics*, vol. 87, no. 1, pp. 18–19, 2013.
- [109] I. Corre, M. Guillonneau, and F. Paris, "Membrane signaling induced by high doses of ionizing radiation in the endothelial compartment. Relevance in radiation toxicity," *International Journal of Molecular Sciences*, vol. 14, pp. 22678–22696, nov 2013.
- [110] N. A. Mayr, W. T. Yuh, V. A. Magnotta, J. C. Ehrhardt, J. A. Wheeler, J. I. Sorosky, C. S. Davis, B. C. Wen, D. D. Martin, R. E. Pelsang, R. E. Buller, L. W. Oberley, D. E. Mellenberg, and D. H. Hussey, "Tumor perfusion studies using fast magnetic resonance imaging technique in advanced cervical cancer: A new noninvasive predictive assay," *International Journal of Radiation Oncology Biology Physics*, vol. 36, pp. 623–633, oct 1996.
- [111] H. E. Barker, J. T. E. Paget, A. A. Khan, and K. J. Harrington, "The tumour microenvironment after radiotherapy : mechanisms of resistance and recurrence," *Nature Publishing Group*, vol. 15, pp. 409–425, jul 2015.
- [112] C.-H. Wang, "Review of treatment assessment using DCE-MRI in breast cancer radiation therapy," *World Journal of Methodology*, vol. 4, p. 46, jun 2014.
- [113] J. Lohrke, T. Frenzel, J. Endrikat, F. C. Alves, T. M. Grist, M. Law, J. M. Lee, T. Leiner, K. C. Li, K. Nikolaou, M. R. Prince, H. H. Schild, J. C. Weinreb, K. Yoshikawa, and

- H. Pietsch, “25 Years of Contrast-Enhanced MRI: Developments, Current Challenges and Future Perspectives,” *Advances in Therapy*, vol. 33, no. 1, pp. 1–28, 2016.
- [114] Y. Yan, X. Sun, and B. Shen, “Contrast agents in dynamic contrast-enhanced magnetic resonance imaging,” *Oncotarget*, vol. 8, pp. 43491–43505, jun 2017.
- [115] A. Jackson, D. L. Buckley, and G. J. M. Parker, *Dynamic Contrast-Enhanced Magnetic Resonance Imaging in Oncology (Medical Radiology / Diagnostic Imaging)*. Springer, Berlin, Heidelberg, 2005.
- [116] M. Rogosnitzky and S. Branch, “Gadolinium-based contrast agent toxicity: a review of known and proposed mechanisms.,” *Biometals : an international journal on the role of metal ions in biology, biochemistry, and medicine*, vol. 29, no. 3, pp. 365–76, 2016.
- [117] Z. Zhou and Z.-R. Lu, “Gadolinium-based contrast agents for magnetic resonance cancer imaging.,” *Wiley interdisciplinary reviews. Nanomedicine and nanobiotechnology*, vol. 5, no. 1, pp. 1–18, 2013.
- [118] B. J. Guo, Z. L. Yang, and L. J. Zhang, “Gadolinium Deposition in Brain: Current Scientific Evidence and Future Perspectives,” *Frontiers in Molecular Neuroscience*, vol. 11, p. 335, 2018.
- [119] P. Marckmann, L. Skov, K. Rossen, A. Dupont, M. B. Damholt, J. G. Heaf, and H. S. Thomsen, “Nephrogenic Systemic Fibrosis: Suspected Causative Role of Gadodiamide Used for Contrast-Enhanced Magnetic Resonance Imaging,” *Journal of the American Society of Nephrology*, vol. 17, pp. 2359–2362, sep 2006.
- [120] T. Grobner, “Gadolinium – a specific trigger for the development of nephrogenic fibrosing dermopathy and nephrogenic systemic fibrosis?,” *Nephrology Dialysis Transplantation*, vol. 21, pp. 1104–1108, apr 2006.

- [121] V. Gulani, F. Calamante, F. G. Shellock, E. Kanal, and S. B. Reeder, "Gadolinium deposition in the brain: summary of evidence and recommendations," 2017.
- [122] N. Murata, L. F. Gonzalez-Cuyar, K. Murata, C. Fligner, R. Dills, D. Hippe, and K. R. Maravilla, "Macrocyclic and Other Non-Group 1 Gadolinium Contrast Agents Deposit Low Levels of Gadolinium in Brain and Bone Tissue," *Investigative Radiology*, vol. 51, pp. 447–453, jul 2016.
- [123] J. W. Choi and W.-J. Moon, "Gadolinium Deposition in the Brain: Current Updates," *Korean Journal of Radiology*, vol. 20, p. 134, jan 2019.
- [124] R. C. Semelka, M. Ramalho, M. AlObaidy, and J. Ramalho, "Gadolinium in Humans: A Family of Disorders," *American Journal of Roentgenology*, vol. 207, pp. 229–233, aug 2016.
- [125] V. P. Mathews, K. S. Caldemeyer, J. L. Ulmer, H. Nguyen, and W. T. C. Yuh, "Effects of contrast dose, delayed imaging, and magnetization transfer saturation on gadolinium-enhanced MR imaging of brain lesions," 1997.
- [126] G. Brix, J. Griebel, F. Kiessling, and F. Wenz, "Tracer kinetic modelling of tumour angiogenesis based on dynamic contrast-enhanced CT and MRI measurements," 2010.
- [127] E. Henderson, B. K. Rutt, and T. Y. Lee, "Temporal sampling requirements for the tracer kinetics modeling of breast disease," *Magnetic Resonance Imaging*, vol. 16, no. 9, pp. 1057–1073, 1998.
- [128] G. H. Jahng, K. L. Li, L. Ostergaard, and F. Calamante, "Perfusion magnetic resonance imaging: A comprehensive update on principles and techniques," *Korean Journal of Radiology*, vol. 15, no. 5, pp. 554–577, 2014.



- [129] N. M. Rofsky, V. S. Lee, G. Laub, M. A. Pollack, G. A. Krinsky, D. Thomasson, M. M. Ambrosino, and J. C. Weinreb, "Abdominal MR Imaging with a Volumetric Interpolated Breath-hold Examination," *Radiology*, vol. 212, no. 3, pp. 876–884, 2013.
- [130] F. H. Epstein, J. P. Mugler, and J. R. Brookeman, "Spoiling of transverse magnetization in gradient-echo (GRE) imaging during the approach to steady state.," *Magnetic resonance in medicine*, vol. 35, pp. 237–45, feb 1996.
- [131] T. A. Bley, O. Wieben, C. J. François, J. H. Brittain, and S. B. Reeder, "Fat and water magnetic resonance imaging," *Journal of Magnetic Resonance Imaging*, vol. 31, no. 1, pp. 4–18, 2010.
- [132] V. L. Yarnykh, "Actual flip-angle imaging in the pulsed steady state: A method for rapid three-dimensional mapping of the transmitted radiofrequency field," *Magnetic Resonance in Medicine*, vol. 57, no. 1, pp. 192–200, 2007.
- [133] S. Chung, D. Kim, E. Breton, and L. Axel, "Rapid B1+mapping using a preconditioning RF pulse with turboFLASH readout," *Magnetic Resonance in Medicine*, vol. 64, no. 2, pp. 439–446, 2010.
- [134] K. K. Brock, S. Mutic, T. R. McNutt, H. Li, and M. L. Kessler, "Use of image registration and fusion algorithms and techniques in radiotherapy: Report of the AAPM Radiation Therapy Committee Task Group No. 132," *Medical Physics*, 2017.
- [135] A. Melbourne, J. Hipwell, M. Modat, T. Mertzaniidou, H. Huisman, S. Ourselin, and D. J. Hawkes, "The effect of motion correction on pharmacokinetic parameter estimation in dynamic-contrast-enhanced MRI," *Physics in Medicine and Biology*, vol. 56, no. 24, pp. 7693–7708, 2011.
- [136] A. L. Martel, M. S. Froh, K. K. Brock, D. B. Plewes, and D. C. Barber, "Evaluating an optical-flow-based registration algorithm for contrast-enhanced magnetic resonance

- imaging of the breast,” *Physics in Medicine and Biology*, vol. 52, pp. 3803–3816, jul 2007.
- [137] Y. Zheng, J. Yu, C. Kambhamettu, S. Englander, M. D. Schnall, and D. Shen, “De-enhancing the dynamic contrast-enhanced breast MRI for robust registration.,” *Medical image computing and computer-assisted intervention : MICCAI ... International Conference on Medical Image Computing and Computer-Assisted Intervention*, vol. 10, no. Pt 1, pp. 933–41, 2007.
- [138] D. Rueckert, C. Hayes, C. Studholme, P. Summers, M. Leach, and D. J. Hawkes, “Non-rigid registration of breast MR images using mutual information,” pp. 1144–1152, Springer, Berlin, Heidelberg, oct 1998.
- [139] F. G. Zöllner, R. Sance, P. Rogelj, M. J. Ledesma-Carbayo, J. Rørvik, A. Santos, and A. Lundervold, “Assessment of 3D DCE-MRI of the kidneys using non-rigid image registration and segmentation of voxel time courses,” *Computerized Medical Imaging and Graphics*, vol. 33, pp. 171–181, 2009.
- [140] C. Tanner, J. a. Schnabel, D. L. G. Hill, D. J. Hawkes, A. Degenhard, M. O. Leach, D. R. Hose, M. a. Hall-Craggs, and S. I. Usiskin, “Quantitative evaluation of free-form deformation registration for dynamic contrast-enhanced MR mammography,” *Medical Physics*, vol. 34, no. 4, p. 1221, 2007.
- [141] E. Hodneland, A. Lundervold, J. Rorvik, and A. Z. Munthe-Kaas, “Normalized gradient fields and mutual information for motion correction of DCE-MRI images,” in *2013 8th International Symposium on Image and Signal Processing and Analysis (ISPA)*, pp. 516–521, IEEE, sep 2014.
- [142] K. Kuczyński, M. Siczek, and R. Stegierski, “DCE-MRI breast image registration for tumour diagnostics,” *Advances in Intelligent and Soft Computing*, vol. 102, pp. 323–329, 2011.

- [143] S. Claude, "A Mathematical Theory of Communication," *The Bell System Technical Journal*, vol. Vol.27, no. 1948, pp. 379–423, 1948.
- [144] R. V. Hartley, "Transmission of Information," *Bell System Technical Journal*, vol. 7, pp. 535–563, jul 1928.
- [145] A. Hill, A. Mehnert, S. Crozier, and K. McMahon, "Evaluating the accuracy and impact of registration in dynamic contrast-enhanced breast MRI," *Concepts in Magnetic Resonance Part B: Magnetic Resonance Engineering*, vol. 35, no. 2, pp. 106–120, 2009.
- [146] D. Rueckert, L. I. Sonoda, C. Hayes, D. L. Hill, M. O. Leach, and D. J. Hawkes, "Nonrigid registration using free-form deformations: application to breast MR images.," *IEEE Transactions on Medical Imaging*, vol. 18, no. 8, pp. 712–21, 1999.
- [147] L. A. Schwarz, *Non-rigid registration using free-form deformations*. PhD thesis, Tech. Univ. Munchen, 2007.
- [148] J. Shackelford, N. Kandasamy, and G. Sharp, *High Performance Deformable Image Registration Algorithms for Manycore Processors*. Morgan Kaufmann, 2013.
- [149] S. Schäfer, U. Preim, S. Glaßer, B. Preim, and K. Tönnies, "Local similarity measures for lesion registration in DCE - MRI of the breast," *Annals of the BMVA*, vol. 2011, no. 3, pp. 1–13, 2011.
- [150] B. L. Daniel, Y. F. Yen, G. H. Glover, D. M. Ikeda, R. L. Birdwell, A. M. Sawyer-Glover, J. W. Black, S. K. Plevritis, S. S. Jeffrey, R. J. Herfkens, L. Daniel, and M. Ikeda, "Breast disease: dynamic spiral MR imaging," *Radiology*, vol. 209, no. 2, pp. 499–509, 1998.
- [151] F. Khalifa, A. Soliman, A. El-Baz, M. Abou El-Ghar, T. El-Diasty, G. Gimel'farb, R. Ouseph, and A. C. Dwyer, "Models and methods for analyzing DCE-MRI: A review," *Medical Physics*, vol. 41, p. 124301, nov 2014.

- [152] J. M. Winfield, G. S. Payne, A. Weller, and N. M. DeSouza, "DCE-MRI, DW-MRI, and MRS in Cancer: Challenges and Advantages of Implementing Qualitative and Quantitative Multi-parametric Imaging in the Clinic.," *Topics in magnetic resonance imaging : TMRI*, vol. 25, pp. 245–254, oct 2016.
- [153] C. A. Cuenod and D. Balvay, "Perfusion and vascular permeability: Basic concepts and measurement in DCE-CT and DCE-MRI," *Diagnostic and Interventional Imaging*, vol. 94, pp. 1187–1204, dec 2013.
- [154] J. Pintaske, P. Martirosian, H. Graf, G. Erb, K. P. Lodemann, C. D. Claussen, and F. Schick, "Relaxivity of gadopentetate dimeglumine (Magnevist), gadobutrol (Gadovist), and gadobenate dimeglumine (MultiHance) in human blood plasma at 0.2, 1.5, and 3 Tesla [published erratum appears in Invest Radiol 2006;41:859]," *Investigative Radiology*, vol. 41, pp. 213–221, mar 2006.
- [155] T. Chikui, M. Obara, A. W. Simonetti, M. Ohga, S. Koga, S. Kawano, Y. Matsuo, T. Kamintani, T. Shiraishi, E. Kitamoto, K. Nakamura, and K. Yoshiura, "The principal of dynamic contrast enhanced MRI, the method of pharmacokinetic analysis, and its application in the head and neck region.," *International journal of dentistry*, vol. 2012, p. 480659, 2012.
- [156] S. P. Sourbron and D. L. Buckley, "Tracer kinetic modelling in MRI: Estimating perfusion and capillary permeability," *Physics in Medicine and Biology*, vol. 57, no. 2, pp. R1–R33, 2012.
- [157] P. S. Tofts and G. J. M. Parker, "DCE-MRI: acquisition and analysis techniques," in *Clinical Perfusion MRI: Techniques and Applications* (P. B. Barker, X. Golay, and G. Zaharchuk, eds.), pp. 58–74, Cambridge University Press, 2013.
- [158] P. S. Tofts, "Modeling Tracer Kinetics in Dynamic Gd-DTPA MR Imaging," *Journal of Magnetic Resonance Imaging*, vol. 7, pp. 91–101, 1997.

- [159] P. Tofts, B. Gunnar, D. L. Buckley, J. L. Evelhoch, E. Henderson, M. V. Knopp, H. B. W. Larsson, T.-Y. Lee, N. A. Mayr, G. J. M. Parker, R. E. Port, J. Taylor, and R. M. Weisskoff, "Estimating kinetic parameters from dynamic contrast-enhanced T1-weighted MRI of a diffusable tracer: Standardized quantities and symbols," *Journal of Magnetic Resonance Imaging*, vol. 10, no. 3, pp. 223–232, 1999.
- [160] G. J. M. Parker, C. Roberts, A. Macdonald, G. A. Buonaccorsi, S. Cheung, D. L. Buckley, A. Jackson, Y. Watson, K. Davies, and G. C. Jayson, "Experimentally-derived functional form for a population-averaged high-temporal-resolution arterial input function for dynamic contrast-enhanced MRI," *Magnetic Resonance in Medicine*, vol. 56, no. 5, pp. 993–1000, 2006.
- [161] S. P. Sourbron and D. L. Buckley, "On the scope and interpretation of the Tofts models for DCE-MRI," *Magnetic Resonance in Medicine*, vol. 66, no. 3, pp. 735–745, 2011.
- [162] M. H. Janssen, H. J. Aerts, R. G. Kierkels, W. H. Backes, M. C. Öllers, J. Buijsen, P. Lambin, and G. Lammering, "Tumor perfusion increases during hypofractionated short-course radiotherapy in rectal cancer: Sequential perfusion-CT findings," *Radiotherapy and Oncology*, vol. 94, pp. 156–160, feb 2010.
- [163] C. Coolens, B. Driscoll, J. Moseley, K. K. Brock, and L. A. Dawson, "Feasibility of 4D perfusion CT imaging for the assessment of liver treatment response following SBRT and sorafenib," *Advances in Radiation Oncology*, vol. 1, pp. 194–203, jul 2016.
- [164] J. D. Winter, F. Y. Moraes, C. Chung, and C. Coolens, "Detectability of radiation-induced changes in magnetic resonance biomarkers following stereotactic radiosurgery: A pilot study," *PLoS ONE*, vol. 13, no. 11, 2018.
- [165] C. Wang, J. K. Horton, F.-F. Yin, and Z. Chang, "Assessment of Treatment Response With Diffusion-Weighted MRI and Dynamic Contrast-Enhanced MRI in Patients With

- Early-Stage Breast Cancer Treated With Single-Dose Preoperative Radiotherapy: Initial Results,” *Technology in Cancer Research & Treatment*, 2015.
- [166] J. S. Detsky, L. Milot, Y.-J. Ko, P. Munoz-Shuffenegger, W. Chu, G. J. Czarnota, and H. T. Chung, “Perfusion imaging of colorectal liver metastases treated with bevacizumab and stereotactic body radiotherapy,” *Physics and Imaging in Radiation Oncology*, vol. 5, pp. 9–12, 2018.
- [167] B. Sawyer, E. Pun, M. Samuel, H. Tay, T. Kron, M. Bressel, D. Ball, and S. Siva, “CT perfusion imaging in response assessment of pulmonary metastases undergoing stereotactic ablative radiotherapy,” *Journal of Medical Imaging and Radiation Oncology*, vol. 59, pp. 207–215, apr 2015.
- [168] Y. S. Huang, J. L. Y. Chen, F. M. Hsu, J. Y. Huang, W. C. Ko, Y. C. Chen, F. S. Jaw, R. F. Yen, and Y. C. Chang, “Response assessment of stereotactic body radiation therapy using dynamic contrast-enhanced integrated MR-PET in non-small cell lung cancer patients,” *Journal of Magnetic Resonance Imaging*, vol. 47, pp. 191–199, jan 2018.
- [169] D. E. Spratt, J. Arevalo-Perez, J. E. Leeman, N. K. Gerber, M. Folkert, N. K. Taunk, K. M. Alektiar, S. Karimi, J. K. Lyo, W. D. Tap, M. H. Bilsky, I. Laufer, Y. Yamada, and J. R. Osborne, “Early magnetic resonance imaging biomarkers to predict local control after high dose stereotactic body radiotherapy for patients with sarcoma spine metastases,” *Spine Journal*, vol. 16, no. 3, pp. 291–298, 2016.
- [170] N. K. Taunk, J. H. Oh, A. Shukla-Dave, K. Beal, B. Vachha, A. Holodny, and V. Hatzoglou, “Early posttreatment assessment of MRI perfusion biomarkers can predict long-term response of lung cancer brain metastases to stereotactic radiosurgery,” *Neuro-Oncology*, vol. 20, pp. 567–575, mar 2018.
- [171] P. Santos, K. K. Peck, J. Arevalo-Perez, S. Karimi, E. Lis, Y. Yamada, A. I. Holodny, and J. Lyo, “T1-Weighted Dynamic Contrast-Enhanced MR Perfusion Imaging Charac-

terizes Tumor Response to Radiation Therapy in Chordoma.," *AJNR. American journal of neuroradiology*, sep 2017.

- [172] H. J. Weinmann, M. Laniado, and W. Mützel, "Pharmacokinetics of GdDTPA/dimeglumine after intravenous injection into healthy volunteers.," *Physiological chemistry and physics and medical NMR*, vol. 16, no. 2, pp. 167–72, 1984.

## Chapter 2

### **2 Reducing the dose of gadolinium-based contrast agents for DCE-MRI guided SBRT: The effects on inter and intra observer variability for preoperative target volume delineation in early stage breast cancer patients**

#### **2.1 Introduction**

The current standard of treatment for early stage breast cancer patients opting for BCT is lumpectomy followed by whole breast radiotherapy delivered over several weeks [1]. This treatment time can be prohibitively long for many patients. APBI techniques can reduce treatment time by treating a smaller volume and increasing the dose per fraction (hypofractionate). Long-term studies [2–4] have found equivalent tumour control and recurrence compared to whole breast radiotherapy. Further studies have shown that performing neoadjuvant to lumpectomy can reduce treatment volumes, allowing further dose escalation [5, 6].

An important aspect of APBI is target volume delineation [7, 8] which relies heavily on image quality. Previous investigations [6] have focused on adjuvant external beam APBI, which use the lumpectomy cavity as the target volume and can be visualized without contrast. Our centre is currently enrolling early-stage breast cancer patients in a neoadjuvant stereotactic radiation therapy trial [9] which requires use of a contrast agent as there is no endogenous contrast at the tumour site. Patients are receiving a dynamic contrast enhanced MRI using



a gadolinium based contrast agent (GBCA). This image sequence is being used for tumour guided delineation as well as to assess patient response to radiotherapy.

Contrast enhanced (CE) techniques involve injecting a contrast agent which causes the tumour to appear hyperintense. This technique can be performed with CT or MRI. Previous studies have shown CE-MRI to be superior to standard CT imaging in the context of breast cancer [7]. For example, in one study [10] comparing contouring the GTV on CE-CT versus CE-MRI in neoadjuvant BCT, observers missed the tumour in 2/14 patients. They also found a significant reduction in GTV definition variability across observers using CE-MRI.

While the use of CE-MRI has increased, recent research has provided evidence for longer term retention of gadolinium in body tissues [11, 12]. This depends on the specific class of GBCA, with higher levels of retention for those GBCAs having ligands with a linear configuration, compared to those where the ligand surrounds the gadolinium (macrocyclic). It also appears to depend on the dose a patient has received. It is not known what effect the retention causes and no pathological risks have been identified from these recent findings. However, the association between nephrogenic systemic fibrosis and GBCAs was not discovered for decades in renally impaired patients [11] and so more time is needed to comprehensively evaluate what this retention may cause, though there are known pathological issues associated with heavy metal toxicities including free gadolinium [11]. It has yet to be established in what form the retained gadolinium exists in the body. In response to these findings, the European Medicines Agency and Health Canada have indicated that the agents found to be more stable (macrocyclic) can still be used but with the lowest possible doses [13, 14], while the FDA is requiring that patients be informed of the currently unknown risk [15]. As such, it is important to investigate methods of minimizing exposure and, hence, any potential health risk to patients. One

way would be to reduce the dose of GBCA given to patients per scan [11]. However, in the context of radiotherapy delivery (particularly in SABR techniques), we must ensure visibility of the tumour is not compromised by reducing the contrast dose.

We hypothesize that reducing the concentration of gadolinium to half of the standard clinical dose will not significantly affect gross target volume as delineated by expert observers. The objective of this study was to quantitatively assess the efficacy of target volume delineation on CE-MR images obtained with half the standard dose of GBCA compared to full dose GBCA for early stage breast cancer patients. Specifically, the quantitative measures of efficacy were based on the inter- and intra- observer variability, volume of delineation, and center of mass of the delineation.

## **2.2 Materials and Methods**

### **Patients**

Data was collected from a phase I/II clinical trial conducted at the London Regional Cancer Program [9]. Inclusion and exclusion criteria are included in the clinical trial document [9]. Patients enrolled in the study had a surgical clip placed adjacent to the tumour at the time of the initial biopsy. A subset of the latest 23 patients within the SIGNAL trial at the time of the experiment were included in this study.

### **Image Acquisition**

Patients were imaged prone with their ipsilateral arm raised above their head to mimic the radiotherapy treatment positioning. For radiotherapy, this was done to minimize the impact

**Table 2.1:** Patient characteristics for the two groups

Characteristic	Full Dose Group	Half Dose Group
Age		
Median	61	69
Range	57-76	58-80
Side		
Left	7	6
Right	7	3

of respiratory motion and reduce inclusion of normal tissue. The contralateral breast was compressed so only the ipsilateral breast was in the coil and the prone breast board. Patients received a planning CT scan (Brilliance Big Bore, Philips Medical Systems, Best, The Netherlands) with a prone board (Aktina Medical, New York, USA) and a DCE-MRI scan on a Siemens Biograph mMR 3T-PET/MRI system (Siemens Medical, Munich, Germany) with a four channel prone breast coil [16].

Three-dimensional fat suppressed fast flow angle shot (FLASH) images were acquired with the following parameters:  $TR = 4.1\text{ms}$ ,  $T_E = 1.5\text{ms}$ , flip angle =  $15^\circ$ , spatial resolution =  $1.0 \times 2.1 \times 2.1\text{ mm}$  interpolated to  $1.0 \times 1.0 \times 1.2\text{ mm}$ , field of view =  $38 \times 38\text{ cm}$ , slab thickness =  $13.4\text{cm}$ , acquisition time of approximately 20s. The DCE series contained a pre-contrast image and 28 post-contrast images as the clinical trial protocol also includes kinetic analysis to assess tumour response using non-invasive perfusion biomarkers [9]. The GBCA used was gadobutrol (Gadavist®). Of the 23 patients, 14 received a clinical dose of  $0.1\text{ mMol/kg}$  with an injection rate of  $2\text{ml/s}$ . Following the findings of gadolinium retention, we decided to reduce the dose to half the standard dose, so patients imaged before and after radiotherapy would only receive a standard dose in total and not increasing their risk for a research only scan (the post-radiation

treatment). Thus far, 9 patients have received half the clinical dose (0.05 mMol/kg) with an injection rate of 0.75ml/s. This injection rate was chosen to match the injection protocol to a population derived arterial input function for DCE-MRI kinetic analysis (outside objective of this study) [17]. A late post-contrast MRI that visually had the highest signal in the tumour was chosen by an expert external to the study to aid the observers in contouring the tumour.

### **Target Volume Delineation**

The patient data from both groups were pooled and randomly ordered for contouring. The CT and late post-contrast CE-MRI scan (that visually showed peak intensity) were fused and manually aligned by a single expert external to this study in MIM (v6.8.0, Mim Software, Cleveland, USA) such that the tumour was in the same location. Five radiation oncologists (ROs), all of whom had enrolled patients on APBI trials, including the SIGNAL trial, RTOG 0413, and the RAPID trial, were asked to delineate the GTV on the CT image with the aid of the fused CE-MRI and the embedded surgical clip. The CT was displayed in grayscale with a soft tissue window/level and the MRI displayed as a heatmap overlaid on the CT with a window/level determined by an expert external to the study and ensured that the window/level settings used were reasonable for all patients. Observers were not allowed to change the display map for the CE-MRI or the window/level though they were able to change the transparency of the CE-MRI heatmap from 0 (only CT shown) to 1 (only CE-MRI shown). The ROs were blinded to each others' contours. After at least 1 month, ROs were asked to recontour the images (randomized again), blinded to their first contouring session and given identical delineation instructions. In accordance with the SIGNAL trial [17], CTV were created by adding a 0.5cm margin to the GTV.

## Data Analysis

The contours were exported from MIM as RTStructs and imported into MATLAB as binary label maps. All metrics were calculated using MATLAB v. 2017a (Mathworks Inc., Natick, MA) using in-house programs. Reporting of multiple metrics is required for accurate characterization of data and comparison to previous results [18]. We chose to use metrics that fall under different categories of characterizing observer agreement: descriptive metrics, spatial or overlap metrics, and statistical metrics [18]. The descriptive and spatial metrics used the first contouring session for analysis [19]. The statistical methodology for comparing groups for each metric is described in the statistical section. For the descriptive metrics, we compared the volumes of the contours and the coefficient of variation (CV). The mean, median, standard deviation, and range of the volume contoured across observers for each patient and both groups were calculated. The CV was calculated for each patient and is defined as the standard deviation of the volume across observers normalized by the average volume across observers [20].

We used three spatial measures to assess differences in contours between observers: the conformity index (CI), the generalized conformity index ( $CI_{gen}$ ), and the distance between centers of mass (dCOM). The CI is a simple measure of overlap and is defined as [10]:

$$CI_{ij} = \frac{v_i \cap v_j}{v_i \cup v_j} \quad (2.1)$$

where  $v_i$  and  $v_j$  are a pair of observers and  $v$  is the volume of the contour. It has a value between 0 and 1 where 1 indicates perfect agreement. For each patient, CI was calculated between all pairs (10 pairs) and averaged across observers [21] and the groups statistically compared.

The  $CI_{gen}$  can be used to compare any number of observers simultaneously and is unbiased by the number of observers included [21]. It is defined as:

$$CI_{gen} = \frac{\sum_{pairsij}(v_i \cap v_j)}{\sum_{pairsij}(v_i \cup v_j)} \quad (2.2)$$

where  $v_i$  and  $v_j$  are a pair of observers and  $v$  is the volume of the contours for those respective observers. It has the same limits as CI (0 to 1). We used the dCOM to determine if there tended to be any difference in systematic shifts between observers. For each patient, the dCOM was calculated for each pair and was averaged across observer and the groups were statistically compared.

Finally, we assessed inter- and intra-observer variability using a statistical methodology that results in two measures termed the reliability coefficients [19, 22–24]. This method allows for the concurrent assessment of inter- and intra-observer reliability by using at least two successive measurements by the same set of observers. In brief, this method ascribes portions of the total variance in the volume measurement to the patients, observers, and inter-/intra-observer random error. These variances are estimated using a two-way random analysis of variance (ANOVA) [23, 24]. We report the variance for each component. From the variances, the inter-observer ( $\rho_{inter}$ ) and intra-observer ( $\rho_{intra}$ ) reliability coefficients, defined as the proportion of the total volume variance ascribed to inter- and intra-observer effects, are reported and compared statistically. Values close to unity indicate perfect reliability.

In addition to the above metrics, we also attempted to quantify differences in the shape of

contours between groups. This was done by calculating the shape circularity (SC):

$$SC = \frac{\text{Area of Contour Slice}}{\text{Area of Bounding Circle}} \quad (2.3)$$

This method assumes more jagged contours will occupy less space of a bounding circle than a “simple” contour. We are interested in the most jagged contour for each patient. As such, this analysis worked as follows: 1) For each expert, for each patient, average ( $SC_{\text{avg}}$ ) and minimum ( $SC_{\text{min}}$ ) SC across all slices was recorded, 2) for each patient, the minimum (and range) across observers was calculated for each patient for  $SC_{\text{min}}$ . In addition, the average value across observers for each patient (and standard deviation of the average values) was calculated for both  $SC_{\text{avg}}$  and  $SC_{\text{min}}$ , 3) full and half dose groups were compared statistically.

### **Statistics**

Statistical analysis was performed using GraphPad Prism v. 6.01 (GraphPad Software, La Jolla, CA) except for the reliability coefficient analysis which was performed using SPSS v. 25 (SPSS, Inc, IBM, Armonk, NY, USA).

The descriptive, spatial and shape circularity were not normally distributed as determined by a Shapiro Wilks test and so a Mann-Whitney U was performed for comparison of the groups. For the reliability coefficients, we used a left-sided F-test with the methods outlined in Eliasziw et al. [24]. A p-level of 0.05 was used.

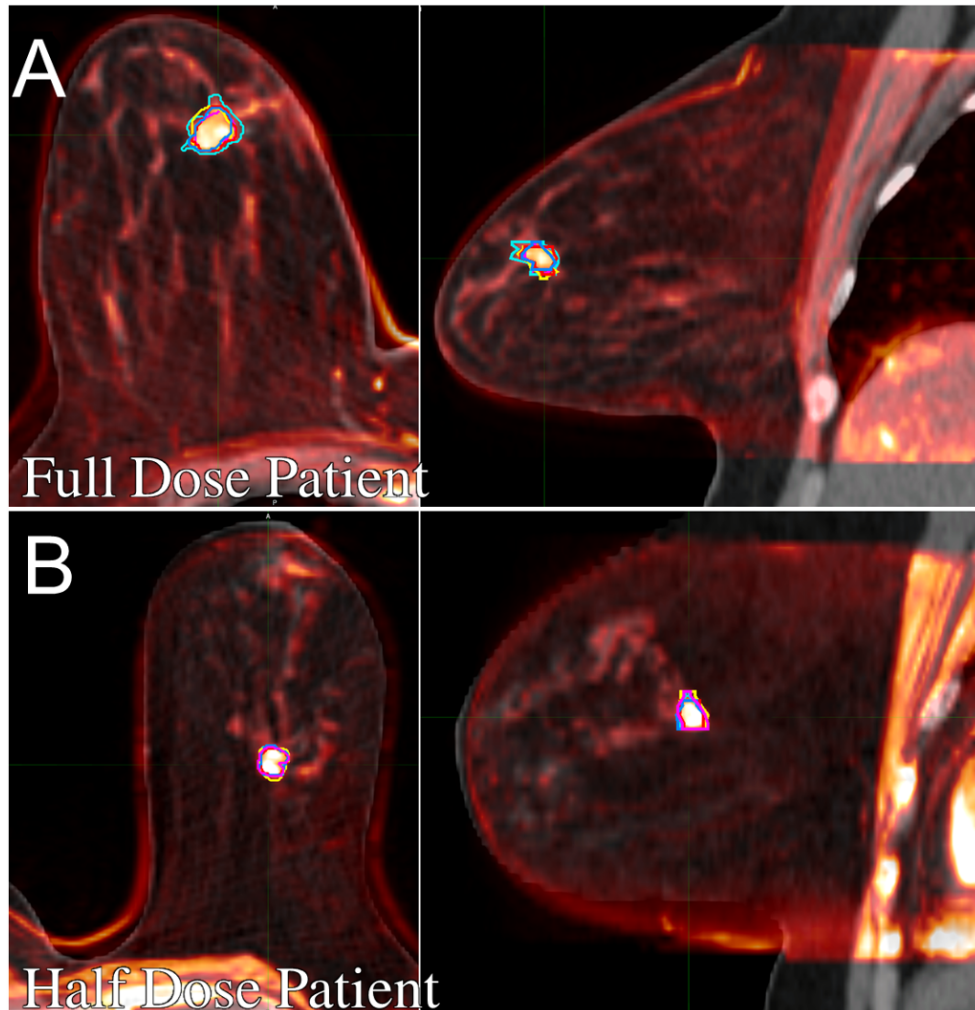
## 2.3 Results

Table 2.1 shows patient characteristics for each dose group. In the process of contouring, no expert missed the tumour for any patient, so each contour was included in the analysis. The average  $\pm$  standard error of the mean post-contrast image timepoint used for the full and half dose group was  $7.30 \pm 0.72$  minutes and  $7.44 \pm 0.76$  minutes respectively signifying essentially no difference in selection of the post-contrast image selected.

Figure 2.1a,b shows the GTV delineations of the five observers on the CT image (grayscale) fused with the CE-MRI image (heat-map) for a representative patient from the full dose group (Figure 2.1a) and the half dose group (Figure 2.1b). In terms of descriptive measures of variability, Figure 2.2a,b shows the volumes for each patient and Figure 2.2c,d shows the CV. There was no significant difference in the volume or CV for the GTV and CTV between the full and half dose group, though there tended to be a reduced volume in the half dose group compared to the full dose group as seen by both the mean (Figure 2.2a,b) and median values (median [range] of  $0.83 [0.37-3.63]$ cc and  $0.57 [0.29-3.33]$ cc for the full and half dose of the GTV,  $5.95 [3.79-15.01]$  and  $4.68 [3.34-13.65]$  for the full and half dose of the CTV). For the spatial metrics, there was a significant difference between the full and half dose group for  $CI_{gen}$ , but no significant difference between groups for CI and dCOM (Table 2.2).

From the statistical comparison, the variability was predominantly due to patients, though there was a larger variability due to inter-observer effects for the full dose group for both the GTV and CTV, though this difference was small. This is reflected in the reliability coefficients (Table 2.3), which show the full dose group had 10% less inter-observer reliability than the





**Figure 2.1:** 3D delineations of the five observers in the axial (left) and sagittal (right) planes for representative patients from the full dose group (A) and the half dose group (B).

half dose group. Following this, a sensitivity analysis was conducted to determine if there was a volume effect in the full dose group. Excluding the top four patients with the largest tumours in the full dose group and recalculating the inter-observer reliability coefficient resulted in a difference of the inter-observer reliability coefficient of approximately 5% between groups.

Shape circularity was used to determine how round a given contour was with higher values indicating rounder contours. We found there was a statistically significant increase in the  $SC_{min}$  for the half dose group compared to the full dose group with an average  $\pm$  standard deviation

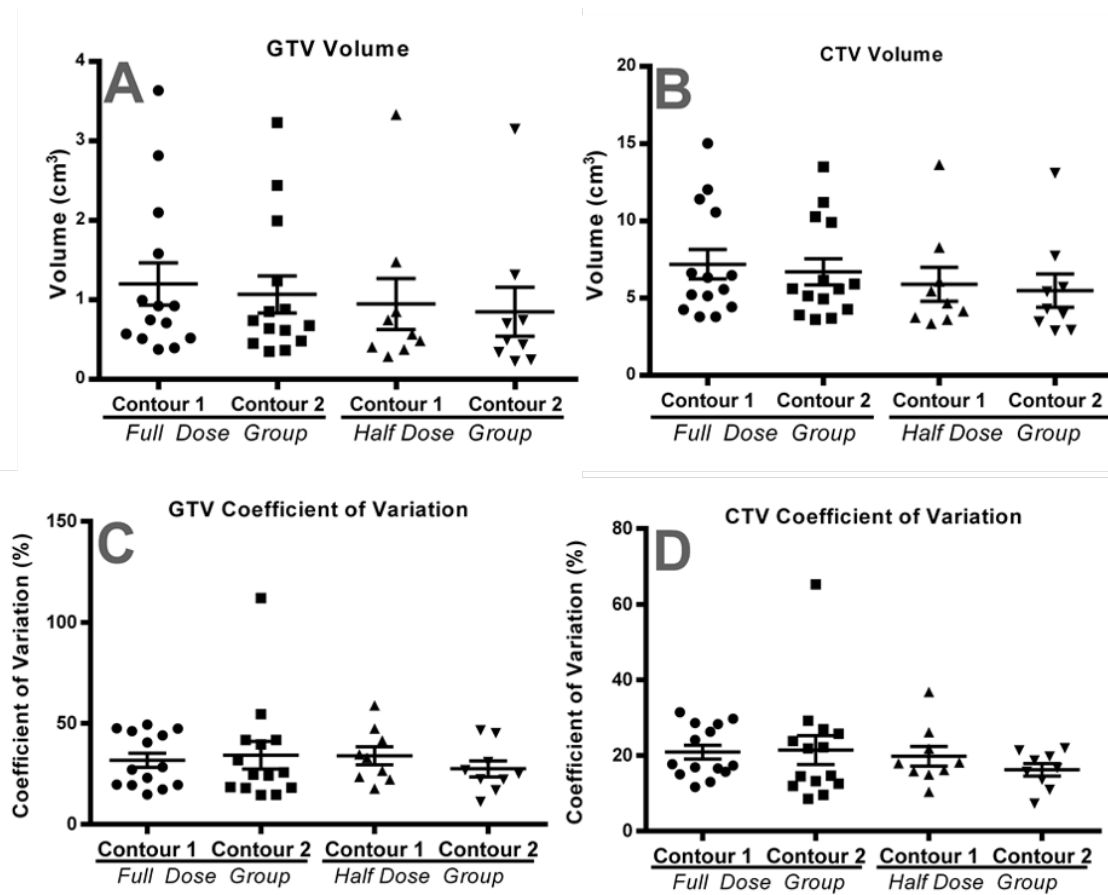


**Figure 2.2:** Column scatter plots of the volume measurements (A,B) and coefficient of variation (C,D) from each patient for the GTV (left column) and CTV (right column) for the full dose group and the half dose group. “Contour 1” and “Contour 2” represent the repeated session. The horizontal bar represents the mean volume across patients and the whiskers represent the standard error of the mean.

value of  $0.48 \pm 0.11$  for the full dose group and  $0.58 \pm 0.11$  for the half dose group for the case where the minimum was taken across observers, indicating contours were less round when using the full dose of contrast. However, there was no significant difference in the average value across all observers for the full dose group ( $0.5 \pm 0.07$ ) versus for the half dose group ( $0.57 \pm 0.08$ ,  $p = 0.7$ ) for  $SC_{\min}$ . For  $SC_{\text{avg}}$ , there was also no significant difference between the full dose group ( $0.60 \pm 0.04$ ) compared to the half dose group ( $0.63 \pm 0.02$ ,  $p = 0.07$ ).

**Table 2.2:** Summary of the spatial metrics CI,  $CI_{gen}$ , and dCOM and significance results comparing the first contouring session for both the GTV and CTV and both dose groups. Normality was violated for most cases and so a Mann-Whitney U test was used. No significance was found in comparing the two groups except for  $CI_{gen}$  though the difference in median value was small.

	Full Dose Group		Half Dose Group		P-Value
	Median	Range	Median	Range	
CI					
GTV	0.58	0.29 – 0.73	0.52	0.46 – 0.69	NS
CTV	0.73	0.60 – 0.81	0.72	0.65 – 0.79	NS
$CI_{gen}$					
GTV	0.61	0.49 – 0.62	0.66	0.61 – 0.69	SIG
CTV	0.73	0.65 – 0.74	0.78	0.74 – 0.79	SIG
dCOM (mm)					
GTV	1.23	0.45 – 2.09	1.24	0.37 – 2.30	NS
CTV	1.46	0.49 – 2.66	1.14	0.46 – 2.09	NS

## 2.4 Discussion

Over the past decade, there has been a large increase in the use of MRI scanning for radiation treatment planning, particularly in the case where soft-tissue contrast is highly desirable. Accurate localization for neoadjuvant radiotherapy or screening requires the use of a GBCA as these lesions are often difficult to localize using CT alone. Due to the finding of long-term retention in brain and bone for gadolinium-based contrast agents, if it is possible to reduce the dose of GBCA to a patient without affecting tumour delineation, then it is imperative we do so. This study showed that it is feasible to reduce the dose of contrast given to early stage breast cancer patients while not affecting both the inter- and intra-observer variability.

Apart from tumour volume delineation, CE-MRI is finding increased use in the clinical workflow for patients [25]. For example, studies have found that it has strong potential as a tool

**Table 2.3:** Inter- and intra-observer reliability coefficients for volume measurements from 5 observers and 1 repetition (2 contour sessions) for both the GTV and CTV

		Reliability Coefficients (%)		
		Full	Half	P-value
$\rho_{inter}$	GTV	82.84	91.97	0.002
	CTV	80.41	91.13	0.001
$\rho_{intra}$	GTV	89.94	95.94	0.103
	CTV	89.19	95.62	0.105

for selecting patients best suited for conserving therapies as well as a screening tool [26, 27]. If CE-MRI is to be used more routinely, reducing the dose of GBCA is an important way to mitigate the deposition in brain and bone [11]. In the context of screening, it is reassuring that even in the half dose group, no targets were missed, especially since tumours included in this study were small (Figure 2.2 a,b).

Regarding the reliability coefficients, an inter-observer reliability  $> 0.6$  implies a substantial agreement and an intra-observer reliability  $> 0.8$  implies an almost perfect agreement [22]. Importantly, using a half dose of GBCA still maintained this threshold i.e., using a half dose of contrast does not alter the inter- or intra-observer variability compared to using a full dose of GBCA.

There is scant literature on observer agreement in the setting of neoadjuvant target volume delineation. In comparing CI and  $CI_{gen}$  reported here to those previous studies, it is important to note that CI and  $CI_{gen}$  are sensitive to the overall volume of the contour [10] which makes comparing to traditional whole-breast contouring studies difficult. In any case, the values of CI for both the GTV and CTV are well within reported ranges [6, 10].

The shape circularity assessment was used to try and account for the better inter-observer

agreement in the half-dose group compared to the full dose group as assessed by  $CI_{gen}$  (Table 2.3) and the reliability coefficients - which showed a 5% increase in the half dose group after the sensitivity analysis was performed. This metric was able to detect differences between groups (using the minimum across observers) when using the slice with the maximum deviation from a circle (minimum SC value). However, averaging across observers and slices resulted in only a trend to significance, most likely due to inadequate sample size and sensitivity of the metric as it is non-specific and only assess deviation from a circle. There may be other metrics more sensitive to differences in shapes between groups.

Furthermore, other factors not considered here that may affect contour variability should be investigated. For example, the use of a heatmap for the overlaid MRI and its window/level was mostly arbitrary which will add a systematic bias to the absolute tumour volume contoured, but because the same expert set the window/level, should not have a large impact on the systematic bias of the gross target volume delineation. However, it may be more appropriate to set the window/level of the MRI based on some characteristic of the signal intensity or to overlay subtraction images (a post-contrast image – a pre-contrast image). However, doing so requires good intra-imaging session registration to avoid motion artifacts and this is not currently being done clinically at our centre. In addition, there may be a confounding effect due to different injection flow rates of the GBCA [28]. Finally, providing additional MRI sequences or imaging modalities (PET) as additional information may be beneficial.

One other notable limitation was that the data was unpaired. This makes absolute comparison between groups difficult since patient biological variability becomes a confounding factor. Furthermore, it does not allow us to make any conclusions on the accuracy of the tumour volume delineated which would require confirmation with pathological specimens. In

addition, our sample size was small, though larger than other studies investigating contouring effects [10, 18].

MRI-guided radiotherapy is showing increasing promise for screening and APBI techniques, though due to recent findings concerning the deposition of contrast agents in brain in bone, it is important we minimize exposure of patients to these contrast agents. The results presented here suggest it is possible to reduce the dose of contrast agent delivered to patients without significantly affecting the efficacy to delineate the volume. Further studies are needed to examine the accuracy of the volumes delineated using a half dose of gadolinium-based contrast agents. The results of this study have prompted our center to reduce the dose of gadolinium in all patients enrolled in the SIGNAL trial.

## 2.5 Bibliography

- [1] S. Darby, P. McGale, C. Correa, C. Taylor, R. Arriagada, M. Clarke, D. Cutter, C. Davies, M. Ewertz, J. Godwin, R. Gray, L. Pierce, T. Whelan, Y. Wang, R. Peto, K. Albain, S. Anderson, R. Arriagada, W. Barlow, J. Bergh, J. Bliss, M. Buyse, D. Cameron, E. Carrasco, M. Clarke, C. Correa, A. Coates, R. Collins, J. Costantino, D. Cutter, J. Cuzick, S. Darby, N. Davidson, C. Davies, K. Davies, A. Delmestri, A. Di Leo, M. Dowsett, P. Elphinstone, V. Evans, M. Ewertz, R. Gelber, L. Gettins, C. Geyer, A. Goldhirsch, J. Godwin, R. Gray, C. Gregory, D. Hayes, C. Hill, J. Ingle, R. Jakesz, S. James, M. Kaufmann, A. Kerr, E. MacKinnon, P. McGale, T. McHugh, L. Norton, Y. Ohashi, S. Paik, H. C. Pan, E. Perez, R. Peto, M. Piccart, L. Pierce, K. Pritchard, G. Pruneri, V. Raina, P. Ravdin, J. Robertson, E. Rutgers, Y. F Shao, S. Swain, C. Taylor, P. Valagussa, G. Viale, T. Whelan, E. Winer, Y. Wang, and W. Wood, “Effect of radiotherapy after breast-conserving surgery on 10-year recurrence and 15-year breast cancer death: Meta-analysis of individual patient data for 10 801 women in 17 randomised trials,” *The Lancet*, vol. 378, pp. 1707–1716, nov 2011.
- [2] M. S. Jawad, C. Shah, J. B. Wilkinson, M. Wallace, C. K. Mitchell, J. Wobb, G. S. Gustafson, D. S. Brabbins, I. S. Grills, and P. Y. Chen, “Seven-Year Outcomes Following Accelerated Partial Breast Irradiation Stratified by ASTRO Consensus Groupings,” in *American Journal of Clinical Oncology: Cancer Clinical Trials*, vol. 40, pp. 483–489, 2017.
- [3] T. J. Whelan, D. H. Kim, and J. Sussman, “Clinical Experience Using Hypofractionated

Radiation Schedules in Breast Cancer,” *Seminars in Radiation Oncology*, vol. 18, no. 4, pp. 257–264, 2008.

- [4] J. S. Haviland, J. R. Owen, J. A. Dewar, R. K. Agrawal, J. Barrett, P. J. Barrett-Lee, J. Dobbs, P. Hopwood, P. A. Lawton, B. J. Magee, J. Mills, S. Simmons, M. A. Sydenham, K. Venables, J. M. Bliss, and J. R. Yarnold, “The UK Standardisation of Breast Radiotherapy (START) trials of radiotherapy hypofractionation for treatment of early breast cancer: 10-year follow-up results of two randomised controlled trials,” [www.thelancet.com/oncology](http://www.thelancet.com/oncology), 2013.
- [5] M. Palta, S. Yoo, J. D. Adamson, L. R. Prosnitz, and J. K. Horton, “Preoperative single fraction partial breast radiotherapy for early-stage breast cancer,” *International Journal of Radiation Oncology Biology Physics*, vol. 82, pp. 37–42, jan 2012.
- [6] T. J. Yang, R. Tao, P. H. Elkhuizen, C. Van Vliet-Vroegindeweij, G. Li, and S. N. Powell, “Tumor bed delineation for external beam accelerated partial breast irradiation: A systematic review,” *Radiotherapy and Oncology*, vol. 108, pp. 181–189, aug 2013.
- [7] E. Weiss and C. F. Hess, “The Impact of Gross Tumor Volume (GTV) and Clinical Target Volume (CTV) Definition on the Total Accuracy in Radiotherapy,” *Strahlentherapie und Onkologie*, vol. 179, pp. 21–30, jan 2003.
- [8] C. W. Hurkmans, J. H. Borger, B. R. Pieters, N. S. Russell, E. P. M. Jansen, and B. J. Mijnheer, “Variability in target volume delineation on CT scans of the breast,” *International Journal of Radiation Oncology Biology Physics*, vol. 50, pp. 1366–1372, aug 2001.



- [9] K. Guidolin, M. Lock, B. Yaremko, N. Gelman, S. Gaede, A. Kornecki, V. Moiseenko, J. Cao, L. Scott, and M. Brackstone, "A phase II trial to evaluate single-dose stereotactic body radiation therapy (SBRT) prior to surgery for early-stage breast carcinoma: SIGNAL (stereotactic image-guided neoadjuvant ablative radiation then lumpectomy) trial," *Journal of Radiation Oncology*, vol. 4, no. 4, pp. 423–430, 2015.
- [10] M. D. den Hartogh, M. E. P. Philippens, I. E. van Dam, C. E. Kleynen, R. J. H. A. Tersteeg, R. M. Pijnappel, A. N. T. J. Kotte, H. M. Verkooijen, M. A. A. J. van den Bosch, M. van Vulpen, B. van Asselen, and H. D. van den Bongard, "MRI and CT imaging for preoperative target volume delineation in breast-conserving therapy," *Radiation oncology (London, England)*, vol. 9, p. 63, feb 2014.
- [11] E. Kanal and M. F. Tweedle, "Residual or Retained Gadolinium: Practical Implications for Radiologists and Our Patients," *Radiology*, vol. 275, pp. 630–634, jun 2015.
- [12] V. Gulani, F. Calamante, F. G. Shellock, E. Kanal, and S. B. Reeder, "Gadolinium deposition in the brain: summary of evidence and recommendations," 2017.
- [13] E. Medicines Agency, "EMA's final opinion confirms restrictions on use of linear gadolinium agents in body scans Recommendations conclude EMA's scientific review of gadolinium deposition in brain and other tissues,"
- [14] H. Canada, "Information Update - New safety information on injectable gadolinium-based contrast agents used in MRI scans Report a Concern," no. 613, 2017.
- [15] FDA, "FDA warns that gadolinium-based contrast agents ( GBCAs ) are retained in the body ; requires new class warnings," pp. 1–4, 2017.

- [16] J. C. Patrick, R. Terry Thompson, A. So, J. Butler, D. Faul, R. Z. Stodilka, S. Yartsev, F. S. Prato, and S. Gaede, “Technical Note: Comparison of megavoltage, dual-energy, and single-energy CT-based  $\mu$ -maps for a four-channel breast coil in PET/MRI,” *Medical Physics*, vol. 44, pp. 4758–4765, sep 2017.
- [17] G. J. M. Parker, C. Roberts, A. Macdonald, G. A. Buonaccorsi, S. Cheung, D. L. Buckley, A. Jackson, Y. Watson, K. Davies, and G. C. Jayson, “Experimentally-derived functional form for a population-averaged high-temporal-resolution arterial input function for dynamic contrast-enhanced MRI,” *Magnetic Resonance in Medicine*, vol. 56, no. 5, pp. 993–1000, 2006.
- [18] I. Fotina, C. Lütgendorf-Caucig, M. Stock, R. Pötter, and D. Georg, “Critical discussion of evaluation parameters for inter-observer variability in target definition for radiation therapy,” *Strahlentherapie und Onkologie*, vol. 188, no. 2, pp. 160–167, 2012.
- [19] Z. B. Popović and J. D. Thomas, “Assessing observer variability: a user’s guide,” *Cardiovascular Diagnosis and Therapy*, vol. 7, pp. 317–324, jun 2017.
- [20] G. Altorjai, I. Fotina, C. Lütgendorf-Caucig, M. Stock, R. Pötter, D. Georg, and K. Dieckmann, “Cone-Beam CT-Based Delineation of Stereotactic Lung Targets: The Influence of Image Modality and Target Size on Interobserver Variability,” *International Journal of Radiation Oncology\*Biology\*Physics*, vol. 82, pp. e265–e272, feb 2012.
- [21] E. Kouwenhoven, M. Giezen, and H. Struikmans, “Measuring the similarity of target volume delineations independent of the number of observers,” *Physics in Medicine and Biology*, vol. 54, pp. 2863–2873, may 2009.

- [22] S. L. Breen, J. Publicover, S. De Silva, G. Pond, K. Brock, B. O’Sullivan, B. Cummings, L. Dawson, A. Keller, J. Kim, J. Ringash, E. Yu, A. Hendler, and J. Waldron, “Intraobserver and Interobserver Variability in GTV Delineation on FDG-PET-CT Images of Head and Neck Cancers,” *International Journal of Radiation Oncology Biology Physics*, vol. 68, no. 3, pp. 763–770, 2007.
- [23] J. R. Mitchell, S. J. Karlik, D. H. Lee, M. Eliasziw, G. P. Rice, and A. Fenster, “The variability of manual and computer assisted quantification of multiple sclerosis lesion volumes,” *Medical Physics*, vol. 23, pp. 85–97, jan 1996.
- [24] M. Eliasziw, S. L. Young, M. G. Woodbury, and K. Fryday-Field, “Statistical methodology for the concurrent assessment of interrater and intrarater reliability: using goniometric measurements as an example.” *Physical therapy*, vol. 74, pp. 777–88, aug 1994.
- [25] F. Sardanelli, C. Boetes, B. Borisch, T. Decker, M. Federico, F. J. Gilbert, T. Helbich, S. H. Heywang-Kö Brunner, W. A. Kaiser, M. J. Kerin, R. E. Mansel, L. Marotti, L. Martincich, L. Mauriac, H. Meijers-Heijboer, R. Orecchia, P. Panizza, A. Ponti, A. D. Purushotham, P. Regitnig, M. Rosselli, D. Turco, F. Thibault, and R. Wilson, “Magnetic resonance imaging of the breast: Recommendations from the EUSOMA working group,” *European Journal of Cancer*, vol. 46, pp. 1296–1316, 2010.
- [26] N. Paudel, K. P. Bethke, L. C. Wang, J. B. Strauss, J. P. Hayes, and E. D. Donnelly, “Impact of breast MRI in women eligible for breast conservation surgery and intra-operative radiation therapy,” *Surgical Oncology*, vol. 27, no. 1, pp. 95–99, 2018.

- [27] C. K. Kuhl, K. Strobel, H. Bieling, C. Leutner, H. H. Schild, and S. Schrading, “Supplemental Breast MR Imaging Screening of Women with Average Risk of Breast Cancer,” *Radiology*, vol. 283, no. 2, pp. 361–370, 2017.
- [28] E. Lancelot, J. Froehlich, O. Heine, and P. Desché, “Effects of gadolinium-based contrast agent concentrations (0.5 M or 1.0 M) on the diagnostic performance of magnetic resonance imaging examinations: Systematic review of the literature,” *Acta Radiologica*, vol. 57, no. 11, pp. 1334–1343, 2016.

## Chapter 3

### 3 The effect of registration on voxel-wise Tofts model parameters and uncertainties from DCE-MRI of early stage breast cancer patients using 3DSlicer

#### 3.1 Introduction

Dynamic contrast enhanced (DCE) MRI is a valuable tool for aiding clinical diagnosis and treatment monitoring of breast cancer. A series of  $T_1$  weighted images are acquired with at least one image prior to the injection of a contrast agent and several images following the injection. From these images, signal enhancement curves are generated either voxel-by-voxel or using the average signals over regions of interest and can be analysed using pharmacokinetic models, empirical models or qualitative methods [1]. Pharmacokinetic model analysis can provide physiological information and has many advantages over using empirical models or qualitative methods [1]. One of the most popular models in breast cancer is the Toft's model [2] from which one can extract two parameters: (1)  $K^{\text{trans}}$  which is the extravasation rate of contrast from the vasculature to the extra-cellular, extra-vascular space, and (2)  $v_e$  which represents the fraction of tissue volume occupied by the extra-vascular, extracellular space. To be physically realistic, measured  $v_e$  values must be at least  $< 1$ .

Inter-scan patient movement during the DCE image series can degrade pharmacokinetic analysis of the curves unless image registration is applied [3, 4]. While several papers [5–10]

have reported on image registration in breast imaging, very little information has been provided on the influence of registration in pharmacokinetic analysis, particularly the Tofts model. Shafer et al. [9], using in-house developed software, investigated the influence of registration on the root-mean-square-error (RMSE) of the data around a fitted curve based on an early version of the Tofts model using an analytic AIF that has shown poor performance compared to more contemporary AIFs [11]. In addition, the assessment of the kinetic fit was based on a voxel averaging method rather than voxel-by-voxel, the registration was only in two dimensions through a single slice of the tumour, and their data set only had 5-6 images with a time resolution of  $> 60$ s on a 1.5T MRI scanner. To our knowledge the influence of registration on measured pharmacokinetic parameters and their uncertainties has not been investigated and not with more recently measured AIF.

While image registration is an important step in pharmacokinetic analysis the computation time can be quite long. This is especially true for deformable registration based on mutual information which is a cost function known to be robust in the presence of local contrast changes such as in the case of DCE [6, 7, 9, 12–14]. Long computation times could be a burden particularly for large clinical studies. For example, our analysis procedure is presently applied for the SIGNAL trial [15] in which registration of 29 DCE images per patient will be performed for more than 100 patients. To reduce computation time for registration, it is possible to use a random subset of the image voxels rather than the full image [16]. Here we use the term percent sampling (PS) to refer to the fraction of voxels sampled within the region of interest. To our knowledge, the effect of under-sampling the image for estimation of the cost metric and its effect on the performance of the kinetic model analysis has not previously been explored quantitatively in the context of DCE-MRI.

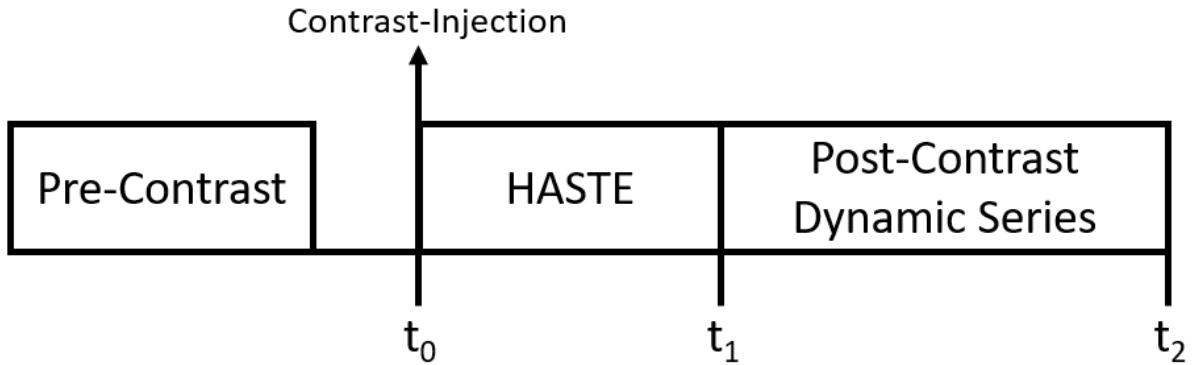


**Figure 3.1:** Timing diagram for the image acquisition. Following contrast injection ( $t_0$ ) a HASTE series is acquired for 15.54 or 18.5 s ( $t_1$ ) which is immediately followed by the post-contrast dynamic contrast enhanced series until approximately 10 minutes has elapsed ( $t_2$ ).

In this paper, we consider the influence of fully 3D deformable registration on pharmacokinetic model voxel-by-voxel analysis using the Tofts model and the AIF from Parker et al. [17] in the context of breast DCE with full breast coverage and relatively high time resolution (18-20 s). In particular, we assess the influence of this registration on parameter values and their uncertainties and on the extent of physically reasonable values for  $v_e$ . We also investigate the efficacy of reduced percent sampling as a means of reducing computation time. In addition to demonstrating the importance of registration on pharmacokinetic analysis in breast DCE and the efficacy of reduced sampling, our results provide the reader with estimates of parameter precision for voxel-by-voxel analysis that can be achieved at 3T with moderate spatial resolution and relatively acquisition times. Finally, we specifically chose an open-source program (3DSlicer) that can be applied for image registration with only minimal time and resource investment for implementation.

## 3.2 Materials and Methods

DCE-MRI breast images were acquired from 13 patients with early stage breast cancer [15]. The median (range) of patient ages was 60 (52-77). The studies were performed on a 3T-PET/MRI system (Siemens Biograph mMR) with a four channel breast coil [18]. Patients were positioned prone to mimic the radiotherapy delivery position with the ipsilateral arm above their head and the contralateral arm at their side.

Figure 3.1 shows a timing diagram for the image acquisition. Three-dimensional fat suppressed fast low angle shot (FLASH) images were acquired with  $TR = 4.1\text{ms}$ ,  $T_E = 1.5\text{ms}$ , flip angle =  $15^\circ$ . The images had a spatial resolution of  $1.0 \times 2.1 \times 2.1$  mm interpolated to  $1.0 \times 1.0 \times 1.2$  mm, a field of view of  $38 \times 38$  cm and a slab thickness of 13.4 cm. Using 6/8 Partial Fourier in two directions and an acceleration factor of two the acquisition time per image was 18-20 s. Each DCE series included one pre-contrast image and 28 post-contrast images following Gadovist (0.1 mMol/kg) injection. Single slice half-Fourier acquisition single-shot turbo spin echo (HASTE) images positioned at the arch of the aorta were acquired for approximately 18-19 seconds immediately following the injection and before the first post contrast DCE image. Time resolution for the HASTE images was 0.37s for nine patients and 0.49s for the remaining four.

Images were registered using the BRAINSFit module [19] of 3DSlicer v4.5.1 [20] on a PC running Windows 10 (16GB ram, Intel i7-4790 CPU). Unless otherwise specified, default values for this version were used for other parameters related to the registration as these have been tuned by the authors of the BRAINSFit over the course of development and generally



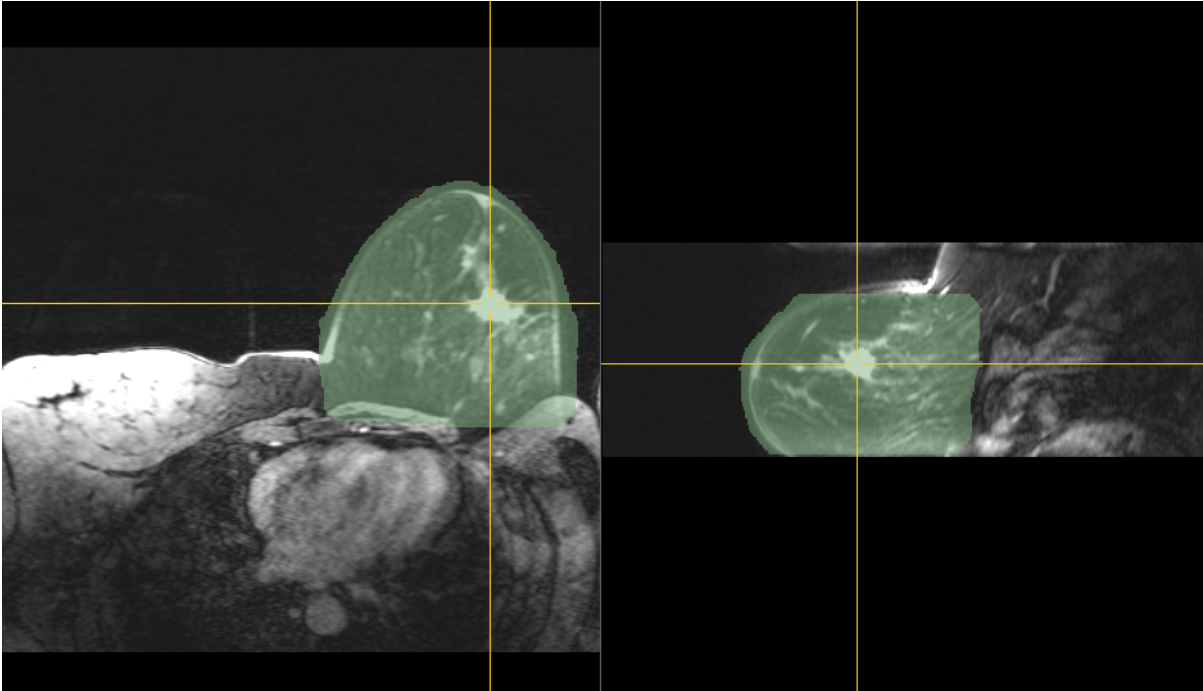


**Figure 3.2:** An example mask defined over a patients' breast for the DCE-MRI intra-session image registration

provide good registrations [19].

The key steps in the registration process are as follows: A mask was defined over the affected breast, extending to approximately the pectoral muscle and dilated to include air around the skin (Figure 3.2). This mask defined the region from where voxels were sampled for estimation of the cost function. The interpolator used for the registration and for final generation of the image output was a windowed sinc. All images were registered to the middle post-contrast image (i.e., the 14th time point) [3, 9, 21]. To correct for gross movement, we performed a sequential affine transformation i.e., a rigid, a rigid + scale, a rigid + scale + skew, and finally an affine. The result of this was used as input into the BSpline registration. The BSpline registration had an approximately 2cm isotropic grid spacing as we were not expecting large deformations.

Registrations were performed using each of the following values of PS: 100%, 20%, 5%,

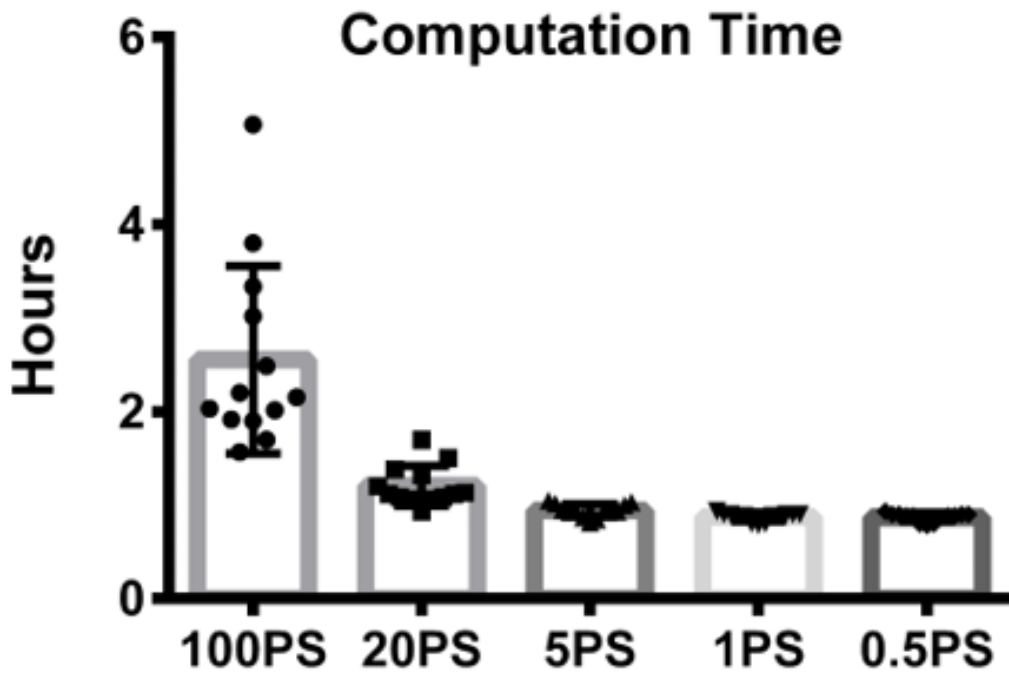


**Figure 3.3:** Computation times for all PS cases for registering the series of 29 images (1 pre-contrast and 28 post-contrast). The bar represents the mean and the whiskers represent the standard deviation. Each point represents a patient.

1% and 0.5%. The PS here refers to the percentage of voxels within the mask used for determination of the cost function and were sampled randomly. The computation time was recorded for each registration procedure applied to each patient. This investigation was performed to determine if registration performance could be maintained while decreasing computation time.

Analysis of the unregistered and registered DCE-MRI data was performed with MATLAB 2016b using in-house code. Otsu's segmentation method [22] was applied to automatically segment the tumour using the last post contrast image. Voxels included in the contour were fit using the Levenberg-Maquardt algorithm (see fit function in matlab or [23]), voxel by voxel, using the Tofts kinetic model [24] and a population derived AIF [17]. The time at which the contrast agent arrived at the arch of the aorta on the HASTE images was considered as a lower

bound on the time of arrival of the contrast bolus to the tumour. Model fitting was applied to voxels that met the following conditions: 1) the signal enhancement was 1.5 times that of the pre-contrast value at any point in the time series and 2) the maximum value of the signal curve did not occur at the last time point. Parameter values of  $K^{\text{trans}}$  (forward rate constant) and  $v_e$  (fractional volume of extracellular, extravascular space) were generated for each voxel within the segmented region of each patient and each registration condition. In addition, the standard errors for  $K^{\text{trans}}$  and  $v_e$  ( $\sigma K^{\text{trans}}$  and  $\sigma v_e$ ) and the root-mean-square-error (RMSE) of the fit were determined for each voxel where the standard error here refers to 1/4 of the 95% confidence interval width. In addition, the percentage of voxels where  $v_e > 1$ , was reported since values of  $v_e > 1$  are unphysical. In addition, to provide an estimate of the error in  $v_e$  ( $\sigma v_e$ ), we calculated the percentage of voxels where  $\sigma v_e$  exceeded four defined thresholds: 0.1, 0.2, 0.5, and 1.

Statistical analysis of parameters included the following: for  $K^{\text{trans}}$ ,  $\sigma K^{\text{trans}}$ , and the RMSE, the median and 90th percentile over all voxels in each of the segmented tumours was calculated for unregistered images and registered images at each PS level. For  $v_e$  and  $\sigma v_e$  we also computed the median values but did not consider 90th percentile metric because for some voxels the extracted values were extremely high. Instead, we determined the number of voxels with  $v_e > 1$  (unphysical) and the number of voxels with  $\sigma v_e > \text{four threshold values (0.1, 0.2, 0.5 and 1.0)}$ . A Wilcoxon sign-rank test was used to compare the values of each parameter obtained from unregistered images to those obtained from registered images. A comparison of values obtained using PS = 100% to values obtained with the lower percent sampling (PS) was also carried out with this test. Theoretically, 100PS should result in the best registration performance.

**Table 3.1:** Results of statistical comparisons between parameters obtained with unregistered images versus registered images (at any PS level). Dashed lines indicate where comparison metrics were not assessed

	Median	90th Percentile	Number of voxels above threshold
$K^{\text{trans}}$	NS	SC	—
$\sigma K^{\text{trans}}$	SR	SR	—
$v_e$	NS	—	SR ( $v_e > 1.0$ )
$\sigma v_e$	SR	—	SR for median and $\sigma v_e > 0.1, 0.2, 0.5, 1.0$
RMSE	SR	SR	—

SR = significant reduction, SC = significant change, NS = no significant difference (all at  $p \leq 0.05$ )

### 3.3 Results

Figure 3.3 shows the mean and standard deviation of the total computation time across patients. Using a lower PS values ( $\leq 20\text{PS}$ ) lead to a dramatic reduction in the computation times compared to 100PS, as well as a large reduction in the standard deviation. However, using 1 or 0.5PS did not further decrease computation time compared to 5PS and so they were omitted from further analysis. For the following paragraphs, Table 3.1 shows a summary of the comparisons of each PS case to the unregistered data.

The top row of Figure 3.4 shows representative parametric maps for  $K^{\text{trans}}$  for 100PS, 20PS, 5PS, and the unregistered case for a representative patient. Large differences can be seen comparing all the PS cases to the unregistered case with subtle variations between PS cases. Figure 3.5 illustrates values of  $K^{\text{trans}}$  and its uncertainty ( $\sigma K^{\text{trans}}$ ) extracted from unregistered and registered images from all PS groups. Comparing unregistered images to registered images (all PS), differences in the uncertainty metrics (median and 90th percentile  $\sigma K^{\text{trans}}$ ) and in the 90th percentile  $K^{\text{trans}}$  are large for some patients and were found to be statistically significant

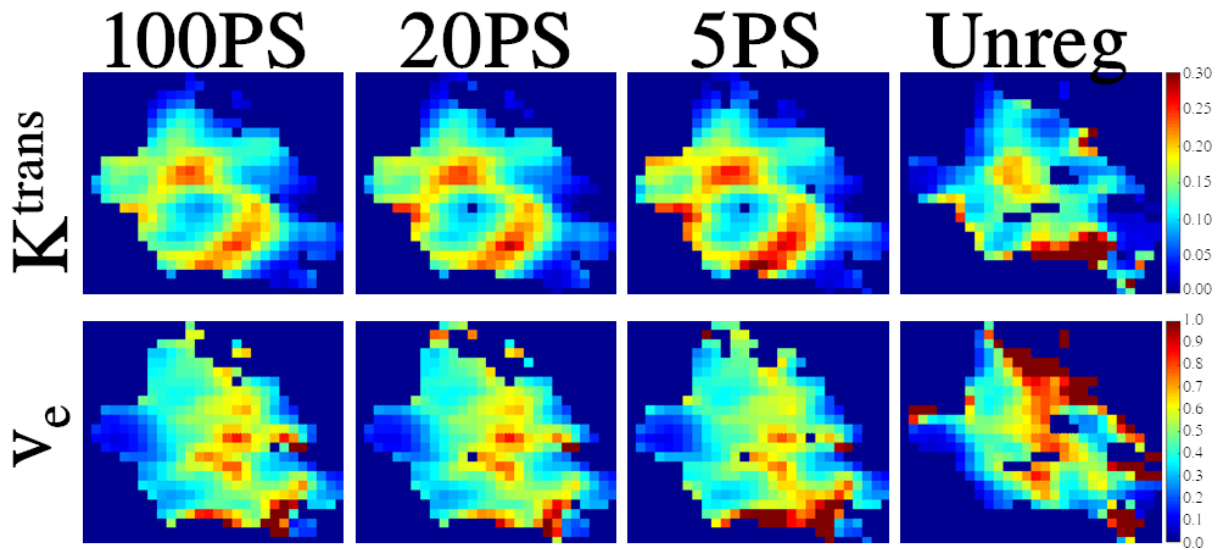


**Figure 3.4:** Parametric maps for  $K^{\text{trans}}$  (top row) and  $v_e$  (bottom row) across percent sampling cases for a representative patient.

(Table 3.1). However, the differences in the median value of  $K^{\text{trans}}$  between unregistered and registered images (all PS) was not significant, though a relatively large difference can be seen for one subject. Any variation in these metrics (Figure 3.5) between PS groups appear to be small. The only difference that was significantly worse than 100PS (but small) was between the median of  $\sigma K^{\text{trans}}$  for 5PS.

The bottom row of Figure 3.4 shows representative parametric maps for  $v_e$  for 100PS, 20PS, 5PS, and the unregistered case for a representative patient. Large differences can be seen comparing all the PS cases to the unregistered case, particularly around the periphery. There are subtle variations between PS cases, again, mostly around the periphery. Figure 3.6 illustrates differences in  $v_e$  and its uncertainty ( $\sigma v_e$ ) extracted from unregistered versus registered images from all PS groups. Comparing unregistered images to registered images (all PS), differences in the uncertainty metrics (median  $\sigma v_e$ ; number of voxels with  $\sigma v_e > 0.2$ ) and in the percentage of unphysical voxels ( $v_e > 1$ ) are large for some patients and were found to be statistically significant (Table 3.1). Significant differences were also found between the

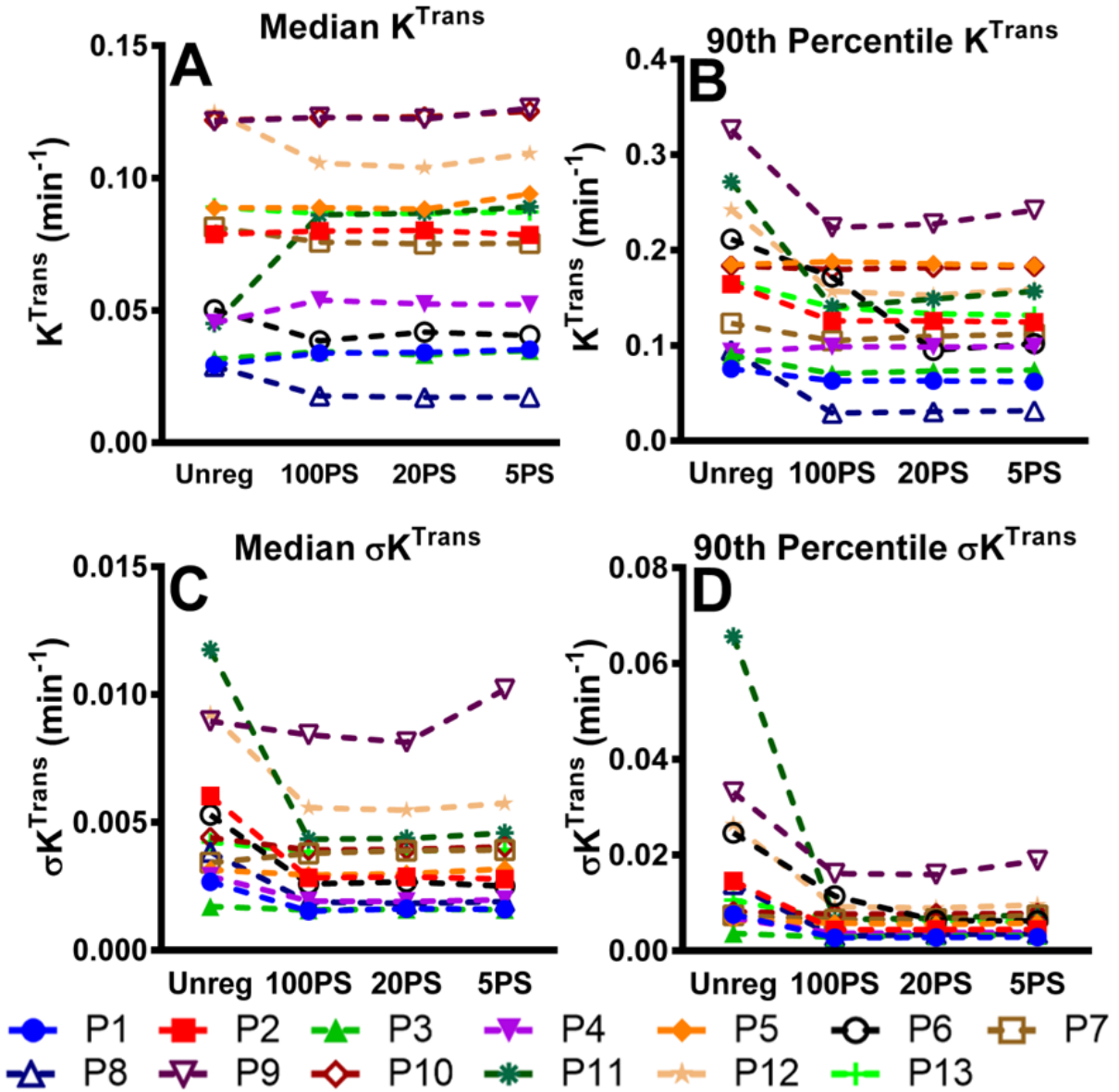


**Figure 3.5:** Median and 90th percentile of  $K^{trans}$  (A,B) and  $\sigma K^{trans}$  (C,D) for unregistered and registered images (all PS cases). Median and 90th percentile was determined over all voxels in the segmented region for each patient. P # represents patient number.

number of voxels with  $\sigma v_e >$  other thresholds tested (Table 3.1, Figure 3.7). However, any difference of the median value of  $v_e$  between unregistered and registered images (all PS) was not significant. Any variation in these metrics (Figure 3.6) between PS cases appear to be small and none were statistically significant.

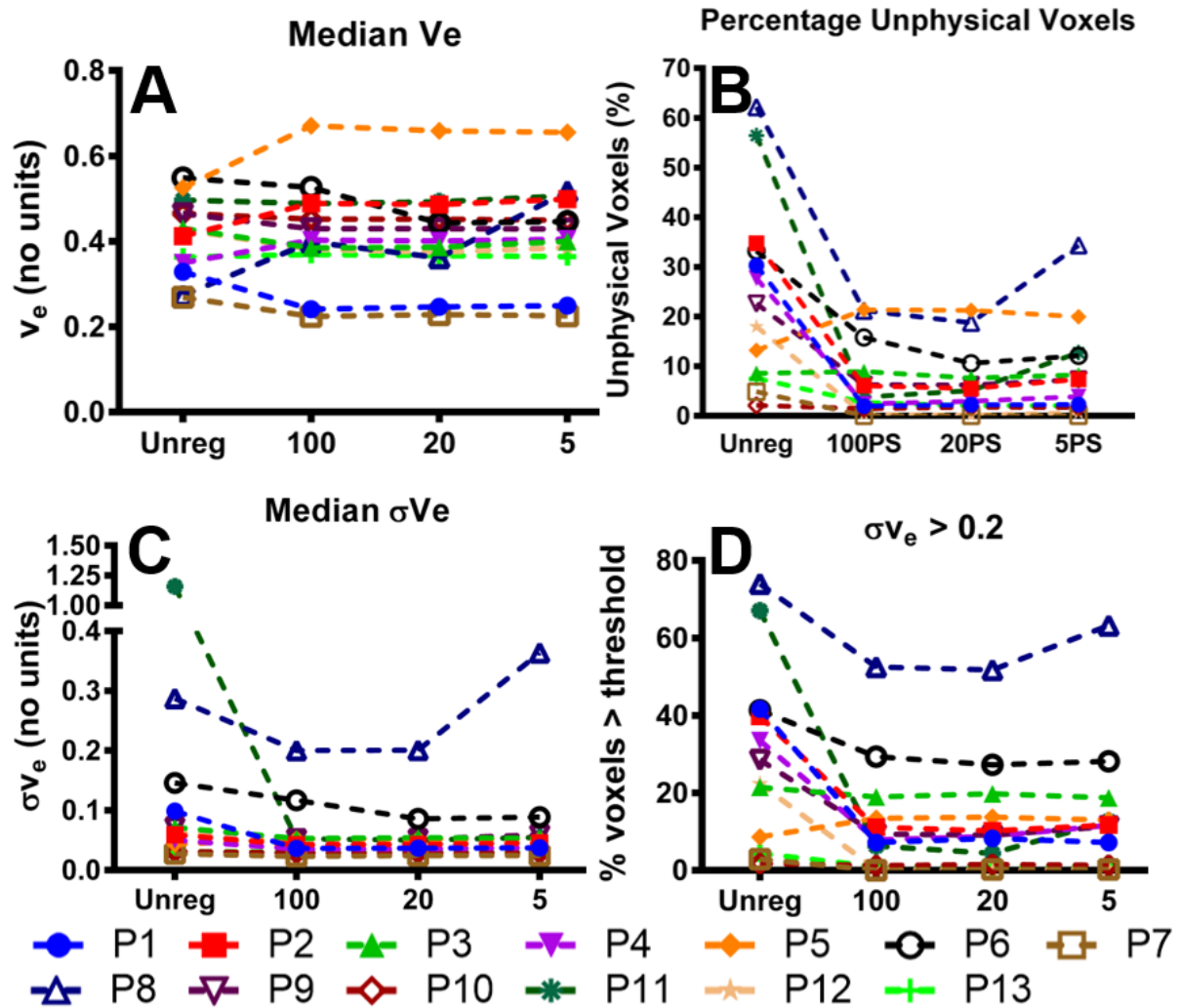


**Figure 3.6:** Median  $v_e$  (A), percentage of voxels with  $v_e > 1$  (B), median  $\sigma v_e$  (C), and percentage of voxels where  $\sigma v_e$  exceeded 0.2 (D) for unregistered and registered images (all PS). P # represents patient number. The median values were determined over all voxels in the segmented region for each patient.

Finally, for the RMSE, the median (Figure 3.8a) and 90th percentile (Figure 3.8b) of all PS cases were significantly reduced compared to the unregistered data (Table 3.1). There were no significant differences between 20 or 5PS compared to 100PS but there was a trend to significance in both the median ( $p = 0.07$ ) and 90th percentile ( $p = 0.08$ ) when comparing 5PS and 100PS.

### 3.4 Discussion

In this study, we investigated the influence of registration on DCE-MRI kinetic parameters in the context of breast imaging using freely available and well tested open source software (3DSlicer and BRAINSFit). We are the first to show how registration can reduce the number of unphysical voxel fits and improve the precision of voxel-wise parameter estimates which is important in the context of assessing response to therapy using these kinetic parameters. In addition, we showed how registration time can be reduced by a factor of two using a smaller sampling of voxels (20PS). To our knowledge, no other publication has quantitatively explored the influence of registration or of reduced PS on the parameter values ( $K^{\text{trans}}$ ,  $v_e$ ) or their associated uncertainties ( $\sigma K^{\text{trans}}$ ,  $\sigma v_e$ ) in DCE-MRI of breast cancer [25].

The methods presented here are being implemented in the SIGNAL clinical trial as mentioned in the introduction [15]. The DCE-MRI imaging protocol has a relatively high time resolution compared to many previous studies [2] that investigate DCE-MRI of breast cancer, with full breast coverage. For our clinical trial, registration of 29 DCE images will be performed for more than 100 patients and in some cases twice per patient as they will be receiving a post-treatment DCE-MRI session. As such, reducing the computation time for registration will be important for maintaining timely assessment of image data. As DCE-MRI improves and 3D images can be acquired faster (which results in more images), ways to mitigate registration time will become even more important. PS reduction is one strategy; however, reducing PS below 5PS had little if any affect on computation time.

In this study we found that registration reduced the number of voxels for which the fitting



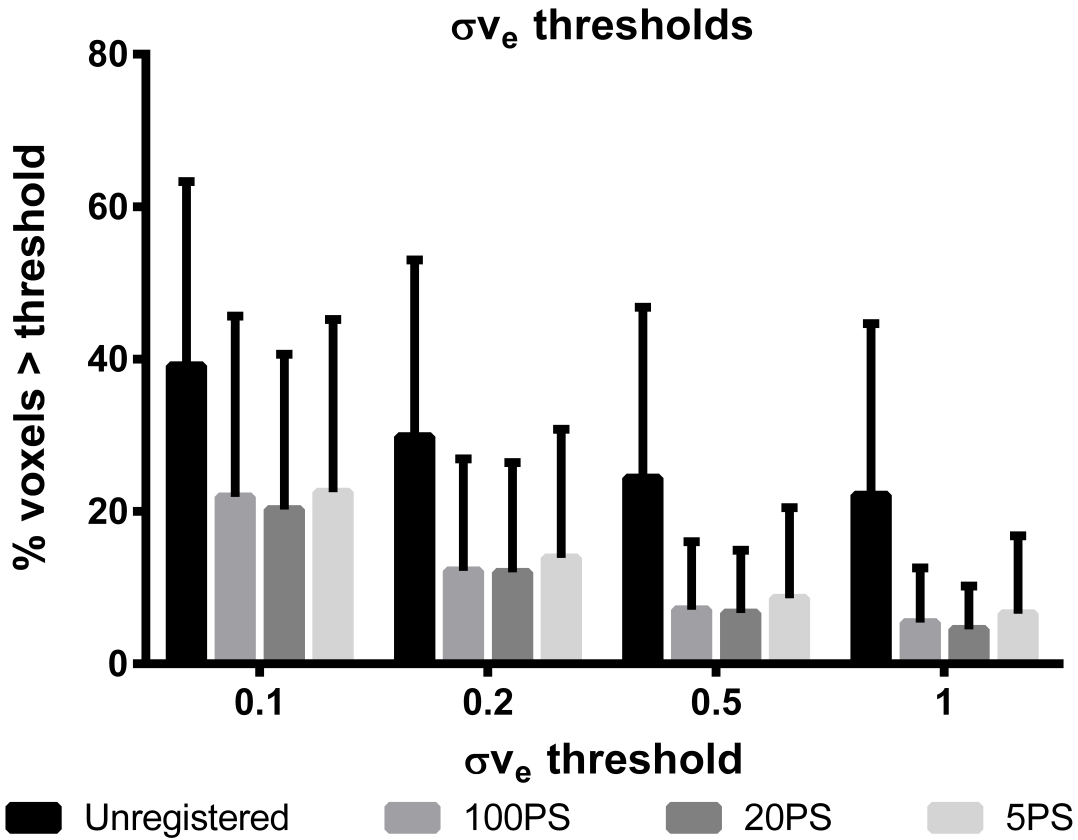


**Figure 3.7:** Percentage of voxels having  $\sigma v_e$  above four different thresholds for different registration cases (PS values). The bar presents the mean across patients and the error bars represent the standard deviation.

with the Tofts model led to an unphysical value for  $v_e$  ( $v_e > 1$ ). This has not been widely considered. However, even with registration the number of such voxels was still substantial (Figure 3.6b) for some patient image sets. From our observation and a previous report [26], this tends to occur for signal enhancement curves that have not reached the washout phase by the end of the dynamic series. For this study, post contrast imaging covered a time period of approximately 10 minutes, but this may not be sufficient for estimating  $v_e$  of voxels near the edges of the tumour which were typically still enhancing by the end of the series. It is unclear how these unphysical voxels affect  $K^{\text{trans}}$  estimation, particularly since the fitting procedure is

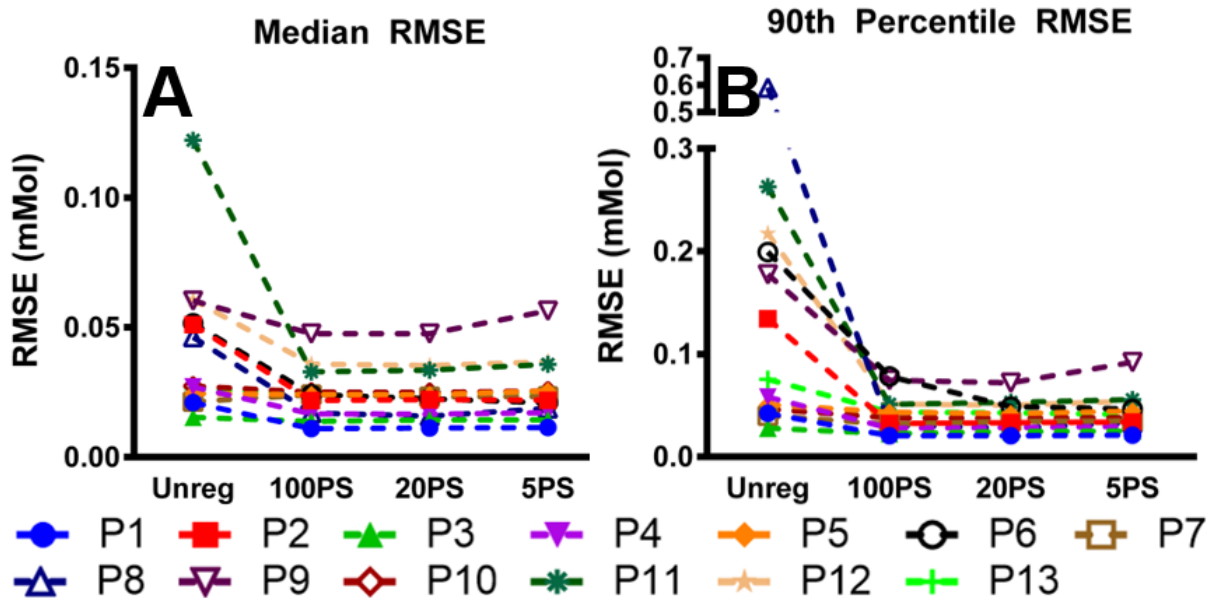


**Figure 3.8:** The median (A) and 90th percentile (B) of the model fit RMSE for unregistered and all PS cases for each patient. Median and 90th percentile were determined over all voxels in the segmented region for each patient. P # represents patient number.

highly non-linear.

Previous studies investigating DCE-MRI registration have not typically reported the effect of registration on model fit parameter outputs and associated uncertainties for the Tofts model. Interestingly, the median values of the parameter values ( $K^{\text{trans}}$  and  $v_e$ ) seemed relatively insensitive to slight misalignment of images as indicated by the lack of significant difference comparing unregistered and registered data. In voxel-by-voxel analysis which has the potential to show the spatial heterogeneity of the tumour, we can see that there is a significant effect of registration on the overall distribution of parameter values as indicated by the significant change in the 90th percentile of  $K^{\text{trans}}$  and the reduction of unphysical voxels. Further, we can significantly reduce the uncertainty in the parameter values ( $\sigma K^{\text{trans}}$ ,  $\sigma v_e$ ), increasing confidence in voxel-wise analysis without a large cost in computation time when a lower PS is used.

Interestingly, there was a large amount of variation in  $K^{\text{trans}}$  (Figure 3.6a,b) and  $v_e$  (Figure 3.7a) across patients even though all patients were early stage breast cancer patients with a similar age [15]. However, this is most likely reflective of the highly heterogeneous nature of tumours. In comparison to reported ranges in the literature for studies that used the Tofts model, it is not uncommon for there to be variability between patients [27, 28].

Our data also demonstrates a large variation between patients regarding the extent to which the RMSE (Figure 3.8), uncertainty metrics ( $\sigma K^{\text{trans}}$ ,  $\sigma v_e$ , Figure 3.3c,d and Figure 3.5c,d) and number of voxels with unphysical values of  $v_e$  (Figure 3.6b) were reduced by image registration. In fact, there are some patients for which any such changes are quite small, suggesting that these patients are able to remain essentially motionless during the 10 min DCE acquisition. It may be that the uncertainty values obtained for these patients might represent an estimate of the potentially achievable fit uncertainties with our protocol (3T, four channel breast coil, 4.4  $\mu\text{L}$  voxel volume, full breast coverage in approximately 20 s). There are several potential factors that could influence the extent to which patients can remain motionless, including level of comfort in this radiotherapy position (one arm overhead), a position that could be challenging for older patients, as those in our study (median (range) of age: 60 (52-77)).

In terms of limitations, we had a small number of patients included in this study. We did not exhaustively investigate all registration parameters and there may be ways to further reduce computation time, such as removing parts of the registration steps before the BSpline i.e., it may only be necessary to perform a rigid and affine before the BSpline without any intermediate steps.

Finally, we would like to highlight the fact that patients included were imaged prone with their ipsilateral arm raised above their head to mimic the radiotherapy position. Typical breast

MR imaging studies are performed with the patient prone with both arms at their side. This difference may affect the extent of patient motion compared to our study. However, the application of MRI for image guidance and treatment monitoring of radiotherapy for breast cancer treatment is growing which means there is a need for MRI studies involving breast patients imaged in the radiotherapy delivery position to assess ways to mitigate motion as well as quantify the optimal imaging and analysis techniques.

### 3.5 Conclusion

In this paper, we investigated the influence of registration using 3DSlicer and percent sampling on extracted kinetic parameters and their uncertainties. Registration resulted in significant reductions in the number of unphysical fits ( $v_e > 1$ ), the standard error (uncertainty) of parameter estimation, as well as the root-mean-square error of the model fit. We also found that computation time could be reduced by a factor of two by using reduced sampling (20PS) without detectable changes in these measures. This computation time reduction will help to improve the practicality of analyzing DCE images with high time resolution for large clinical studies and for studies that include a large number of post-contrast injection images.

### 3.6 Bibliography

- [1] F. Khalifa, A. Soliman, A. El-Baz, M. Abou El-Ghar, T. El-Diasty, G. Gimel'farb, R. Ouseph, and A. C. Dwyer, "Models and methods for analyzing DCE-MRI: A review," *Medical Physics*, vol. 41, p. 124301, nov 2014.
- [2] C.-H. Wang, "Review of treatment assessment using DCE-MRI in breast cancer radiation therapy," *World Journal of Methodology*, vol. 4, p. 46, jun 2014.
- [3] A. Lausch, *Nonrigid Registration of Dynamic Contrast-Enhanced MRI data using Motion Informed Intensity Corrections*. PhD thesis, Western University, 2011.
- [4] M. L. Giger, N. Karssemeijer, and J. A. Schnabel, "Breast Image Analysis for Risk Assessment, Detection, Diagnosis, and Treatment of Cancer," *Annu. Rev. Biomed. Eng.*, vol. 15, pp. 327–57, 2013.
- [5] I. D. Dmitriev, C. E. Loo, W. V. Vogel, K. E. Pengel, and K. G. A Gilhuijs, "Fully automated deformable registration of breast DCE-MRI and PET/CT," *Phys. Med. Biol.*, vol. 58, pp. 1221–1233, feb 2013.
- [6] E. R. Denton, L. I. Sonoda, D. Rueckert, S. C. Rankin, C. Hayes, M. O. Leach, D. L. Hill, and D. J. Hawkes, "Comparison and evaluation of rigid, affine, and nonrigid registration of breast MR images.," *Journal of computer assisted tomography*, vol. 23, no. 5, pp. 800–5, 1999.

- [7] A. Hill, A. Mehnert, S. Crozier, and K. McMahon, "Evaluating the accuracy and impact of registration in dynamic contrast-enhanced breast MRI," *Concepts in Magnetic Resonance Part B: Magnetic Resonance Engineering*, vol. 35, no. 2, pp. 106–120, 2009.
- [8] D. Rueckert, L. I. Sonodaa, E. Denton, S. Rankina, C. Hayesc, M. Leachc, D. Hula, and D. J. Hawkesa, "Comparison and evaluation of rigid and non-rigid registration of breast MR images," in *Medical Imaging 99*, vol. 3661, pp. 78–88, 1999.
- [9] S. Schäfer, U. Preim, S. Glaßer, B. Preim, and K. Tönnies, "Local similarity measures for lesion registration in DCE - MRI of the breast," *Annals of the BMVA*, vol. 2011, no. 3, pp. 1–13, 2011.
- [10] A. L. Martel, M. S. Froh, K. K. Brock, D. B. Plewes, and D. C. Barber, "Evaluating an optical-flow-based registration algorithm for contrast-enhanced magnetic resonance imaging of the breast," *Physics in Medicine and Biology*, vol. 52, pp. 3803–3816, jul 2007.
- [11] D. K. Woolf, N. J. Taylor, A. Makris, N. Tunariu, D. J. Collins, S. P. Li, M.-L. Ah-See, M. Beresford, and A. R. Padhani, "Arterial input functions in dynamic contrast-enhanced magnetic resonance imaging: which model performs best when assessing breast cancer response?," *The British journal of radiology*, vol. 89, p. 20150961, jul 2016.
- [12] D. Rueckert, L. I. Sonoda, C. Hayes, D. L. Hill, M. O. Leach, and D. J. Hawkes, "Non-rigid registration using free-form deformations: application to breast MR images.," *IEEE Transactions on Medical Imaging*, vol. 18, no. 8, pp. 712–21, 1999.

- [13] C. Tanner, J. a. Schnabel, D. L. G. Hill, D. J. Hawkes, A. Degenhard, M. O. Leach, D. R. Hose, M. a. Hall-Craggs, and S. I. Usiskin, "Quantitative evaluation of free-form deformation registration for dynamic contrast-enhanced MR mammography," *Medical Physics*, vol. 34, no. 4, p. 1221, 2007.
- [14] V. V. Chebrolu, D. Shanbhag, R. Bedair, S. Gupta, P. Hervo, S. Reid, F. Gilbert, A. Patterson, M. Graves, and R. Mullick, "Impact of Non-rigid Motion Correction on Pharmacokinetic Analysis for Breast Dynamic Contrast-Enhanced MRI," *Proceedings 23rd Scientific Meeting, International Society for Magnetic Resonance in Medicine*, p. 668, 2015.
- [15] K. Guidolin, M. Lock, B. Yaremko, N. Gelman, S. Gaede, A. Kornecki, V. Moiseenko, J. Cao, L. Scott, and M. Brackstone, "A phase II trial to evaluate single-dose stereotactic body radiation therapy (SBRT) prior to surgery for early-stage breast carcinoma: SIGNAL (stereotactic image-guided neoadjuvant ablative radiation then lumpectomy) trial," *Journal of Radiation Oncology*, vol. 4, no. 4, pp. 423–430, 2015.
- [16] H. J. Johnson and M. M. McCormick, "The ITK Software Guide Book 1 : Introduction and Development Guidelines Fourth Edition Updated for ITK version 4 . 8," 2015.
- [17] G. J. M. Parker, C. Roberts, A. Macdonald, G. A. Buonaccorsi, S. Cheung, D. L. Buckley, A. Jackson, Y. Watson, K. Davies, and G. C. Jayson, "Experimentally-derived functional form for a population-averaged high-temporal-resolution arterial input function for dynamic contrast-enhanced MRI," *Magnetic Resonance in Medicine*, vol. 56, no. 5, pp. 993–1000, 2006.

- [18] J. C. Patrick, R. Terry Thompson, A. So, J. Butler, D. Faul, R. Z. Stodilka, S. Yartsev, F. S. Prato, and S. Gaede, “Technical Note: Comparison of megavoltage, dual-energy, and single-energy CT-based  $\mu$ -maps for a four-channel breast coil in PET/MRI,” *Medical Physics*, vol. 44, pp. 4758–4765, sep 2017.
- [19] H. J. Johnson, G. Harris, K. Williams, N. K. Williams, and K. Williams, “BRAINSFit: Mutual Information Rigid Registrations of Whole-Brain 3D Images, Using the Insight Toolkit,” Tech. Rep. 10, 2007.
- [20] A. Fedorov, R. Beichel, J. Kalpathy-Cramer, J. Finet, J.-C. Fillion-Robin, S. Pujol, C. Bauer, D. Jennings, F. Fennessy, M. Sonka, J. Buatti, S. Aylward, J. V. Miller, S. Pieper, and R. Kikinis, “3D Slicer as an image computing platform for the Quantitative Imaging Network.,” *Magnetic resonance imaging*, vol. 30, pp. 1323–41, nov 2012.
- [21] A. Melbourne, J. Hipwell, M. Modat, T. Mertzaniidou, H. Huisman, S. Ourselin, and D. J. Hawkes, “The effect of motion correction on pharmacokinetic parameter estimation in dynamic-contrast-enhanced MRI,” *Physics in Medicine and Biology*, vol. 56, no. 24, pp. 7693–7708, 2011.
- [22] N. Otsu, “A Threshold Selection Method from Gray-Level Histograms,” *IEEE Transactions on Systems, Man, and Cybernetics*, vol. 9, pp. 62–66, jan 1979.
- [23] MATLAB, “Least-Squares (Model Fitting) Algorithms - MATLAB & Simulink.”
- [24] P. Tofts, B. Gunnar, D. L. Buckley, J. L. Evelhoch, E. Henderson, M. V. Knopp, H. B. W. Larsson, T.-Y. Lee, N. A. Mayr, G. J. M. Parker, R. E. Port, J. Taylor, and R. M. Weisskoff, “Estimating kinetic parameters from dynamic contrast-enhanced T1-weighted MRI of a



- diffusable tracer: Standardized quantities and symbols,” *Journal of Magnetic Resonance Imaging*, vol. 10, no. 3, pp. 223–232, 1999.
- [25] C. A. Cuenod and D. Balvay, “Perfusion and vascular permeability: Basic concepts and measurement in DCE-CT and DCE-MRI,” *Diagnostic and Interventional Imaging*, vol. 94, pp. 1187–1204, dec 2013.
- [26] P. S. Tofts and G. J. Parker, “DCE-MRI: Acquisition and analysis techniques,” in *Clinical Perfusion MRI: Techniques and Applications* (P. Barker, X. Golay, and G. Zaharchuk, eds.), vol. 9781107013, pp. 58–74, Cambridge: Cambridge University Press, 2010.
- [27] C. Hayes, A. R. Padhani, and M. O. Leach, “Assessing changes in tumour vascular function using dynamic contrast-enhanced magnetic resonance imaging,” *NMR in Biomedicine*, vol. 15, pp. 154–163, apr 2002.
- [28] T. E. Yankeelov, M. Lepage, A. Chakravarthy, E. E. Broome, K. J. Niermann, M. C. Kelley, I. Meszoely, I. A. Mayer, C. R. Herman, K. McManus, R. R. Price, and J. C. Gore, “Integration of quantitative DCE-MRI and ADC mapping to monitor treatment response in human breast cancer : initial results,” *Magnetic Resonance Imaging*, vol. 25, pp. 1–13, jan 2007.

## Chapter 4

### **4 DCE-MRI assessment of response to neoadjuvant SABR in early stage breast cancer: Comparisons of single versus three fraction schemes and two different imaging time delays post-SABR**

#### **4.1 Introduction**

The current standard of breast conserving therapy for early stage breast cancer patients is a lumpectomy followed by whole breast radiotherapy delivered over 5-7 weeks [1]. This treatment time is prohibitively long for many patients [1, 2]. Accelerated partial breast irradiation (APBI) is being investigated to reduce treatment time by treating local to the tumour [3] while attempting to maintain the same efficacy as the current standard. The treatment volume can be further reduced by treating before surgery [4] allowing large doses to be delivered per fraction and facilitating the use of stereotactic ablative radiotherapy (SABR). With pre-surgical radiotherapy it becomes possible to use imaging to assess the physiological effects of the radiation and investigate potential tumour response biomarkers. Determination of tumour control at an early stage could potentially allow patient-specific radiotherapy adaption.

It has been shown that microvascular damage from radiotherapy plays a key role in tumour regression [5,6]. Dynamic contrast enhanced (DCE) MRI provides a means to assess microvasculature function and potential damage. Parameters extracted from DCE-MRI include the rate

at which a gadolinium contrast agent exits capillaries into the extracellular-extravascular space ( $K^{\text{trans}}$ ) and the volume of the extracellular, extravascular space ( $v_e$ ). Using these metrics we can non-invasively assess response to the SABR treatment [7].

Pre-clinical and clinical studies have demonstrated early vs late changes in tumour response parameters related to blood flow and vessel permeability. Early changes have been attributed to acute inflammatory reactions which can cause increased vessel permeability, and endothelial cell death within irradiated volumes [5, 6, 8]. Determination of the optimal time post-radiotherapy for DCE-based assessment of response without confounding acute effects remains an unanswered question.

In addition to the effect of high doses of radiation within the tumour it is important to consider the influence of irradiation on the surrounding tissue, which has been seldomly studied in humans. Pre-clinical studies have suggested there may exist a threshold dose (8-12 Gy) above which a cascade of events leads to endothelial apoptosis in normal vasculature [6, 9–12].

To our knowledge, only one study has investigated DCE-MRI after SABR in the context of breast cancer [13]. DCE-MRI parameters ( $K^{\text{trans}}$ ,  $v_e$ , area under enhancement curve) were quantified one week following single-fraction SABR (15, 18, or 21 Gy). Measurements were limited to region-of-interest enhancement curves (rather than voxel-wise curves) for the gross, clinical, and planning target volumes (GTV, CTV, PTV). However, no values of  $K^{\text{trans}}$  or  $v_e$  for the GTV, which most closely relates to the tumour region, were reported. Finally, the authors used an arterial input function proposed by Weinmann in 1984 [14] that has shown to have poor performance [15].

The purpose of the present study was twofold. First, we aimed to compare potential DCE-MRI measures of response obtained from early stage breast cancer patients at one-week post

SABR versus 2-3 weeks. This information is important in developing a protocol for monitoring SABR response as one would hope to monitor response as early as possible while avoiding potential confounding factors (e.g., inflammatory changes). Our second aim was to compare DCE-MRI measures obtained from patients exposed to single high dose (21Gy/1fraction) versus a fractionated scheme (30Gy/3fractions every other day). While these two schemes provide equivalent tumour cell killing according to the linear quadratic model and universal survival curves [2], we wanted 1) to verify that the two schemes lead to similar tumour response as assessed by DCE-MRI and 2) to determine if DCE-MRI measures are consistent with expectations that the fractionated scheme would lead to a differential effect in the surrounding tissue due to the higher biologically effective dose in the single fraction scheme in the surrounding tissue. To investigate the influence of SABR on tissue surrounding the tumour, the changes in enhancing tissue volume from pre to post-SABR were quantified. To investigate tumour response, we applied the Tofts pharmacokinetic model to assess pre to post-SABR changes within the tissue enhancing in the pre-SABR scan.

## 4.2 Methods

Figure 4.1 is a flowchart that summarizes the order of methods used to analyse the DCE-MRI data.

### 4.2.1 Patients

Images were acquired as part of a phase I/II clinical trial called SIGNAL [2]. Early stage breast cancer patients were treated with neoadjuvant SABR, and randomly assigned to either 21Gy/1

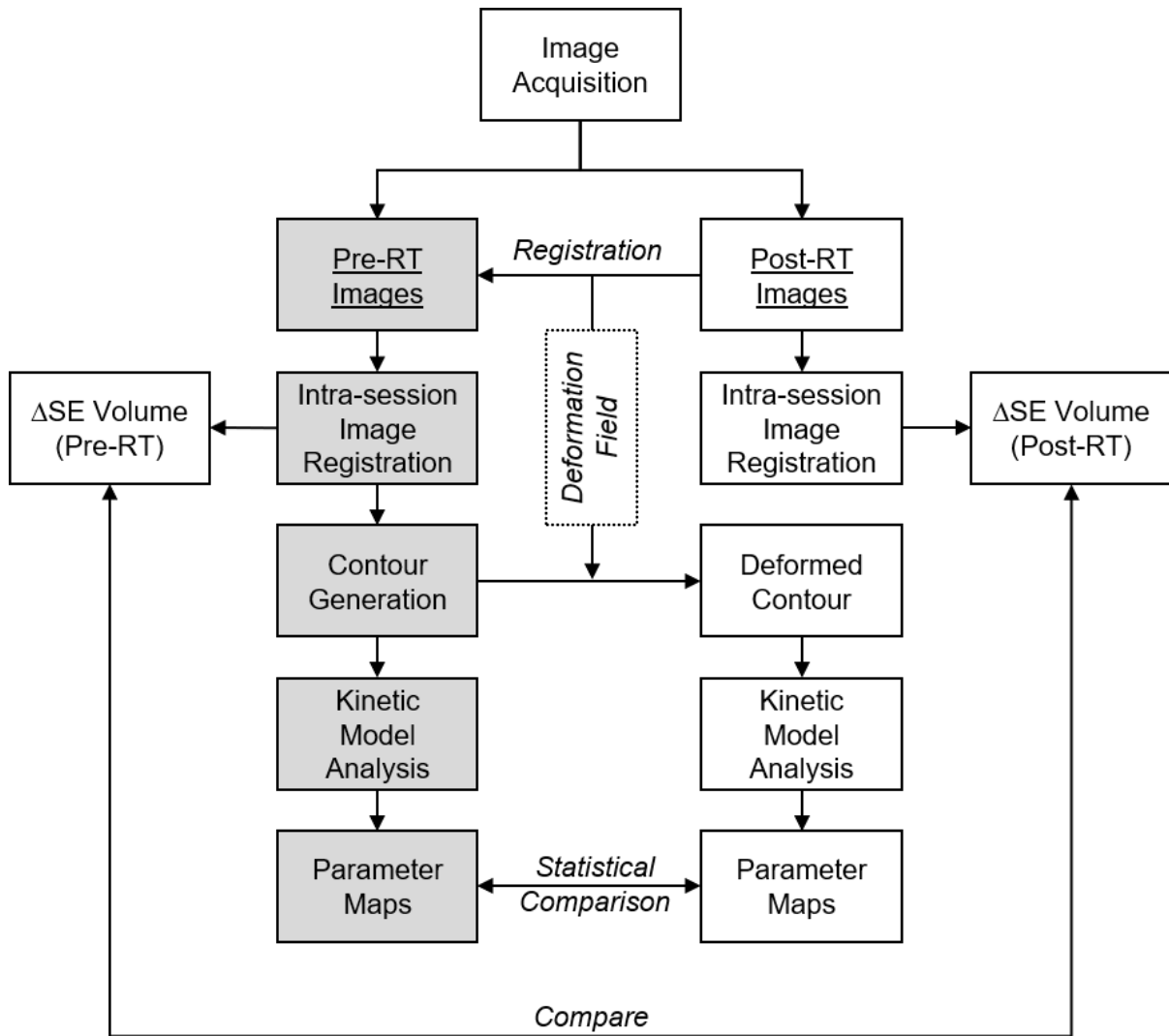


**Figure 4.1:** Flowchart outline image processing and analysis for this study. Two comparisons were performed, one between the signal enhancement volume changes, and a separate comparison between the parameters involved in the kinetic model analysis. The kinetic analysis was localized to tumour contours. RT = radiotherapy, SE = signal enhancement.

fraction or 30Gy/3 fractions every other day. A surgical clip was placed either adjacent to or within the tumour at the time of initial biopsy. All patients underwent an MRI scan prior to and following SABR, with the post-SABR as close to the lumpectomy as possible. Patients were categorized into three groups (Table 4.1) as follows: Group 1 patients received 21Gy/1 fraction with imaging scheduled to be as close as possible to one-week post-SABR. Group 2 and group 3 patients received 21Gy/1 fraction and 30Gy/3 fractions, respectively, with post-SABR MRI

**Table 4.1:** Study/patient information, image timing and SABR treatment scheme separated by group. Note that for the 3 fraction patients, imaging time post-treatment is the time delay from the conclusion of radiation therapy to the MRI scan.

	# Patients	Dose Scheme	Median (Range) Imaging Time Post-SABR (days)	Breast Affected	Mean Age
Group 1	5	21Gy/1FX	6 (6-7)	3L / 2R	72
Group 2	6	21Gy/1FX	16 (16-19)	3L / 3R	69
Group 3	6	30Gy/3FX	16 (15-18)	3L / 3R	69

FX = fraction, L / R = Left or right sided breast affected, SABR = stereotactic ablative radiotherapy

scans schedule to be as close to three weeks as possible.

## 4.2.2 Image Acquisition

Images were acquired on a Siemens Biograph mMR 3T-PET/MRI system (Siemens Medical, Erlangen, Germany) with a four channel prone breast coil [16]. Prior to contrast injection native  $T_1$  relaxation time ( $T_{10}$ ) maps were generated using the variable flip angle (VFA) method [17] for conversion of signal to concentration [7].  $B_1$  maps were acquired to determine the true flip angle for both  $T_{10}$  mapping and DCE-MRI [7]. Due to a scanner upgrade, two different sequences for  $B_1$  quantification were used- the Actual Flip Angle (AFI) [18] and the “slice-selective pre-conditioning RF pulse” (SS-Pre) [19] methods. Imaging parameters for both methods are provided in Table 4.2.  $T_{10}$  maps were reconstructed in MATLAB v. 2018a (Mathworks Inc., Natick, MA).

Three-dimensional fat suppressed fast low angle shot (FLASH) images were acquired with field of view = 38x38cm, slab thickness = 13.4cm, time of acquisition = 20s using 6/8 partial Fourier in two directions and an acceleration factor of two. The DCE series included a pre-contrast and 28-post gadobutrol (Gadavist®) contrast injection images using half a clinical

**Table 4.2:** Acquisition Parameters for MRI sequences used in this study.

Acquisition	Nominal FA	TR (ms)	TE (ms)	Spatial Resolution (mm)	Interpolated voxel size (mm)
HASTE	10°	489.6 / 521.4	1.16 / 1.36	1.4 x 2.0 x 5	1.4 x 1.4 x 5
DCE-MRI	15°	4.1	1.5	1.0 x 2.1 x 2.1	1.0 x 1.0 x 1.2
VFA (T1 map)	5 or 6 FAs (1° to 17°)	4.9 or 5.1	1.9 or 2.5	1.0 x 1.1 x 2.11 or 1.0 x 2.1 x 2.0	1 x 1 x 1.2 or 1.0 x 1.0 x 1.0
AFI B1 Map	50°	TR1 = 20 TR2 = 100	2.46	2.4 x 4.0 x 2.4	2.4 x 2.4 x 2.4
SS-Pre B1 Map	80°	10000	2	5.94 x 5.94 x 5	N/A

VFA = variable flip angle, AFI B1= actual flip angle B1 mapping sequence, SS-PRE B1 = slice-selective pre-conditioning RF pulse B1 mapping sequence

dose of 0.05 mmol/kg and an injection rate of 0.75ml/s. Immediately after injection but prior to post-contrast images, single slice HASTE image, positioned at the arch of the aorta were acquired for 18-19s.

### 4.2.3 Image Registration

To correct for intra-session motion, DCE images were deformably registered to the mid-time point post-contrast image using BRAINSFit [20] in 3DSlicer v4.8.0 [21] and Mattes mutual information as the similarity metric [22] (see chapter 3). To correct for patient movement between the B<sub>1</sub> and T<sub>10</sub> mapping, scans relative to the DCE-MRI, deformable registration was performed using MIM v6.8.5 (v6.8.0, MIM Software, Cleveland, USA) and its multi-modality metric [23, 24].

Following intra-session registration, a post- to pre-radiotherapy registration was performed. The post-radiotherapy, pre-contrast image was deformably registered to the pre-radiotherapy pre-contrast image (MIM v6.8.0, MIM Software, Cleveland, USA), creating a deformation

field linking the pre-radiotherapy space to the post-radiotherapy space.

#### **4.2.4 Analysis**

##### **Signal Enhancement Volume**

The purpose of this analysis was to compare the change in the absolute volume of enhancement between the pre- and post-radiotherapy setting. A 3D rectangular cuboid centered on the tumour and sized to encompass all visibly enhancing tissue (excluding skin) was manually drawn on the 9th post-contrast (3.3 minutes post-injection) DCE-MRI image in the pre-radiotherapy setting. The same sized cuboid was used for the post-radiotherapy data for a given patient. A signal enhancement map was calculated by dividing the 9th post-contrast DCE-MRI image by the pre-contrast image for both the pre-radiotherapy and post-radiotherapy data. Within the cuboid region, the signal enhancement volume  $\geq$  signal enhancement thresholds ranging from 1-5 with increments of 0.01 was calculated, generating threshold vs signal enhancement volume curves. The area under these curves (AUC) was calculated (higher values indicating greater volume of enhancement). The percent change from pre- to post-SABR was used to compare differences.

##### **Tumour Segmentation**

The tumour was automatically segmented in the pre-SABR DCE-MRI images. Figure 4.2A shows this process schematically. Initial filtering was performed using Otsu's segmentation method [25] on a subtraction image (last post-contrast – pre-contrast). Then, a k-means clustering algorithm using three clusters was applied using five features: 1-3) XYZ spatial position



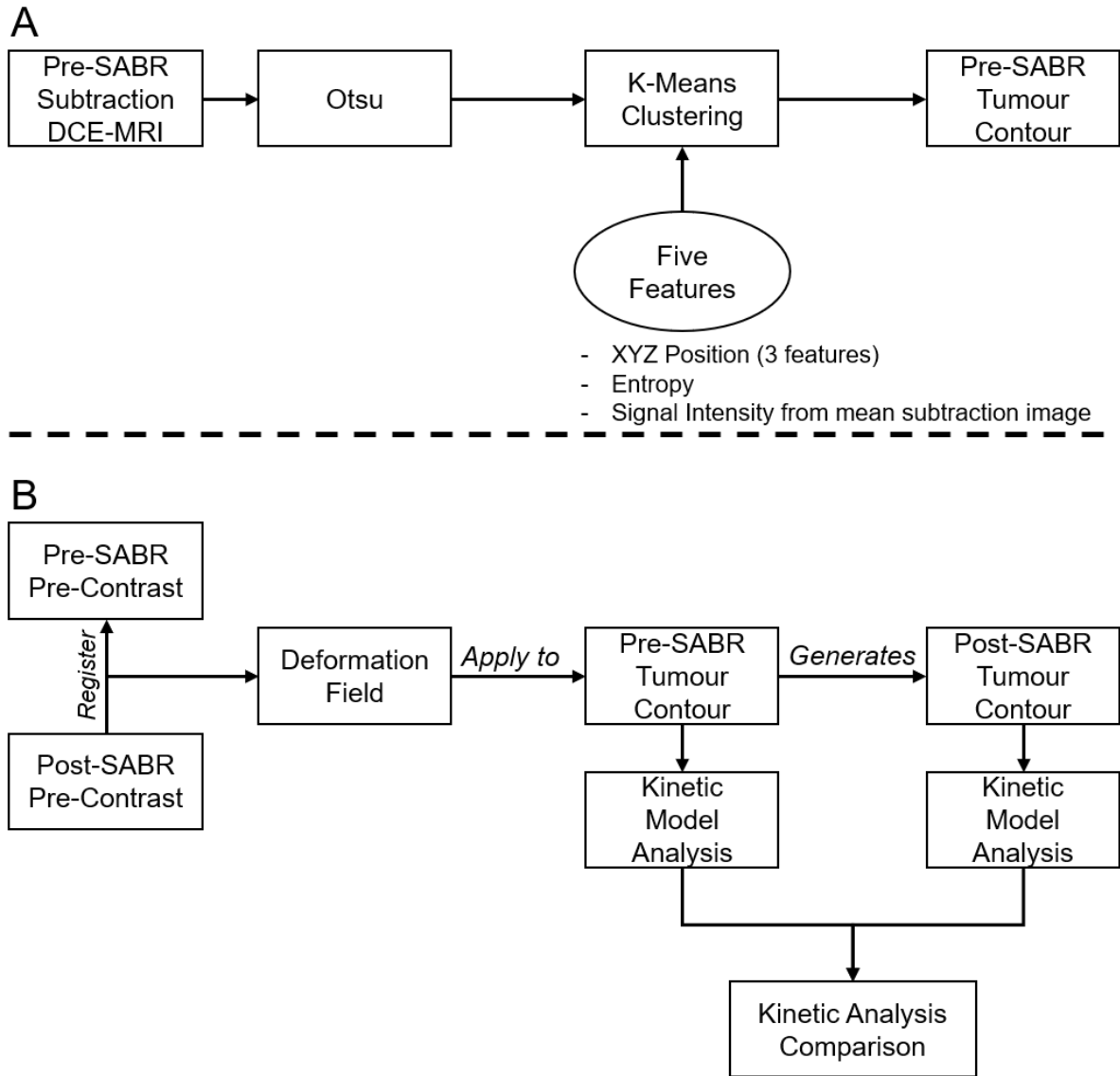


**Figure 4.2:** Schematic representation of the process in generating the (A) pre-SABR tumour contour and (B) post-SABR tumour contour. The pre-SABR contour was generated using a k-means clustering algorithm with 5 features. Following this, the post-SABR pre-contrast image was registered to the pre-SABR pre-contrast image and the deformation field was applied to the pre-SABR contour.

of each voxel, 4) the entropy of a voxel (MATLAB `entropyfilt` with 9,9 neighborhood) [26], and 5) the signal intensity of a mean subtraction image generated by taking the average of the last 5 post-contrast images subtracting the pre-contrast image. Each feature was normalized to have a mean of zero and standard deviation of 1 [27]. Voxels not connected in 3D to the central

tumour contour were eliminated and a morphological fill was used to remove holes. The post- to pre-SABR deformation field was applied to the pre-SABR tumour contour resulting in a post-SABR tumour contour (Figure 4.2B).

### **Kinetic analysis**

The first step in the kinetic analysis was to estimate  $T_{10}$  values. Beginning with the contour generated above, the surgical clip was automatically segmented and removed followed by a 2 pixel in-plane erosion to remove partial volume voxels. The average  $B_1$  and  $T_{10}$  over each tumour was calculated. Pre- and post-SABR data were compared to determine if differences in  $B_1$  or  $T_{10}$  from pre- to post-SABR were statistically significant. Following this, the average across all patients was calculated, and this population derived average  $T_{10}$  [28] was used to convert signal enhancement to concentration [7] using a relaxivity of  $4.5\text{s}^{-1}\text{mM}^{-1}$  [29].

The Tofts kinetic model [30] was applied voxel-by-voxel to the concentration curves within the tumour contour using a population derived arterial input function (AIF) [31], with amplitude adjusted to our dose. An adjustable fit parameter was included to account for the delayed bolus arrival with a lower time bound set using the time the contrast agent arrived at the aortic arch as determined from the HASTE images. From this,  $K^{\text{trans}}$  and  $v_e$  were extracted from the model fit. For each tumour, the mean ( $K^{\text{trans}}$ ,  $v_e$ ) and standard deviation ( $\sigma K^{\text{trans}}$ ,  $\sigma v_e$ ) of the parameters were calculated. The median absolute difference method [32] was used to remove  $v_e$  values that were outliers in each tumour.

### Statistical Analysis

A Wilcoxon signed-rank test was used to test for significant within-subject changes between pre- and post-radiotherapy parameters ( $\alpha=0.05$ , SPSS Inc. v25.0 Chicago). For  $T_{10}$ , differences between pre- and post-SABR in group 1 could not be tested in 3 out of 5 patients due to small tumours as well as clip placement.

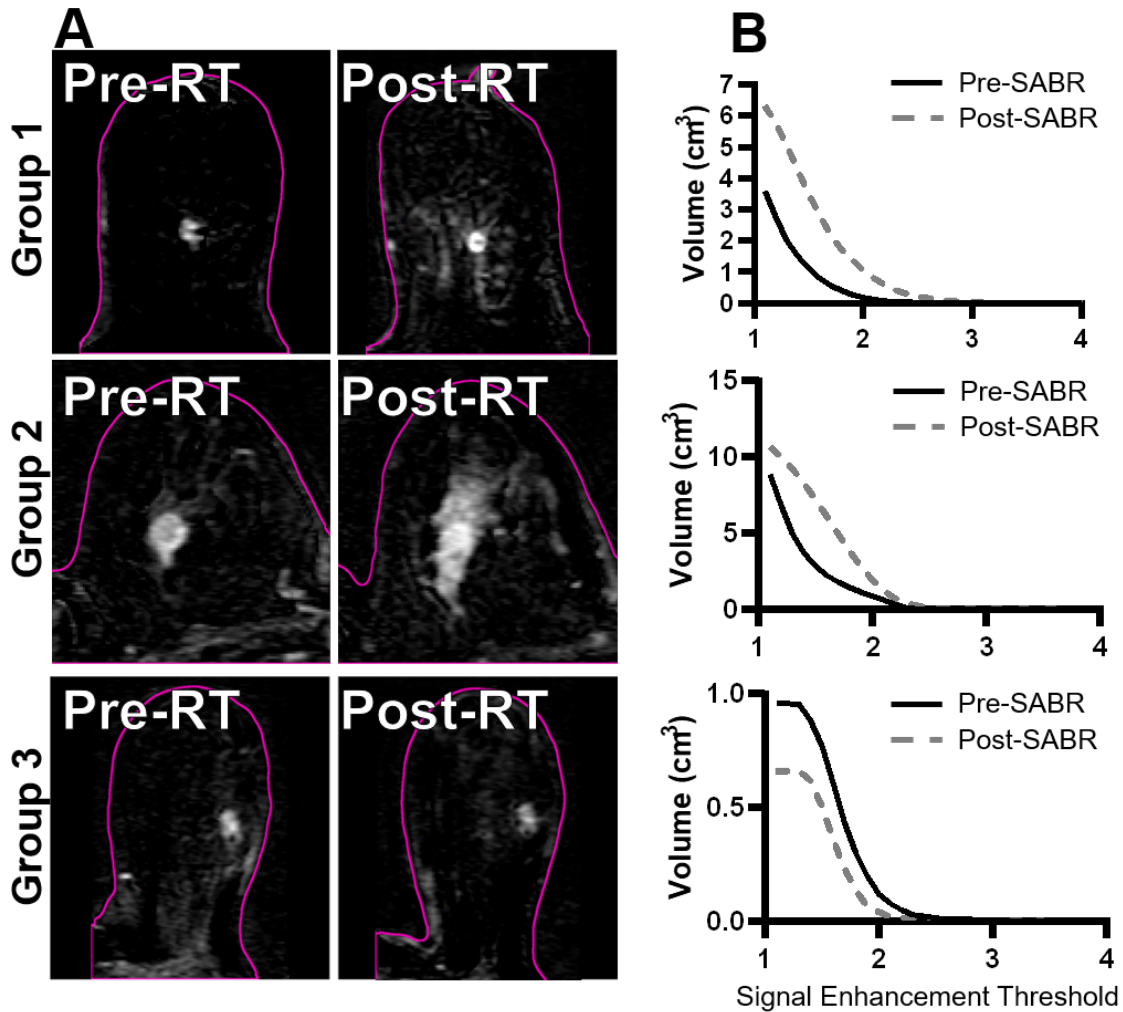
## 4.3 Results

Table 4.1 shows patient characteristics by group. The mean (standard deviation) time between initial biopsy and pre-SABR imaging was 35 (9) days. Median days post-SABR delays for groups 2 and 3 was 16 days and substantially longer than for group 1 (6 days).

Table 4.3 shows AUC percent change values and the pre-SABR contour volume for each patient by group. The AUC increased in all group 1 patients and in 4/6 group 2 patients, whereas it decreased in all group 3 patients. Figure 4.3a shows subtraction images from three representative patients for the three groups pre and post-SABR, demonstrating the increased enhancement in the tissue surrounding the tumour for single fraction patients. Figure 4.3b shows representative signal enhancement threshold volume vs threshold curves.

Regarding  $T_{10}$ , the average  $\pm$  standard deviation for pre- and post-SABR was  $1571 \pm 264$ ms and  $1656 \pm 204$ ms, respectively. This difference was not significant (see appendix D). Therefore, the average of these two values (1613ms) was applied for conversion of enhancement signal to contrast concentration.

Figure 4.4a and 4.4b illustrate pre- to post-SABR changes in the mean values of  $K^{\text{trans}}$



**Figure 4.3:** Subtraction images (A) and associated signal enhancement threshold vs volume curves (B) from representative patients for each of the three groups. The slices are approximately through the center of the tumour. The pink outline represents the skin/air interface. The single fraction images show clear evidence of an increase in the signal enhancement volume local to the tumour following SABR, and this is not seen in the 30Gy/3 fraction patient.

and  $v_e$ , respectively, referring to the mean across each contoured region. Mean  $K^{\text{trans}}$  values for group 1 increased 76% ( $p=0.043$ ) but decreased for groups 2 and 3 by 15% ( $p=0.028$ ) and 34% ( $p=0.028$ ), respectively. Mean values of  $v_e$  increased 25% ( $p=0.046$ ) for group 2 and showed a trend to increase of 32% ( $p=0.075$ ) for group 3, but did not reach significance. Group 1 showed no significant change ( $p=0.138$ ).

**Table 4.3:** Pre-SABR contour volume and pre to post SABR percent change for signal enhancement area under the curve (AUC) for each patient in the different groups. Bold indicates an increase in the AUC value from pre- to post-SABR

	Patient #	Pre-SABR Contour Volume (cm3)	Percent change (%) for Signal Enhancement AUC
Group 1	1	0.07	<b>1932</b>
	2	2.22	<b>598</b>
	3	0.6	<b>295</b>
	4	0.49	<b>64</b>
	5	0.11	<b>1829</b>
Group 2	6	1.23	<b>180</b>
	7	0.72	<b>52</b>
	8	1.27	-18
	9	0.33	-31
	10	1.93	<b>144</b>
	11	0.47	<b>45</b>
Group 3	12	0.66	-42
	13	0.62	-28
	14	2.26	-77
	15	1.37	-14
	16	0.57	-87
	17	0.77	-40

Figures 4.4c and 4.4d illustrate pre to post-SABR changes in  $\sigma K^{\text{trans}}$  and  $\sigma v_e$ , respectively, representing the spatial variability across contoured regions. For group 1,  $\sigma K^{\text{trans}}$  increased 100% ( $p=0.043$ ), but decreased by 31% ( $p=0.028$ ) for group 3. No significant change of  $\sigma K^{\text{trans}}$  was found for group 2 ( $p=0.173$ ). For  $\sigma v_e$ , group 2 and 3 showed increases of 36% ( $p=0.046$ ) and 113% ( $p=0.028$ ), respectively. There was no significant change in  $\sigma v_e$  for group 1 ( $p=0.225$ ).

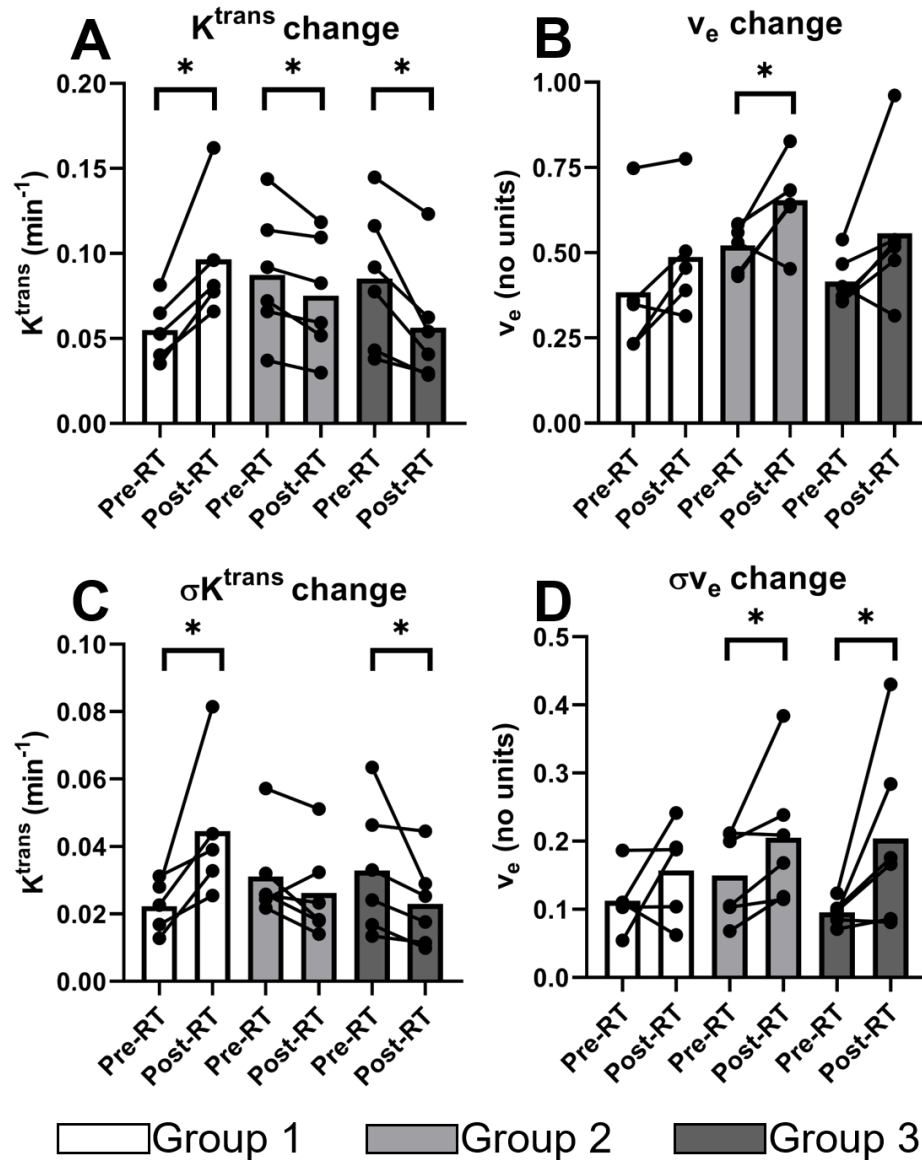


**Figure 4.4:** Pre SABR vs Post SABR changes in the mean and standard deviation of kinetic model parameters  $K^{\text{trans}}$  (A, C) and  $v_e$  (B, D) for the three patient groups. These measures refer to the mean and standard deviation over all voxels within the tumour contours of each patient. Circles connected by a line represent an individual patient's pre- and post-SABR values. The bars represent the median across patients. The asterisks represent significance ( $p < 0.05$ ).

## 4.4 Discussion

In this study, we investigated changes in quantitative DCE-MRI parameters post-SABR with two different fractionation schedules and two different imaging times for the single fraction

scheme. Our results show a differential tumour response depending on time-delay post-SABR. In addition, we found a signal enhancement volume increase following single fraction SABR that was also seen 2.5 weeks post-SABR in most patients. To our knowledge, no study has reported this signal enhancement volume change (Figure 4.3, Table 4.3).

In the context of previous studies, our results suggest that 2.5 weeks post-SABR is a sufficient time-delay in order to minimize acute transient inflammatory effects. In other sites, it has been shown that at short times post-stereotactic radiotherapy (~1-2 weeks post-therapy), there are transient increases in  $K^{\text{trans}}$  following therapy, primarily attributed to endothelial cell death, and permeability increases accompanying acute inflammatory effects [5, 13, 33–37]. A recent early stage breast cancer study [13] found significant increases in the initial area under an enhancement curve for the entire GTV at one-week post single dose SABR. However, when assessing response at later times (>1month) in other cancer sites, decreases in  $K^{\text{trans}}$  were associated with pathologically complete response [38–40]. Two of these reports [38, 40] also indicated that decreases in  $\sigma K^{\text{trans}}$  was indicative of response.

Our results suggest that a three-fraction scheme spares surrounding tissue while providing an equivalent or stronger response at three weeks post-SABR. The magnitude of change in the mean  $K^{\text{trans}}$  was greater for the three-fraction group compared to the single fraction group at three weeks post-SABR (34% vs 15%). However, only the single fraction scheme led to an increase in enhancement volume for the surrounding tissue for some patients (4/6). This implies that fractionation of SABR may reduce the impact of radiation on tissue surrounding the tumour. We suspect that this differential effect on surrounding tissue is related to an endothelial cell death dose threshold which has been hypothesized to be on the order of 8-12 Gy delivered in a single dose [5, 9, 10, 41–44]. With endothelial cell death, gadolinium contrast would be

freer to diffuse into the extra-cellular, extra-vascular space and result in enhancement outside the tumour. Long-term follow-up studies are needed to understand the long-term implications of this in terms of post-radiotherapy toxicities.

The application of  $v_e$  as a metric for response assessment remains unclear. It is expected that vascular and cellular death would lead to increases in  $v_e$  [5, 13]. We found a significant increase in group 2 and a trend to increase in group 3, but not for group 1 (one-week post-SABR). However, Wang et al. [13] showed a significant increase in  $v_e$  at 1 week post-SABR for the PTV and CTV, but did not report  $v_e$  for the GTV which most closely corresponds to the volumes used in our study. On the contrary, Winter et al. [35] found significant decreases in  $v_e$  20 days post stereotactic radiosurgery for brain metastases. Furthermore, most studies do not find a significant change following therapy [33–35, 38, 40]. These variable results may be due to the long scan times required for precise measurement of  $v_e$  [5, 45].

Our study had a few limitations. First, our sample size for each group was small. However, there were consistent trends within each group with similar directions of change observed for  $K^{\text{trans}}$  and most patients showing similar direction of change for  $v_e$ . Second, for  $T_{10}$  we used an average value over all patients because of non-optimal surgical clip location and particularly small tumours in two patients. Third, we did not image at one-week post-SABR for the 30Gy/3fraction treatment and cannot determine if surrounding tissue enhancement would occur in this case. Fourth, physiological changes associated with tumour core biopsy may confound the 1 versus 3 week comparison but at the same time, there was more than a month, on average, between pre-SABR imaging and the biopsy which should minimize these effects. Finally, pathological analysis to investigate vasculature structure of tumours and surrounding tissue was not performed.



## 4.5 Conclusion

Our results suggest that performing breast DCE-MRI one-week post-SABR may be too early for response assessment, whereas 2.5 weeks appears sufficiently long to minimize confounding transient acute effects. In addition, kinetic parameters measured within tumours at 2.5 weeks post-SABR in both single fraction and three-fraction groups were indicative of response, but only the single-fraction protocol led to enhancement in tissue surrounding the tumour. This indicates that while both schemes may lead to response within the tumour, greater sparing of surrounding tissue may be achieved with the three-fraction scheme. Longer-term follow-up of tissue toxicity is needed to confirm this potential benefit of fractionated delivery in this context.

## 4.6 Bibliography

- [1] C. F. Njeh, M. W. Saunders, and C. M. Langton, “Accelerated Partial Breast Irradiation (APBI): a review of available techniques,” *Radiation Oncology*, vol. 5, no. 90, pp. 1–28, 2010.
- [2] K. Guidolin, M. Lock, B. Yaremko, N. Gelman, S. Gaede, A. Kornecki, V. Moiseenko, J. Cao, L. Scott, and M. Brackstone, “A phase II trial to evaluate single-dose stereotactic body radiation therapy (SBRT) prior to surgery for early-stage breast carcinoma: SIGNAL (stereotactic image-guided neoadjuvant ablative radiation then lumpectomy) trial,” *Journal of Radiation Oncology*, vol. 4, no. 4, pp. 423–430, 2015.
- [3] G. N. Marta, C. Rufino Macedo, H. De Andrade Carvalho, A. Hanna, J. L. Fernandes Da Silva, and R. Riera, “Systematic review Accelerated partial irradiation for breast cancer: Systematic review and meta-analysis of 8653 women in eight randomized trials,” *Radiotherapy and Oncology*, vol. 114, pp. 42–49, 2015.
- [4] E. Nichols, S. B. Kesmodel, E. Bellavance, C. Drogula, K. Tkaczuk, R. J. Cohen, W. Citron, M. Morgan, P. Staats, S. Feigenberg, and W. F. Regine, “Preoperative Accelerated Partial Breast Irradiation for Early-Stage Breast Cancer: Preliminary Results of a Prospective, Phase 2 Trial,” *International Journal of Radiation Oncology Biology Physics*, vol. 97, pp. 747–753, mar 2017.
- [5] R. García-Figueiras, V. J. Goh, A. R. Padhani, S. Baleato-González, M. Garrido, L. León, and A. Gómez-Caamaño, “CT perfusion in oncologic imaging: A useful tool?,” *American*

*Journal of Roentgenology*, vol. 200, pp. 8–19, jan 2013.

- [6] H. J. Park, R. J. Griffin, S. Hui, S. H. Levitt, C. W. Song, H. Levitt, and C. W. Song, “Radiation-Induced Vascular Damage in Tumors: Implications of Vascular Damage in Ablative Hypofractionated Radiotherapy (SBRT and SRS),” *Radiation Research*, vol. 177, no. 3, pp. 311–327, 2012.
- [7] C.-H. Wang, “Review of treatment assessment using DCE-MRI in breast cancer radiation therapy,” *World Journal of Methodology*, vol. 4, p. 46, jun 2014.
- [8] H. B. Stone, C. N. Coleman, M. S. Anscher, and W. H. McBride, “Effects of radiation on normal tissue: Consequences and mechanisms,” 2003.
- [9] T. Hellevik and I. Martinez-Zubiaurre, “Radiotherapy and the Tumor Stroma: The Importance of Dose and Fractionation,” *Frontiers in Oncology*, vol. 4, p. 1, jan 2014.
- [10] M. T. Milano, L. S. Constine, and P. Okunieff, “Normal tissue toxicity after small field hypofractionated stereotactic body radiation,” *Radiation Oncology*, vol. 3, no. 1, 2008.
- [11] R. G. Figueiras, A. R. Padhani, V. J. Goh, J. C. Vilanova, S. B. Gonzalez, C. V. Martin, a. G. Caamano, A. B. Naveira, and P. L. Choyke, “Novel Oncologic Drugs: What They Do and How They Affect Images,” *Radiographics*, vol. 31, no. 7, pp. 2059–2091, 2011.
- [12] C. W. Song, M. S. Kim, L. C. Cho, K. Dusenbery, and P. W. Sperduto, “Radiobiological basis of SBRT and SRS,” 2014.
- [13] C. Wang, J. K. Horton, F.-F. Yin, and Z. Chang, “Assessment of Treatment Response With Diffusion-Weighted MRI and Dynamic Contrast-Enhanced MRI in Patients With

Early-Stage Breast Cancer Treated With Single-Dose Preoperative Radiotherapy: Initial Results,” *Technology in Cancer Research & Treatment*, 2015.

- [14] H. J. Weinmann, M. Laniado, and W. Mützel, “Pharmacokinetics of GdDTPA/dimeglumine after intravenous injection into healthy volunteers.,” *Physiological chemistry and physics and medical NMR*, vol. 16, no. 2, pp. 167–72, 1984.
- [15] A. E. Othman, F. Falkner, D.-e. Kessler, P. Martirosian, J. Weiss, S. Kruck, S. Kaufmann, R. Grimm, U. Kramer, K. Nikolaou, and M. Notohamiprodjo, “Comparison of different population-averaged arterial-input-functions in dynamic contrast-enhanced MRI of the prostate : Effects on pharmacokinetic parameters and their diagnostic performance,” *Magnetic Resonance Imaging*, vol. 34, no. 4, pp. 496–501, 2016.
- [16] J. C. Patrick, R. Terry Thompson, A. So, J. Butler, D. Faul, R. Z. Stodilka, S. Yartsev, F. S. Prato, and S. Gaede, “Technical Note: Comparison of megavoltage, dual-energy, and single-energy CT-based  $\mu$ -maps for a four-channel breast coil in PET/MRI,” *Medical Physics*, vol. 44, pp. 4758–4765, sep 2017.
- [17] S. C. Deoni, B. K. Rutt, and T. M. Peters, “Rapid combined T1 and T2 mapping using gradient recalled acquisition in the steady state,” *Magnetic Resonance in Medicine*, vol. 49, pp. 515–526, mar 2003.
- [18] V. L. Yarnykh, “Actual flip-angle imaging in the pulsed steady state: A method for rapid three-dimensional mapping of the transmitted radiofrequency field,” *Magnetic Resonance in Medicine*, vol. 57, no. 1, pp. 192–200, 2007.

- [19] S. Chung, D. Kim, E. Breton, and L. Axel, "Rapid B1+mapping using a preconditioning RF pulse with turboFLASH readout," *Magnetic Resonance in Medicine*, vol. 64, no. 2, pp. 439–446, 2010.
- [20] H. J. Johnson, G. Harris, K. Williams, N. K. Williams, and K. Williams, "BRAINSFit: Mutual Information Rigid Registrations of Whole-Brain 3D Images, Using the Insight Toolkit," Tech. Rep. 10, 2007.
- [21] A. Fedorov, R. Beichel, J. Kalpathy-Cramer, J. Finet, J.-C. Fillion-Robin, S. Pujol, C. Bauer, D. Jennings, F. Fennessy, M. Sonka, J. Buatti, S. Aylward, J. V. Miller, S. Pieper, and R. Kikinis, "3D Slicer as an image computing platform for the Quantitative Imaging Network.," *Magnetic resonance imaging*, vol. 30, pp. 1323–41, nov 2012.
- [22] M. Mouawad, H. Biernaski, M. Brackstone, M. Klassen, M. Lock, F. S. Prato, R. T. Thompson, S. Gaede, and N. Gelman, "Sci-Fri AM: MRI and Diagnostic Imaging - 03: The influence of sampling percentage in deformable registration on kinetic model analysis results in DCE-MRI of the breast," *Medical Physics*, vol. 43, pp. 4951–4951, aug 2016.
- [23] M. P. Heinrich, M. Jenkinson, M. Bhushan, T. Martin, F. V. Gleeson, S. M. Brady, and J. A. Schnabel, "MIND: Modality independent neighbourhood descriptor for multi-modal deformable registration," *Medical Image Analysis*, vol. 16, pp. 1423–1435, oct 2012.
- [24] S. Pirozzi, A. Kruzer, H. Richmond, and A. Nelson, "Evaluation of Three Deformable Image Registration Techniques Between CT and CBCT in Prostate Cancer Radiation Therapy," *International Journal of Radiation Oncology\*Biography\*Physics*, vol. 102, pp. e546–e547, nov 2018.

- [25] N. Otsu, "A Threshold Selection Method from Gray-Level Histograms," *IEEE Transactions on Systems, Man, and Cybernetics*, vol. 9, pp. 62–66, jan 1979.
- [26] R. C. Gonzalez, R. E. Woods, and B. R. Masters, *Digital Image Processing, Third Edition*, vol. 14. 2009.
- [27] M. E. Celebi, H. A. Kingravi, and P. A. Vela, "A comparative study of efficient initialization methods for the k-means clustering algorithm," *Expert Systems with Applications*, vol. 40, no. 1, pp. 200–210, 2013.
- [28] H. M. Reynolds, B. K. Parameswaran, M. E. Finnegan, D. Roettger, E. Lau, T. Kron, M. Shaw, S. Chander, and S. Siva, "Diffusion weighted and dynamic contrast enhanced MRI as an imaging biomarker for stereotactic ablative body radiotherapy (SABR) of primary renal cell carcinoma," *PLoS ONE*, vol. 13, no. 8, 2018.
- [29] J. Pintaske, P. Martirosian, H. Graf, G. Erb, K. P. Lodemann, C. D. Claussen, and F. Schick, "Relaxivity of gadopentetate dimeglumine (Magnevist), gadobutrol (Gadovist), and gadobenate dimeglumine (MultiHance) in human blood plasma at 0.2, 1.5, and 3 Tesla," *Investigative Radiology*, vol. 41, pp. 213–221, mar 2006.
- [30] P. Tofts, B. Gunnar, D. L. Buckley, J. L. Evelhoch, E. Henderson, M. V. Knopp, H. B. W. Larsson, T.-Y. Lee, N. A. Mayr, G. J. M. Parker, R. E. Port, J. Taylor, and R. M. Weisskoff, "Estimating kinetic parameters from dynamic contrast-enhanced t1-weighted MRI of a diffusable tracer: Standardized quantities and symbols," *Journal of Magnetic Resonance Imaging*, vol. 10, no. 3, pp. 223–232, 1999.

- [31] G. J. M. Parker, C. Roberts, A. Macdonald, G. A. Buonaccorsi, S. Cheung, D. L. Buckley, A. Jackson, Y. Watson, K. Davies, and G. C. Jayson, “Experimentally-derived functional form for a population-averaged high-temporal-resolution arterial input function for dynamic contrast-enhanced MRI,” *Magnetic Resonance in Medicine*, vol. 56, no. 5, pp. 993–1000, 2006.
- [32] C. Leys, C. Ley, O. Klein, P. Bernard, and L. Licata, “Detecting outliers: Do not use standard deviation around the mean, use absolute deviation around the median,” *Journal of Experimental Social Psychology*, vol. 49, pp. 764–766, jul 2013.
- [33] M. H. Janssen, H. J. Aerts, R. G. Kierkels, W. H. Backes, M. C. Öllers, J. Buijsen, P. Lambin, and G. Lammering, “Tumor perfusion increases during hypofractionated short-course radiotherapy in rectal cancer: Sequential perfusion-CT findings,” *Radiotherapy and Oncology*, vol. 94, pp. 156–160, feb 2010.
- [34] C. Coolens, B. Driscoll, J. Moseley, K. K. Brock, and L. A. Dawson, “Feasibility of 4D perfusion CT imaging for the assessment of liver treatment response following SBRT and sorafenib,” *Advances in Radiation Oncology*, vol. 1, pp. 194–203, jul 2016.
- [35] J. D. Winter, F. Y. Moraes, C. Chung, and C. Coolens, “Detectability of radiation-induced changes in magnetic resonance biomarkers following stereotactic radiosurgery: A pilot study,” *PLoS ONE*, vol. 13, no. 11, 2018.
- [36] J. S. Detsky, L. Milot, Y.-J. Ko, P. Munoz-Shuffenegger, W. Chu, G. J. Czarnota, and H. T. Chung, “Perfusion imaging of colorectal liver metastases treated with bevacizumab

- and stereotactic body radiotherapy,” *Physics and Imaging in Radiation Oncology*, vol. 5, pp. 9–12, 2018.
- [37] B. Sawyer, E. Pun, M. Samuel, H. Tay, T. Kron, M. Bressel, D. Ball, and S. Siva, “CT perfusion imaging in response assessment of pulmonary metastases undergoing stereotactic ablative radiotherapy,” *Journal of Medical Imaging and Radiation Oncology*, vol. 59, pp. 207–215, apr 2015.
- [38] Y. S. Huang, J. L. Y. Chen, F. M. Hsu, J. Y. Huang, W. C. Ko, Y. C. Chen, F. S. Jaw, R. F. Yen, and Y. C. Chang, “Response assessment of stereotactic body radiation therapy using dynamic contrast-enhanced integrated MR-PET in non-small cell lung cancer patients,” *Journal of Magnetic Resonance Imaging*, vol. 47, pp. 191–199, jan 2018.
- [39] D. E. Spratt, J. Arevalo-Perez, J. E. Leeman, N. K. Gerber, M. Folkert, N. K. Taunk, K. M. Alektiar, S. Karimi, J. K. Lyo, W. D. Tap, M. H. Bilsky, I. Laufer, Y. Yamada, and J. R. Osborne, “Early magnetic resonance imaging biomarkers to predict local control after high dose stereotactic body radiotherapy for patients with sarcoma spine metastases,” *Spine Journal*, vol. 16, no. 3, pp. 291–298, 2016.
- [40] N. K. Taunk, J. H. Oh, A. Shukla-Dave, K. Beal, B. Vachha, A. Holodny, and V. Hatzoglou, “Early posttreatment assessment of MRI perfusion biomarkers can predict long-term response of lung cancer brain metastases to stereotactic radiosurgery,” *Neuro-Oncology*, vol. 20, pp. 567–575, mar 2018.
- [41] S. L. Brown, T. N. Nagaraja, M. P. Aryal, S. Panda, G. Cabral, K. A. Keenan, R. Elmghirbi, T. Mikkelsen, D. Hearshen, R. A. Knight, N. Wen, J. H. Kim, and J. R.



- Ewing, "MRI-Tracked Tumor Vascular Changes in the Hours after Single-Fraction Irradiation," *Radiation Research*, vol. 183, pp. 713–721, jun 2015.
- [42] B. P. Venkatesulu, L. S. Mahadevan, M. L. Aliru, X. Yang, M. H. Bodd, P. K. Singh, S. W. Yusuf, J.-I. Abe, and S. Krishnan, "Radiation-Induced Endothelial Vascular Injury," *JACC: Basic to Translational Science*, vol. 3, no. 4, pp. 563–572, 2018.
- [43] Y. Cao, "The Promise of Dynamic Contrast-Enhanced Imaging in Radiation Therapy," *Seminars in Radiation Oncology*, vol. 21, pp. 147–156, apr 2011.
- [44] H. E. Barker, J. T. E. Paget, A. A. Khan, and K. J. Harrington, "The tumour microenvironment after radiotherapy : mechanisms of resistance and recurrence," *Nature Publishing Group*, vol. 15, pp. 409–425, jul 2015.
- [45] P. S. Tofts and G. J. Parker, "DCE-MRI: Acquisition and analysis techniques," in *Clinical Perfusion MRI: Techniques and Applications* (P. Barker, X. Golay, and G. Zaharchuk, eds.), vol. 9781107013, pp. 58–74, Cambridge: Cambridge University Press, 2010.

## **Chapter 5**

### **5 Conclusions and Future Works**

#### **5.1 Summary and Conclusions**

The introductory chapter of this thesis provides motivation for the use of APBI; specifically that long treatment times have resulted in the under-utilization of BCT in early stage breast cancer patients. APBI has the potential to address this short-coming by treating smaller volumes (the tumour) and allowing for higher doses per fraction to be used resulting in shorter treatment times. While various techniques can be used to deliver APBI, there is a strong motivation for using EB-APBI due to its ease of access and non-invasive nature, so long as its shortcomings can be addressed. Specifically, several studies have found worse cosmesis in patients which is likely caused by the fact that large margins are needed to account for setup error and patient motion and the use of somewhat dated conformal radiotherapy techniques (i.e., 3D-CRT) which do not allow for sufficiently conformal doses and normal tissue sparing. Treating patients before surgery, prone, and with stereotactic techniques would allow for sufficiently conformal dose distributions to spare the normal tissue and would potentially bring EB-APBI on-par with cosmesis outcomes of WBRT but treating in a significantly shorter treatment time.

The SIGNAL trial was introduced with a summary of the protocol. Highlighted in this was the fact that treating neoadjuvant provides a unique opportunity to investigate non-invasive

response biomarkers using functional imaging techniques while the tumour is still intact. Response biomarkers would allow for early assessment of treatment response, potentially providing a means to confirm tumour control as well as possible adaptation of treatment on a patient by patient basis at a very early stage in their care. In addition, imaging following high dose radiotherapy could provide novel insights into the early radiobiological response to SABR treatments. To our knowledge, very little information about the response, in-vivo, is available (particularly in breast).

The primary goal of this thesis was to investigate response to SABR using DCE-MRI at an early timepoint post SABR in early stage breast cancer patients. However, before this could be investigated, it was necessary to address two issues related to the acquisition and analysis of DCE-MRI. First, contrast agent safety issues lead to a temporary halt to the post-SABR imaging in SIGNAL. We decided to reduce the contrast agent dose that patients would receive to half the standard clinical dose. While the radiation oncologists involved in SIGNAL found that using the reduced dose of contrast agent the tumour conspicuity was sufficient for radiotherapy planning, nevertheless, we wanted to quantitatively investigate what effect this reduced dose would have on target volume delineation for MRI guided radiotherapy planning. Second, we wished to quantify the effect that registration had on parameter values, precision, and model goodness of fit from application of the commonly used Tofts model. Finally, we also considered the effect of strategies to reduce computation time and how it affected these same parameters.

The three objectives of this thesis were:

1. To quantitatively assess the potential of reducing the dose of gadolinium contrast agent

for DCE-MRI-based radiotherapy target volume delineation. More specifically the aim was to compare using a full versus half clinical dose of contrast agent on the inter- and intra-observer variability (Chapter 2).

2. To quantitatively evaluate the impact of 3D deformable registration on voxel-by-voxel parameter values, associated uncertainties, and goodness of fit extracted from application of the Tofts model to DCE-MRI data from breast cancer patients.
3. To determine tumour and the surrounding tissue response to SABR in early stage breast cancer patients using two different SABR fractionations and two different time delays post-SABR.

Chapter 2 addressed the first objective. The major conclusion from this study was that using a half-dose of contrast did not significantly decrease inter- and intra-observer variability as assessed by several metrics. This is one of the first studies to investigate half the standard dose of gadolinium in a clinical setting. Gadolinium-based contrast agents are used in many different MRI applications, several of which require repeated administrations, and so, we expect that my study will provide motivation for investigating the impact of reduced contrast agent dose in the context of other MRI applications. The conclusions of our study provided evidence to support the continuation of the post-SABR imaging for response assessment to the SABR treatment in SIGNAL.

Chapter 3 addressed the second objective by investigating the impact of registration on the the values of model fit parameter estimates and their uncertainties. The primary conclusion was that registration significantly reduced the uncertainties of Tofts model parameter estimates and significantly decreased the percentage of voxels that were fit with unphysical  $v_e$  values.

This study is the first to demonstrate deformable registration leads to a reduction in the number of voxels for which unphysical values of  $v_e$  are extracted. We also showed that computation time could be decreased by a factor of two without affecting the parameter estimates by using a lower sampling of the image for estimation of the registration similarity metric.

Finally, chapter 4 addressed the third objective of assessing response to SABR within tumour and surrounding tissue, in early stage breast cancer patients, using DCE-MRI. We investigated the effect of both fractionation and time delay post-SABR on the response. The changes in surrounding tissue have not been previously studied. Also kinetic parameter changes within the tumor have not been reported. We found a profound increase in contrast uptake in the surrounding tissue for patients who were exposed to a single fraction of SABR at both 1 and 2.5 weeks post-SABR but not when exposed to three fraction SABR assessed 2.5 weeks post-SABR - a result which has not been previously reported. An important finding was that a delay of 2.5 weeks post-SABR was sufficient to assess response without confounding acute effects using either single or 3 fraction SABR. The methods and results presented here will play an important role in designing future clinical trials for early stage breast cancer treatment (see section 5.3).

## 5.2 Limitations

A common limitation across all three studies presented in this thesis was the relatively small sample size which inhibits generalizations of the conclusions. However, the finding of statistically significant changes with this small sample size (and with lower than standard contrast agent doses in chapters 2 and 4) is also encouraging. For example, the finding of statistically

significant pre- to post-SABR changes of kinetic parameters in chapter 4, despite the relatively small number of patients, suggests that the metrics have potential for providing strong sensitivity to response. Further work will look to add more patient data as more patients are accrued to the SIGNAL trial.

In Chapter 2, the most important limitation was the fact that data was unpaired which acts as a potential confounder when making comparisons between groups due to the introduction of biological variability. A systematic analysis should be performed to investigate the effect that changing the contrast agent dose has on an observer's ability to contour a target. Most likely, this could not be performed from images acquired using different contrast agent doses on the same patients due to ethical concerns. However, it may be possible to investigate this either by using a large animal model or by manipulating acquired patient data and simulating different contrast doses and associated changes in signal enhancement. The simulation experiment is discussed in section 5.3.

In Chapter 3, we assessed the influence of registration on voxel-by-voxel application of the commonly used Tofts model. Specifically, we considered deformable registration impact on parameter estimates and associated uncertainties, and goodness of fit. However, the analysis used here does not provide a means to assess the effect of registration on parameter accuracy due to the lack of ground truth data.

In Chapter 4, a novel analysis scheme was developed in an attempt to separate tumour from surrounding tissue effects. However, there are still areas that need to be improved. We chose to use a population averaged  $T_{10}$ , based on  $T_{10}$  measurements from our patients, instead of patient-specific voxel-by-voxel  $T_{10}$  values. The primary reason for this choice of methodology was to minimize partial volume averaging of tumour tissue (especially from smaller tumors)

with the surgical clip or with the surrounding fat tissue in patients where fat suppression was not used for  $T_{10}$  measurements. Through simulation, we determined that these partial volume effects could severely affect the curve fitting for  $T_{10}$  estimation (see appendix B). Another limitation is that we did not correct for intra-session motion between the images used for  $T_{10}$  estimation due to the drastically changing contrast between the different flip angle images. It may be possible to register these images and the DCE-MRI data set simultaneously using novel group-wise registration techniques that register all images together (rather than in pairs) [1]. However, this was not explored in this study.

### 5.3 Future Work

Registration played an important role in this thesis. In chapter 3, we investigated how registration affected precision of Tofts model estimates. Future work should look to investigate other registration software and algorithms that may provide better results [2], or compare DCE-MRI specific cost metrics that may be able to better account for the local changes in contrast. For example, using a principle component analysis based metric has been shown to outperformed mutual information based metrics since they can incorporate the intensity change over time information [3,4]. However, there has been a lack of consideration for computation time and should likely be considered in future work, especially since the temporal resolution of DCE-MRI studies will only continue to increase resulting in a large number of images per data set.

In chapter 4 we showed that single fraction but not three fraction radiotherapy led to increased gadolinium contrast agent in the tissue surrounding the tumour. We suspect that this is due to vascular permeability changes accompanying acute inflammatory effects [5] and pos-

sibly due to a hypothesized endothelial cell death threshold [6]. At this time, we have begun acquiring simultaneous  $^{18}\text{F}$ -Fluorodeoxyglucose (FDG)-PET in addition to the DCE-MRI images for patients enrolled in the pre- and post-imaging arm of SIGNAL. The PET data may serve to provide additional information related to the response of the normal and tumour tissue to SABR – not only by measuring the glucose activity of the tumour itself, but also potentially serving as a marker of macrophage activity [7–9]. Studies have shown that macrophage polarization (M1 versus M2) may mediate tumour response to radiation [10] and that the predominant type of macrophage (i.e., M1 or M2) may depend on fractionation scheme [11]. FDG-PET will potentially help to understand the role the immune system plays in response to SABR for both the tumour and the surrounding tissue.

In chapter 4 we observed differential effects in the tissue surrounding the tumour which we suspect is due to vascular permeability changes accompanying acute inflammatory effects [5] and possibly due to a hypothesized endothelial cell death threshold [6]. Perhaps our PET-MRI study (mentioned in the previous paragraph) may be able to provide insight into the inflammatory and immune response following SABR [7]. The FDG PET signals may also serve as a potential imaging biomarker - though this may be difficult at the early stages when acute inflammatory and immune response may be the predominant effect and, hence, may confound tumour FDG uptake measurements [12]. Furthermore, it has been shown that FDG uptake is variable in breast cancer due to varying degrees of metabolic activity [13]. However, it may be possible to separate response values in tumours from those that are due to immune response using a time-point method [13, 14] and this will be the subject of future work. It may be beneficial as well to use more specific tracers if FDG is not specific enough. Several PET tracers are being investigated in the context of assessing tumour response to treatment such as FLT



(which measures cellular proliferation), fluoroazomycin arabinoside (FAZA) (which measures hypoxia), or more breast cancer specific tracers such as those based on estrogen and progesterone receptors [15]. However, these are still under active investigation and are costly and so, their role is unclear in patient care.

In addition to complementary imaging information, future studies will include additional information from immunohistochemistry performed on the surgical specimens following SABR (see “lumpectomy” in figure 1.3). This will help to elucidate the vascular changes following radiotherapy and confirm the hypothesis of vascular permeability changes and potential endothelial cell death as a cause for the increased contrast uptake in the tissue surrounding the tumour as speculated in chapter 4. In particular, immunohistochemistry analysis could include assessment of the following: 1) general "bulk" changes following SABR in tumour and the surrounding tissue using a hematoxylin and eosin (H&E) stain [16], 2) Disruption of the vasculature and extracellular matrix using CD31 staining [17], and 3) apoptosis assessed using the TUNEL assay [18]. Inflammation will be investigated in the future as well under the purview of SIGNAL which will quantify the change in the following immunomarkers: 1) CD8 which indicates the presence of infiltrating leukocytes, 2) Anti-PDL1 which plays a role in immune response suppression, and 3) Ki-67 which indicates cellular proliferation.

Another area of future work is in the delivery of SABR. Advances in technology have made during-treatment (intra-session) delivery monitoring possible through the use of the kV fluoroscopic imaging system mounted 90°s to the gantry treatment head. Currently, this is being used clinically in SIGNAL to confirm that the tumour and surgical clip are within the prescribed margins and act as a confirmation that the target received the prescribed dose. However, it may be possible to utilize the series of 2D kV images to estimate the 3D trajectory of the tumour

and better inform the statistical margins needed for generation of the PTV [19].

The doses used for SIGNAL (30 Gy/3 fraction or 21 Gy/1 fraction) are biologically equivalent to the traditional treatment regime of 50 Gy in 25 fractions. However, it may be possible in the future to escalate the dose even further. The dose that can be achieved will depend on a variety of factors such as breast size, tumour location compared to the chest wall and skin, as well as advances in treatment planning and setup accuracy. In a future iteration of SIGNAL, the London Regional Cancer Program is proposing a dose escalation study. Using a 3+3 design [20], the dose will be continually escalated in early stage breast cancer patients to determine the maximum tolerable dose. Lumpectomy will still be performed and analyzed at each dose level to see if tumour control is achieved before surgery is performed. In this way, it may be possible to deliver a sterilizing dose of radiation to the tumour such that surgery is no-longer needed. An integral part to investigating this treatment scheme is adequate response imaging and so, the work presented in this thesis sets the stage for investigating further improvements to early stage breast cancer patient care.

## 5.4 Bibliography

- [1] A. Hallack, M. A. Chappell, M. J. Gooding, and J. A. Schnabel, “A new similarity metric for groupwise registration of variable flip angle sequences for improved T10 estimation in DCE-MRI,” in *Lecture Notes in Computer Science (including subseries Lecture Notes in Artificial Intelligence and Lecture Notes in Bioinformatics)*, vol. 8545 LNCS, pp. 154–163, Springer, Cham, 2014.
- [2] A. P. Keszei, B. Berkels, and T. M. Deserno, “Survey of Non-Rigid Registration Tools in Medicine,” 2017.
- [3] A. Melbourne, J. Hipwell, M. Modat, T. Mertzaniidou, H. Huisman, S. Ourselin, and D. J. Hawkes, “The effect of motion correction on pharmacokinetic parameter estimation in dynamic-contrast-enhanced MRI,” *Physics in Medicine and Biology*, vol. 56, no. 24, pp. 7693–7708, 2011.
- [4] M. J. A. Jansen, H. J. Kuijf, W. B. Veldhuis, F. J. Wessels, M. S. Van Leeuwen, and J. P. W. Pluim, “Evaluation of motion correction for clinical dynamic contrast enhanced MRI of the liver,” *Physics in Medicine and Biology*, vol. 62, no. 19, pp. 7556–7568, 2017.
- [5] R. García-Figueiras, V. J. Goh, A. R. Padhani, S. Baleato-González, M. Garrido, L. León, and A. Gómez-Caamaño, “CT perfusion in oncologic imaging: A useful tool?,” *American Journal of Roentgenology*, vol. 200, pp. 8–19, jan 2013.
- [6] T. Hellevik and I. Martinez-Zubiaurre, “Radiotherapy and the Tumor Stroma: The Importance of Dose and Fractionation,” *Frontiers in Oncology*, vol. 4, p. 1, jan 2014.

- [7] T. Belhocine, D. Blockmans, R. Hustinx, J. Vandevivere, and L. Mortelmans, “Imaging of large vessel vasculitis with 18FDG PET: Illusion or reality? A critical review of the literature data,” sep 2003.
- [8] T. Satomi, M. Ogawa, I. Mori, S. Ishino, K. Kubo, Y. Magata, and T. Nishimoto, “Comparison of Contrast Agents for Atherosclerosis Imaging Using Cultured Macrophages: FDG Versus Ultrasmall Superparamagnetic Iron Oxide,” *Journal of Nuclear Medicine*, vol. 54, pp. 999–1004, jun 2013.
- [9] L. Zhu, Q. Zhao, T. Yang, W. Ding, and Y. Zhao, “Cellular Metabolism and Macrophage Functional Polarization,” *International Reviews of Immunology*, vol. 34, pp. 82–100, jan 2015.
- [10] X. Shi and S. L. Shiao, “The role of macrophage phenotype in regulating the response to radiation therapy,” *Translational research : the journal of laboratory and clinical medicine*, vol. 191, pp. 64–80, 2018.
- [11] K. M. Arnold, N. J. Flynn, A. Raben, L. Romak, Y. Yu, A. P. Dicker, F. Mourtada, and J. Sims-Mourtada, “The Impact of Radiation on the Tumor Microenvironment: Effect of Dose and Fractionation Schedules,” *Cancer Growth and Metastasis*, vol. 11, p. 117906441876163, jan 2018.
- [12] H. Cliffe, C. Patel, R. Prestwich, and A. Scarsbrook, “Radiotherapy response evaluation using FDG PET-CT—established and emerging applications,” *The British Journal of Radiology*, vol. 90, p. 20160764, mar 2017.

- [13] R. Kumar, V. A. Loving, A. Chauhan, H. Zhuang, S. Mitchell, and A. Alavi, "Potential of Dual-Time-Point Imaging to Improve," *Journal of nuclear medicine*, vol. 46, no. 11, pp. 1819–1824, 2005.
- [14] O. Schillaci, "Use of dual-point fluorodeoxyglucose imaging to enhance sensitivity and specificity," *Seminars in Nuclear Medicine*, vol. 42, no. 4, pp. 267–280, 2012.
- [15] I. Peñuelas, I. Domínguez-Prado, M. J. García-Velloso, J. M. Martí-Climent, M. Rodríguez-Fraile, C. Caicedo, M. Sánchez-Martínez, and J. A. Richter, "PET Tracers for Clinical Imaging of Breast Cancer," *Journal of Oncology*, vol. 2012, pp. 1–9, 2012.
- [16] M. N. Gurcan, L. E. Boucheron, A. Can, A. Madabhushi, N. M. Rajpoot, and B. Yener, "Histopathological Image Analysis: A Review," *IEEE Reviews in Biomedical Engineering*, vol. 2, pp. 147–171, 2009.
- [17] D. Wang, C. R. Stockard, L. Harkins, P. Lott, C. Salih, K. Yuan, D. Buchsbaum, A. Hashim, M. Zayzafoon, R. W. Hardy, O. Hameed, W. Grizzle, and G. P. Siegal, "Immunohistochemistry in the evaluation of neovascularization in tumor xenografts." *Biotechnic & histochemistry : official publication of the Biological Stain Commission*, vol. 83, pp. 179–89, jun 2008.
- [18] Z. Darzynkiewicz, D. Galkowski, and H. Zhao, "Analysis of apoptosis by cytometry using TUNEL assay," *Methods (San Diego, Calif.)*, vol. 44, pp. 250–4, mar 2008.
- [19] P. R. Poulsen, B. Cho, and P. J. Keall, "A Method to Estimate Mean Position, Motion Magnitude, Motion Correlation, and Trajectory of a Tumor From Cone-Beam CT Pro-

jections for Image-Guided Radiotherapy,” *International Journal of Radiation Oncology Biology Physics*, vol. 72, no. 5, pp. 1587–1596, 2008.

- [20] C. Le Tourneau, J. J. Lee, and L. L. Siu, “Dose escalation methods in phase I cancer clinical trials,” *Journal of the National Cancer Institute*, vol. 101, pp. 708–20, may 2009.

## Appendix A

### A SIGNAL inclusion/exclusion criteria

For completeness, the entire inclusion/exclusion criteria for SIGNAL is included for ease of reading. Note that this is from an internal revised protocol, named “SIGNAL 2.0” but should closely match those stipulated in reference [1].

#### *Eligibility Criteria*

The following criteria must all be met:

- Age  $\geq$  50 years and postmenopausal
- Tumor size < 3cm on pre-treatment imaging
- Any grade of disease, estrogen receptor (ER) positive
- Unicentric/unifocal disease
- Invasive ductal carcinoma or other favorable subtypes of epithelial breast malignancy (lobular, medullary, papillary, colloid, mucinous, or tubular) .
- Clinically node-negative (based upon pre-treatment physical examination and/or axillary ultrasound).
- Surgical expectation that a > 2mm margin can be obtained.
- Lesion is 1 cm or greater from the skin surface.

- Able to have surgery within 14-20 days of radiation therapy.
- Able to lie comfortably in the prone position with arms raised above the head for extended periods of time.

### ***Ineligibility Criteria***

Any of the following renders a patient ineligible for enrollment:

- Previous RT to the same breast
- Evidence of suspicious diffuse microcalcifications in the breast prior to the start of radiation.
- Local metastatic spread into ipsilateral axilla and/or supraclavicular region and/or neck nodes and/or internal mammary nodes diagnosed on clinical examination or any imaging assessment (unless such sites can be confirmed as negative following biopsy)
- Distant metastases
- Involvement of contralateral axillary, supraclavicular, infraclavicular or internal mammary nodes (unless there is histologic confirmation that these nodes are negative)
- Prior non-hormonal therapy or radiation therapy for the current breast cancer
- Patients with Paget's disease of the nipple.
- Skin involvement, regardless of tumor size.
- Patients with a breast technically unsatisfactory for radiation therapy.
- Inability to lie prone with arms raised above head for extended periods of time.



- Patients not appropriate for BCS due to expectation of poor cosmetic result, even without RT
- Collagen vascular disease (particularly lupus, scleroderma, dermatomyositis)
- Inability or unwillingness to provide informed consent.
- Any other malignancy at any site (except non-melanomatous skin cancer) < 5 years prior to study enrollment
- Patients who are pregnant or lactating

## Appendix B

### B The Effect of Partial Volume on $T_{10}$ Estimation Using the Variable Flip Angle Method

**Purpose:** In chapter 4, the tumour contour was altered in an attempt to remove  $T_{10}$  values that may have been influenced by partial volume averaging with the surrounding fat. The images acquired for  $T_{10}$  were not fat-suppressed for the majority of patients. Initially we acquired these images without fat suppression to avoid the small gaps in the sequence that slightly perturbs the magnetization. However, we found that the partial volume problem created a substantial challenge for analysis, especially for small tumors.

This appendix demonstrates the effects of partial volume effects on  $T_{10}$  estimation when fat is not suppressed.

**Methods:** To generate the simulated signals for fat and fibroglandular tissue the SPGRE equation was used:

$$S = PD \frac{1 - \exp(-TR/T_{10}) \sin(\theta)}{1 - \cos(\theta) \exp(-TR/T_{10})} \quad (\text{B.1})$$

where  $PD$  is the proton density which was assumed to be equal to 1 for both fat and fibroglandular tissue,  $TR$  is the repetition time = 4.97ms (as per SIGNAL),  $\theta$  is the flip angle, and  $T_{10}$  is the native longitudinal relaxation time. Signal equations for fat and fibroglandular tissue were simulated using a  $T_{10}$  of 366.78 ms and 1444.83ms, respectively [2]. For initial generation of the signal curves, we used flip angles from 1 to 50 degrees.

To determine the total signal observed, we must first calculate the angle offset between the fibroglandular and fat tissue magnetizations:

$$\Delta\theta = \Delta\omega_0 T_E \quad (\text{B.2})$$

where  $\Delta\theta$  is the angular difference between the two vectors in radians,  $\Delta\omega$  is the frequency difference between water and fat ( $440 \cdot 2\pi$  Hz at 3T), and  $T_E$  is the echo time, set to 1.5ms as per the imaging protocol. Using this and the law of cosines, the total signal was calculated from the individual signal curves using relative percentages of fat and fibroglandular tissue (Figure B.1):

$$S_{total} = \sqrt{(P_{fat}S_{fat})^2 + [(1 - P_{fat})S_{fibro}]^2 - 2(P_{fat}S_{fat})(1 - P_{fat})S_{fibro}(-\cos(\Delta\theta))} \quad (\text{B.3})$$

where  $P_{fat}$  is the proportion of fat,  $S_{fat}$  and  $S_{water}$  are the signals calculated from equation B.1, and  $-\cos(\Delta\theta)$  is to calculate for the interior angle of the triangle.

$S_{total}$  was sampled at flip angles 1, 3, 5, 8, and 14 which correspond to the range and number of flip angles used in SIGNAL. No noise was added to the curve. Using non-linear fitting, the  $T_{10}$  was estimated from the sampled  $S_{total}$  curve.

**Results:** Figure B.2 shows the results of this analysis. Depending on the proportion of fat, there is over or under estimation of the  $T_{10}$  value.

**Discussion/Conclusion:** Even with just a small partial volume effect, there are overestimations of  $T_{10}$  - and this was in the absence of any noise. This result provides motivation for

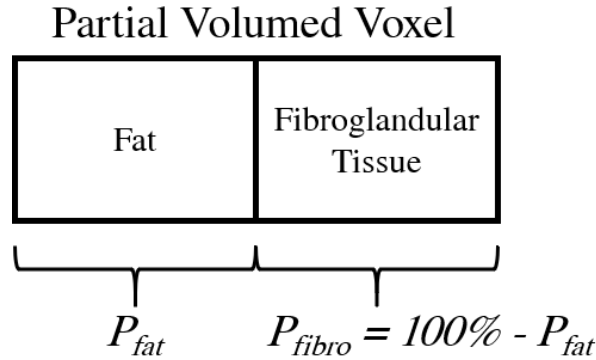


**Figure B.1:** Representation of a partial voxel with different percentages ("P") of fat and fibroglandular tissue

our decision to use a population average  $T_{10}$  value for patient tumours in all patients. This population average  $T_{10}$  was determined by averaging the measured  $T_{10}$  values across all of our patients scans. Both pre and post SABR  $T_{10}$  values were included in the average since differences between average values for pre vs post SABR were very small and not statistically significant.

A particular limitation of this analysis is that we assumed that the fibroglandular tissue and the surrounding adipose tissue have equal proton density. This was based on the fact that the  $1^\circ$  flip angle images (which are almost proton density weighted) had essentially no contrast between fibroglandular and the surrounding fat tissue.

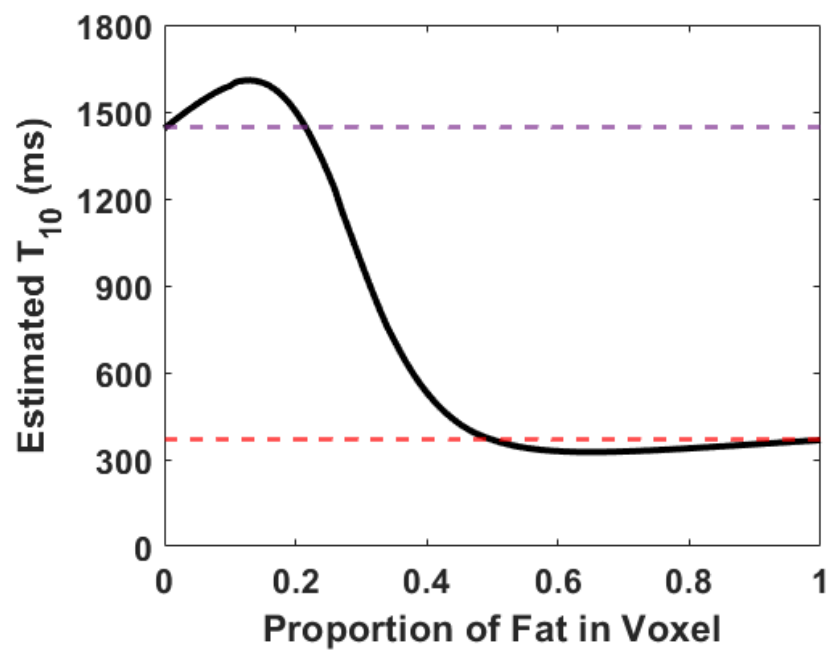


**Figure B.2:** Estimated  $T_{10}$  values as a function of the percentage of fat in the partial volumed voxel. The purple dashed line represents the “true” value of fibroglandular tissue and the red dashed lines is the “true” value of fat

## Appendix C

### C Response assessment - detailed methodology for image registration and post-SABR contour generation

In chapter 4, a brief methodology was given to fit within the constraints of the journal publication. In this appendix, a detailed account of the methodology used for response assessment is given. The general overview given in Figure 4.1 is a good reference for a high-level overview of the methodology.

#### Intra-session image registration

The first step in the registration process was to register the intra-session images. Chapter 3 provides an account of how this was performed and is not re-iterated here. All images that were not part of the DCE-MRI series were registered in MIM (v6.8.0, MIM Software, Cleveland, USA) using the multi-modality metric. The motivation for using MIM and its multi-modality metric rather than 3DSlicer is that I found this was better able to deal with registrations between the non-fat suppressed variable flip angle images and the fat-suppressed DCE-MRI images. Figure C.1 shows a schematic overview of the registration process for aligning the  $T_1$  images and the  $B_1$  to the DCE registered series. Bias correction was performed to remove slowly varying spatial intensity changes across the image based on the N4ITK algorithm [3]. The bias corrected image with the largest flip angle that was part of the  $T_{10}$  image set was registered to bias corrected pre-contrast DCE image. This deformation field was then applied to each of

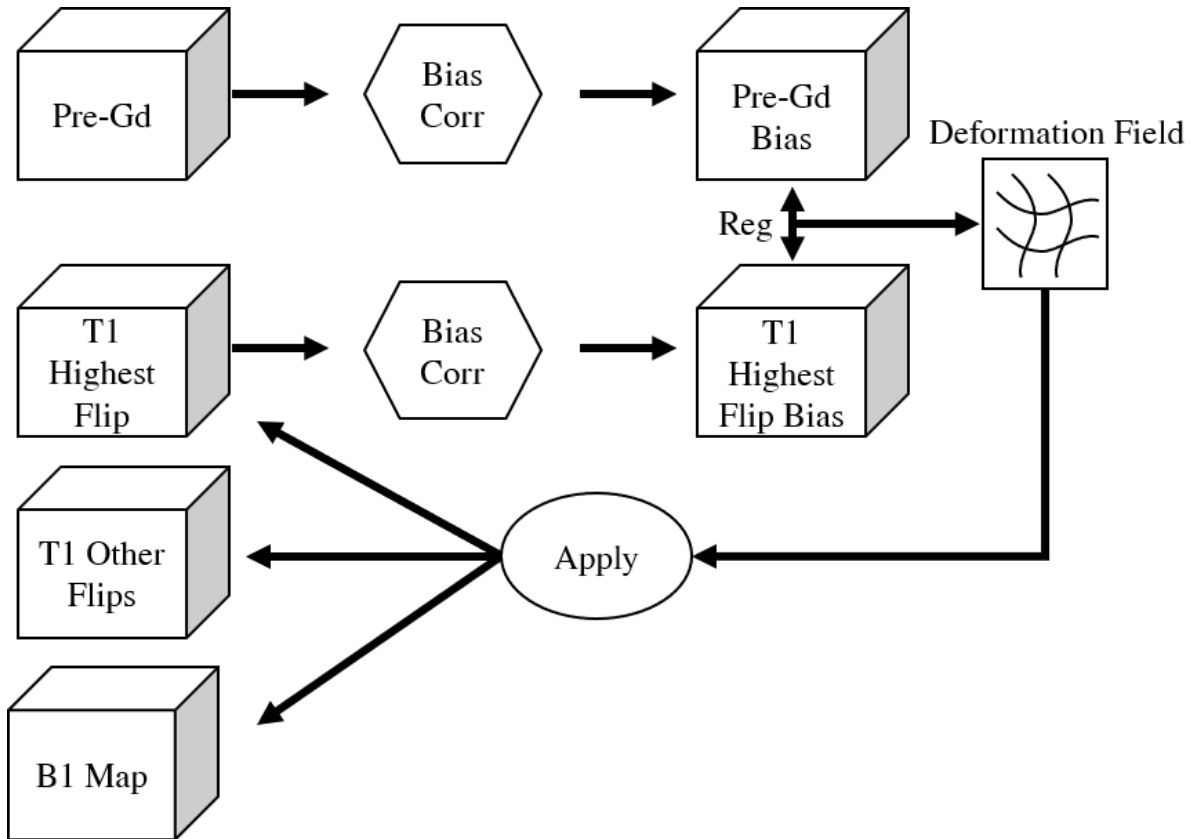


**Figure C.1:** Schematic of how the different images that comprise the variable flip angle sequence and  $B_1$  image were registered within a session to the pre-contrast DCE-MRI. Corr = correction, Gd = gadolinium contrast

the acquired images used for  $T_1$  mapping and  $B_1$  map, resulting in a fully intra-session motion corrected data set.

### Post-SABR to Pre-SABR Registration for Post-SABR Contour Generation

Due to the presence of signal enhancement surrounding the tumour in the post-SABR setting, we attempted to preserve the tumour volume by generating a contour in the pre-SABR setting and transfer it to the post-SABR setting using deformable registration. Figure C.2 shows this process schematically. The registered (intra-session) pre-contrast images were bias corrected and then deformably registered to each other. The deformation field was then applied to the

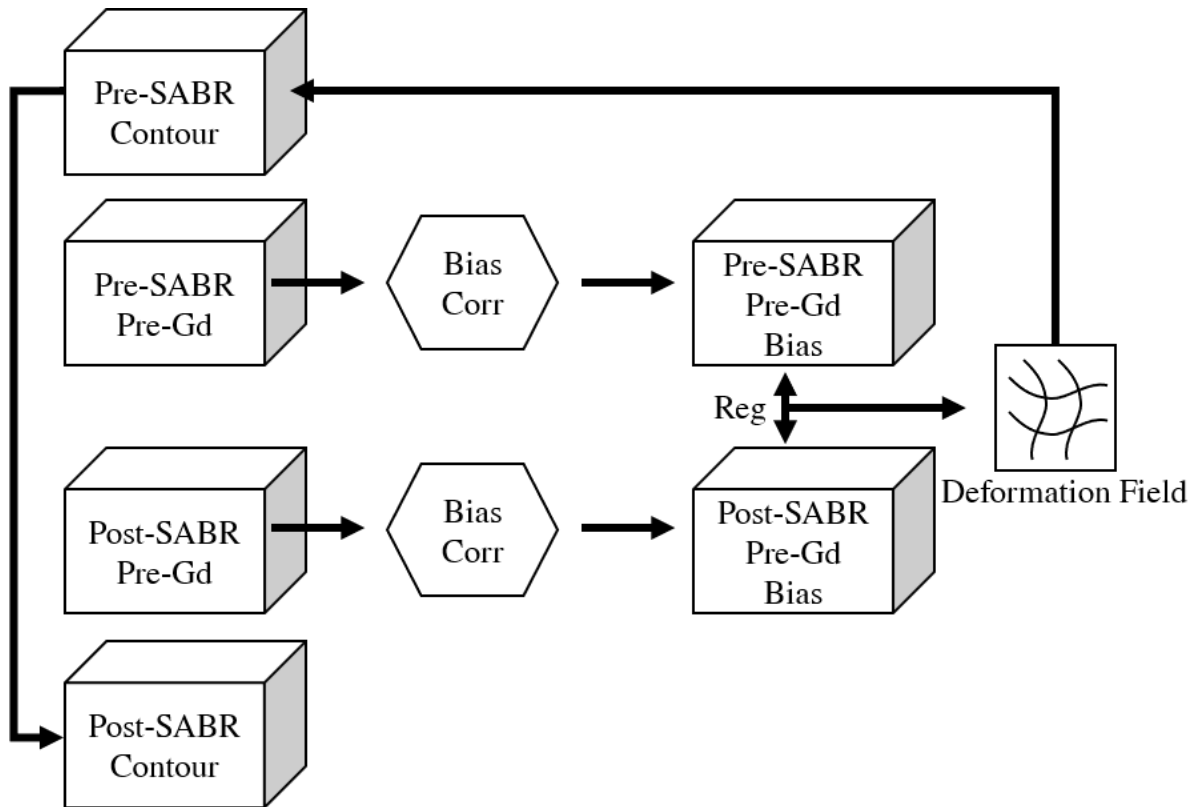


**Figure C.2:** Schematic of how the post-SABR contour was generated from the pre-SABR tumour contour. Corr = correction, Gd = gadolinium contrast

pre-SABR contour to generate the post-SABR contour.



## Appendix D

### **D Response assessment - $B_1$ and $T_{10}$ variation within the tumour for Chapter 4**

In chapter 4 we indicated that an average  $B_1$  and  $T_{10}$  was used. In this appendix, the average value across voxels for each patient is provided for the reader. Figure D.1a shows the  $B_1$  values across patients for the three groups under study. There was essentially no variation in  $B_1$  values measured even though two different  $B_1$  correction techniques were used (see 1.7.4). Figure D.1b shows  $T_{10}$  variation across patients. There were larger differences in group 1, likely due to smaller tumours being included and a larger effect of partial voluming with the clip and surrounding fat tissue. In groups 2 and 3 there was essentially no difference pre- and post-SABR.

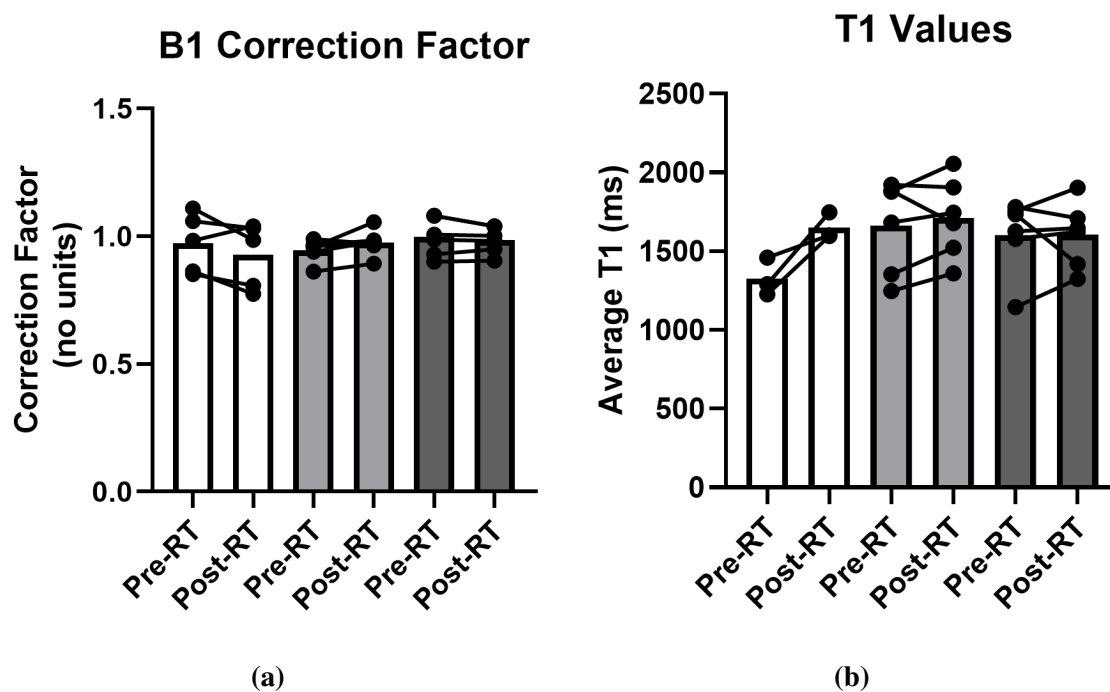


**Figure D.1:** Additional Results for Chapter 4 showing variation of  $B_1$  (a) and  $T_{10}$  (b) across patients

## Appendix E

### E Appendix A-C Bibliography

#### E.1 Bibliography

- [1] K. Guidolin, M. Lock, B. Yaremko, N. Gelman, S. Gaede, A. Kornecki, V. Moiseenko, J. Cao, L. Scott, and M. Brackstone, “A phase II trial to evaluate single-dose stereotactic body radiation therapy (SBRT) prior to surgery for early-stage breast carcinoma: SIGNAL (stereotactic image-guided neoadjuvant ablative radiation then lumpectomy) trial,” *Journal of Radiation Oncology*, vol. 4, no. 4, pp. 423–430, 2015.
- [2] R. Rakow-Penner, B. Daniel, H. Yu, A. Sawyer-Glover, and G. H. Glover, “Relaxation times of breast tissue at 1.5T and 3T measured using IDEAL,” *Journal of Magnetic Resonance Imaging*, vol. 23, no. 1, pp. 87–91, 2006.
- [3] N. J. Tustison, B. B. Avants, P. A. Cook, Y. Zheng, A. Egan, P. A. Yushkevich, and J. C. Gee, “N4ITK: Improved N3 bias correction,” *IEEE Transactions on Medical Imaging*, vol. 29, pp. 1310–1320, jun 2010.

## Appendix F

### **F Stereotactic Image-Guided Neoadjuvant Ablative Single Dose Radiation Then Lumpectomy (Signal) For Early Breast Cancer: A Prospective Single Arm Trial Of Single Dose Radiation Therapy**

#### **F.1 Introduction**

The modern management of low-risk breast cancer involves the use of breast conserving surgery (BCS) plus radiotherapy (RT), which can be hypofractionated without sacrificing efficacy or safety when compared to standard RT (i.e. 50 Gy in 25 fractions) [1–7]. Recently, APBI was postulated as a viable treatment option for low-risk disease since most local recurrences are located in the lumpectomy cavity [8,9]. The most accelerated example of APBI is single-fraction radiotherapy (SFRT), which is well established in the literature and has been used to treat large cohorts of women with low-risk breast cancer, with acceptable clinical outcomes [10,11]. It is more convenient and may reduce health-care costs by freeing space on the radiation treatment units. SFRT may entice more women to undergo standard of care treatment (i.e. breast conserving surgery with RT), because the primary reasons for the underutilization of adjuvant radiotherapy following breast conserving surgery are the time, travel and effort required [12,13]. Despite such benefits, SFRT is associated with an increased risk of treatment-related toxicity compared to standard techniques, and it has historically required

treatment planning and delivery platforms that were not widely available, which limit its use in North America [14]. In Canada, intra-operative radiation is cost-prohibitive due to the expense of disposable components and is currently used in very few centres. With the movement toward hypofractionation in the radiotherapeutic management of low-risk carcinoma of the breast in general, a discussion of how best to implement and to incorporate SFRT into routine clinical practice is very timely.

We therefore developed SIGNAL (Stereotactic Image-Guided Neoadjuvant Ablative radiation then Lumpectomy), a single-arm, single-institution clinical trial, wherein a cohort of women with early-stage low-risk carcinoma of the breast was treated with neoadjuvant radiotherapy delivered one week prior to lumpectomy [15]. We selected 21 Gy in one fraction based on a dose escalation trial and another single arm trial, and radiobiological calculations described previously, delivered prone using external beam volumetric modulated arc therapy, with dosimetry planning on computerized tomography (CT) simulation images co-registered with magnetic resonance imaging (MRI) images [15–17]. Our objectives were to evaluate the feasibility and safety of this approach in a pilot design, as a guide for future randomized-controlled studies. Our hypothesis was that for selected patients with low-risk breast carcinoma, neoadjuvant partial-breast hypofractionated SBRT would be technically feasible, with acceptable toxicity and cosmesis. Here, we report the toxicity and cosmesis outcomes observed in a cohort of patients treated according to this regimen.

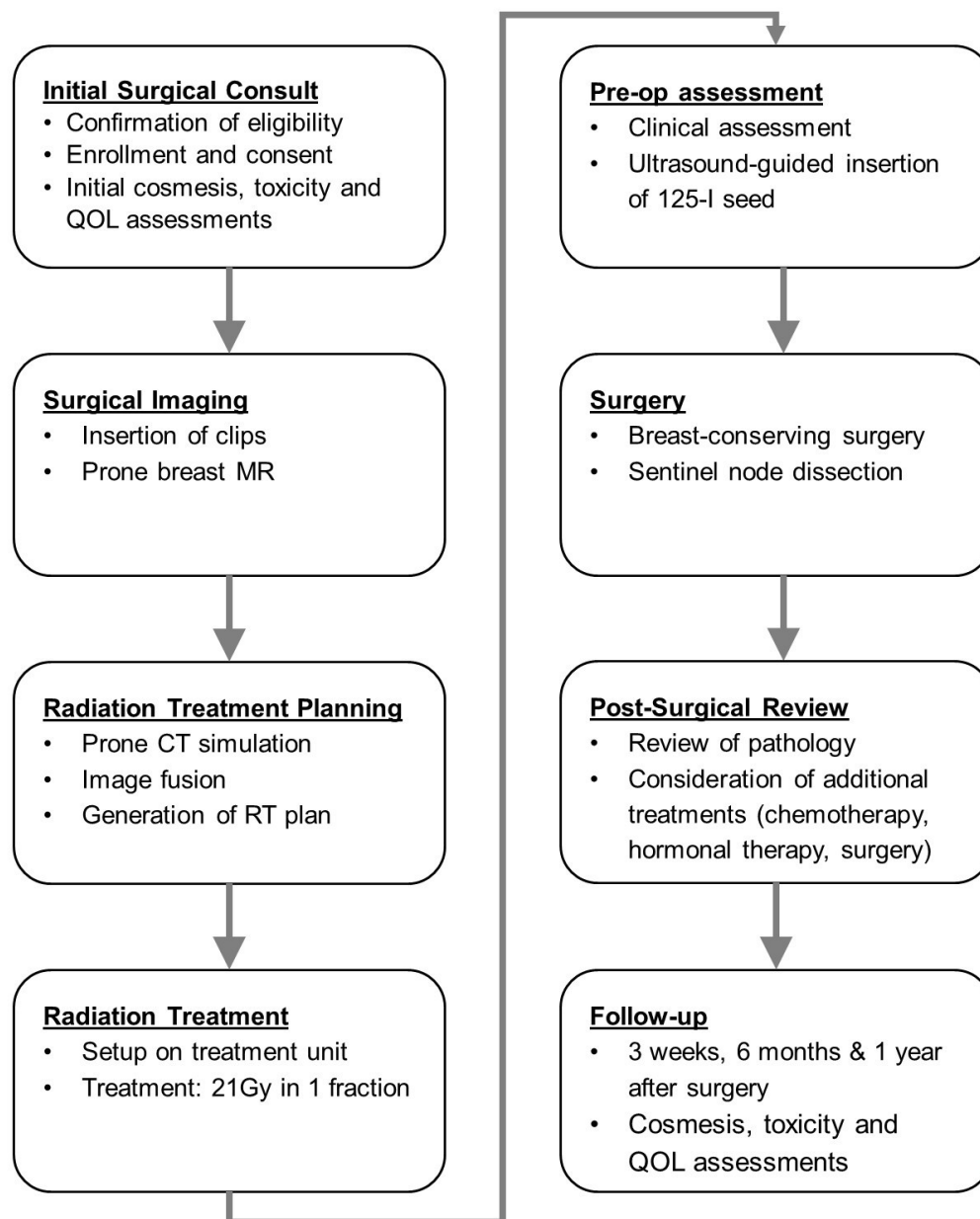


**Figure F.1:** Study schema showing the entire course of the experimental protocol undergone by patients in this study

## F.2 Methods

The SIGNAL protocol has been previously published, and the study schema is shown in Figure F.1 [15]. SIGNAL had two primary endpoints: radiation toxicity and feasibility. Radiation toxicity was defined as grade  $\geq 2$  toxicity, such as fibrosis, measured using the Common Terminology Criteria for Adverse Events (CTCAE) [18]. Feasibility was defined as the ability to deliver treatment in accordance with the study-defined dosimetry constraints in  $\geq 90\%$  of patients. Secondary endpoints were (i) cosmesis, scored by the patient and radiation oncologist or surgeon, using the Modified Harvard-Harris Cosmetic Scale [19]; and (ii) quality of life (QOL), measured using the Functional Assessment of Cancer Therapy - Breast (FACT-B) tool [20]. Post-operative complications were also collected, analyzed, and reported. SIGNAL was approved by Western University's Health Sciences Research Ethics Board (HSREB Number 105643) and was registered with Clinicaltrials.gov (identifier: NCT02212860).

All post-menopausal women presenting for surgical consultation between 2014 and 2016 with a new diagnosis of early stage (size  $< 3$ cm, node-negative), estrogen receptor (ER) positive, unifocal breast cancer were approached for participation. If initial ultrasound suggested sufficient distance (i.e.  $\geq 2$  cm) between both the lesion and skin, and the lesion and chest wall, patients were enrolled. Once enrolled, patients underwent ultrasound-guided insertion of a surgical clip as a fiducial marker. They were then immobilized on a prone breast board and were imaged by contrast-enhanced prone breast MRI. If MRI confirmed unifocal disease less than 3 cm, sufficiently distant from the skin and the chest wall, patients proceeded on to radiation treatment planning: all patients were again positioned and immobilized on a prone

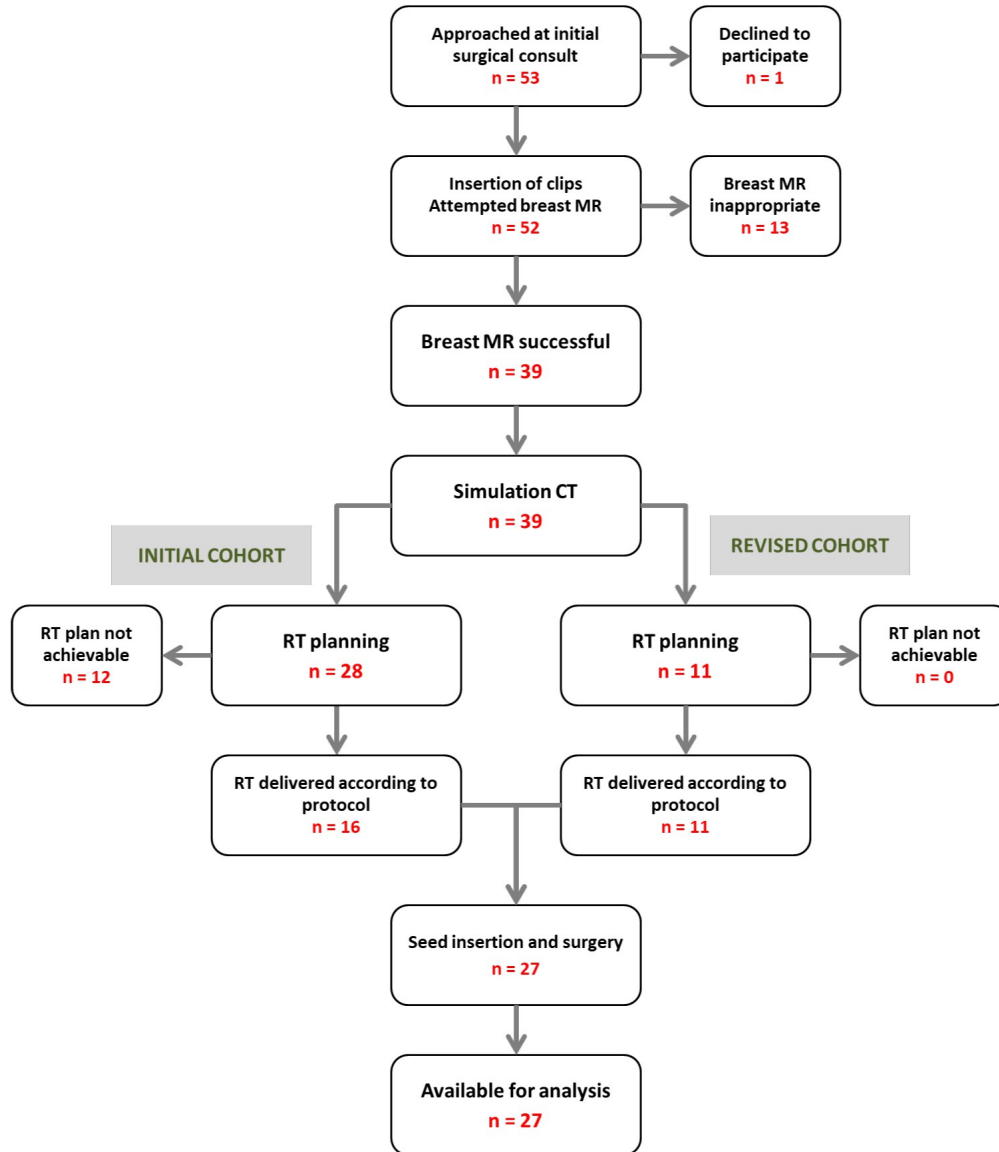


**Figure F.2:** Sample size of the different cohorts of patients included in SIGNAL

breast board for CT simulation. The prone breast MRI was fused onto the prone CT simulation images using rigid body registration. The GTV was defined as the primary breast lesion seen on MRI. The CTV was defined as the GTV plus a 5 mm margin. The PTV was defined as



the CTV plus a 5 mm margin. Radiation treatment plans were devised to deliver a prescription dose of 21 Gy to the PTV in a single fraction. 21 Gy was delivered using SBRT with the patient in prone position, using cone-beam CT imaging to confirm patient positioning and accuracy of delivery by localizing the tumour via the surgical clip. Real-time image acquisition was used to monitor patient positioning and allowed the beam to be disabled if the patient moved significantly. Relevant, as-treated dosimetric constraints were based upon a thorough review of relevant published literature, published SBRT-based clinical trials and general radiobiological principles (Table F.1). Following induction radiotherapy, radiolocalizing I-125 seeds were placed adjacent to the surgical clip to facilitate localization and guided excision. All patients underwent breast conserving surgery and sentinel node biopsy (where clinically indicated), ideally within 1 week of radiotherapy. Older patients could opt out of sentinel node biopsy in accordance with clinical guidelines. Toxicity, cosmesis (patient-assessed and physician-assessed) and QOL measures were collected at baseline, 3 weeks post-operation, 6 months post-operation, and 1 year post-operation. Toxicity was reported as the number of patients who experienced any grade 2 or higher toxicity at each time point, and these were compared to baseline using Fisher's exact test. The cosmesis score (excellent, good, fair, poor) was collapsed into the proportion of patients or physicians rating the cosmesis as excellent/good or as fair/poor, in order to allow for comparisons to other publications using the Modified Harvard-Harris Cosmetic Scale in breast irradiation trials. The proportion of patients or physicians reporting a good or excellent cosmetic score at each time point were compared to baseline using the Fisher's exact test. The QOL total score was compared at each time point to baseline using the Student's t-test.

### F.3 Results

Between February 2014 and September 2016, 53 patients were approached for participation, and 52 patients were initially enrolled (Figure F.2). Of these, 13 were excluded at the time of MRI: 2 were upstaged by MRI; 5 did not fit in the MRI bore or were unable to remain still; and 6 failed due to proximity of disease to skin or chest wall as-measured on MRI. Of the remaining 39 who met the criteria for breast MRI and went on to radiation treatment planning, the study-specified dosimetric constraints could not be met in 12 of them (in every case, it was the chest wall and/or skin constraints that could not be met). These patients were taken off study protocol and instead went on to surgery and standard whole-breast adjuvant radiotherapy.

The remaining patients fell into one of two distinct cohorts depending upon when they were treated (Figure F.2). The first of these cohorts comprised the first 36 patients approached (the “Initial Cohort”). Of these, 8 were excluded at the time of MRI: 2 were upstaged by MRI; 2 did not fit in the MRI bore; 4 failed due to proximity of disease to skin or chest wall. Of the remaining 28 patients, the study-defined dosimetric constraints could not be met in 12 of them (the same 12 detailed above). Therefore, in the Initial Cohort, only 16 of 28 patients meeting the study criteria by breast MRI went on to receive the study-defined treatment, representing a cohort-specific success rate of 57%. This was deemed a failure of the approach, triggering an interim review as-required by protocol. During the interim review, we concluded that our dosimetric constraints were too restrictive, especially regarding dose to skin. We similarly concluded that our original definition of skin (external contour less 5 mm) was too restrictive and more conservative than that used in similar published clinical trials employing SFRT [21].

**Table F.1: Normal Tissue Dosimetric Limits – Original and Revised.** Our initial study cohort (n=16) was treated according to the original limits (2014). Following an interim review and quality assurance assessment, we adopted a new set of limits (2016) (n=11 completed treatment). SE = Standard Error; D [x cm<sup>3</sup>] = dose delivered to a volume of x cm<sup>3</sup>.

Structure	Original Cohort (n=16)		Revised Cohort (n=11)	
	Dose (Gy)	Specification	Dose (Gy)	Specification
Uninvolved Ipsilateral Breast	10	≤50%	10.5	≤50%
	18	≤20%	20	≤47%
	21	≤47cm <sup>3</sup>	21	Point Dose
Contralateral Breast	0.6	Point Dose	1	Point Dose
Total Lung	-	-	11	≤35%
Ipsilateral Lung	6	≤15%	7.5	≤15%
	10	≤10%		
Contralateral Lung	3	≤5%	1.7	≤15%
Heart	3	≤5%	22	Point Dose
	1	≤40%	3	<5cm <sup>3</sup>
			16	≤15%
Thyroid	1.8	Point Dose	1.1	Point Dose
Skin	16	Point Dose	18.3	<5cm <sup>3</sup>
	10	≤10cm <sup>3</sup>		
Chest wall	10	≤10cm <sup>3</sup>	10	<10cm <sup>3</sup>
	15	Any Point	16	<2cm <sup>3</sup>

Revised dosimetric constraints were therefore developed (Table F.1) and implemented to treat the next 16 patients who were accrued (the “Revised Cohort”). Of these 16, 5 were excluded at the time of MRI: 2 were upstaged by MRI; 3 did not fit in the MRI bore; 2 failed due to proximity of disease to skin or chest wall. Of the remaining 11 patients, all of them went on to receive the study-defined treatment, representing a cohort-specific success rate of 100%. The actual mean doses delivered in both patient cohorts were similar between the cohort who underwent treatment at the initial dosimetric constraints and the cohort treated under the revised constraints (F.2).

**Table F.2: As-Treated Target Dosimetry.** Numbers represent the as-treated dosimetry doses averaged over the initial cohort (n = 16), the subsequent revised cohort (n=11), and the total study cohort (n=27). SE = Standard Error

	Original (n=16)	Revised (n=11)	Total (n=27)
Dosimetry	Mean Dose $\pm$ SE	Mean Dose $\pm$ SE	Mean Dose $\pm$ SE
Prescription dose (Gy)	21	21	21
Prescription isodose (%)	95.7 $\pm$ 0.4	96.5 $\pm$ 0.30	95.9 $\pm$ 0.3
Delivered dose at isocentre (Gy)	22.0 $\pm$ 0.09	22.2 $\pm$ 0.36	22.0 $\pm$ 0.11
Minimum dose to 100% PTV (Gy)	19.5 $\pm$ 0.2	19.1 $\pm$ 0.45	19.3 $\pm$ 0.22
Minimum dose to 95% PTV (Gy)	21.0 $\pm$ 0.1	21.0 $\pm$ 0.06	21.0 $\pm$ 0.05

All treated patients underwent local excision of the primary tumour to negative margins within 7 days of radiation without any delay or complication. No patients showed signs of erythema at the time of surgery, none described any pain, and every patient expressed pleasure with the entire process. None of the surgeries were made more complicated as a result of the pre-operative radiation, and in fact the tissues appeared healthy and normal. No post-operative complications were encountered. No patients required in situ drains and none had prolonged seroma, wound dehiscence, skin necrosis or infections in the post-operative period.

Patient demographic and tumour details are presented in Table F.3. Toxicity, cosmesis (patient-assessed and physician-assessed) and QOL measures (all assessed at baseline, 3 weeks, 6 months, and 1 year post-operation) are presented in Table F.4. No patients experienced CTCAE toxicity grade 2 or higher at baseline, 3 weeks, or 1 year postoperatively, and one patient out of 27 had a grade 2 delayed wound infection at the 6-month postop visit, which was not significantly different from baseline (p=1.0). Physician-rated cosmesis (Harvard-Harris score) was slightly worse than baseline (100% good/excellent) at the 3-week (93% good/excellent, p=0.16), 6-month (96% good/excellent, p=0.29), and 1-year (92%

**Table F.3: Patient Demographics: Baseline and Tumour Characteristics.** The baseline patient and tumour characteristics are represented for the entire study cohort (n=27). Age and tumour size are represented as mean +/- standard deviation, while all other categorical data are represented as number of patients (percentage of cohort). Tumour size in ultrasound represents the best pre-treatment estimate of baseline tumour size (using imaging), while tumour size reported by pathologist represents the best estimate of post-treatment tumour size. The two were compared using paired Student's t-test.

N = 27	Baseline (mean $\pm$ SD) or N (%)
Age (years)	38.7 $\pm$ 6.5
Laterality	
Left	14 (60.9%)
Right	9(39.1%)
Tumour Size (cm)	
Ultrasound	1.2 $\pm$ 0.63
Pathology	1.17 $\pm$ 0.63
Pathological Nodal Stage	
N0	21 (91.4%)
N1mic	1 (4.3%)
N1	1 (4.3%)
Grade	
1	10 (43.5%)
2	12 (52.2%)
3	1 (4.3%)
ER+	23 (100%)
PR+	18 (78.3%)
HER2+	2 (8.7%)

good/excellent,  $p=0.13$ ) postoperative periods, but none of these differences were statistically significant. Physicians rated 96% of patients' cosmetic outcomes as good/excellent at baseline versus 93% at 3 weeks ( $p=0.60$ ), 92% at 6 months ( $p=0.53$ ), and 96% at 1 year ( $p=0.98$ ); again, none of these changes were statistically significant. Compared to baseline, QOL was significantly improved compared to baseline at 3 weeks ( $p=0.01$ ), and 1 year post-operation ( $p=0.001$ ), and was elevated, though not significantly, at 6 months post-operation ( $p=0.09$ ).

**Table F.4: Toxicity, Cosmesis, and Quality of Life Outcomes Pre- and Post-Treatment** Toxicity is graded from 0-5 (CTCAE), cosmesis rated 1-4 (Modified Harvard-Harris), quality of life rated out of a total 148 possible points (FACT-B), each scored 0-4. Three week, 6-month and 1-year postop outcomes of patient and physician cosmesis as well as toxicity were each compared to baseline values using fisher's exact test. Paired Student's t-test for was used to compare FACT-B mean quality of life score at each time point to baseline.

N = 27	Baseline (mean $\pm$ SD or N(%))	3-week F/U (mean $\pm$ SD)	p-value (3 wk. vs baseline)	6-month F/U (mean $\pm$ SD)**	p-value (6 mo. vs baseline)	1 yr F/U (mean $\pm$ SD)**	p-value (1 yr vs baseline)
Toxicity <sup>§</sup> ( $\geq$ grade 2)	0	0	p=1.0	1	p=1.0	0	p=1.0
Cosmesis <sup>†</sup> (physician rated)	100%	93%	p=0.16	96%	p=0.29	92%	p=0.13
Cosmesis <sup>†</sup> (patient rated)	96%	93%	p=0.60	92%	p=0.53	96%	p=0.98
Quality of Life Score (FACT-B)	118.68 $\pm$ 16.8	123.56 $\pm$ 16.9	p=0.01*	122.48 $\pm$ 15.7	p=0.09	127.15 $\pm$ 15.4	p=0.001*

\*statistically significant,  $\alpha=0.05$

\*\*n=24 (1 patient diagnosed with advanced renal cell carcinoma, 1 patient diagnosed with glioblastoma, 1 patient diagnosed with metastatic breast cancer from prior remote contralateral breast cancer).

<sup>§</sup>Only 1 patient had a grade 2 toxicity (delayed wound infection), felt to be treatment related.

<sup>†</sup>Percentage rated good or excellent.

## F.4 Discussion

SIGNAL represents a novel approach to the radiotherapeutic management of early-stage, low-risk carcinoma of the breast. The classic approach for such patients, established over many decades, is surgery followed by radiotherapy. The benefit of adjuvant radiotherapy in such a setting is well known, and so too are its toxicities. In principle, neoadjuvant radiotherapy holds several advantages over adjuvant radiotherapy, including improved tumor oxygenation, reduced dose to the surrounding normal tissues due to a smaller target volume, and of course the ability to recognize and to delineate the disease in situ. This latter benefit was of particular

interest to us given the availability of MRI for radiation treatment planning with image co-registration. Hypofractionation is now established in the treatment of multiple malignancies. As SFRT, SBRT and other hypofractionated techniques likewise become more established in the management of breast cancer, it is incumbent upon us to understand as fully as possible the potential benefits and toxicities of this approach.

The unique aspects of this trial include the use of VMAT with strict dosimetry constraints to skin and normal tissues, avoiding any early erythema or dermatitis to the skin, as well as any delayed fibrosis or telangiectasias by latest follow-up at 1 year. The co-registration of prone breast imaging allowed for high fidelity treatment delivery, minimizing dose to skin which, if these low risk patients had requested mastectomy, would not require radiation at all, but when radiated does contribute to a worsening cosmetic outcome and patient satisfaction. This may explain why our cosmetic outcomes were better than those reported by Pinnaro in their SFRT trial using intensity-modulated radiotherapy (59% of patients reporting good/excellent cosmetic outcome), and similar or better than other larger trials looking at cosmesis with more standard radiation regimens (ranging from 81-95% reporting good/excellent cosmesis) [17, 20, 22].

As a pilot study, SIGNAL's primary endpoints were feasibility and safety. Our results suggested that SFRT, when delivered in the manner specified by SIGNAL, was certainly tolerable and well-liked by the patients. Our approach was not feasible with the first cohort of patients using the initial dosimetry constraints but became feasible after revisions of the conservative constraints permitted successful treatment of all eligible patients. In that initial patient cohort, 12 patients who appeared eligible by breast MRI were not able to have acceptable radiation treatment plans generated. For these 12 patients, the primary reason for ineligibility was prox-

imity of the GTV to the skin (8 patients) and chest wall (4 patients), thereby rendering it impossible to meet the study-defined dosimetric limits. We therefore realized that our limits were simply too restrictive and would limit generalizability of the trial to a breast cancer population commonly seen in practice. This difficulty was most obvious for skin. We initially defined skin as the external contour contracted isotropically by 5 mm; and we likewise required that the PTV could not extend into the skin. In addition, we imposed a maximum point-dose of 16 Gy to the skin. Such definitions severely limited our ability to devise an acceptable treatment plan in patients whose disease was located more than 2 cm away from the skin surface. The situation was even less tenable when the PTV was situated in areas where the external breast contour was changing rapidly in three dimensions, such as in the retro-areolar region, where the PTV was surrounded by “skin” on every side except posteriorly. In addition, for lesions located very medially, buildup of dose was less, necessitating delivery of somewhat higher dose both superficially and also through the chest wall in order to attain the prescription dose.

When we devised the original normal tissue dosimetric limits for SIGNAL, we reviewed multiple published studies of SFRT [11, 17, 21, 23, 24] and APBI [25, 26], delivered using a variety of techniques, in both the pre-operative and post-operative settings. Most of these studies did not state specific skin constraints, even though the primary toxicity in most cases appeared to be skin toxicity. Therefore, our original dosimetric limits were chosen to be conservative, recognizing that there was limited clinical data available at this dose-fractionation. Our revised dosimetric criteria were based upon re-review of the published literature, and upon our limited clinical experience gained up to that point. Once the dosimetric limits were revised, 100% of MRI-eligible patients accrued to the study were successfully treated, which met our a priori feasibility threshold of 90%. Therefore, we feel that SIGNAL (using the revised dosimetric



constraints) could be considered a feasible method of delivering single-dose neoadjuvant radiation therapy.

Our second primary end-point was radiation toxicity, which is related to secondary end-points cosmesis and QOL, since changes to the skin and underlying soft tissue of the breast could be immediately visible as discolorations. The mean toxicity score was not significantly different from baseline at 3 weeks, 6 months, or 1 year (Table F.4). A few grade 1 post-surgical toxicities were reported (such as transient post-surgical thickening at scar), while one patient in the entire study suffered a grade 2 toxicity (delayed wound infection at 6 months postop), representing an expected breast wound infection rate from surgery alone. Neither patient nor physician-rated cosmesis scores changed significantly from baseline at 3 weeks or 6 months postop (Table F.1). Finally, patients reported significantly improved QOL at 3 weeks compared to baseline, although this returned to baseline by 6 months.

The main limitation is the small sample size and relatively short follow up of this single-arm study. SIGNAL was designed to determine overall feasibility, to identify any early concerns regarding toxicity and safety, and to assess patient interest to inform the design of future prospective randomized clinical trials. SIGNAL was certainly well received by our patients (only 1 of 53 patients declined participation). Once we identified workable dosimetry constraints, we were successful in treating patients in a very timely manner, something that was very popular with our local patient population, with many of them living several hours away. Although acute toxicity and cosmesis were certainly acceptable, it is not possible to comment upon late radiation toxicity as we simply have not followed our patients for a sufficiently long time to enable such an assessment to be made. The determination of late radiation toxicity is especially relevant with SFRT given that the estimation of equivalent radiobiologic effects

at higher dose per fraction is notoriously difficult. Nonetheless, we are satisfied with our selected dose (21 Gy in a single fraction) for several reasons. It was selected based upon both the standard linear-quadratic formulation as well as newer approaches such as the “universal survival curve” which models effects at high doses per fraction more accurately [27]. In addition, our selected dose was consistent with that delivered in several other similar studies [11, 17]. Finally, the use of MRI enabled us to define the GTV very accurately, and the fact that the prescription dose was confined to the area targeted for excision likely reduced any significant impact on acute and delayed [28]. To ensure safety we used very stringent criteria including requiring lesions to be at least 2 cm from the skin. To ensure accurate localization, we fused a breast MRI for each patient. Furthermore, we moved to a prone set up to minimize the impact of respiratory motion and day-to-day set up of the breast. These three components of our treatment are not readily available in all institutions and would limit the generalizability. However, to maximize safety, to provide sufficient dose, and to ensure reliability for this new technique, these components were included. These components could easily be adopted in most centres and an assessment of the need for each of these (especially MRI) will be published separately.

In conclusion, neoadjuvant single fraction (21 Gy) partial breast stereotactic radiation therapy followed by breast conserving surgery appears to be a feasible, safe and well-tolerated method for delivering radiation in the prone position using external beam radiotherapy and equipment available at standard radiation treatment facilities. The findings of this study need to be confirmed in a prospective, randomized clinical trial.

**Citation:** Keegan Guidolin, Brian Yaremko, Kalan Lynn, Stewart Gaede, Anat Kornecki, Giulio Muscedere, Ilanit BenNachum, Olga Shmuilovich, Matthew Mouawad, Edward Yu,

Tracy Sexton, Neil Gelman, Vitali Moiseenko, Muriel Brackstone, Michael Lock, *Current Oncology*, 2019, Vol 26 (3), Copyright Holder: *Keegan Guidolin*.

## F.5 Bibliography

- [1] B. Fisher, C. Redmond, R. Poisson, R. Margolese, N. Wolmark, L. Wickerham, E. Fisher, M. Deutsch, R. Caplan, Y. Pilch, A. Glass, H. Shibata, H. Lerner, J. Terz, and L. Sidorovich, "Eight-year results of a randomized clinical trial comparing total mastectomy and lumpectomy with or without irradiation in the treatment of breast cancer," *Obstetrical and Gynecological Survey*, vol. 44, pp. 618–619, mar 1989.
- [2] U. Veronesi, R. Zucali, and A. Luini, "Local control and survival in early breast cancer: The milan trial," *International Journal of Radiation Oncology, Biology, Physics*, 1986.
- [3] A. P. Forrest, H. J. Stewart, D. Everington, R. J. Prescott, C. S. McArdle, A. N. Harnett, D. C. Smith, and W. D. George, "Randomized controlled trial of conservation therapy for breast cancer: 6-year analysis of the Scottish trial," *Lancet*, 1996.
- [4] T. J. Whelan, J.-P. Pignol, M. N. Levine, J. A. Julian, R. MacKenzie, S. Parpia, W. Shelley, L. Grimard, J. Bowen, H. Lukka, F. Perera, A. Fyles, K. Schneider, S. Gulavita, and C. Freeman, "Long-Term Results of Hypofractionated Radiation Therapy for Breast Cancer," *New England Journal of Medicine*, vol. 362, pp. 513–520, feb 2010.
- [5] FAST Trialists group, R. K. Agrawal, A. Alhasso, P. J. Barrett-Lee, J. M. Bliss, P. Bliss, D. Bloomfield, J. Bowen, A. M. Brunt, E. Donovan, M. Emson, A. Goodman, A. Harnett, J. S. Haviland, R. Kaggwa, J. P. Morden, A. Robinson, S. Simmons, A. Stewart, M. A. Sydenham, I. Syndikus, J. Tremlett, Y. Tsang, D. Wheatley, K. Venables, and J. R. Yarnold, "First results of the randomised UK FAST Trial of radiotherapy hypofractiona-

- tion for treatment of early breast cancer (CRUKE/04/015),” *Radiotherapy and Oncology*, vol. 100, pp. 93–100, jul 2011.
- [6] K. Holli, P. Hietanen, R. Saaristo, H. Huhtala, M. Hakama, and H. Joensuu, “Radiotherapy After Segmental Resection of Breast Cancer With Favorable Prognostic Features: 12-Year Follow-Up Results of a Randomized Trial,” *Journal of Clinical Oncology*, vol. 27, pp. 927–932, feb 2009.
- [7] J. S. Haviland, J. R. Owen, J. A. Dewar, R. K. Agrawal, J. Barrett, P. J. Barrett-Lee, H. J. Dobbs, P. Hopwood, P. A. Lawton, B. J. Magee, J. Mills, S. Simmons, M. A. Sydenham, K. Venables, J. M. Bliss, J. R. Yarnold, and START Trialists’ Group, “The UK Standardisation of Breast Radiotherapy (START) trials of radiotherapy hypofractionation for treatment of early breast cancer: 10-year follow-up results of two randomised controlled trials,” *The Lancet. Oncology*, vol. 14, pp. 1086–1094, oct 2013.
- [8] C. Correa, E. E. Harris, M. C. Leonardi, B. D. Smith, A. G. Taghian, A. M. Thompson, J. White, and J. R. Harris, “Accelerated Partial Breast Irradiation: Executive summary for the update of an ASTRO Evidence-Based Consensus Statement,” *Practical radiation oncology*, vol. 7, pp. 73–79, mar 2017.
- [9] C. Polgár, E. V. Limbergen, R. Pötter, G. Kovács, A. Polo, J. Lyczek, G. Hildebrandt, P. Niehoff, J. L. Guinot, F. Guedea, B. Johansson, O. J. Ott, T. Major, and V. Strnad, “Patient selection for accelerated partial-breast irradiation (APBI) after breast-conserving surgery: Recommendations of the Groupe Européen de Curiethérapie-European Society

- for Therapeutic Radiology and Oncology (GEC-ESTRO) breast cancer working group  
ba,” *Radiotherapy and Oncology*, vol. 94, no. 3, pp. 264–273, 2010.
- [10] U. Veronesi, R. Orecchia, P. Maisonneuve, G. Viale, N. Rotmensz, C. Sangalli, A. Luini,  
P. Veronesi, V. Galimberti, S. Zurrada, M. C. Leonardi, R. Lazzari, F. Cattani, O. Gentilini,  
M. Intra, P. Caldarella, and B. Ballardini, “Intraoperative radiotherapy versus external  
radiotherapy for early breast cancer (ELIOT): A randomised controlled equivalence trial,”  
*The Lancet Oncology*, vol. 14, pp. 1269–1277, 2013.
- [11] J. S. Vaidya, M. Baum, J. S. Tobias, F. Wenz, S. Massarut, M. Keshtgar, B. Hilaris,  
C. Saunders, N. R. Williams, C. Brew-Graves, T. Corica, M. Roncadin, U. Kraus-  
Tiefenbacher, M. Sütterlin, M. Bulsara, and D. Joseph, “Long-term results of targeted in-  
traoperative radiotherapy (Targit) boost during breast-conserving surgery.,” *International  
journal of radiation oncology, biology, physics*, vol. 81, pp. 1091–7, nov 2011.
- [12] K. Guidolin, M. Lock, L. Richard, G. Boldt, and M. Brackstone, “Predicting which pa-  
tients actually receive radiation following breast conserving therapy in Canadian popula-  
tions,” *Canadian Journal of Surgery*, vol. 59, pp. 358–360, oct 2016.
- [13] E. H. Wang, H. S. Park, C. E. Rutter, C. P. Gross, P. R. Soulos, J. B. Yu, and S. B. Evans,  
“Association between access to accelerated partial breast irradiation and use of adjuvant  
radiotherapy.,” *Cancer*, vol. 123, pp. 502–511, feb 2017.
- [14] I. A. Olivotto, T. J. Whelan, S. Parpia, D. H. Kim, T. Berrang, P. T. Truong, I. Kong,  
B. Cochrane, A. Nichol, I. Roy, I. Germain, M. Akra, M. Reed, A. Fyles, T. Trotter,  
F. Perera, W. Beckham, M. N. Levine, and J. A. Julian, “Interim cosmetic and toxicity

- results from RAPID: A randomized trial of accelerated partial breast irradiation using three-dimensional conformal external beam radiation therapy,” *Journal of Clinical Oncology*, 2013.
- [15] K. Guidolin, M. Lock, B. Yaremko, N. Gelman, S. Gaede, A. Kornecki, V. Moiseenko, J. Cao, L. Scott, and M. Brackstone, “A phase II trial to evaluate single-dose stereotactic body radiation therapy (SBRT) prior to surgery for early-stage breast carcinoma: SIGNAL (stereotactic image-guided neoadjuvant ablative radiation then lumpectomy) trial,” *Journal of Radiation Oncology*, vol. 4, no. 4, pp. 423–430, 2015.
- [16] J. K. Horton, R. C. Blitzblau, S. Yoo, J. Geradts, Z. Chang, J. A. Baker, G. S. Georgiade, W. Chen, S. Siamakpour-Reihani, C. Wang, G. Broadwater, J. Groth, M. Palta, M. Dewhirst, W. T. Barry, E. A. Duffy, J.-T. A. T. A. Chi, and E. S. Hwang, “Preoperative Single-Fraction Partial Breast Radiation Therapy: A Novel Phase 1, Dose-Escalation Protocol With Radiation Response Biomarkers,” *International Journal of Radiation Oncology Biology Physics*, vol. 92, pp. 846–855, jul 2015.
- [17] P. Pinnarò, S. Arcangeli, C. Giordano, G. Arcangeli, F. A. Impiombato, V. Pinzi, G. Iaccarino, A. Soriani, V. Landoni, and L. Strigari, “Toxicity and cosmesis outcomes after single fraction partial breast irradiation in early stage breast cancer,” *Radiation oncology (London, England)*, vol. 6, p. 155, jan 2011.
- [18] U.S. Department of Health and Human Services, “Common Terminology Criteria for Adverse Events (CTCAE) and Common Toxicity Criteria (CTC),” vol. 2009, p. 65, 2010.

- [19] J. R. Harris, M. B. Levene, G. Svensson, and S. Hellman, "Analysis of cosmetic results following primary radiation therapy for stages I and II carcinoma of the breast," *International Journal of Radiation Oncology, Biology, Physics*, vol. 5, pp. 257–261, feb 1979.
- [20] M. J. Brady, D. F. Cella, F. Mo, A. E. Bonomi, D. S. Tulsky, S. R. Lloyd, S. Deasy, M. Cobleigh, and G. Shiimoto, "Reliability and validity of the Functional Assessment of Cancer Therapy-Breast quality-of-life instrument.," *Journal of Clinical Oncology*, vol. 15, pp. 974–986, mar 1997.
- [21] R. C. Blitzblau, R. Arya, S. Yoo, J. A. Baker, Z. Chang, M. Palta, E. Duffy, and J. K. Horton, "A phase 1 trial of preoperative partial breast radiation therapy: Patient selection, target delineation, and dose delivery.," *Practical radiation oncology*, vol. 5, pp. e513–e520, sep 2015.
- [22] M. Sayan, D. Hard, K. Wilson, C. Nelson, H. Gagne, D. Rubin, and R. Heimann, "Long-term cosmesis following a novel schedule of accelerated partial breast radiation in selected early stage breast cancer: result of a prospective clinical trial," *Radiation Oncology Journal*, vol. 35, pp. 325–331, dec 2017.
- [23] U. Veronesi, R. Orecchia, A. Luini, V. Galimberti, S. Zurrada, M. Intra, P. Veronesi, P. Arnone, M. C. Leonardi, M. Ciocca, R. Lazzari, P. Caldarella, N. Rotmensz, C. Sangalli, D. Sances, and P. Maisonneuve, "Intraoperative radiotherapy during breast conserving surgery: a study on 1,822 cases treated with electrons.," *Breast cancer research and treatment*, vol. 124, pp. 141–51, nov 2010.



- [24] B. S. Hoppe, B. Laser, A. V. Kowalski, S. C. Fontenla, E. Pena-Greenberg, E. D. Yorke, D. M. Lovelock, M. A. Hunt, and K. E. Rosenzweig, "Acute skin toxicity following stereotactic body radiation therapy for stage I non-small-cell lung cancer: who's at risk?," *International journal of radiation oncology, biology, physics*, vol. 72, pp. 1283–6, dec 2008.
- [25] F. van der Leij, S. C. Bosma, M. J. van de Vijver, J. Wesseling, S. Vreeswijk, S. Rivera, C. Bourgier, J.-R. Garbay, T. Foukakis, T. Lekberg, D. H. van den Bongard, C. van Vliet-Vroegindeweyj, H. Bartelink, E. J. Rutgers, and P. H. Elkhuizen, "First results of the preoperative accelerated partial breast irradiation (PAPBI) trial," *Radiotherapy and Oncology*, vol. 114, pp. 322–327, mar 2015.
- [26] S. C. Formenti, H. Hsu, M. Fenton-Kerimian, D. Roses, A. Guth, G. Jozsef, J. D. Goldberg, and J. K. Dewynngaert, "Prone accelerated partial breast irradiation after breast-conserving surgery: Five-year results of 100 patients," *International Journal of Radiation Oncology Biology Physics*, vol. 84, pp. 606–611, nov 2012.
- [27] C. Park, L. Papiez, S. Zhang, M. Story, and R. D. Timmerman, "Universal Survival Curve and Single Fraction Equivalent Dose: Useful Tools in Understanding Potency of Ablative Radiotherapy," *International Journal of Radiation Oncology Biology Physics*, vol. 70, pp. 847–852, mar 2008.
- [28] J. M. Kurtz, "The clinical radiobiology of breast cancer radiotherapy," *Radiotherapy and Oncology*, vol. 75, pp. 6–8, apr 2005.

# Appendix G

## G Chapter 2 copyright form

5/8/2019

Rightslink® by Copyright Clearance Center



RightsLink®

Home

Create Account

Help



**Title:** Reducing the dose of gadolinium-based contrast agents for DCE-MRI guided SBRT: The effects on inter and intra observer variability for preoperative target volume delineation in early stage breast cancer patients

**Author:** Matthew Mouawad, Heather Biernaski, Muriel Brackstone, Michael Lock, Brian Yaremko, Tracy Sexton, Edward Yu, Robert E. Dinniwel, Kalan Lynn, George Hajdok, Frank S. Prato, Robert Terry Thompson, Neil Gelman, Stewart Gaede

**Publication:** Radiotherapy and Oncology

**Publisher:** Elsevier

**Date:** February 2019

© 2018 Elsevier B.V. All rights reserved.

### LOGIN

If you're a **copyright.com user**, you can login to RightsLink using your copyright.com credentials.

Already a **RightsLink user** or want to [learn more?](#)

Please note that, as the author of this Elsevier article, you retain the right to include it in a thesis or dissertation, provided it is not published commercially. Permission is not required, but please ensure that you reference the journal as the original source. For more information on this and on your other retained rights, please visit: <https://www.elsevier.com/about/our-business/policies/copyright#Author-rights>

BACK

CLOSE WINDOW

Copyright © 2019 [Copyright Clearance Center, Inc.](#) All Rights Reserved. [Privacy statement](#). [Terms and Conditions](#). Comments? We would like to hear from you. E-mail us at [customercare@copyright.com](mailto:customercare@copyright.com)

## **Appendix H**

### **H Curriculum Vitae**

# Matthew Mouawad | Curriculum Vitae

## EDUCATION

---

<b>PhD in Medical Biophysics</b> <i>Western University</i>	<b>2014-Present</b> <i>London, Ontario</i>
<b>CAMPEP Accredited Masters in Clinical Medical Biophysics</b> <i>Western University</i>	<b>2018</b> <i>London, Ontario</i>
<b>Honors Bachelor of Medical Sciences: Specialization in Medical Biophysics</b> <i>Western University</i>	<b>2014</b> <i>London, Ontario</i>

## RESEARCH EXPERIENCE

---

<b>Photon Technology International</b> <i>Application Lab Assistant</i>	<b>2012-2013</b> <i>London, Ontario</i>
--	--

## TEACHING EXPERIENCE

---

<b>Mentorship, 4th Year Medical Biophysics Undergraduate</b> <i>Western University</i> <i>Delivery Verification of Respiratory-Gated Volumetric-Modulated Arc Therapy for Liver Cancer Using During Treatment Imaging</i>	<b>2018-2019</b> <i>London, Ontario</i>
<b>Mentorship, 3rd Year Medical Biophysics Undergraduate</b> <i>Western University</i> <i>Monitoring Breast Cancer Response to Radiotherapy Using Pharmacokinetic Modelling</i>	<b>2018-2019</b> <i>London, Ontario</i>
<b>Teaching Assistant: Mathematical Transform Applications</b> <i>Western University</i>	<b>2015-2017</b> <i>London, Ontario</i>

## PUBLICATIONS

---

Mouawad, M., Biernaski H., Brackstone M., Lock M., Yaremko B., Sexton T., Yu E., Dinniwell R.E., Lynn K., Hajdok G., Prato F.S., Thompson R.T., Gelman N., Gaede S. (2019) <b>Reducing the Dose of Gadolinium-based Contrast Agents for DCE-MRI Guided SBRT: The Effects on Inter and Intra Observer Variability for Preoperative Target Volume Delineation in Early Stage Breast Cancer Patients.</b> <i>Radiotherapy and Oncology.</i> <a href="https://doi.org/10.1016/j.radonc.2018.11.020">https://doi.org/10.1016/j.radonc.2018.11.020</a>	<b>2019</b>
Mouawad, M., Biernaski H., Brackstone M., Lock M., Kornecki A., Shmuilovich O., Nachum I.B., Prato F.S., Thompson R.T., Gaede S., Gelman N. (2019) <b>The effect of registration on voxel-wise Tofts model parameters and uncertainties from DCE-MRI of early stage breast cancer patients using 3DSlicer.</b> <i>Journal of Digital Imaging.</i> <i>UNDER REVIEW</i>	<b>2019</b>

- Guidolin K., Yaremko B., Lynn K., Gaede S., Kornecki A., Muscedere G., Ben-Nachum I., Shmuilovich O., Mouawad M., Yu E., Sexton T., Gelman N., Moiseenko V., Brackstone M., Lock M. (2019) **Stereotactic image-guided neoadjuvant ablative single dose radiation then lumpectomy (signal) for early breast cancer: a prospective single arm trial of single dose radiation therapy.** Current Oncology. *IN PRESS*. 2019
- Kamińska, I., Fronc, K., Sikora, B., Mouawad, M., Siemiarczuk, A., Szewczyk, M., ... & Paszkowicz, W. (2015) **Upconverting/magnetic: Gd 2 O 3:(Er 3+, Yb 3+, Zn 2+) nanoparticles for biological applications: effect of Zn 2+ doping.** Royal Society of Chemistry Advances. 2015

## PEER REVIEWED ABSTRACTS

---

- Matthew Mouawad, Heather Biernaski, Muriel Brackstone, Michael Lock, Brian Yaremko, Anat Kornecki, Olga Shmuilovich, Ilanit Nachum, Giulio Muscedere, Kalan Lynn, Frank Prato, R. Terry Thompson, Stewart Gaede, Neil Gelman (2019) **The influence of single fraction versus three fraction neoadjuvant stereotactic ablative radiotherapy and imaging delay time post-radiotherapy on dynamic contrast enhanced MRI response assessment in early stage breast cancer patients.** Research and Education Day 2019. *SNAP ORAL PRESENTATION* 2019
- Matthew Mouawad, Heather Biernaski, Muriel Brackstone, Michael Lock, Brian Yaremko, Anat Kornecki, Olga Shmuilovich, Ilanit Nachum, Giulio Muscedere, Kalan Lynn, Frank Prato, R. Terry Thompson, Stewart Gaede, Neil Gelman (2019) **The Influence of SABR Fractionation and Imaging Delay Time On Post-Radiotherapy DCE-MRI Response Assessment in Early Stage Breast Cancer Patients.** The 2019 AAPM Annual Scientific Meeting. *ORAL PRESENTATION* 2019
- Oi Wai Chau, Omar El-Sherif, Matthew Mouawad, Frank Prato, Stewart Gaede (2019) **Assessing Myocardial Perfusion After Cardiac Irradiation Using Dynamic Contrast Enhanced Hybrid PET/MRI.** The 2019 AAPM Annual Scientific Meeting. *POSTER PRESENTATION* 2019
- Matthew Mouawad, Heather Biernaski, Muriel Brackstone, Michael Lock, Brian Yaremko, Anat Kornecki, Olga Shmuilovich, Ilanit Nachum, Giulio Muscedere, Kalan Lynn, Frank Prato, R. Terry Thompson, Stewart Gaede, Neil Gelman (2019) **The influence of delay between radiotherapy and imaging on DCE-MRI assessment of tumour response to high dose single fraction radiotherapy in early stage breast cancer patients.** London Health Research Day 2019. *POSTER PRESENTATION* 2019
- Matthew Mouawad, Heather Biernaski, Muriel Brackstone, Michael Lock, Brian Yaremko, Tracy Sexton, Edward Yu, Robert E. Dinniwell, George Hajdok, Frank S. Prato, R. Terry Thompson, Neil Gelman, Stewart Gaede. (2018) **Effect of Reduced Dose of Gadolinium Contrast in Tumour Volume Delineation Aided by DCE-MRI for Single Fraction Radiotherapy in Early Stage Breast Cancer Patients.** The 2018 CARO-COMP-CAMRT Joint Scientific Meeting. *ORAL PRESENTATION* 2018

- Matthew Mouawad, Heather Biernaski, Muriel Brackstone, Michael Lock, Anat Kornecki, Olga Shmuilovich, Ilanit Nachum, Frank Prato, R. Terry Thompson, Stewart Gaede, Neil Gelman (2018) **Signal Enhancement Volume Increase in DCE-MRI After Single Fraction SBRT of Early Stage Breast Cancer**. The 2018 CARO-COMP-CAMRT Joint Scientific Meeting. *POSTER PRESENTATION* 2018
- Matthew Mouawad, Heather Biernaski, Muriel Brackstone, Michael Lock, Anat Kornecki, Olga Shmuilovich, Ilanit Nachum, Frank Prato, R. Terry Thompson, Stewart Gaede, Neil Gelman (2018) **Tumour Signal Enhancement Volume Increase in DCE-MRI After Single Fraction SBRT of Early Stage Breast Cancer**. The 2018 AAPM Annual Scientific Meeting. *EPOSTER PRESENTATION* 2018
- Matthew Mouawad, Heather Biernaski, Muriel Brackstone, Michael Lock, Anat Kornecki, Olga Shmuilovich, Ilanit Ben Nachum, Frank S. Prato, R. Terry Thompson, Stewart Gaede, Neil Gelman (2018) **Large signal enhancement volume changes in DCE-MRI after single fraction SBRT of early stage breast cancer**. Research and Education Day 2018. *POSTER PRESENTATION* 2018
- Matthew Mouawad, Heather Biernaski, Muriel Brackstone, Michael Lock, Anat Kornecki, Olga Shmuilovich, Ilanit Ben Nachum, Frank S. Prato, R. Terry Thompson, Stewart Gaede, Neil Gelman (2018) **Signal Enhancement Volume Increase in DCE-MRI After Single Fraction SBRT of Early Stage Breast Cancer**. Imaging Network of Ontario 2018. *POSTER PRESENTATION* 2018
- Matthew Mouawad, Heather Biernaski, Muriel Brackstone, Michael Lock, Anat Kornecki, Olga Shmuilovich, Ilanit Ben Nachum, George Hajdok, Frank S. Prato, R. Terry Thompson, Stewart Gaede, Neil Gelman (2018) **Effect of Reduced Contrast Agent on Kinetic Analysis of early stage breast cancer patients**. Imaging Network of Ontario 2018. *POSTER PRESENTATION* 2018
- Matthew Mouawad, Heather Biernaski, Muriel Brackstone, Michael Lock, Anat Kornecki, Olga Shmuilovich, Ilanit Ben Nachum, Frank S. Prato, R. Terry Thompson, Stewart Gaede, Neil Gelman (2018) **Large signal enhancement volume changes in DCE-MRI after single fraction SBRT of early stage breast cancer**. London Health Research Day 2018. *POSTER PRESENTATION* 2018
- Matthew Mouawad, Heather Biernaski, Muriel Brackstone, Michael Lock, Anat Kornecki, Olga Shmuilovich, Ilanit Ben Nachum, Robert Terry Thompson, Frank S. Prato, Stewart Gaede, Neil Gelman (2017) **Reducing computation time for registration in Breast DCE-MRI: Effects of percent sampling on kinetic analysis model parameters, uncertainties, and goodness of fit**. International Society of Magnetic Resonance in Medicine (ISMRM) 2017 Annual Scientific Meeting. *POSTER PRESENTATION* 2017

- Matthew Mouawad, Heather Biernaski , Muriel Brackstone, Michael Lock, Anat Kornecki, Olga Shmuilovich, Ilanit Ben Nachum, Robert Terry Thompson, Frank S. Prato, Stewart Gaede, Neil Gelman (2017) **Reducing computation time for registration in Breast DCE-MRI: Effects of percent sampling on kinetic analysis model parameters, uncertainties, and goodness of fit.** Imaging Network of Ontario 2017. *POSTER PRESENTATION* 2017
- Matthew Mouawad, Heather Biernaski , Muriel Brackstone, Michael Lock, Anat Kornecki, Olga Shmuilovich, Ilanit Ben Nachum, Robert Terry Thompson, Frank S. Prato, Stewart Gaede, Neil Gelman (2017) **Reducing computation time for registration in Breast DCE-MRI: Effects of percent sampling on kinetic analysis model parameters, uncertainties, and goodness of fit.** London Health Research Day 2017. *POSTER PRESENTATION* 2017
- Matthew Mouawad, Heather Biernaski , Muriel Brackstone, Michael Lock, Anat Kornecki, Olga Shmuilovich, Ilanit Ben Nachum, Robert Terry Thompson, Frank S. Prato, Stewart Gaede, Neil Gelman (2016) **Deformable Registration of Dynamic Contrast Enhanced Breast MRI: The Influence of B-Spline Grid Size on Enhancement Curves and Computation Time.** London Health Research Day 2016. *POSTER PRESENTATION* 2016
- Matthew Mouawad, Heather Biernaski , Muriel Brackstone, Michael Lock, Anat Kornecki, Olga Shmuilovich, Ilanit Ben Nachum, Robert Terry Thompson, Frank S. Prato, Stewart Gaede, Neil Gelman (2016) **Deformable Registration of Dynamic Contrast Enhanced Breast MRI: The Influence of Sampling Percent on Enhancement Curves and Computation Time.** Imaging Network of Ontario (IMNO) 2016. *POSTER PRESENTATION* 2016
- Matthew Mouawad, Heather Biernaski , Muriel Brackstone, Michael Lock, Anat Kornecki, Olga Shmuilovich, Ilanit Ben Nachum, Robert Terry Thompson, Frank S. Prato, Stewart Gaede, Neil Gelman (2016) **How Does Sampling Percentage affect computation time and accuracy in Deformable Registration Influence Kinetic Model Analysis Results in DCEMRI of the Breast?.** Research And Education Day 2016. *POSTER PRESENTATION* 2016
- Matthew Mouawad, Heather Biernaski , Muriel Brackstone, Michael Lock, Anat Kornecki, Olga Shmuilovich, Ilanit Ben Nachum, Robert Terry Thompson, Frank S. Prato, Stewart Gaede, Neil Gelman (2016) **How Does Sampling Percentage affect computation time and accuracy in Deformable Registration Influence Kinetic Model Analysis Results in DCEMRI of the Breast?.** The 2016 COMP Annual Scientific Meeting. *POSTER PRESENTATION* 2016

## SCHOLARSHIPS

---

- Translational Breast Cancer Studentship funded in part by the Breast Cancer Society of Canada 2014-2019
- ISMRM 2017 annual meeting stipend 2017

## AWARDS

---

- Runner-up for Best Oral Presentation, COMP-CARO-CAMRT Annual Scientific Meeting 2018

## COMMITTEES

---

**Strategic Planning Committee**

*London Regional Cancer Program*  
Student Representative

**2017-2019**

*London, Ontario*

**CAMPEP steering committee**

*Department of Medical Biophysics, Western University*  
Student Representative

**2015-2018**

*London, Ontario*

**Graduate Recruitment Committee**

*Department of Medical Biophysics, Western University*  
Student Representative

**2015-2017**

*London, Ontario*